BrJAC

Brazilian Journal of Analytical Chemistry

an International Scientific Journal

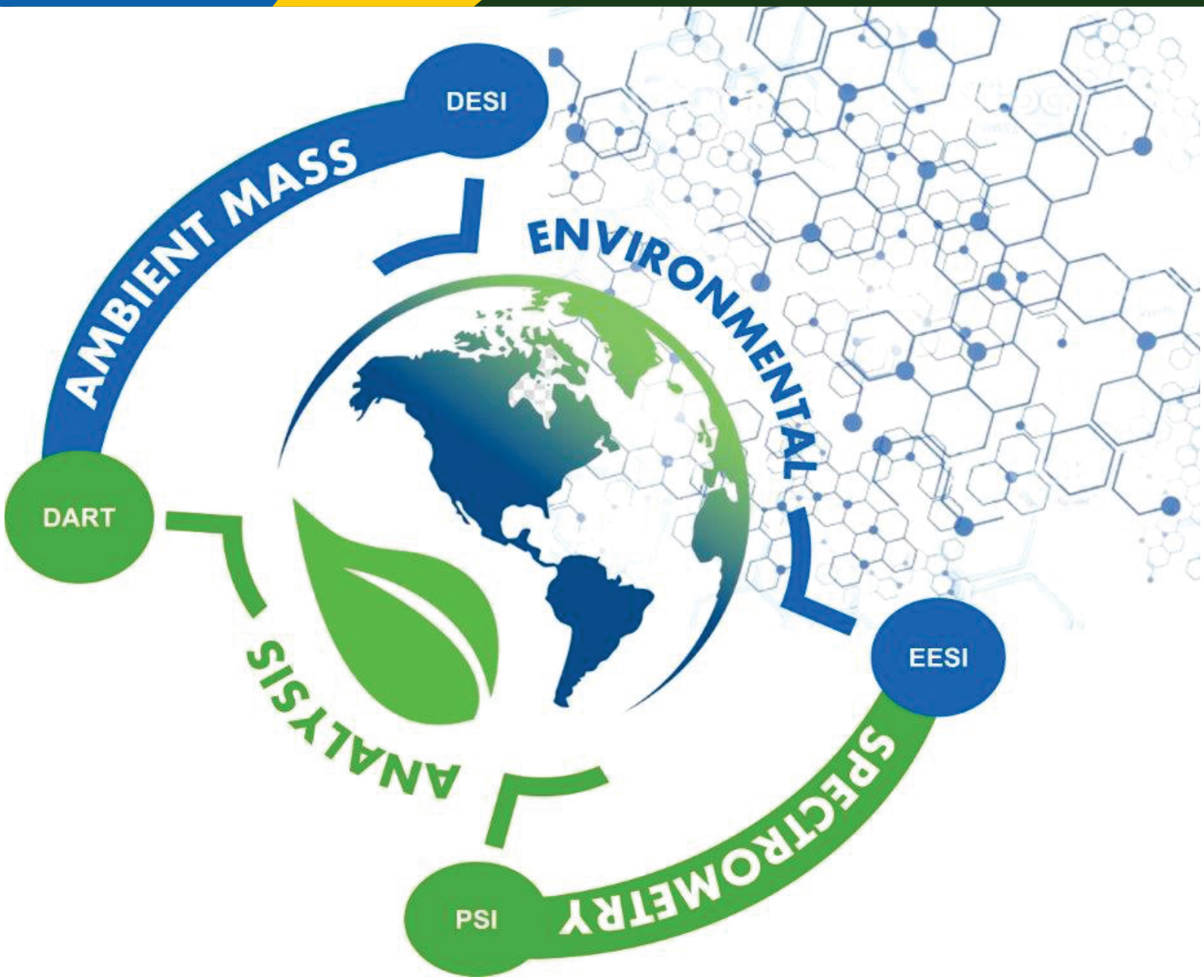

Ambient Ionization Mass Spectrometry: Applications and New Trends for Environmental Matrices Analysis

Andréa Rodrigues Chaves, Rafael Oliveira Martins, Lanaia Ítala Louzeiro Maciel, Allyster Rodrigues Silva, Daniel Vieira Gondim, Júlia Martins Fortalo, Steffany de Souza Santos, Jussara Valente Roque, Boniek Gontijo Vaz

July – September 2022 Volume 9 Number 36

DECEMBER
10-15, 2022

RIO DE JANEIRO - BRAZIL

3rd IBEROAMERICAN CONFERENCE OF MASS SPECTROMETRY

Sheraton Grand Rio Hotel & Resort

Organization

Sociedad Brasileira de Espectrometria de Masas

Venue

SHERATON

EST. 1937

Brazilian Journal of Analytical Chemistry

VISÃO FOKKA - COMMUNICATION AGENCY

The *Braz. J. Anal. Chem.* (BrJAC) is a peer-reviewed, open access, scientific journal intended for professionals and institutions acting mainly in all branches of analytical chemistry.

ISSN 2179-3425 printed ISSN 2179-3433 eletronic

Scope

BrJAC is dedicated to the diffusion of significant and original knowledge in all branches of Analytical Chemistry and Bioanalytics. BrJAC is addressed to professionals involved in science, technology and innovation projects in Analytical Chemistry at universities, research centers and in industry.

BrJAC is a quarterly journal that publishes original, unpublished scientific articles, reviews and technical notes that are peer reviewed in the double-blind way. In addition, it publishes interviews, points of view, letters, sponsor reports, and features related to analytical chemistry. Once published online, a DOI number is assigned to the paper.

Manuscripts submitted for publication in BrJAC cannot have been previously published or be currently submitted for publication in another journal.

For complete information on ethics and policies on conflicts of interest, copyright, reproduction of already published material and preprints, in addition to the manuscript submission and peer review system, please visit “About us” and Guidelines for Authors at www.brjac.com.br

Indexing Sources

Scopus

CiteScore 2020: 0.3; SJR: 0.131; SNIP: 0.146. CiteScore Tracker 2021: 0.6 Access source details

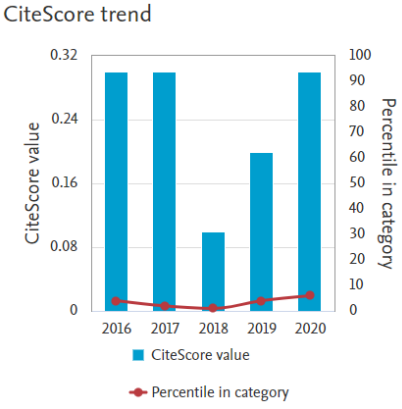

CLARIVATE ANALYTICS
EMERGING SOURCES CITATION INDEX
INDEXED

CAPES QUALIS

Google scholar

Cited by		VIEW ALL
	All	Since 2017
Citations	311	237
h-index	7	6
i10-index	3	1

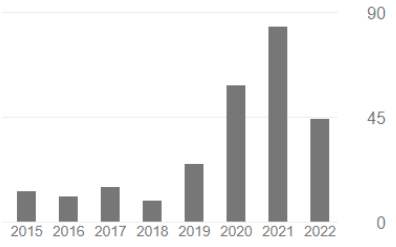

Production Editor
Silvana Odete Pisani, PhD

Publisher
Lilian Freitas
MTB: 0076693/ SP
lilian.freitas@visaofokka.com.br

Advertisement
Luciene Campos
luciene.campos@visaofokka.com.br

Art Director: Adriana Garcia

WebMaster: Daniel Letieri

BrJAC’s website: www.brjac.com.br / Contact: brjac@brjac.com.br
Like BrJAC on Facebook: https://www.facebook.com/brjachem

ABEC BRASIL
BrJAC is associated to the Brazilian Association of Scientific Editors

VISÃO FOKKA
BrJAC is published quarterly by:
Visão Fokka Communication Agency
Av. Washington Luiz, 4300 - Bloco G - 43
13042-105 – Campinas, SP, Brazil
contato@visaofokka.com.br
www.visaofokka.com.br

EDITORIAL BOARD

EDITORIAL ADVISORY BOARD

EDITORIAL ADVISORY BOARD (Continuation)

CONTENTS

CONTENTS

Brazilian Journal of Analytical Chemistry
2022, Volume 9, Issue 36, pp 1-2
doi: 10.30744/brjac.2179-3425.editorial.mbertotti.N36

BrJAC

EDITORIAL

About this Issue

Mauro Bertotti
Full Professor at the Institute of Chemistry at the University of São Paulo (IQ-USP), São Paulo, SP, Brazil
Associate Editor of the Braz. J. Anal. Chem.

This BrJAC issue starts with an interview with Edenir R. Pereira Filho, an Associate Professor at the Federal University of São Carlos (UFSCar). His research spans multiple sectors, including spectroanalytical methods for direct solid sample analysis, especially electronic waste. He is also an expert in designing experiments using chemometric tools and has a YouTube channel to share his research group´s contributions. He finished his pleasant interview with an important comment: “Treat your students with special care.”.

The point of view shows an interesting and relevant discussion on the limit of detection (LOD) and the use of significant digits. The author’s conclusion is clearly stated: “The LOD must be reported with a single digit, which is significant but uncertain”. I completely agree with such a claim and reinforce that as scientists that handle numbers, we have to be aware that all measurements contain some kind of uncertainty, and significant figures show us what that uncertainty is.

Nanomaterials have been increasingly studied for medical applications, and one crucial aspect that has drawn attention is the safety concerns of handling and using nanoparticles. Do the benefits outweigh the risks? Accordingly, the letter presents a thorough discussion on nanostructured materials and provides an update on the challenges associated with nanomaterials production with a focus on nanomedicine.

Analytical chemistry has always been associated with the needs of society, and two reviews address issues involving environmental analysis. One of them gives an overview of arsenic speciation methods and the challenges represented by contamination in soil, water, and food supplements. The other reports the analysis of compounds using minimal or no sample preparation. Such an approach includes the development of less invasive and more continuous testing, resulting in devices that cover the trend of point-of-care (POC) analysis.

Two exciting articles have been included in this BrJAC issue. The first reports on the synthesis, characterization, and application of zeolitic imidazolate frameworks for adsorption processes. The authors have demonstrated that their material presents excellent adsorption capacity and can be successfully employed to remove arsenic species from aquatic environments. The other article describes a thorough study on a cost-effective sorbent (a lignin-based bio-alkyd resin) prepared from the reaction between oxidized lignin with a mixture of palmitic acid and glycerol. Molybdenum (in the form of a Mo/thiocyanate complex) can be selectively extracted from complex samples (mice liver, pharmaceuticals, water, and fertilizer samples) for further spectrophotometric detection with enhanced sensitivity.

As for technical notes, the issue presents two attractive studies. The first shows how the combination of threshold QTOF-MS measurements and quantum-chemical calculations allows for the understanding of the increased stability of sodiated sucralose compared to the protonated one. Neodymium and praseodymium can be found in permanent magnets at very low levels, and a method to determine both metals with high accuracy and precision is presented in the other work.

Cite: Bertotti, M. About this Issue. *Braz. J. Anal. Chem.,* 2022, *9* (36), pp 1-2. https://dx.doi.org/10.30744/brjac.2179-3425.editorial.mbertotti.N36

It is exciting to see the growing interest of researchers worldwide for BrJAC, as shown in this issue. The articles reveal that analytical chemistry is a long-standing example of an interdisciplinary approach to scientific research, pushing the field into emerging topics of societal importance. I hope you enjoy reading!

Mauro Bertotti is currently Full Professor at the Institute of Chemistry at the University of São Paulo (IQ-USP), São Paulo, SP, Brazil. Works mainly on Electroanalytical Chemistry, with emphasis on Microelectrodes, Electrochemical Sensors, and Scanning Electrochemical Microscopy.

CV

Brazilian Journal of Analytical Chemistry
2022, Volume 9, Issue 36, pp 3-7
doi: 10.30744/brjac.2179-3425.interview.erpfilho

INTERVIEW

Professor Edenir Pereira Filho, a researcher with a broad and solid background in science and also a YouTuber, recently gave an interview to BrJAC

Edenir Rodrigues Pereira Filho
Associate Professor in the Department of Chemistry at the Federal University of São Carlos, São Carlos, SP, Brazil

Edenir R. Pereira Filho holds a degree in Chemistry from the Pontifical Catholic University of Campinas (1996), a Master's degree in Chemistry (1999) from the State University of Campinas (Unicamp), a Master's degree in Mathematics (2022) from the Federal University of São Carlos (UFSCar), and a doctorate (2003) in Science (Unicamp). He is currently an Associate Professor at UFSCar. He works mainly on spectroanalytic, with an emphasis on Inductively Coupled Plasma Optical Emission Spectroscopy (ICP OES), Flame Atomic Absorption Spectrometry (FAAS), and Laser Induced-Breakdown Spectroscopy (LIBS), and applications of chemometric tools (Design of Experiments, DoE) in atomic spectrometry.

Would you tell us where you were born and what your childhood was like?

I was born in Colatina, Espírito Santo state, on May 24, 1975. My relatives are originally from Minas Gerais state, and during my first years, we moved from Espírito Santo to Minas Gerais. My father worked in a company dedicated to civil construction (mainly railways and infrastructure), and we moved to several Brazilian states (Espírito Santos, Maranhão, Minas Gerais again, and São Paulo) and cities (6 different locations). From the end of 1980 to the beginning of 1990, we lived in Montes Claros (North of Minas Gerais state). In this case, my first years were rich in different cultures (north and south) of our country.

What early influences encouraged you to study chemistry? Did you have any influencers, such as a teacher?

I attended a chemistry technician course in Montes Claros (from 1989 to 1992) (old high school). I also assisted some professors during laboratory classes. This activity exposed me to several aspects of chemistry: mainly physical chemistry and analytical chemistry. Several professors influenced my decision to focus on chemistry in the next steps of my career (university). In addition, during this period, I also visited several chemical industries (cement, metallic magnesium and silicon production, and water treatment) and had contact with chemists and engineers.

Cite: Pereira Filho, E. R. Professor Edenir Pereira Filho, a researcher with a broad and solid background in science and also a YouTuber, recently gave an interview to BrJAC**.** *Braz. J. Anal. Chem.,* 2022, *9* (36), pp 3-7. http://dx.doi.org/10.30744/brjac.2179-3425.interview.erpfilho

When did you decide to study chemistry? What motivated you? How was the beginning of your career?

I decided to follow the chemistry career after the chemistry technician course (at the beginning of the 1990s). My relatives moved to Valinhos (São Paulo state), and I attended several universities then. In 1993, I enrolled in my first chemistry class at Pontifical Catholic University of Campinas (PUC-Campinas). During my undergraduate course, the classes were at night. I worked as an industry supervisor in a paint manufacturer in Campinas. Later, I was approved as a scientific assistant at the Brazilian Agricultural Research Corporation (Embrapa), Environmental Research Center at Jaguaríuna (São Paulo State). At Embrapa, I worked in an analytical chemistry laboratory and operated several analytical chemistry instruments, such as a spectrophotometer (UV-Vis), flame atomic absorption spectrometer (FAAS), and graphite furnace atomic absorption spectrometer for water, plant, and soil analysis. In 1997, I left Embrapa and started a Master's course in chemistry at Campinas State University (Unicamp) under the supervision of Prof. Dr. Marco Aurélio Zezzi Arruda. I finished my Master's course in 1999 and started the Ph.D. course in Science under the supervision of Prof. Arruda and the co-supervision of Prof. Dr. Roney Poppi. In 2001, I performed part of my Ph.D. course in Germany under the guidance of Prof. Dr. Harald Berndt. In 2003, I defended my thesis. Both Master's and Ph.D. projects were financed by São Paulo Research Foundation (Fapesp). From 2004 to 2006, I worked at the Federal University of Alfenas (Minas Gerais state), Unifal (former School of Pharmacy and Odontology, EFOA), and PUC-Campinas. In the middle of 2006, I was approved and appointed as a professor at the Chemistry Department of the Federal University of São Carlos (UFSCar).

Prof. Edenir Pereira Filho at the Group of Applied Instrumental Analysis (GAIA), Dept. of Chemistry, UFSCar.

What has changed in the student's profile, ambitions and performance since the time you started your career?

Nowadays, students have more information, and the professional possibilities are almost infinite. Requirements such as a second or a third language or international experience are no longer intangible activities and are now natural and required steps. The students are more connected; it is necessary to have other required characteristics such as social abilities (soft skills), teamwork, and capacity to solve complex problems using different knowledge (not only the technical).

Could you comment briefly on the recent evolution of analytical chemistry, considering your contributions?

Analytical Chemistry has a fundamental characteristic: the possibility to quickly interact with other areas of chemistry and other sciences — the analytical chemistry professional must know data science, mining, and processing. In addition, it is possible to interact with mathematics and statistics. In my research line, for instance, I am applying several mathematical and statistical techniques, and this combination is a science named Chemometrics. I believe that Chemometrics is a powerful Science, and I am very tempted to learn more and more. For instance, in 2019, I started a Master's course in Mathematics, and my dissertation entitled "Chemistry and Mathematics' synergism: Teaching Design of Experiments in undergraduate and graduate courses of Chemistry at UFSCar" was defended in 2022. Finally, the future of analytical chemistry is to spread its interactions with other areas and solve complex problems related to calibration and data science.

What are your lines of research? You have published many scientific papers. Would you highlight any?

My research line is mainly devoted to developing analytical methods for direct solid sample analysis. In the last 10 years, I have been working with a very complex type of sample: electronic waste (waste electrical and electronic equipment, WEEE). The WEEE has more than 40 chemical elements in its different parts: printed circuit boards (PCBs), polymers, batteries, and screens. Several elements are potentially and economically recoverable. In addition, I am also interested in the application of chemometric techniques to propose calibration models focusing on solid sample analysis. Up to 2022, I have almost 200 publications in different international journals. Instead, to highlight a specific paper, I would like to invite the reader to see and join my YouTube channel: https://www.youtube.com/c/EdenirPereiraFilho. This channel presents several contributions of my research group (more than 300 videos): design of experiments (DoE) with two tutorials, chemometrics (principal component analysis, PCA), laser induced-breakdown spectroscopy (LIBS), calibration strategies for direct solid sample analysis, bibliometric analysis, chemical equilibrium, the interaction between academy and industry (professional Master's course), WEEE characterization, and the use of Excel, Octave, Matlab, R, and Python. Part of the channel's content was prepared with the help of my former Ph.D., Master's, and undergraduate students, and the work is completely voluntary. Please, spread the word!!!

"... the interaction between Brazilian researchers and industry must be more collaborative, and the dialogue should be improved..."

What is your opinion on the current progress of research in chemistry in Brazil? What are the most recent advances and challenges in scientific research in Brazil?

Chemistry research has improved a lot in Brazil in the last 20 years. Nowadays, we have access to sophisticated and advanced technologies and instrumentation. In addition, it is possible to have close contact with research centers worldwide. The main challenges are having a regular source of financial support and establishing a healthy interaction with the industry. In my opinion, the interaction between Brazilian researchers and industry must be more collaborative, and the dialogue should be improved. There are several initiatives, but it is necessary to propose clear rules and a governmental incentive.

For you, what have been the most important recent achievements in analytical chemistry research? What are the landmarks? What has changed in the scenario with the pandemic?

From the point of view of solid sample analysis and data science, I think the use of X-ray fluorescence (XRF) and LIBS in a rover sent to Mars is a significant development. During the pandemic, for example, and describing one of my activities, it was possible to interact, even remotely, with researchers and students from different parts of Brazil and the world. I discussed several research activities with national and international students, and some presented webinars for graduate students. Now, it is also possible to attend webinars presented by Nobel Prize winners. During the pandemic period, I offered a discipline about DoE on four different occasions (2020, 2021, and 2022). More than 300 students from 17 states of Brazil and Argentina, Peru, and Colombia participated in this discipline. I saw the pandemic period as a unique opportunity to present my research line and scientific achievements on social media (YouTube and LinkedIn) and try to show to society how their financial investment is used.

There are in Brazil, and in the world, several conferences on chemistry. To you, how important are these meetings to the scientific community? How do you see the development of national chemistry meetings in Brazil?

These meetings are essential, but it is necessary to propose activities to include all the community partners, mainly students. In addition, the researchers and students need to feel valued and considered by the scientific societies. When students prepare a poster for presentation, for example, they want to show their work and not comply with a protocol.

Dr. Edenir R. Pereira Filho, Associate Professor in the Department of Chemistry at the Federal University of São Carlos (UFSCar).

What is the importance of awards in the development of science and new technologies?

All awards are important and healthy to the scientific community and can be used as an additional stimulus.

For you, what is the importance of the national funding agencies for the scientific development of Brazil?

These agencies are vital and need to receive regular investments for better support. On the other hand, the researchers also need the effort to obtain financial support from others, such as industry and international cooperation.

At the moment, the situation for scientific research in Brazil is one of decreasing investment. How do you see this situation, and what would you say to young researchers?

We need to pay more attention to our political representatives. The present government was established by the people that made an unthinkable and unhappy choice. Soon, we need to choose better and study the proposition of the candidates and see its commitment with the Science.

What advice would you give to a young scientist who wants to pursue a career in chemistry?

Treat your students with special care. They are your business card. Remember that you were a student a few years ago. Try to establish beneficial scientific collaborations. Answer your e-mails and be polite. Do not ignore your colleagues. Keep studying and observe which gaps need to be filled. Keep a distance from toxic (from the psychological point of view) people and organizations. Be authentic and do not pay attention to what others will think. Work hard!!!

How would you like to be remembered?

I would like to be remembered for contributing to solid sample analysis using LIBS and the bald guy with an interesting and useful YouTube channel.

Brazilian Journal of Analytical Chemistry
2022, Volume 9, Issue 36, pp 8-9
doi: 10.30744/brjac.2179-3425.point-of-view-gldonati-N36

BrJAC

POINT OF VIEW

The Case of the Limit of Detection

George L. Donati
Associate Research Professor at the Department of Chemistry
Wake Forest University, Winston-Salem, NC, USA

Students learn early on in science courses that reliable results can only be achieved from accurate measurements. In some of the first general chemistry classes, but even more intensively in analytical chemistry classes, students are introduced to the concept of significant figures.[1] They learn that a measurement is only as true and precise as the instrument used to carry it out, and that the level of skill of the measurer (and how they interpret and report the measurement) is also important. A classic example to introduce significant figures involves the measurement of an object's length using a ruler. Let us say that the object is a string, and one has two rulers available to measure it. The first ruler has 1-cm markings, while the second one presents 0.1-cm markings. When performing any measurement, students learn that more accurate results will be achieved if one estimates and includes an additional digit to the measurement. Thus, as an example, let us say that the string's length is determined to be between 3 and 4 cm using the first ruler. The measurer will then estimate the tenths decimal place and report the string's length as 3.4 cm, for example. Although considered significant, the tenths place (*i.e.*, 4) is an estimate and, therefore, it is uncertain. The other digit (*i.e.*, 3) is both significant and certain. Using the second ruler, the string's length falls between 3.4 and 3.5 cm. The measurer will again estimate an additional decimal place and report the length as 3.48 cm. In this example, the digits 3 and 4 are both significant and certain, while the hundredths place (*i.e.*, 8) is significant but uncertain.

Now, how does the concept of significant figures relate to limit of detection (LOD)?

There are different interpretations for LOD,[2-5] but it simply is the lowest concentration of analyte generating an instrument response that is statistically different from (and higher than) that recorded for the blank. According to the International Union of Pure and Applied Chemistry (IUPAC), the LOD is calculated as three times the standard deviation of the instrument response for the blank (S_b), divided by the calibration curve slope (m), *i.e.*, LOD = $3S_b/m$. The value S_b is calculated from repeated measurements of the blank solution, usually 10 - 20 replicates (n = 10 - 20). Considering a normal distribution, 99.86% of the data is < $(\bar{x} + 3S)$ (*i.e.*, < than the value corresponding to three standard deviations above the mean). Therefore, the LOD calculated at $3S_b$ is statistically different from, and has a 99.86% chance of being larger than the blank.[4]

At the LOD, the instrument response recorded for the analyte is certainly not due to the random variation of the blank signal (almost 100% certain). However, there is no certainty associated with the analyte concentration. In other words, one knows the analyte is present, but cannot quantify it with an adequate level of confidence. Considering S_b as noise, the analyte's signal-to-noise ratio (S/N) at the LOD is 3 (*i.e.*, the instrument response recorded for the analyte is three times higher than the noise). Because S/N is the reciprocal of the relative standard deviation (RSD), analyte signal variations higher than 33% (RSD = 1/3) are expected at the LOD. Therefore, the concentration corresponding to the LOD is, by definition, uncertain. Going back to the concept of significant figures, the LOD must be reported with a single digit, which is significant but uncertain.

Cite: Donati, G. L. The Case of the Limit of Detection. *Braz. J. Anal. Chem.,* 2022, *9* (36), pp 8-9. http://dx.doi.org/10.30744/brjac.2179-3425.point-of-view-gldonati-N36

Many researchers fail to follow these fundamental concepts of statistics and analytical chemistry, as LODs are often reported with several significant figures (!). Perhaps, it is due to a natural difficulty to connect concepts learned at different points in one's education. Nevertheless, "the case of the LOD" may foster an awareness that could facilitate the identification of instances in which the connection between different concepts is essential: from adequate reporting of analytical results to new ideas and discoveries.

REFERENCES

(1) Skoog, D. A.; West, D. M.; Holler, F. J.; Crouch, S. R. Fundamentals of Analytical Chemistry, 8th ed., Brooks/Cole Cengage Learning, Belmont, **2004**.
(2) IUPAC, Compendium of chemical terminology, second ed. (The "Gold Book"). Compiled by A. D. McNaught and A. Wilkinson, Blackwell Scientific Publications, Oxford, 1997. Online version (2019-) created by S. J. Chalk, 0-9678550-9-8. https://doi.org/10.1351/goldbook
(3) Boqué, R.; Heyden, Y. V. The Limit of Detection. *LC GC Europe* **2009**, *22* (2), 82-85.
(4) Long, G. L.; Winefordner, J. D. Limit of detection. A closer look at the IUPAC definition. *Anal. Chem*. **1983**, *55* (7), 712A-724A. https://doi.org/10.1021/ac00258a001
(5) Krishnamoorthy, K.; Mallick, A.; Mathew, T. Model-Based Imputation Approach for Data Analysis in the Presence of Non-detects. *Ann. Occup. Hyg*. **2009**, *53* (3), 249-263. https://doi.org/10.1093/annhyg/men083

George L. Donati is currently an Associate Research Professor at the Department of Chemistry of Wake Forest University, teaching analytical chemistry courses and directing a research program in analytical instrumentation for trace element analysis. George received his M.Sc. in Analytical Chemistry at the Federal University of São Carlos (SP, Brazil, 2006) and PhD in Chemistry at Wake Forest University (Winston-Salem, NC, EUA, 2010). His research at WFU focuses on the development of portable instrumentation and novel calibration methods for spectrochemical analysis, as well as the use of atomic spectrometry and advanced statistical tools to diagnose and understand diseases.

Brazilian Journal of Analytical Chemistry
2022, Volume 9, Issue 36, pp 10-13
doi: 10.30744/brjac.2179-3425.letter.jrdejesus.N36

BrJAC

LETTER

Nanostructured Materials as an Analytical Strategy to Unravel and Treat Human Diseases: The Practical Challenges Behind the Theory

Jemmyson Romário de Jesus

Departamento de Química, Universidade Federal de Viçosa, Avenida Peter Henry Rolfs, s/n Campus Universitário, 36570-900, Viçosa, Minas Gerais, Brazil

In recent years, the world has witnessed important progress in the field of nanotechnology, which has strongly impacted the various fields of science and industry, creating new applications in electronics,[1] medicine,[2] and energy storage.[3] In this sense, several nanoscale materials with different compositions have been produced and reported in the literature.

Nanomaterials can be classified according to their composition. For example, silicon dioxide (SiO_2),[4] quantum dots (QDs),[5] carbon dots (CDs),[6] and nanoparticles (metallic and non-metallic),[7] among others, have been widely synthetized and applied in several area. In nanomedicine, more specifically, the literature shows that nanoscale materials have shown numerous advantages, including unravelling and/or treating human diseases.[8] In theory, due to unique optical properties, relative stability, high brightness, high quantum yield, biocompatibility, and biodegradability,[9] some nanomaterials can be used as promising tools to assist in the generation of bioimages,[2] diagnosis,[10] and treatments of human diseases (Figure 1).[11]

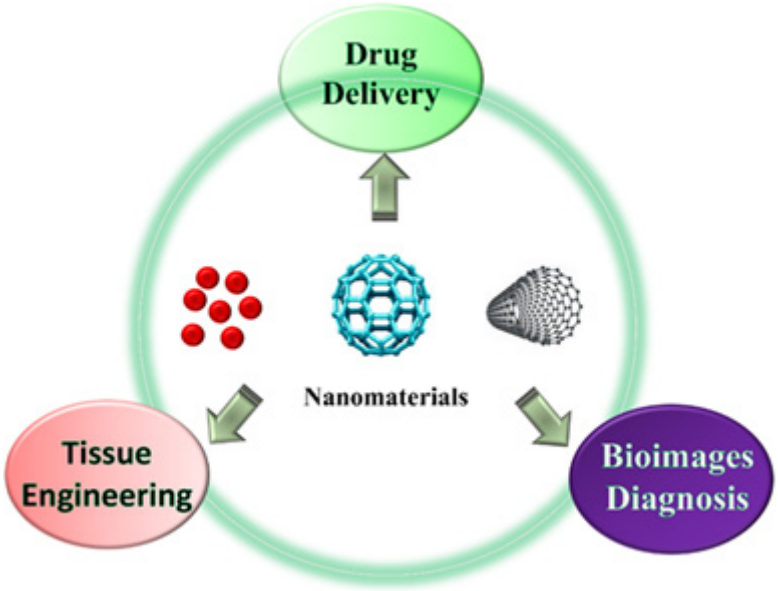

Figure 1. General use of nanomaterials in clinical applications.

Cite: de Jesus, J. R. Nanostructured Materials as an Analytical Strategy to Unravel and Treat Human Diseases: The Practical Challenges Behind the Theory. *Braz. J. Anal. Chem.,* 2022, *9* (36), pp 10-13. http://dx.doi.org/10.30744/brjac.2179-3425.letter.jrdejesus.N36

To guarantee specific interactions between nanoparticles and cells, the adsorptive properties of nanomaterials are altered by the selective functionalization of the particles, allowing different clinical applications.[8] For example, Zhang et al.[12] reported a new method for cancer identification called multiplexed nanomaterial-assisted laser desorption/ionization for cancer identification (MNALCI). In this study, Au/SiO_2 core/shell nanoparticles were used as the nanostructured material. The MNALCI was applied to 1,183 subjects, including 233 healthy controls and 950 patients with different types of cancer from two independent cohorts. MNALCI demonstrated a sensitivity of 93% to 91% to distinguish cancers from healthy controls. Satisfactory accuracy and minimal sample consumption make MNALCI a promising solution for non-invasive cancer diagnosis. In another study, magnetic NPs (MNPs), combined with oligomer-specific antibodies targeting neurotoxic beta-amyloid oligomers (AβOs), were evaluated *in vitro* and *in vivo* for imaging neurodegenerative diseases.[2] Furthermore, nanocomposites (natural or synthetic) have been used as nanocarriers to carry out controlled drug delivery to target regions and even for reconstitution of necrotic tissues (tissue engineering).[11,13]

However, the lack of adequate techniques to detect and characterize nanomaterials has exacerbated concerns about the potential risk of using nanomaterials in clinical applications, as the properties of nanomaterials depend on controlling size, shape, specific functional group, and synthesis conditions.[3,8,14] Therefore, more studies are needed to develop an adequate, reproducible, and validated method that allows for the synthesis and characterization of safe nanomaterials for medical practices. In general, there are at least three major challenges regarding nanomaterials production with a focus on nanomedicine.[8,14,15] The first is associated with the development of easy and efficient methods for the large-scale production of high-quality and safe nanomaterials.[14] In other words, although several syntheses are reported in the literature, many of them have low yield, making large-scale production difficult. The second challenge reflects the concern to control the size and shape of particles. Many physicochemical properties of the nanomaterials change with increasing or decreasing size, and therefore the pattern of toxicity may also change.[9] In general, some particle properties vary with decreasing particle size due to surface energy impacts. For example, the properties of metallic particles change when they are smaller than 5 nm. In the literature, there are few studies that report on the toxicity patterns of nanomaterials or the physicochemical properties that are impacted by size variation. For example, the energy levels of QDs are examples of changes in the properties of particles that suffer due to size variation.

Finally, the third challenge is associated with the stability and functionalization of nanomaterials.[14] Aggregation into nanoparticles in solution occurs when physical processes bring the surfaces of particles into contact with each other. The short-range thermodynamic interactions allow bonding between the particles and, consequently, the aggregation. For particles below 100 nm in size, Brownian diffusion controls the long-range forces between individual nanoparticles, causing collisions between particles and the resulting aggregation.[14] Aggregation may represent the low stability of the prepared nanomaterials. In this sense, nanomaterials with low stability can be a risk in clinical application due to nanotoxicity.[15] Therefore, the evaluation of the toxicity of nanoscale materials in the field of nanomedicine implies another important challenge, which is the need for highly detailed *in vitro* and *in vivo* studies on nanotoxicity.[9]

Although, important practical challenges are found in nanoscience, there is no doubt that nanostructured materials present considerable opportunities for advances in nanotechnology applied to nanomedicine. Therefore, more studies are needed to develop easy, efficient, reproducible, and validated methods to ensure the applicability of nanomaterials with a low risk of toxicity.

REFERENCES

(1) Wang, C. T.; Wu, S. W.; Kuo, C. C. Silver nanoparticle-embedded titania nanobelts with tunable electronic band structures and plasmonic resonance for photovoltaic application. *Mater. Sci. Semicond. Process.* **2022**, *138*. http://dx.doi.org/10.1016/j.mssp.2021.106317

(2) Viola, K. L.; Sbarboro, J.; Sureka, R. De M.; Bicca, M. A.; Wang, J.; Vasavada, S.; Satpathy, S.; Wu, S.; Joshi, H.; Velasco, P. T.; Macrenaris, K.; Waters, E. A.; Lu, C.; Phan, J.; Lacor, P.; Prasad, P.; Dravid, V. P.; Klein, W. L. Towards non-invasive diagnostic imaging of early-stage Alzheimer's disease. *Nat. Nanotechnol.* **2015**, *10*, 91–98. http://dx.doi.org/10.1038/nnano.2014.254

(3) Yu, X.; Tang, Z.; Sun, D.; Ouyang, L.; Zhu, M. Recent advances and remaining challenges of nanostructured materials for hydrogen storage applications. *Prog. Mater. Sci.* **2017**, *88*, 1–48. https://doi.org/10.1016/j.pmatsci.2017.03.001

(4) Distasi, C.; Ruffinatti, F. A.; Dionisi, M.; Antoniotti, S.; Gilardino, A.; Croci, G.; Riva, B.; Bassino, E.; Alberto, G.; Castroflorio, E.; Incarnato, D.; Morandi, E.; Martra, G.; Oliviero, S.; Munaron, L.; Lovisolo, D. SiO_2 nanoparticles modulate the electrical activity of neuroendocrine cells without exerting genomic effects. *Sci. Rep.* **2018**, *8*, 2760. http://dx.doi.org/10.1038/s41598-018-21157-8

(5) Xiao, G.; Chen, B.; He, M.; Hu, B. Dual-mode detection of avian influenza virions (H9N2) by ICP-MS and fluorescence after quantum dot labeling with immuno-rolling circle amplification. *Anal. Chim. Acta* **2020**, *1096*, 18–25. http://dx.doi.org/10.1016/j.aca.2019.10.063

(6) Jamaludin, N.; Rashid, S. A.; Tan, T. Natural biomass as carbon sources for the synthesis of photoluminescent carbon dots. In: Rashid, S. A.; Othman, R. N. I. R.; Hussein, M. Z. (Editors) *Synthesis, Technology and Applications of Carbon Nanomaterials*. Elsevier, **2018**, Chapter 5, 109–134. http://dx.doi.org/10.1016/B978-0-12-815757-2.00005-X

(7) de Jesus, J. R.; Fernandes, R. S.; Pessoa, G. S.; Raimundo Jr., I. M.; Arruda, M. A. Z. Depleting high-abundant and enriching low-abundant proteins in human serum: An evaluation of sample preparation methods using magnetic nanoparticle, chemical depletion and immunoaffinity techniques. *Talanta* **2017**, *170*, 199–209. http://dx.doi.org/10.1016/j.talanta.2017.03.091

(8) Albalawi, F.; Hussein, M. Z.; Fakurazi, S.; Masarudin, M. J. Engineered nanomaterials: The challenges and opportunities for nanomedicines. *Int. J. Nanomed.* **2021**, *16*, 161–184. http://dx.doi.org/10.2147/IJN.S288236

(9) Khan, I.; Saeed, K.; Khan, I. Nanoparticles: Properties, applications and toxicities. *Arabian J. Chem.* **2019**, *12* (7), 908–931. https://doi.org/10.1016/j.arabjc.2017.05.011

(10) Xu, Y.; Zhao, M.; Zhou, D.; Zheng, T.; Zhang, H. The application of multifunctional nanomaterials in Alzheimer's disease: A potential theranostics strategy. *Biomed. Pharmacother.* **2021**, *137*, 111360. http://dx.doi.org/10.1016/j.biopha.2021.111360

(11) Yadid, M.; Feiner, R.; Dvir, T. Gold Nanoparticle-Integrated Scaffolds for Tissue Engineering and Regenerative Medicine. *Nano Letters* **2019**, *19*, 2198–2206. http://dx.doi.org/10.1021/acs.nanolett.9b00472

(12) Zhang, H.; Zhao, L.; Jiang, J.; Zheng, J.; Yang, L.; Li, Y.; Zhou, J.; Liu, T.; Xu, J.; Lou, W.; et al. Multiplexed nanomaterial-assisted laser desorption/ionization for pan-cancer diagnosis and classification. *Nat. Commun.* **2022**, *13*, 617. http://dx.doi.org/10.1038/s41467-021-26642-9

(13) Sun, Y.; Zheng, L.; Yang, Y.; Qian, X.; Fu, T.; Li, X.; Yang, Z.; Yan, H.; Cui, C.; Tan, W. Metal–Organic Framework Nanocarriers for Drug Delivery in Biomedical Applications. *Nano-Micro Letters* **2020**, *12*. http://dx.doi.org/10.1007/s40820-020-00423-3

(14) Baer, D. R.; Amonette, J. E.; Engelhard, M. H.; Gaspar, D. J.; Karakoti, A. S.; Kuchibhatla, S.; Nachimuthu, P.; Nurmi, J. T.; Qiang, Y.; Sarathy, V.; et al. Characterization challenges for nanomaterials. *Surf. Interface Anal.* **2008**, *40* (3-4), 529–537. https://doi.org/10.1002/sia.2726

(15) Neuberger, T.; Schöpf, B.; Hofmann, H.; Hofmann, M.; von Rechenberg, B. Superparamagnetic nanoparticles for biomedical applications: Possibilities and limitations of a new drug delivery system. *J. Magn. Magn. Mater*. **2005**, *293* (1), 483–496. https://doi.org/10.1016/j.jmmm.2005.01.064

Jemmyson Romário de Jesus has a Ph.D. in Sciences with emphasis in Analytical Chemistry by the University of Campinas (Unicamp, Brazil). He is an Assistant Professor in the Department of Chemistry at the Federal University of Viçosa (Minas Gerais, Brazil). De Jesus has experience in the field bioanalytics, dealing in proteomics and metallomics studies and environmental analysis, as well as developing new materials and sample preparation methods to simplify complex samples. He is a Member of the Advisory Board of some scientific journal in the area.
CV

Brazilian Journal of Analytical Chemistry
2022, Volume 9, Issue 36, pp 14-51
doi: 10.30744/brjac.2179-3425.RV-119-2021

BrJAC

REVIEW

Regional and Global Scale Challenges for Controlling Arsenic Contamination in Agricultural Soil, Water Supplies, Foods and Ayurvedic Medicines

Victor G. Mihucz
ELTE – Eötvös Loránd University, Institute of Chemistry, H-1117 Budapest, Pázmány Péter stny 1/A, Hungary

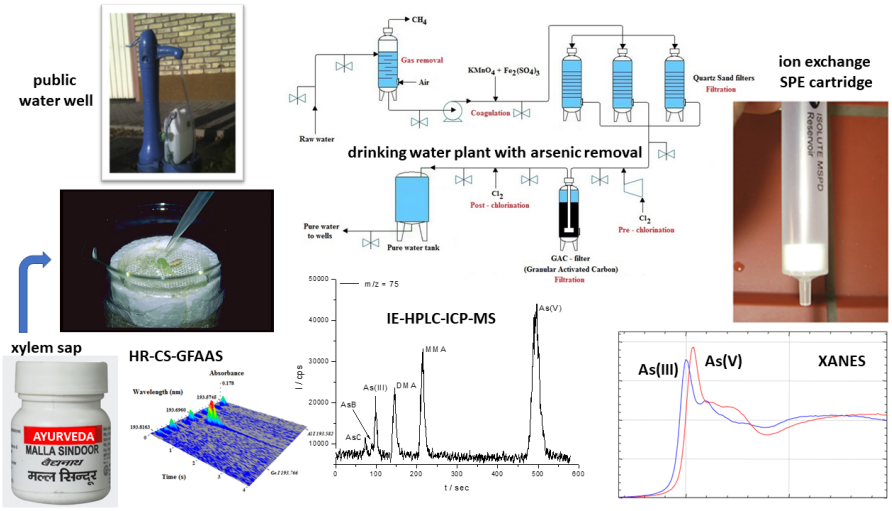

Arsenic is naturally present at high concentration levels in aquifers adversely affecting the life of some 200 million people in a number of countries on four continents. Human exposure to As from dietary sources such as marine fish, seafood, poultry, cereals is generally much lower compared to exposure through drinking contaminated water, using contaminated water in food preparation and irrigation of crops. Arsenic toxicity depends on its four valences [As(-III), As^0, As(III) and As(V)] and chemical compounds. Thus, in seafood, As is mainly found in its less toxic organic forms. The qualitative and quantitative determinations of individual As species are crucial to understand the environmental fate and behavior of As. The aim of the present review is to give a brief overview on the main As speciation methods and to present how to control As contamination at local and global scales in several environmental (soil, waters) and biological (crops, basic and processed food) samples, as well as complementary and alternative medicinal products marketed as food supplements. In terms of chromatographic separation, emphasis is placed on separation by thin layer chromatography and solid phase extraction. Some approaches to address As contamination (e.g., stabilization in soil, provision of a safe water supply in affected communities) at global and regional scales are also presented.

Keywords: arsenate, arsenite, drinking water, organic arsenicals, speciation

Cite: Mihucz, V. G. Regional and Global Scale Challenges for Controlling Arsenic Contamination in Agricultural Soil, Water Supplies, Foods and Ayurvedic Medicines. *Braz. J. Anal. Chem.* 2022, *9* (36), pp 14-51. http://dx.doi.org/10.30744/brjac.2179-3425.RV-119-2021

Submitted 30 November 2021, Resubmitted 23 January 2022, Accepted 6 February 2022, Available online 29 March 2022.

Abbreviations used in this Review

Acronym	Meaning	Acronym	Meaning
AC	activated charcoal	K_a	acid dissociation constant
AsB	arsenobetaine	LA	laser ablation
AsC	arsenocholine	LC	linear combination
ASE	accelerated solvent extraction	LD_{50}	median lethal dose
ASHRAM	Arsenic health risk assessment and molecular epidemiology	LMWOA	low molecular weight organic acid
ATR-FTIR	attenuated total-reflection Fourier—transformed infrared spectroscopy	LOD	limit of detection
BCR	Bureau Communautaire de Référence or (European) Community Bureau of Reference	MMA(III)	monomethylarsonous acid
BMDL	benchmark dose limit	MMA(V)	monomethylarsonic acid
BW	body weight	MOE	margin of exposure
CAM	complementary and alternative medicine	MW	microwave
DMA(III)	dimethylarsinous acid	NIST	National Institute for Standards and Technology
DMA(V)	dimethylarsinic acid (cacodylic acid)	OPLC	overpressured layer chromatography
DSHEA	Dietary Supplement Health and Education Act	PEI	polyethylene imide
DW	deionized water	PTFE	polytetrafluoroethylene
EC	European Commission	Q-ICP-MS	quadrupole inductively coupled plasma mass spectrometry
EDTA	ethylene diamine tetraacetic acid	R_f	retention factor
EDXRF	energy dispersive X-ray fluorescence	RSD	relative standard deviation (%)
EXAFS	extended X-ray absorption fine structure	SAM	*S*-adenosyl methionine
FAO	Food and Agriculture Organization of the United Nations	SAX	strong anion exchanger
FIA	flow injection analysis	SPE	solid phase extraction
FRW	fresh root weight	SRM	standard reference material
FTIR	Fourier-transformed infrared spectroscopy	SR-XANES	synchrotron radiation X-ray absorption near edge spectroscopy

Continues on the next page.

Abbreviations used in this Review (Continuation)

Acronym	Meaning	Acronym	Meaning
GFAAS	graphite furnace atomic absorption spectrometry	TETRA	tetramethylarsine
GSH	reduced glutathione	TMA	trimethylarsine
HG-AAS	hydride generation atomic absorption spectrometry	TFA	trifluoroacetic acid
HPLC	high performance liquid chromatography	THGA	transversely heated graphite atomizer
HR-CS-GFAAS	high resolution continuum source graphite furnace atomic absorption spectrometry	TMAO	trimethylarsine oxide
iAs(III)	arsenite	TXRF	total-reflection X-ray fluorescence (spectrometry)
iAs(V)	(hydrogen) arsenate ions	TLC	thin layer chromatography
ICP-(SF)-MS	inductively coupled plasma (sector field) mass spectrometry	WHO	World Health Organization
IRMM	Institute for Reference Materials and Measurements	XANES	X-ray absorption near edge spectroscopy
JECFA	Joint FAO/WHO Expert Committee on Food Additives	μ-XRF	μ-X-ray fluorescence

RATIONALE OF THIS REVIEW

In the 21st century, not only did the pace of scientific development accelerate tremendously, but thanks to infocommunications, our way of life has been completely transformed. We spend nearly 90% of our time indoors, and global warming has led to the creation of energy-efficient air-conditioned buildings. There is a growing demand for healthy diet. At the same time, more and more people are turning to traditional medicine due to the lack of empathy often experienced in public health. These alternative pharmaceutical preparations are generally sold over-the-counter and considered dietary supplements.

Due to its controversial properties, arsenic (As) came early into the sight of humanity. It can occur in many chemical forms, from poisonous to harmless species. However, even small amounts of its toxic forms can have therapeutic and corroborative effects. In soil, the availability of As is mainly determined by the chemistry of iron (Fe). Arsenic phytotoxicity is closely related to the composition and pH of the soil and, last but not least, the tolerance of the plant to As. Biomethylation produces less toxic organic As compounds. The As contamination of many of the aquifers is of geological origin, adversely affecting the everyday life of some 200 million people. In Europe, the south-eastern part of Hungary is mainly affected by naturally occurring As contamination. Recently, significant efforts have been made in Hungary to comply with the 10 μg L^{-1} health limit for the concentration of As in drinking water set out in European Commission Directive 98/83/EC.[1] However, the choice of technological solution for As removal is primarily determined by the chemical form of As. The pace of development of analytical measurement techniques is extremely fast, and the development of elemental speciation analysis is also supported by the knowledge gained in many other fields of science. In addition to the coupling of separation techniques and atomic spectrometric measurement techniques, speciation procedures include a number of sample preparation procedures that can be a separate source of error. These may occur during sampling in the form of unwanted interconversion of the species, but the interference caused by sample matrix components may

also be significant. In parallel with the need to improve analytical performance, it would be useful to develop cost-effective, speciation methods applicable to different matrices that could be routinely used in analytical laboratories.

The aim of the present review is to give a brief overview on main As speciation methods and to present how to address the challenges represented by As contamination at local and global scales in several environmental (e.g., soil, waters) and biological (e.g., crops, basic and processed food) samples, as well as complementary and alternative medicinal (CAM) products marketed as food supplements with special emphasis on As speciation.

ARSENIC SPECIES AND THEIR TOXICITY

Arsenic is a highly toxic metalloid that can occur in soil even at extreme concentration (e.g., 250 g kg^{-1}) due to both geogenic and anthropogenic activities.[2] Arsenic toxicity depends on its valence and chemical environment. Thus, As(III) species are more toxic than As(V) ones and inorganic As (iAs) compounds are more toxic than organic As ones. The median lethal dose (LD_{50}) values of the most common As compounds determined by oral exposition to rats have been summarized in Table I.[3]

Table I. Toxicity of arsenic species expressed as median lethal dose (LD_{50}) values*

As species	LD_{50} (mg kg^{-1})
AsH_3 (arsine)	3
As_2O_3 (arsenic trioxide)	20
Na_3AsO_3 (sodium arsenite)	60
Na_3AsO_4 (sodium arsenate)	120
$CH_3AsO(OH)_2$ [monomethylarsonic acid, MMA(V)]	700
elementary state As (As^0)	763
$(CH_3)_3As$ (trimethyl arsine, TMA)	787
$(CH_3)_4As^+$ (tetramethyl arsine, TETRA)	890
$(CH_3)_2AsO(OH)$ [dimethylarsinic acid (cacodylic acid), DMA(V)]	1600
$CH_3AsO(ONa)_2$ (disodium monomethyl arsonate)	1800
$(CH_3)_2AsO(ONa)$ (sodium cacodylate)	2600
$(CH_3)_3As^+(CH_2)_2OH$ (arsenocholine, AsC)	6500
$(CH_3)_3As^+CH_2COO^-$ (arsenobetaine, AsB)	10000
$(CH_3)_3AsO$ (trimethylarsine oxide, TMAO)	10600

*oral exposition to rats

The high toxicity of arsenite [iAs(III)] – also confirmed by the Pearson acid-base theory – can be explained by its significant affinity for the sulfur (S) atom. Thus, As can bind to the sulfhydryl group of enzymes and inhibits their function, causing cell death. The toxicity of (hydrogen)arsenate ion [iAs(V)] is due to the fact

that its chemical structure is very similar to that of phosphate ion. This latter ion plays a role in the energy balance of living organisms through phosphorylation. Arsenate can be accumulated, mainly in the nails and hair. The iAs(V) taken up by plants, when replaced by phosphate ions, interfere the energy balance.

The iAs species are more toxic compared to organic derivatives such as e.g., arsenobetaine (AsB) and arsenocline (AsC). However, both dimethylarsinic acid [DMA(V)] and monomethylarsonic acid [MMA(V)] can decrease the levels of hepatic reduced glutathione (GSH) and serum alanine aminotransferase and increase those of cytochrome P450. These events were more intensive in rats at doses of 679 mg kg^{-1} MMA(V) and 387 mg kg^{-1} DMA(V) in the liver and lungs. At the same time, organ-specific DNA damage has been demonstrated.[4] Dimethylarsinous acid [DMA(III)] is a toxic intermediate of DMA(V) that can also be detected in urine in the case of As poisoning.[5] Monomethylarsonous acid [MMA(III)] is a carcinogenic and toxic human xenobiotic metabolite formed during the detoxification of GSH and MMA(V) in the liver during acute and minor As poisoning. It is then converted to DMA(V) by oxidative methylation upon reaction with *S*-adenosyl-L-methionine (SAM)[6] (Figure 1). The major metabolites of the typically non-toxic arsenic sugars, AsB and AsC, are also excreted in the urine (Figure 1). If As enters the human body in large quantities at the same time, it causes vomiting, diarrhea, increased sweating and cramps. The sodium salts of MMA(V) and DMA(V) have also been widely used as insecticides (e.g., currently still permitted in weed control for cotton cultivation).[7] Arsenic has also been used to pickle wood e.g., in the USA.[3] Among the organic As species, roxarsone should be mentioned, used mainly in poultry as a feed additive to increase weight gain and as a coccidiostat. Due to the increased concentration of iAs detected in meat from breeding animals and poultry after metabolization, the use of roxarsone was banned in the US since 2013[8] and also in the EU as early as 1999. However, it is still widely used in China and many developing countries.[9]

Among the human aspects of As toxicity, the harmful effects on health due to the chronic exposure to the consumption of As-containing drinking water in Hungary should also be mentioned. Thus, according to the results of the ASHRAM (Arsenic Health Risk Assessment and Molecular Epidemiology) research project funded by the European Commission and carried out in Hungary between 2002 and 2004, there was a positive correlation between As exposure and skin, lung, bladder and kidney cancer in several settlements located in the Hungarian Great Plain.[10] In the settlements of one the affected regions, for which the As concentration of drinking water exceeded 100 µg L^{-1}, an increase of 1.5 – 2 was observed in the number of spontaneous abortions and stillbirths compared to the control settlements.[11]

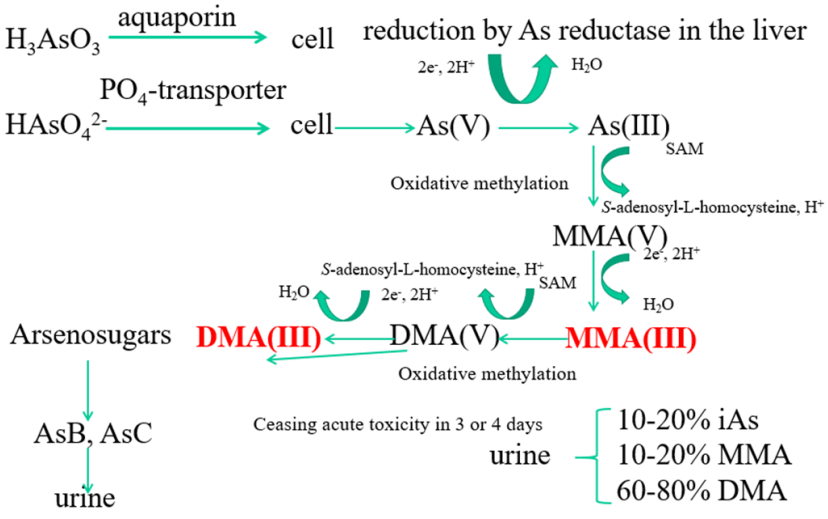

Figure 1. Mechanism of arsenic detoxification in liver for acute inorganic arsenic toxicity. Notations: iAs(III) = arsenite; iAs(V) = arsenate; AsB = arsenobetaine; AsC = arsenocholine; DMA(III) = dimethylarsinous acid acid; DMA(V) = dimethylarsinic acid; MMA(III) = monomethylarsonous acid; MMA(V) = monomethylarsonic acid; SAM = *S*-adenosyl-L-methionine.

ANALYTICAL TECHNIQUES FOR DETERMINATION OF As IN ENVIRONMENTAL AND FOOD SAMPLES AS WELL HYPHENATION POSSIBILITIES FOR As SPECIATION

Several analytical techniques have been proposed for As speciation. Analytical techniques suitable for qualitative and quantitative determination of As discussed in the present review have been compiled in Table II. It is worth mentioning that, in terms of As speciation, hydride generation atomic absorption spectrometry (HG-AAS) and synchrotron radiation X-ray absorption near edge spectroscopy (SR-XANES) allow discrimination between As(III) and As(V). Since the toxicity of As depends significantly on its chemical form, it is advisable to determine not only the total concentration of As in the samples but also that of each species. Thus, several chromatographic methods have been proposed for the separation of As species such anion/cation exchange, reversed-phase, ion pair, and size exclusion chromatography.[12] Separation of As species has traditionally been performed by high performance liquid chromatography (HPLC) using ion exchange columns. The most common species – iAs(III), iAs(V), MMA(V) and DMA(V) – are separated on an anion exchange column, while AsB and AsC are separated on a cation exchanger. In a recent review by Reid *et al.*,[12] suitability of hydrophilic interaction liquid chromatography, multiple separation mechanisms, and testing of fluorophenyl and graphene oxide stationary phases has also been discussed. Quantification of the separated species is performed using an appropriate atomic spectrometric technique connected to the chromatographic device on-line. Nowadays, inductively coupled plasma mass spectrometry (ICP-MS) is the most commonly used for this purpose.

Table II. Analytical techniques discussed in the present review suitable for As determination in environmental and food samples

Analytical technique	Sample preparation	Sample matrix	Remarks	Speciation	Ref.
Qualitative determination					
ATR-FTIR	–	food waste-derived charcoal added to As-contaminated soil	elucidation of As adsorption mechanism	n.a.	[13]
EDXRF	–	Ayurvedic ointment		– *	[14]
LA-DRC-ICP-MS	extraction	rice	monitoring of ^{13}C, ^{121}Sb and ^{75}As	off-line with PEI-TLC/OPLC	[15]
SR-XANES	–	xylem sap	LC of standard spectra	discrimination between As(III) and As(V)	[16]
Quantitative determination					
HR-CS-GFAAS	dilution with DW	thermal / well water		off-line with IE-SPE	[17,18]
HG-AAS	dry ashing	solid foods		use of pre-reducing agent (e.g., KI, L-cysteine)	[19-21]
Q-ICP-MS	dilution with DW	water	mathematical correction	[on-line with IE-HPLC & off-line with IE-SPE]	[19]
	MW-assisted acid digestion	aqueous food samples			[19]

Continues on the next page.

Table II. Analytical techniques discussed in the present review suitable for As determination in environmental and food samples (Continuation)

Analytical technique	Sample preparation	Sample matrix	Remarks	Speciation	Ref.
SF-ICP-MS	dilution with DW	water	HR when HCl is used	on-line with IE-HPLC & off-line with IE-SPE	[22]
	MW-assisted acid digestion (+H_2O_2 for organic matter)	aqueous food samples; rice; Ayurvedic formulations			[14]
	Enzymatic extraction with sonotrode	rice	for As speciation		[23]
	–	xylem sap	FIA for total As & R = 4000		[24]
TXRF	–	water		off-line with IE-SPE	[18]
	MW-assisted acid digestion	plant extracts (root, leaves)	for speciation, extraction with $NH_4H_2PO_4$ (pH=5.6)	off-line with PEI-TLC/OPLC	[25]
μ-XRF (confocal)	–	rice grains	individual item analysis	–	[26]

For acronyms see list of abbreviations; * = phase analysis.

Speciation of arsenic using solid phase extraction cartridges

One of the pivotal points of elemental speciation is to prevent interconversion of species during sampling and analysis; therefore, it is a great advantage to be able to use an analytical technique that requires minimal and cost-effective sample preparation. Significant efforts in this direction have been seen mainly in the As speciation of water. Cost-efficient separation of iAs species can be successfully performed at the sampling site using solid phase extraction (SPE) cartridges filled with strong anion exchange (SAX) resins.[27-33] When using SAX resins it is not possible to retain iAs(III) as it is a very weak acid (Figure 2). However, by coupling two miniature columns in series and oxidation by $KMnO_4$, iAs(III) can also be retained on the microcolumn.[34] Connection in series of SPE cartridges filled with strong anion and cation exchange resins have also been shown to be robust in field studies for speciation of As characterized by samples up to 30 mL of 10 mg L^{-1} As and complex matrix materials.[33] If necessary, MMA(V) can be determined after selective elution performed with acetic acid, while DMA(V) binds upon passing the fraction not retained on the SAX cartridge through the cation exchanger one (Figure 2).[28]

Alternatively, cartridges filled with Al-containing sorbent may be used.[35] In this case, a breakthrough of the otherwise retained iAs(V) was also observed when ions competing for Al silicate sorption sites were also present in the water.[36] Other SPE cartridges for *in situ* separation of the methylated forms of iAs have also been prepared. Such sorbents include nanometer-size titanium dioxide particles immobilized on silica gel,[37] octadecyl groups,[38] yeast immobilized on controlled pore size glass,[39] PTFE turnings,[40] cetyltrimethylammonium bromide-modified alkyl silica,[41] 3-(2-aminoethylamino) propyltrimethoxysilane-modified mesoporous silica,[42] macrocyclic materials,[43] hybride resins activated with hydrated Fe oxides and silver chloride,[44] carbon nanofibers,[45] as well as nanotubes[46] and eggshell membrane.[47]

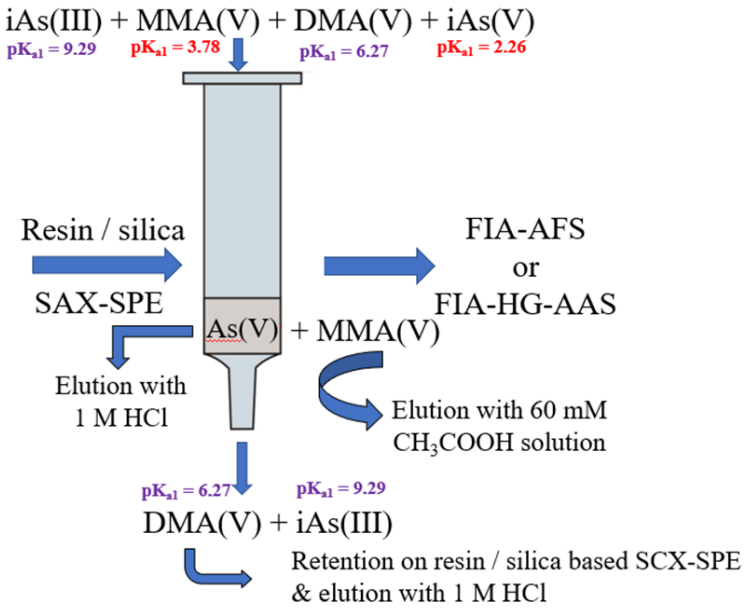

Figure 2. Diagram of a solid phase extraction process involving a cartridge filled with a strong anion exchange for *in situ* separation of arsenic species. (Figure adapted from Ref. 28.) Notations: iAs(III) = arsenite; iAs(V) = arsenate; DMA(V) = dimethylarsinic acid; MMA (V) = monomethylarsonic acid; pK_a = minus logarithm of base 10 of the corresponding acid dissociation constant.

ENVIRONMENTAL AND FOOD ANALYTICAL APPLICATIONS

Arsenic in soil

Occurrence of arsenic species in soil

Arsenic is present in many soil types at an average concentration between 0.1 and 40 mg kg^{-1}. As main constituent, it occurs in more than 200 minerals, mostly along with S. Its most important mineral is arsenopyrite (FeAsS), but realgar (α-As_4S_4) and auripigment (As_2S_3) are also noteworthy. In addition, it can occur in many sulfide minerals, mainly as a substitute for S. The concentration of As in igneous rocks is low, averaging 1.5 mg kg^{-1}. The concentration range for sedimentary rocks varies from 5 to 10 mg kg^{-1}. The concentration of As in the metamorphic rocks reflects the characteristics of the precursor igneous or sedimentary rock. Unconsolidated sediments typically contain 3-10 mg kg^{-1} of As, although this also depends on the texture and constituent minerals.[48]

In soil, the availability of As is mainly determined by the chemistry of Fe. In soils and groundwater, iAs(V) dominates. Inorganic As(V) are more likely to occur under aerobic, while iAs(III) under anaerobic conditions.[49] Inorganic As species are methylated in soils due to microbial activity (Figure 3).[48,50] Demethylation converts organic As compounds to iAs.[48] Biomethylated As(V) species account for up to 15.5–16.7% of the total As concentration of surface geothermal waters.[51] Oxyhydroxides of Fe, Al and Mn as well as clays, and mineral oxyanions (e.g., sulfates, phosphates and carbonates) in soil and sediments immobilize As.[52] Fine particles of clay minerals and (oxy)hydroxides adsorb As due to their high specific surface area.

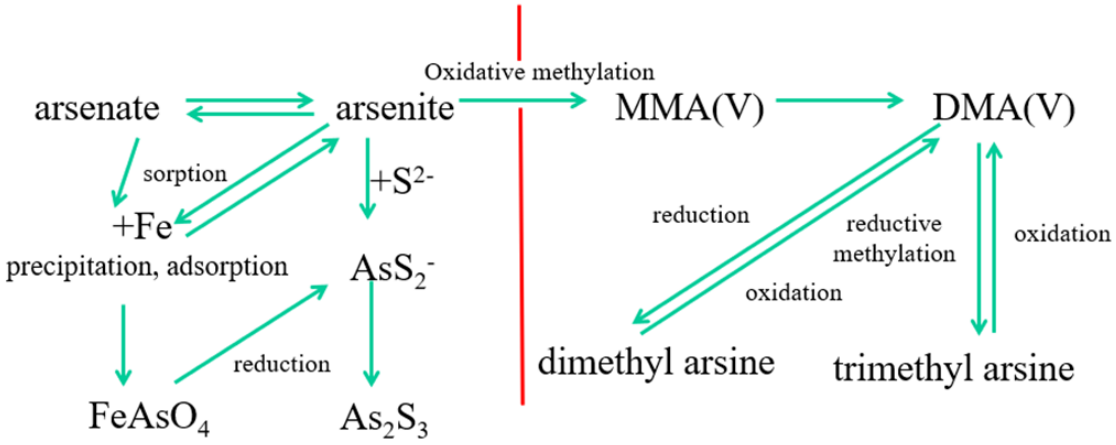

Figure 3. Simplified mechanism for the illustration of the connection of inorganic arsenic species to iron chemistry as well as bacterial methylation of in soil. Notations: $(CH_3)_2As$ = dimethylarsine; MMA(V) = monomethyl arsonic acid; DMA(V) = dimethylarsinic acid; TMA = trimethylarsine.

At regional scale, for example in Hungary, the concentration of As in soils varies between <2.5-230 mg kg^{-1}.[53] The limit value of As in Hungarian soils is 15 mg kg^{-1} dry weight (DM).[54] The European Economic Community has classified As a priority risk pollutant, i.e., As is a hazardous substance in all cases.[54] Concentrations of As in floodplain and riverbed sediments in the geochemical regions of Hungary range from 1 to 60 mg kg^{-1}.

The origin of As contamination of soils in Hungary has not been well elucidated yet (Figure 4). However, several theories have been suggested. Among the geochemical landscapes of Hungary (Figure 4), the second one is characterized by the accumulation of Ca, Mg and Sr, but As can also be found in the floodplain sediments of the Danube River. Moreover, As occurs in the southern part of the Danube-Tisza interfluve with exceptionally high values, probably due to the fact that As bound to Fe oxyhydroxides during the ice age is mobilized nowadays.[55,56] In the 3rd geochemical landscape, the dead ground originating from mining non-ferrous and precious metals (Ag, As, Au, Cd, Cu, Pb, Sb, Zn) in Transylvania (Romania) and the highlands of Slovakia, is carried by rivers to the shallow basin of the Great Plain. In this case, As is an accompanying element of non-ferrous metals.

Figure 4. Arsenic containing geochemical landscapes in Hungary. (Figure adapted from Ref. 55.)

Estimation of As concentration in agricultural soils through sequential extraction

First of all, it is important to estimate the total concentration of As in the contaminated soil. Then, it is advisable to perform sequential extraction of As on the soil. In the case of agricultural soils, As is most likely present in the form of iAs(V), so a two-step modified BCR (Bureau Communautaire de Référence) soil extraction procedure[13] is appropriate. Briefly, the water-soluble and carbonate fractions are extracted with 0.11 M acetic acid. This step is followed by extraction of the fraction bound to amorphous Fe(III)/Mn(IV) oxides with 0.5 M hydroxylamine hydrochloride solution at pH = 2. The initial samples as well as the extraction residues can be analyzed by ICP-SF-MS after MW-assisted acid digestion.[13] If appropriate soil CRMs are not available, another atomic spectrometric technique, e.g., total-reflection X-ray fluorescence (TXRF) spectrometric analysis of the same extracts can be used to check the accuracy of the results.[13] To calculate recovery, the concentration of As in the different extracts should be summed and compared to the pseudo-total concentration.[13]

Stabilization of arsenic in contaminated agricultural soils

Remediation of soils contaminated with toxic elements (e.g., As) is still a complex task of great importance nowadays, as toxic inorganic constituents cannot be easily removed from contaminated soil.[57,58] Usually *in situ* immobilization or stabilization by physical and chemical methods[59-61] have been proposed for toxic inorganic contaminants. The latter is an attractive alternative as it is a cost-effective and non-destructive process, yet suitable for remediating slightly or moderately contaminated soils. The purpose of immobilization is not only to minimize the mobility of toxic elements, but also to preserve soil structure and fertility. The most commonly used substances for stabilizing heavy metals are various minerals and organic substances [e.g., humic substances, ethylenediaminetetraacetate (EDTA), activated charcoal (AC)].[61-69]

Despite its many advantages, AC is hardly suitable for soil improvement due to its high production costs involving pyrolysis at 1000 °C for 24 h in an inert atmosphere for charring.[70] Charcoal has been used in agriculture for a long while.[71,72] However, due to its homonuclear structure, adsorption on charcoal is mainly characterized by van der Waals interaction.[73-75] The production costs of AC can be significantly reduced by choosing a large amount of available biomass waste as a feedstock. These raw materials do not always prove to be efficient enough, so activation and/or functionalization is required after charring involving mainly sulfuric or nitric acids.

However, As, the most common form of oxyanion, is not easy to stabilize in soil because plant adsorbents have a cation exchange capacity. Depending on pH of the media, iAs(III) and iAs(V) differ not only in valence but also in electrical charge significantly influencing their mobility.[76,77] Due to the carboxyl and hydroxyl functional groups contained in them, plant-derived ion exchangers are not suitable for binding negatively charged iAs(V) at soil pH. However, biomass wastes (e.g., peanut shells) are available in large quantities. The production of AC from peanut shell was carried out with concentrated sulfuric acid (H_2SO_4) for cost-effectiveness reasons. To increase the mechanical stability of the produced AC particles, composite formation with silicate-containing compounds (e.g., Florisil®) was applied.[13] Composite formation and the binding of As to AC were studied by Fourier transform infrared (FTIR) spectroscopy in attenuated total reflection (ATR) mode.[13] For example, acidic (pH = 5) sandy soil was incubated for four weeks with 15-30 mg kg^{-1} iAs(V). Freundlich isotherm proved to adequately model adsorption of As.[78] The highest adsorption rate was observed at pH=5 for Florisil®-modified AC. The slope of the line fitted for adsorption was about 30% higher at pH=5 than at pH=8 for Florisil®-AC. However, at pH 8, the rate of As adsorption decreased with Florisil®-modified AC. This suggested that the adsorption of iAs(V) is due to the formation of a covalent bond between the AC carboxyl group and one of the O atoms of iAs(V) while a water molecule is eliminated (Equation 1), as it was confirmed by the ATR-FTIR analysis:

$$\mathrm{Res-COOH + H_2AsO_4^- \rightarrow Res-COO-HAsO_3^- + H_2O} \qquad \text{Equation 1}$$

Formation of this mixed acid anhydride does not occur at alkaline pH, which was also proved by ATR-FTIR analyses.

Depending on the AC modification used, the proportion of immobilized As was approx. 30-40%, of which the soil alone immobilized about 15-20% As. The best results were obtained with Florisil®-modified AC. The amount of immobilizable As increased almost proportionally with increasing AC application dose and doubling the treatment concentration of iAs(V).[13]

Being electrically neutral over a wide pH range, iAs(III) can be more efficiently stabilized by ACs, e.g., formation of H-bonds. However, oxidation of iAs(III) → iAs(V) must also be taken into account. This cost-effective approach may be successful for acidic agricultural soils slightly contaminated with As.

Arsenic in water

Arsenic in groundwater in aquifers

The concentration of As in groundwater varies very widely (0.1-5000 μg L^{-1}).[48] This is especially problematic if the water body serves as a drinking water base. Several theories have been formulated for the large As contamination in natural water.

1) During the extraction of sulfide ores, As originating from their weathering first binds to Fe(III) (oxy) hydroxides; in parallel with the reduction of Fe(III) to Fe(II), As is released and dissolved in the groundwater in the mining areas.
2) Oxidation of As-rich pyrite or arsenopyrite results in the dissolution of As in groundwater.[79] The reductive dissolution of Fe(III) (oxy)hydroxides in groundwater under anaerobic conditions by microorganisms, e.g., may be catalyzed by *Acidithiobacillus ferrooxidans* and *Leptospirillum ferrooxidans*.[52,80]
3) A third theory that is characteristic of the Pannonian Basin in Hungary is that As is brought to the surface by thermal water that erupts from the depths.[81]

Arsenic can be accumulated in aquifers or highly reducing layers of inland/closed basins (semi-)desert areas.[48] Both of these different geological environments contain young sediments in flat, low-lying, and slow groundwater flow areas. Waters with high As concentrations (up to 5000 μg L^{-1}) adversely affect the drinking water supply of some 200 million people worldwide.[48] The As contamination of many aquifers is of geological origin. This affects the western part of the North American continent, the vast areas of Chile and Argentina in the southern hemisphere, parts of China, and the Gulf of Bengal and its associated delta region in Asia.[48] Studies in the US suggest that changes in As concentration over time cannot be clearly correlated with wet/dry seasons[82] or pre- or post-monsoon periods in the Indian subcontinent.[83] Arsenic contamination can also be attributed to a lesser extent to anthropogenic activity.[84]

Arsenic in surface and drinking water

In rivers, the As concentration is around 0.1-0.8 μg L^{-1}, which is also influenced by the flow of the rivers, lithology of the river bed and water replenishment of the area. The As concentration in lakes is close to or less than that of rivers.

For the *in situ* separation of As species from water samples taken from public wells in Hungary, the method described by Le *et al.*[28] was also suitable. For As determination in the samples, ICP-SF-MS was used. High-resolution mode (R = 10000) had to be applied only for As speciation. The sum of the As concentration in the SPE fractions was compared to the values of the total As one obtained for the corresponding original samples. Organic As species [e.g., MMA(V) or DMA(V)] could not be detected in the samples. Even a four-fold enrichment could be applied to the iAs(V)-containing fractions. After regeneration, the SPE microcolumns could be reused at least 15 more times by analyzing repeatedly carbonated mineral water samples with a salt content of 450 mg L^{-1} between pH 6 and 8 spiked to 150 μg L^{-1} iAs(V). This approach was applied to determine the ratio of iAs(III) and iAs(V) in water taken from public wells of settlements belonging to different geochemical landscapes of Hungary affected by natural As contamination (Figure 5). The total concentration of As in the samples taken from the public wells of

settlements of the Csongrád plain, located east of the Tisza River and belonging to the 2nd geochemical landscape (Figure 4), reached even 210 μg L^{-1}.

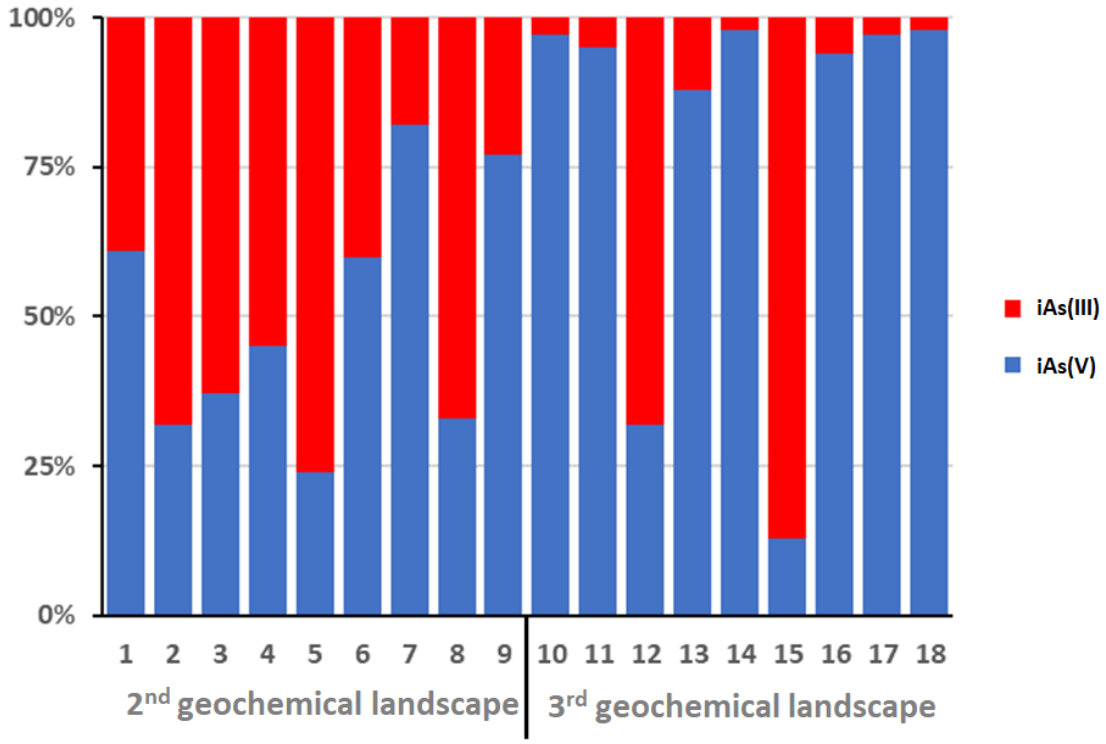

Figure 5. Arsenic distribution between arsenate [iAs(V)] (blue) and arsenite iAs(III) (red) in water samples taken from public wells in settlements located in the 2nd and 3rd geochemical landscapes affected by natural As contamination in Hungary. Grouping of data according to the relative distance of the settlements from each other. (Figure adapted from Ref. 22.)

The results obtained were in agreement with the geochemical theories on the mobility of As in soil. Thus, mobility of As deposited in flat areas from river sediments situated in the 3rd geochemical landscape, can be attributed to the iAs(V) species. The anaerobic conditions favor the formation of iAs(III) and Fe(II) in the deeper layers. In the southern part of the Danube-Tisza interfluve, located in the 2nd geochemical landscape (Figure 4), mobilization of iAs(V) adsorbed onto Fe(III) (oxo)hydroxides during the ice age could only be achieved if Fe(III) → Fe(II) reduction took place due to anaerobic conditions. The mobility of iAs(III) is due to the increased water solubility of the resulting Fe(II) compounds, and the fact that this species is electrically neutral over a wide pH range. Thus, iAs(III) is believed to be mobilized nowadays.[55,56] However, iAs(III) is again converted to iAs(V) species under aerobic conditions.

For *in situ* separation of As species, the SPE method described by Le *et al.*[28] was also applicable to samples taken from a geothermal well.[17] The As content of the samples was determined by high resolution continuum source graphite furnace atomic absorption spectrometry (HR-CS-GFAAS) using an Xe arc lamp as a continuous-spectrum primary radiation source equipped with a transversely heated graphite tube atomizer (THGA).[17] A linear response to As in the concentration range of 5 – 200 μg L^{-1} was obtained by external calibration. In addition, the absorbance values up to an As concentration of 500 μg L^{-1} could be properly fitted with a quadratic polynomial equation. The LOD value of the method was 0.6 μg L^{-1}. This method was characterized by adequate RSD and recovery. When the 150 μg L^{-1} of an iAs(III) fraction acidified with HNO_3 and stored for up to 30 days was analyzed by HR-CS-GFAAS, the oxidation rate of As(III) → As(V) was less than 10%. The iAs speciation could be performed with sufficient accuracy (± 5%)

up to pH 8.[17] A mass balance could be set up for the As species determined by SPE-HR-CS-GFAAS. The total As concentration was about 400 μg L^{-1}. Chloride and sulphate ions in natural waters above 100 and 50 mg L^{-1}, respectively, caused interference in the determination of As by the continuum source GFAAS method.[85] The effect of high concentration of sulphate and chloride ions generated by magmatic gases in volcanic water on the As measurements was minimized by two-fold dilution of the samples before HR-CS-GFAAS analysis. The proportion of iAs(III) in the geothermal water was about 55%. However, it was reported that the proportion of iAs(III) can be more than 70% in geothermal waters.[86] Slow cooling of the water below 66 °C did not change the proportion of As species in the samples. The SAX-SPE has been shown to be effective for As speciation in water with high salinity at about 85 °C. Due to the total concentration of As (i.e., 400 μg L^{-1}) in the water sample, almost half of which was iAs(III), the analyzed water cannot be used for recreational and/or aquaculture purposes.

For the separation and enrichment of iAs species in tap, lake and well waters, the same Dowex 1-X8 SAX-type SPE charge using electrothermal AAS was suitable for the determination of As in the fractions eluted from the cartridges.[87] Arsenic speciation of surface[88] and groundwater[89] was performed using silica gel-based SAX-SPE- HG-AAS hyphenated technique.

Arsenic removal technologies from drinking water

Arsenic has a complex water chemistry and exists in a variety of inorganic and organic forms in waters, depending on pH, salinity, acid dissociation constants (K_a) of As oxyacids, as well as redox potential of the iAs(V)/iAs(III). Chemical oxidation, co-precipitation, adsorption, ion exchange, reverse osmosis, and membrane filtration are used to remove As from (waste)water.[90-93]

From a technological point of view, As removal processes can be divided into three major groups[94]: 1) conventional technologies (coagulation, Fe-Mn removal, lime softening); 2) sorption processes (ion exchange, activated Al); 3) membrane technologies (reverse osmosis, nanofiltration, micro- or ultrafiltration). The removal efficiencies and main characteristics of the six most commonly used As removal technologies for the two iAs species present in water are summarized in Table III.[94,95]

Table III. Main features of some arsenic removal technologies

Technological solution	Removal efficiency (%)		Notes
	iAs(III)	iAs(V)	
Coagulation with Fe, sedimentation/filtration	60	95	1. filtration through 0.1 or 1.0 μm pore size 2. pH dependent
Coagulation with Al, sedimentation/filtration	15	80	also suitable for removal of fluoride
Lime softening	70	99	1. for hard water 2. soft water must be acidified
Ion exchange	-	>95	1. independent of pH; 2. SO_4^{2-}interference
Activated Al oxide	-	98	1. iAs(V) exchanges OH^- on the surface of Al_2O_3 2. pH dependent
Reverse osmosis	60	>95	treated water not suitable for human consumption

iAs(III) = arsenite; iAs(V) = arsenate.

As shown in Table III, each of the technologies is more efficient for the iAs(V) species, so oxidation of iAs(III) is often applied first. Oxidation by simple direct aeration is slow, but there are several chemical agents that can speed up the process such as chlorine gas, hypochlorite, ozone, $KMnO_4$, hydrogen peroxide, Mn oxides, and UV radiation.[95]

The main water treatment steps applied in the waterworks operating settlements located in the southern regions affected by natural As contamination in Hungary are summarized in Table IV.

Table IV. Steps of drinking water quality improvement technologies applied in the waterworks of the monitored settlements

Step	Water treatment step	Target compound	Notes
1	Gas removal by purging with air	CH_4	
2	Flocculation and oxidation	iAs(III), Fe(II), Mn(II)	2-4 w/w% $KMnO_4$ + 40 w/w% $Fe_2(SO_4)_3$
3	Quartz sand filtration	products of oxidation *cf.* step 2	
4	Pre-chlorination	NH_4^+	5 mg L^{-1} Cl_2
5	Granular activated carbon filtration	by-products of step 4	
6	Post-chlorination (Cl_2, ClO_2, NaOCl)	—	0.3-0.5 mg L^{-1} free Cl_2 concentration after chlorination

Water samples were also analyzed by HR-CS-GFAAS and TXRF after *in situ* separation of the As species by SPE. The total concentration of As in the raw water samples taken from the wells of the waterworks varied between 42.9 and 118 µg L^{-1}. In well waters, iAs(III) (> 80% of total As) was the predominant species in each settlement. After the addition of oxidizing and flocculant and filtration on quartz sand, the total concentration of As decreased below 10 µg L^{-1} during the applied water treatment technology. This value was typically about 5 µg L^{-1}. Regarding the proportion of species, iAs(V) was the predominant species. Arsenite was not detected in the samples taken after water treatment. Application of As speciation allowed fine tuning of the reagent use (e.g., $KMnO_4$) for the oxidation step.

In addition, application of TXRF has the advantage to provide multi-element information. Thus, changes in the concentration of other elements of interest in Directive 98/83/EC in water samples could be monitored after the addition of the oxidizing ($KMnO_4$) and flocculant [Fe(III) sulfate]. Thus, it was demonstrated that the concentrations of Mn and Fe in drinking water fell far short of the values laid down in Directive 98/83/EC. After the addition of the oxidizing agent and the flocculant, the Fe, Mn and S constituents were retained by the SPE microcolumn, but the cartridges could be regenerated with HNO_3 solution.

Moreover, dilution of contaminated water with that of adequate quality to reduce As contamination of drinking water is an accepted practice, as well. For example, the proportion of iAs(V) in the drinking water of some settlements established on the floodplain soil of the Ráckeve branch of the Danube belonging to the 2nd geochemical landscape with a total As concentration larger than 10 mg L^{-1} was found to be decreased after repeating sampling and analysis after 5 years. However, the proportion of As species was almost the same as in the samples originally taken. This result means that the reduction of the As concentration was achieved by dilution with water of adequate water quality.

Arsenic in plants and the importance of xylem sap analysis

The first studies on the accumulation of As in plants were published first in the 1970s. It was found that, the As content in plants grown on As-contaminated soils was slightly higher than in lightly contaminated soils (0.01-5 mg kg^{-1} As), but As accumulation was not observed.[13] The fern native to China (*Pteris Vittata* L.) was the first plant to be found to be capable of hyperaccumulation of As (> 20 g kg^{-1} DM). Arsenic can also be taken up in larger amounts by rice (*Oryza sativa* L.).[96] However, the As content of carrots (*Daucus carota* L.) can also reach up to 1 mg kg^{-1}.[97] Arsenic is found primarily in the roots of plants, and

its concentration can be up to 75-fold higher than that determined in the shoot.[98,99] The vast majority of As is localized in the apoplastic space of the root.[100] In the rice plant grown under reducing conditions, 1% of the total As concentration (2.3 mg kg^{-1}) was transported to the shoot. In the root, 60% and 39% of the apoplastic and non-apoplastic fractions contained As, respectively.[100] In addition, the hyperaccumulative fern contained about 1/6 of the total As in the apoplast.[101]

Arsenic species found in terrestrial and aquatic plants, lichens, and fungi are divided primarily into hydrophilic and lipophilic compounds.[102] In terrestrial plants, mainly inorganic species of As, namely, iAs(V) and iAs(III), are detected, although methylated derivatives of iAs(V), DMA(V) and MMA(V), may be present in small amounts.[103]

Since iAs(V) is the most stable species in the soil under aerobic conditions, it is expected that plants will absorb it mainly in this form. Iron deposition on the root surface can significantly bind iAs(V) species.[100] In the reducing environment of root cells, iAs(V) is readily reduced to iAs(III). This reduction is thought to be an essential process in the detoxification of As, as the resulting more toxic iAs(III), being electrically neutral over a wide pH range, is transported to senescent leaves.[104] It has not been clearly demonstrated whether organic As compounds detected in plant tissues can be taken up directly from the soil. There is also no clear evidence that iAs species are methylated by microorganisms living in root symbiosis or by the plants themselves.[103]

The MMA(V) species is converted to DMA(V) in the root or xylem sap of the As hyperaccumulative fern (*Pteris Vittata* L.).[105,106] However, microorganisms may also be involved in methylation. Study of As in terrestrial plants provides a two-fold information since: (i) it may indicate the bioaccessibility of As, and (ii) As taken up by plants may enter the food chain. The phytotoxicity of As also depends on the pH, phosphate, composition (e.g., Fe, Al and organic matter content) of the soil and the tolerance of plants for As.[107] Since various As species have different toxicities, the information obtained from their identification and distribution within the plant may provide an answer to the plant metabolism of As and an assessment of the health risks posed by the introduction of As into the food chain.

The study of xylem sap playing a central role in the transport of toxic and essential elements and nutrients to plant shoots, is particularly advantageous for elemental speciation, as it requires minimal sample preparation. Xylem sap from cucumber plants (*Cucumis sativus* L.) is easily collected and a single sample preparation step consisting of filtration through 0.22 μm membrane filters should be used for chromatographic studies.[108-118] The roots of most plants should be placed in a pressurized chamber filled with an inert gas (e.g., nitrogen gas) to enhance exudation. This, together with the fact that interconversion of As species can occur relatively easily, makes it difficult to perform As speciation in xylem sap. Pickering *et al.*[114] confirmed that only a small amount of As was transported to the shoot of Indian mustard (*Brassica juncea* L. var. Czern) applying a treatment of 250 μmol L^{-1} iAs(III) or iAs(V) by XANES measurements. The iAs(V) taken up was stored by the plant both in the root and shoot mainly in the form of As(III) tris(thiolate) complexes. Kertulis *et al.*[106] have been detected mainly iAs(V) in the xylem sap of *P. vittata* L. treated with either iAs(III) or iAs(V) at concentrations up to 50 mg L^{-1}, regardless of the type of treatments used. In the case of treatments with MMA(V) or DMA(V), As was transported to the shoot in these methylated forms. However, iAs(III) has always been detected at the apex of the fern leaf, suggesting that reduction of iAs(V) occurs in the plant shoot.

Plant growth experiments conducted in nutrient solution have shown that the concentration of As(V) (2–10 μmol L^{-1}) and the iAs(V):phosphate ion concentration ratio of the hydroponics (1:100, 1:1, and 100:1) play an important role in the development cucumber plants. This phenomenon is due to the similar structure of hydrogen arsenate and hydrogen phosphate ion, taken up and transported within the plant by the same mechanism. To eliminate competition between iAs(V) and phosphate, it is advisable to set their concentration ratio in the medium to 1:1. However, the seedlings showed a severe phosphate deficiency at a phosphate ion concentration of 2 μmol L^{-1}, which could only be eliminated at a concentration of 250 μmol L^{-1}. Therefore, in plant growth experiments, it is advisable to keep the phosphate concentration at this value and to reduce it to the As concentration only at the start of As treatment.[24]

Speciation analysis of the nutrient solutions also confirms the different uptake mechanisms of the two species – electrically neutral iAs(III) and ionic iAs(V) at physiological pH.[24] As the pK_{a1} values of H_3AsO_3 and H_3AsO_4 differ significantly, i.e., 9.3 and 2.3, respectively,[105] and taking into account the pH of the hydroponics (pH 4.7–5.9), the electrical charge of these two species is significantly different. The iAs(V) uptake is similar to that of phosphate ions, with electrically neutral iAs(III) being taken up through aquaporin.

When sampling xylem sap from cucumber plants treated with As, the rate of exudation with respect to sampling time and fresh root weight (FRW) was very similar for both As treatments: 12.4 and 11.2 μL h^{-1} FRW^{-1} for iAs(V) and iAs(III) treatments, respectively.[24] Three As species – iAs(III), DMA(V) and iAs(V) – could be identified in the xylem sap. Regardless of the As treatment, the following concentration order was determined: iAs(III) > iAs(V) > DMA(V). The proportion of DMA(V) in the xylem sap did not reach 5%. The mass of the As species in the xylem sap collected for 1 h taking into account the exudation rate, was very similar: 17.65 and 16.55 ng h^{-1} for the iAs(V) and iAs(III) treatments, respectively. Arsenobetaine and AsC were not detectable in the samples by cation exchange HPLC-ICPSF-MS. The predominance of iAs(III) in xylem sap of cucumber plants grown in As containing hydroponics was consistent with literature data.[104] Zabłudowska *et al.*[119] found that As present as iAs(V) in aerobic soils was taken up by the phosphate transport system of ferns. Subsequently, a portion of the iAs(V) is reduced to the iAs(III) specific in the root by the arsenate reductase[120,121] and further translocated to the shoot *via* the xylem.[122,123] Reduction is an important process in As tolerance, as iAs(III) can react with highly reactive compounds containing SH groups,[124] such as thiol compounds, e.g. phytochelatins or GSH – and is thus immobilized by complex formation. The iAs(III) ratio was also greater than 60% in xylem sap of rice, tomatoes, wheat, cabbage, and barley. However, methylated As species are rarely detected.[114,123-126] The presence of iAs(V) in the xylem sap of plants treated with the iAs(III) species can be attributed to the partial oxidation of iAs (III) to iAs (V) in the hydroponics.

Cucumber plants also take up DMA(V) species in an unaltered way. Zhao *et al.*[127] found that not only in cucumber plants, but also in xylem sap or different tissues of common velvet grass (*Holcus lanatus*)[128] and sunflower (*Helianthus annuus*)[129] grown in iAs-containing hydroponics, methylated As species could be determined only in traces. This provided indirect evidence that the biomethylation capacity of the plants was low.

Arsenic containing xylem saps can also be studied by XANES for As speciation purposes. The normalized profile of the absorption edge of the As K shell for a xylem sap sample taken from cucumber plants (*Cucumis sativus* L.) treated with iAs(V) is shown in Figure 6. These studies also confirmed that iAs(III) is the predominant species in xylem sap regardless of the chemical form of As used for plant growth.

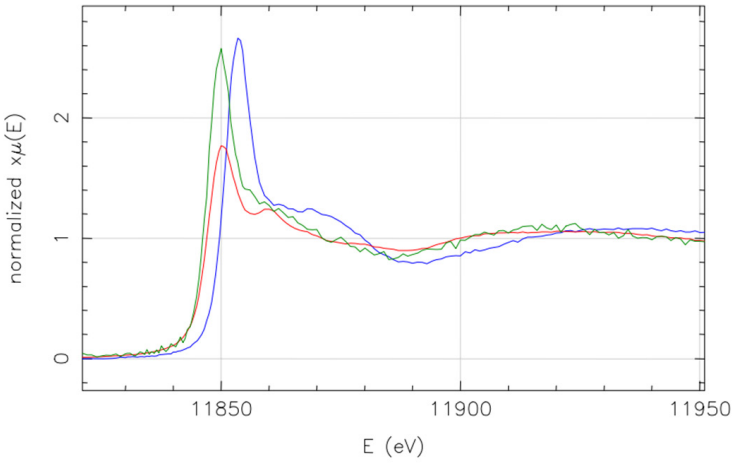

Figure 6. Spectra of a xylem sap taken from cucumber plants (*Cucumis sativus* L.) treated with iAs(V) as well as those of arsenite (red line) and arsenate (blue line) standards by near near-edge X-ray absorption spectroscopy. (unpublished figure)

The XANES spectra of nutrient solutions and xylem saps can be simulated by linear combinations (LC) of XANES spectra of iAs(III) and iAs(V) standards. Thus, LC calculations confirmed that >80% of As detected in xylem sap corresponds to the iAs(III) species regardless of the type of As treatment.[16] This is consistent with the results obtained by HPLC-ICP-MS, as the proportion of iAs(III) in those similar samples was 86%.[24]

As speciation studies on cucumber plants can be performed by applying off-line polyethylene imide thin layer chromatography – total-reflection X-ray fluorescence (PEI-TLC-TXRF) spectrometric method using acetone: acetic acid:water. The elution of the different As species was as follows: iAs(V) (R_f = 0.06) <iAs(III) (R_f = 0.38) < MMA(V) (R_f = 0.59) < DMA(V) (R_f = 0.91).[25] Due to the reproducible operating conditions ensured by overpressured layer chromatography (OPLC) such as controlled flow rate, external application of pressure and accurate flushing volume, as well as doubling of the running distance, the separation was faster and resolution was better for each 25 ng of iAs(III), iAs(V), MMA(V), and DMA(V) expressed in elemental As in a multicomponent standard solution (Figure 7).

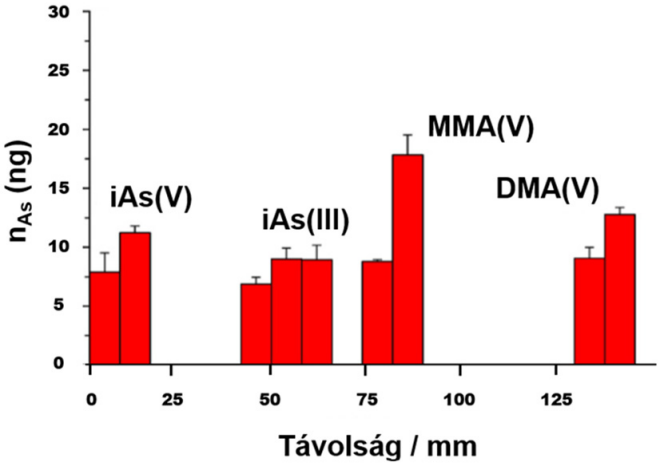

Figure 7. Off-line PEI- OPLC-TXRF chromatogram of multicomponent standard solution of arsenite [iAs(III)], arsenate [iAs(V)], monomethylarsonic acid [MMA(V)] and dimethylarsinic acid [DMA(V)] containing 25 ng of As each. [Reprinted (adapted) with permission from Ref. 25: Mihucz, V. G.; Móricz, Á. M.; Kröpfl, K.; Szikora, S.; Tatár, E.; Parra, L. M. M.; Záray, G. Development of off-line layer chromatographic and total reflection X-ray fluorescence spectrometric methods for arsenic speciation. *Spectrochim. Acta, Part B* **2006**, 61, 1124–1128. https://doi.org/10.1016/j.sab.2006.08.011 Copyright© (2022), Elsevier.]

The efficiency of As extraction from the roots of cucumber plants treated with iAs(III) species was 92%.[25] To quantify As by the developed off-line PEI-OPLC-TXRF method, the extract should have been applied in triplicate onto the plate. However, due to the high concentration of nutrient cations in the root samples and the electrostatic repulsion between positively charged PEI cellulose, this was not feasible. Only iAs(V) and iAs(III) species could be detected by applying 4 µL of the root extract. The presence of iAs(V) in the samples is due to the oxidation of iAs(III) to iAs(V) in the nutrient solution during treatment. In addition, the time-consuming extraction process could not be performed in an inert gas atmosphere.

A faster As speciation method can be achieved by introducing the different As species separated on the PEI-TLC layer into the ICP-MS by laser ablation (LA). Even much smaller amounts of As (different As species containing 3 ng As each) can be detected with this hyphenated technique than with the PEI-TLC/OPLC-TXRF method. The R_f values calculated for the separated species also showed a good agreement with the data obtained by the PEI-TLC-TXRF method[15]. Arsenobetaine and AsC were detected together at the sampling point. The resolution calculated for each adjacent peak ranged from 1.5 to 2.5, and no OPLC separation was required. The method has significant potential for rapid identification of As-contaminated samples, which was verified on enzymatically extracted NIST SRM 1568a rice flour. Thus, up to 10 pg

MMA(V) could be distinguished from the background value. This proposed TLC-LA-ICP-MS method was later modified for silica gel-based high-efficiency TLC plates[130] for Cr speciation. It has recently been further optimized using an iAs(V)-imprinted polymer to separate iAs(III) species. The developed μ-TLC-LA-ICP-MS method has been successfully applied to mine water spiked with iAs(III) and iAs(V) species. Using the optimal conditions, the detection limit of As was 0.3 μg L^{-1}.[131]

Dietary As intake and As speciation in rice grains using simple kitchen technology operations

For the population not exposed to As-contaminated drinking water, nutrition is the most significant source of iAs intake.[132] A close to linear relationship was observed between the As concentration of foods containing more than 40% water (e.g., soups, soft drinks, soda water, beer) and that of the water used for their production.[19] Moreover, the As concentration of the samples with high water content was positively correlated with that of the water used (i.e., Pearson's correlation coefficient was 0.830-0.923).[19] However, in Bangladesh, it has been shown that a partial reduction of As contamination in drinking water was not sufficient to significantly reduce the amount of As ingested.[133] In Europe, the population consumes an average of 153 g of vegetables per day, compared to around 250 g in Asia.[134] In Chile, the total As and iAs content of cooked vegetables from an As-contaminated area was studied. During the study it was found that the concentration of As in the drinking water used for cooking varied between 41 and 572 μg L^{-1}. The results also showed that foods made a significant contribution to iAs intake, which also posed a higher health risk for those 15 years of age and younger.[135] Exposure of school children (n=55) to As-contaminated well water was assessed in several areas of Mexico. The considerable As concentration in the water showed a clear correlation with that of determined in the hair samples of children. According to the authors, As-contaminated water used for cooking may have been the main source of As exposure.[136] The use of poor-quality glass and unglazed earthenware can also cause As poisoning.[137] The concentration of As dissolved by soaking in unglazed earthenware varied from 30.9 to 800 μg L^{-1}, while the As concentration obtained in the same experiments with glazed earthenware often fell below the detection limit (<0.5 μg L^{-1}), but maximally reached only 30.6 μg L^{-1}. Valentine *et al.*[138] compared the dietary habits of the population in two As-contaminated areas (Mexico and California) where there are geographical differences in the prevalence of skin diseases. Although the population exposure to As was similar to that of drinking water, there was a difference in the diet (vitamin A consumption) for the groups studied. The issue of dietary intake has been studied in detail in Latin America.[13] The dietary exposure of the population to As has been extensively studied in different regions of France and Catalonia[140,141] as well as in Hong Kong.[142] The main route of bioavailability of As is the food chain (diet and drinking water consumption).[143,144] According to Yost *et al.,*[145] 21-40% of As ingested by terrestrial foods in North America is of inorganic origin. The average concentration of As in vegetables is around 20 μg kg^{-1}.[146]

One of the staple foods for human consumption, rice (*Oryza sativa* L.) is also often contaminated with As, at concentrations of up to 280 μg kg^{-1}.[96] Also in the United States, rice consumption is a significant source of children exposure to As.[147-149] According to the Food and Agriculture Organization (FAO), the People's Republic of China is the largest rice producer in the world. China is followed by India, Indonesia, Bangladesh and Vietnam. In many areas of these countries, groundwater is highly contaminated with As.[80] The relatively high As content of rice suggests considerable uptake and translocation of this element. According to Liang *et al.,*[150] the rice grains are first husked by grinding (and friction), i.e. the husks (bran layers) covering the grains are removed. The rice grains, stripped of their husks, are polished with a (conical) grinder and bleached with glucose or talcum. The 8-10% of the initial weight of brown rice is removed, mainly in the form of bran. As with most cereals, the distribution of the amounts of elements within the rice grain is heterogeneous. Consequently, it is worth examining the effect of milling rice grains on element content. Of the trace elements accumulating in rice, special attention is paid to the highly toxic Cd.[151-154] However, several other toxic elements have already been determined in various milled rice cultivars.[155,156] Rice plants are basically classified into two classes. We distinguish between short and long grain rice. The two most common subspecies are *indica* and *japonica*. Short-grained and cooked rice is

a subspecies of *japonica*, while long-grained rice is of Indian origin. *Indica* subspecies are usually grown on water-flooded arable land, while *japonica* species can be grown on dry soil. In general, rice crops and grains grown by the flood method are studied.[152,153] However, Rascio *et al.*[154] studied Vialone Nano rice grown in the province of Verona (Italy) used to make risottos.

The rice grains must be subjected to solvent or enzymatic extraction before chromatographic separation. Methanol is often used for solvent extraction. Thus, e.g., 76% of the concentration of As in the NIST 1568a in the rice sample could be recovered by extraction with methanol-water (1:1 v/v) using ultrasonication. In the case of extraction with trifluoroacetic acid (TFA) solution at 100 °C for 6 h, the recovery in As-spiked rice samples was quantitative as opposed to methanol extraction.[155] In the latter case, the recovery varied between 31 and 72%.[155] However, a reduction in iAs (V) was observed using TFA. According to Huang *et al.,*[157] quantitative extraction could be achieved by using dilute HNO_3 solution for As speciation in rice grains.[157] By extracting As species from freeze-dried rice produced at the IRMM with water or methanol:water mixtures of different compositions (1:1, 9:1 and 1:1 then 9:1 v/v), Pizarro *et al.*[156] found that about 80% of the total concentration of As can be extracted with a 1:1 v/v mixture of methanol:water using a single extraction step. Accelerated solvent extraction (ASE) is similar to conventional solid-liquid extraction, but it is performed at higher temperatures and pressures, reducing the time required for extraction. However, depending on the type of solvent, the temperature and the pressure used, ASE causes the rice grains to swell.[155] Nevertheless, ASE has been successfully used to extract As species of marine fish[158] and seaweed.[143]

The biggest disadvantage of enzymatic extraction methods is their high time demand, which can result in the interconversion of As species.[159] To break down starch, Heitkemper *et al.* used α-amylase[155] for As determination in rice prior to extraction with methanol: water (1:1 v/v). Under these conditions, an extraction efficiency of 59% was achieved for white rice grains. However, for the NIST 1568a rice sample, this value was found to be 97%. Although the best results were obtained using TFA, it was found that iAs(V) was partially reduced to iAs(III) during extraction. In addition, Pizarro *et al.*[156,160] rejected the use of TFA for As-speciation from rice by HPLC-ICP-MS because in this case poor chromatographic resolution of the extracted As species was observed. Focused ultrasonic treatment coupled with enzymatic hydrolysis has been successfully applied to the extraction of As from rice grains for speciation purposes[23,161] as well as to other samples of biological origin.[162]

Rice is dominated by iAs(III), iAs(V), DMA(V), and MMA(V).[96,156,158-162] Arsenic speciation can be performed in rice seedlings[163] as well as in rice grains.[96,156,158-162] In raw rice grains, iAs(III) is the predominant species, accounting for about 50% of the samples.[23] The other major As species present in the samples is iAs(V), the percent of which varied between 25 and 33%.[23] At the same time, the percent of DMA(V) ranged from 8 to 10%, while that of AsC from 6 to 10%.[23] In 2015, the European Commission revised Directive 2006/1881/EC on maximum levels for iAs in food. Thus, the sum of the concentrations of iAs(III) and iAs(V) in rice used for food processing in the case of infants and young children under Regulation (EC) No 2015/1006 may not exceed 0.1 mg kg^{-1}.[164] Study of 24 high-As rice samples grown in the United States revealed that they contained mainly iAs(III) and DMA(V) species. The DMA(V) content increased proportionally with the total As content, while the concentration of iAs(III) (approximately 0.1 mg kg^{-1}) did not change significantly. From this, the authors concluded that rice can be divided into two groups according to its As content: DMA(V) and iAs rice. According to this theory, varieties grown in the United States belong to the first category, while those growing in Europe and Asia to the second one. It was suggested that this difference was due to plant genetic reasons. Although this theory cannot be completely ruled out, the type of soil composition and irrigation is more likely to be responsible for the high DMA(V) content. Furthermore, the recent use of pesticides containing DMA(V) and MMA(V) in the central and southern parts of the United States may play a role.[165,166]

It is common practice to perform As speciation of rice in ground form. This is understandable since rice flour is used for cooking in Asia and also from an analytical chemistry point of view, as the homogeneity of the sample is a key issue to obtain reliable results. In China, rice is usually cooked with small aliquots

of water. In this way, rice absorbs the available water. However, this approach does not provide real information for estimating the As exposure from rice consumption for example, in the so-called Western societies, where rice is usually consumed as a side dish, so it is cooked in plenty of water and the remaining water is poured off. Thus, there is a need to perform As speciation also according to this latter kitchen technology methods. On the other hand, milk rice, risotto, etc. requires a different approach. The As speciation performed on rice cooked in As-containing water diluted with varying degrees of deionized water (DW) (1:1 to 4:1 v/v) demonstrated the ability of rice grains to absorb As during cookin.[167] Bae *et al.*[168] reached to a similar conclusion by determining the total As concentration of rice cooked with local water in Bangladeshi households.

Extraction of rice grains with room temperature and boiling DW provides valuable information on the removal of toxic elements in them. By simulating two simple kitchen technologies (washing and cooking) corresponding to one of the possible ways of preparing rice, it is possible to determine the extent to which the As content of the rice grains can be removed.[26] The minimum cooking time was chosen so that the rice grains would soften in line with the recommendations for cooking instant and long grain rice. The total As concentrations of the investigated rice samples did not exceed 171.3 ± 7.1 μg kg^{-1}, which was also in agreement with previous literature data.[96] When determining the As content of polished rice samples taken from different geographical areas of ten countries, seven-fold differences were found in the median value. Samples from Egypt (0.04 mg kg^{-1}) and India (0.07 mg kg^{-1}) had the lowest As concentration, while the United States (0.25 mg kg^{-1}) and France (0.28 mg kg^{-1}) had the highest one.[169] Since 2014, the health limit value for iAs set by WHO/FAO is 0.2 mg kg^{-1} in polished rice.[170] According to the water extraction results, 8–17% and 29–42% of As could be removed from the studied rice grains by washing room with temperature DW and cooking, respectively.[23] These results are also consistent with results reported by Bae *et al*.,[168] according to which 57-81% of As remained in varieties of rice cooked in Bangladeshi households.

For removal of elements by washing and cooking, it also plays a role if metal contamination affects the surface of the rice grains or its deeper layers.[171] Cooking may increase the diffusion rate of these ions[171]. Confocal μ-XRF analysis provides an opportunity to track the extraction of the elements and interpret the results obtained by measurements in bulk phase (e.g., ICP-MS). By confocal μ-XRF analysis, normalization of the intensity confirmed that the intensity of the X-ray fluorescent signal of most elements was higher in the near-surface part of the studied rice grains.[26] Thus, elements (e.g., As) were enriched from the surface of the rice grain to a depth of about 80 μm.[26]

In terms of As speciation in washed and cooked rice, the main extractable chemical form of As was also iAs(III), with proportions ranging from about 40 to 70% in white rice grains at room temperature and between 60 and 75% in boiling DW extracts.[23] Arsenocholine, DMA(V) and iAs(V) could also be determined in these samples. In contrast, cooked samples were generally dominated by the presence of iAs(V), suggesting that iAs(III) was partially oxidized during cooking.[23] Pal *et al.* reached to the same conclusion by performing As speciation following cooking of rice grown in As-contaminated areas of West Bengal in distilled water.[172]

Arsenic intake by breastfeeding

Exclusive breastfeeding is recommended for the first six months after birth for infants, because of providing optimal conditions for the immunological and psychological development of the newborn. However, potential inorganic contaminants in breast milk (e.g., As) are transmitted to the neonate through breastfeeding.[173] Toxic elements are absorbed to a greater extent in neonates than in adults, and bile excretion is low in the first weeks after delivery.[174] Arsenic occurrence in breast milk is mainly due to a diet rich in marine fish and seafood.[175] The As concentration of breast milk in endemic As-contaminated areas (e.g., aquifers) was found to be lower than expected.[176] According to the Joint FAO/WHO Expert Committee on Food Additives, the lower limit of the benchmark dose ($BDML_{0.5}$) with iAs-induced lung cancer as the end point of toxicity effect is 3 μg kg^{-1} BW.[177]

Twenty-four-hour pooled samples taken from the same mother[178] would be ideal for elemental analysis in breast milk. Since this is not possible, usually, samples are collected from only one mammal gland that has not been involved in breastfeeding for 2-3 hours prior to sampling.[178] The most common sample preparation procedure is MW-assisted acid digestion using a mixture of concentrated HNO_3 and hydrogen peroxide solutions. If freeze-drying is applied before analysis,[178-180] the sample demand is smaller.[180] The digested samples are nowadays analyzed by ICP-MS.[181-183]

A recent study conducted in Hungary on the determination of As in breast milk of non-smoking, exclusively breastfeeding volunteers with an average body mass index and with no occupational exposure to As in the early stages of breastfeeding, the mean concentration of As in the samples was 0.41 ± 0.20 μg L^{-1}. However, the median values of the As concentrations determined for all samples were 0.35 μg L^{-1}, respectively, indicating an almost symmetric distribution of the concentration dataset.[184] The median As concentration in the abovementioned study was approximately 45% larger than in the Hungarian mature milk samples published in 1991 and analyzed by neutron activation analysis.[185] Unlike in 1991, the results of the recent study showed that As was detectable in all samples. This is due not only to the advances in instrumental analysis, but also to the changes in the dietary habits of the last 30 years. Today, more poultry meat is consumed, because it is considered healthier, and a larger selection of seafood and marine fish is available in Hungary. Lovreglio *et al.*[186] found that less toxic AsB and AsC occur even in poultry meat. Concentration values of As in samples taken in Taiwan and Sweden were also similar to those obtained in the aforementioned recent study.[187] Higher As concentrations have been reported from Greece.[175] Outside Europe, higher values have been reported from Pakistan (0.5 μg L^{-1}),[188] Iran (0.85 μg L^{-1}),[189] Bangladesh (1 μg L^{-1}),[190] Japan (1.4 μg L^{-1})[191] and Lebanon (2.3 μg L^{-1}).[192] In mature breast milk samples analyzed in Portugal, As concentration was about 5.8 μg L^{-1}, presumably due to regular consumption of fish and seafood, while the Pb concentration was lower.[193]

Estimation of the intake of As in breast-fed infants can be performed by the method applied by Rebelo and Caldas[194] consisting of expressing the ratio between the determined concentration and the benchmark dose limit (BMDL) value. The value thus obtained is called margin of exposure (MOE). Its estimated value is inversely proportional to the risk to public health posed by a certain toxic element.[195] In the US, this value is typically above 50 for As.[196] According to literature data, the MOE values for As in Europe are about 50 or higher.[194] No significant relationship could be found between the age of the volunteers and the As concentrations in breastmilk samples.[184] In return, the MOE values calculated for Pb proved that this element continues to pose a potential risk to infants.[184] Moreover, the Pb concentration in breast milk was significantly correlated with the age of the mothers.[184,197]

Organs playing an important role in reproduction and offspring care are protected against As, As-speciation is difficult to achieve.

Potential threat represented by As in complementary and alternative medicinal products

General considerations

According to the WHO, traditional medicine is defined as CAM. This category includes traditional Chinese medicine, the Ayurvedic or Indian medicine system, the Tamil Siddha, the Persian - Arabic Unani, and homeopathy. Of these, Ayurveda is only surpassed in popularity by traditional Chinese medicine. The main difference between these two systems is that Ayurvedic preparations can not only contain herbs but also minerals and elementary state elements (e.g., Hg, S). From an analytical chemistry point of view, Ayurvedic preparations can be classified as herbal, herbomineral and animal ones. Of the metals used to make Ayurvedic preparations, Hg is of primary importance. Among the minerals, those containing As such as realgar (α-As_4S_4) and auripigment (As_2S_3) are common constituents. Through the current numerous infocommunication channels, these products have become available worldwide. Online sales of Ayurvedic products have recently skyrocketed.[198] By performing elemental analysis of 193 Ayurvedic preparations purchased at random from the Internet, the authors of the study found that Pb, Hg or As were detectable in 21% of the products. The order of detection frequency of these toxic elements in the investigated

products was: Pb> Hg> As. Heavy metal and As contamination was twice as common in herbomineral products as in other types of products. In the Netherlands, about 20% of the labels of 292 traditional herbal preparations used in Ayurveda, traditional Chinese and Tibetan medicine, indicated the presence of Hg, As or Pb. These elements could be determined by ICP-MS in 64% of the samples. In about 20% of the investigated samples (n = 59), the amount of these elements exceeded the maximum allowable intake for humans with a single recommended dose. For 26 products, the estimated weekly As intake was 0.53 and 427 mg.[199] The European Commission classifies Ayurvedic preparations only as food supplements under Directive 2002/46/EC. In the United States, where Ayurvedic preparations are subject to the requirements of the Food Supplements Act 1994 (DSHEA - Dietary Supplement Health and Education Act), there is no need to demonstrate the safe use or efficacy of these products.[198]

The large number of scientific communications on Ayurvedic research published in peer reviewed journals contain relatively less information from analytical chemistry point of view. Elemental content of Ayurvedic products has been studied by neutron activation analysis,[200] voltammetry,[201] XRF spectroscopy[199,202] or ICP-MS.[199] The advantage of XRF is that it is a non-destructive analytical technique, although not suitable for the determination of trace elements, while ICP-MS has extremely low detection limits, its acquisition and maintenance costs are much higher, and sample preparation is a much more time-consuming process. Literature data are difficult to be compared due to the wide range of Ayurvedic products. An attempt is presented hereby. Khandpur *et al.*[203] investigated eight different Ayurvedic formulations, the As concentrations in these products were ranging from 5 to 248 mg kg^{-1}. The concentration of As in a blood sample from a patient undergoing Ayurvedic treatment was 0.202 mg L^{-1}, although the normal value is generally <0.06 µg L^{-1}. Saper *et al.* studied 70 Ayurvedic formulations purchased in stores[204] and 193 online[198] in the United Stated by X-ray fluorescence spectrometry. Of the 70 samples investigated, Pb, Hg, and As were quantifiable in 14. The concentration of As ranged from 0.037 to 8.13 g kg^{-1}.[204]

In a recent study, analysis by ICP-SF-MS after MW-assisted acid digestion of six different Ayurvedic products purchased online from India and one purchased in Hungary showed that the As concentration was relatively low, i.e., 0.41 ± 0, 05 mg kg^{-1} in the plant-derived sample (containing *Centella Asiatica*).[14] The concentrations of As in the rest of the investigated samples ranged from 0.04 to 771 mg kg^{-1}. The concentration of As (106 ± 13 g kg^{-1}) was the highest in an As_2O_3-containing preparation.[14] Due to its significant As content, an Ayurvedic ointment was only worth analyzing by energy dispersive X-ray fluorescence (EDXRF). Thus, the spectra of the ointment recorded by EDXRF confirmed that As was the major component of the sample.

Arsenic bioaccessibility in Ayurvedic complementary and alternative medicines

Knowledge of the total concentration of a toxic element (e.g., As) is necessary but not sufficient to estimate adverse health risks, so it is important to quantify the amounts of element(s) that could be assimilated after ingestion of a certain dose. However, application of *in vivo* experiments raises ethical issues. Thus, several *in vitro* procedures have been developed to simulate the effects of the human digestive process.[205]

Data from only a few complex analytical studies on bioaccessible concentrations of toxic elements in Ayurvedic formulations have been reported.[206-208] Giacomino *et al.*[209] used a mixture of hydrochloric acid, sodium chloride and pepsin to simulate gastric juice. Pancreatin, potassium dihydrogen phosphate and sodium hydroxide solution were used to simulate duodenal fluid. However, As_2O_3 and As sulfides can hardly be dissolved in HCl due to their (thio)acid anhydride properties, so their dissolution is expected only in alkaline media. However, due to their high initial concentration, As uptake by the human body may still be significant. For samples containing As_2O_3/cinnabar red and α-As_4S_4/HgS, the estimated daily intake exceeded the WHO recommended daily dose of 3.0 µg iAs BW kg^{-1} by a factor of 11.1 to 21.4.[14]

After incubation of 17 products purchased from pharmacies and local markets in Italy and India, respectively, in suspensions of gastric and duodenal fluids, a remarkable dissolution was observed for As.[209,210]

Koch *et al.*[206] characterized the elemental content of CAMs by ICP-MS and XANES, focusing on the bioaccessibility of As and Pb, respectively, by incubation in a model suspension containing pancreatic

and bile extract, respectively. Interestingly, *bhasma* formulations characterized by a strong covalent bond between As(III) and S atoms increased the bioacessibility of As. The authors explained this phenomenon by the oxidation of As(III), which was confirmed by XANES measurements. In addition, the estimated dietary intake using the bioaccessible As concentration values in several cases was greater than the daily tolerable limit set by California Proposition 65.[211] Bolan *et al.*[208] investigated bioaccessibility of As-containing rice and some Ayurvedic products of plant origin by using an exhaustive sequential extraction method proposed by Tessier *et al.*[212] as well as in simulated gastric and duodenal fluids. The concentration of bioaccessible As was highly dependent on the procedure used. However, pancreatin is one of the most preferred compounds for simulating duodenal fluid.[206,213-217] Extraction efficiencies determined by modeling bioaccessibility resulted in large differences. Therefore, it would be important to develop and adopt an appropriate extraction method.[207]

Arsenic speciation in phosphate-rich bioaccessible fractions of Ayurvedic preparations

Arsenic speciation in bioaccessible fractions is not a routine procedure. Until now, elemental speciation has been performed directly on Ayurvedic samples in solid state of matter using X-ray-based analytical techniques (e.g., XANES, extended X-ray absorption fine structure, EXAFS) due to the high toxic element concentration of the formulations.[206-208] In herbal preparations, the predominant As species were organic, while in mineral-containing Ayurvedic products, As occurs in inorganic form.

Two Ayurvedic formulations containing As in moderate concentration were studied after spiking to 150 μg kg^{-1} iAs(V) standard solution, incubation in a pH = 6.8 suspension simulating duodenal fluid and SAX-SPE separation. The highest recovery of about 80% for the iAs(V) species was obtained when the model solution did not contain phosphate ions. The presence of sodium hydroxide did not affect the recovery of iAs(V). Oxidation of iAs(III) was observed using optimal SPE conditions for two Ayurvedic (herbo)mineral preparations with high As content. Thus, 6.3% of the iAs(III) in the bioaccessible fractions were oxidized in the sample containing As_2O_3 and cinnabar red, compared to 33% in the formulation containing realgar and HgS. Spiking a simple homeopathic sample matrix containing theoretically As_2O_3 with a 1 μg L^{-1} iAs(V) standard solution, recovery of total As and iAs(V) of samples subjected to SAX-SPE were about 97% and 95%, respectively.[14] The recovery of total As and iAs(V) was approximately 90% and 80%, respectively, when the homeopathic product was spiked to 10 μg L^{-1} iAs(V) and then incubated with the duodenal modeling suspension without the addition of phosphate ions. Study of the homeopathic remedy has also shown that it was mainly phosphate ions that prevent the separation of As species with SPE and not the matrix constituents. Breakthrough results in this area with efficient As-speciation methods have yet to be published.

CONCLUSIONS

In recent decades, several As speciation methods have been developed, many of which are cost-effective as alternatives to the original on-line hyphenated techniques consisting of an HPLC separation followed by atomic spectroscopic detection. In the case of TLC, the OPLC-TXRF method provides reproducible operating conditions, resulting in faster separation and better resolution. Laser ablation for PEI-TLC plates followed by ICP-MS measurements proved to be suitable for the screening of biological samples. *In situ* separation of As species in water with SAX-SPE can be easily accomplished from matrices up to pH<9 with higher enrichment and/or dilution, followed by laboratory analysis of acid-preserved samples. The cost-efficient TXRF spectrometry allows the simultaneous determination of several other trace elements in drinking water. At the regional level (e.g., in Hungary), the exposure of the population to As has been significantly reduced since 2017 by drilling new wells and establishing new waterworks in settlements of poor water quality. To the best of my knowledge, however, As speciation has not been widely used in the development of As removal technologies. To date, there is no real breakthrough in the use of As speciation methods. Arsenic contamination is challenging since inorganic As species cannot easily be decomposed compared to purely organic contaminants. Thus, the removed As is concentrated in hazardous waste disposal, which is also costly. Another possibility is to immobilize As e.g., in the soil. In this respect, bio-

waste is a promising raw material after conversion to AC with concentrated H_2SO_4. In order to increase mechanical stability and adsorption, it is advisable to use a silicate-containing material after charring to stabilize As (e.g., Florisil®). Although Florisil® is a widespread chromatographic adsorbent, it is expensive, but simple charring processes can keep the cost of producing ACs low (e.g., no application of energy-demanding pyrolysis).

In the lack of a definitive solution for the removal of As from drinking water, it is important to estimate the exposure of the population in areas with extensive natural As pollution. Dietary intake is the major source for nonoccupational exposure to As. Washing and cooking rice in plenty of water is advisable in regions affected by As-contaminated water. In this way, large amounts of As can be removed. According to a recent study, significant efforts are still being made in several parts of the world (e.g., West Bengal) to develop intervention procedures to reduce As pollution of waters.[218]

The estimated intake of As from the bioaccessible fractions of Ayurvedic formulations poses a health risk. If public health employees were more empathetic to their patients, or if a significant portion of the contemporary society did not reject the results of scientific research, there would be no demand for such dubious quality drugs. A recent review paper[219] highlighted the need to (i) elucidate the mechanisms of incorporation of toxic elements into CAM formulations, (ii) to understand the biogeochemical cycles of these elements and in particular their metabolites; (iii) to develop appropriate speciation methods to study the *in vitro* bioaccessibility of toxic elements; and (iv) conducting clinical trials and developing stricter legislation. In accordance with the current practice, elemental speciation in Ayurvedic preparations containing high concentrations of toxic elements is performed directly in the solid state by X-ray-based analytical techniques (XANES, EXAFS). Although the success of X-ray measurement techniques is undeniable, more accurate information could be obtained using appropriate *in vitro* methods to study bioaccessibility, but extreme pH and complex sample/extraction matrix represent real obstacles.

Even today, several reviews deal with the estimation of health risks caused by dietary As intake[220,221] and the development of As speciation methods.[222] Regarding the reduction of As contamination in environmental compartments and food items, many questions still should be addressed in the future.

Conflicts of interest

There have not been any financial conflicts of interest for writing this manuscript.

Acknowledgements

This review has not received any funding.

REFERENCES

(1) European Commission Directive 98/83/EC of 3 November 1998 on the quality of water intended for human consumption. Official Journal L 330, 05/12/1998, 0032 – 0054. https://eur-lex.europa.eu/legal-content/EN/TXT/HTML/?uri=CELEX:31998L0083&from=HU [Accessed 28 November 2021].

(2) Mikutta, C.; Mandaliev, P. N.; Mahler, N.; Kotsev, T.; Kretzschmar, R. Bioaccessibility of Arsenic in Mining-Impacted Circumneutral River Floodplain Soils. *Environ. Sci. Technol.* **2014**, *48*, 13468-13477. https://doi.org/10.1021/es502635t

(3) Prohaska, T.; Stingeder, G. Speciation of Arsenic: Arsenic and Arsenic Species in Environment and Human Nutrition. In: Cornelis, R.; Caruso, J.; Crews, H.; Heumann, K. (Eds.). *Handbook of Elemental Speciation II – Species in the Environment, Food, Medicine and Occupational Health,* Vol. 2. Wiley, Chichester, **2005**, 69-85. https://doi.org/10.1002/0470856009

(4) Brown, J. L.; Kitchin, K. T.; George, M. Dimethylarsinic acid treatment alters six different rat biochemical parameters: Relevance to arsenic carcinogenesis. *Teratog. Carcinog. Mutagen*. **1997**, *17*, 71–84. https://doi.org/10.1002/(sici)1520-6866(1997)17:2<71::aid-tcm3>3.0.co;2-b

(5) Human Metabolome Database (HMDB). Showing metabocard for Dimethylarsinous acid. http://www.hmdb.ca/metabolites/HMDB0012216 [Accessed 28 November 2021].

(6) Human Metabolome Database (HMDB). Showing metabocard for Methylarsonite. http://www.hmdb.ca/metabolites/HMDB0012259 [Accessed 28 November 2021].
(7) Odanaka, Y.; Tsuchiya, N.; Matano, O.; Goto, S. Characterization of arsenic metabolites in rice plant treated with DSMA (disodium methanearsonate). *J. Agric. Food Chem*. **1985**, *33*, 757–763. https://doi.org/10.1021/jf00064a050
(8) U.S. Food & Drug Administration (FDA). *Arsenic-based Animal Drugs*. https://www.fda.gov/animal-veterinary/product-safety-information/arsenic-based-animal-drugs [Accessed 28 November 2021].
(9) Chen, G.; Liu, H.; Zhang, W.; Li, B.; Liu, L.; Wang, G. Roxarsone exposure jeopardizes nitrogen removal and regulates bacterial community in biological sequential batch reactors. *Ecotox. Environ. Safe*. **2018**, *159*, 232-239. https://doi.org/10.1016/j.ecoenv.2018.05.012
(10) European Commission. *Arsenic health risk assessment and molecular epidemiology.* http://cordis.europa.eu/result/rcn/44352_en.html [Accessed 28 November 2021].
(11) Hamza, J. *Arsenic derogation for drinking water and related measures*. https://prezi.com/zjt6lvskaxs4/copy-of-az-ivoviz-arzen-derogacio-es-az-azzal-kapcsolatbanszukseges-intezkedesek/ [Accessed 28 November 2021].
(12) Reid, M. S.; Hoy, K. S.; Schofield, J. R. M.; Uppal, J. S.; Lin, Y.; Lu, X.; Peng, H.; Le, X. C. Arsenic speciation analysis: A review with an emphasis on chromatographic separations. *TrAC, Trends Anal. Chem*. **2020**, *123*, 115770. https://doi.org/10.1016/j.trac.2019.115770
(13) Anemana, T.; Óvári, M.; Varga, M.; Mihály, J.; Uzinger, N.; Rékási, M.; Yao, J.; Tatár, E.; Streli, C.; Záray, G.; et al. Granular activated charcoal from peanut (*Arachis hypogea*) shell as a new candidate for stabilization of arsenic in soil. *Microchem J*. **2019**, *149*, 104030. https://doi.org/10.1016/j.microc.2019.104030
(14) Kovács, D.; Veszely, Á.; Enesei, D.; Óvári, M.; Záray, G.; Mihucz, V. G. Feasibility of ion-exchange solid phase extraction inductively coupled plasma mass spectrometry for discrimination between inorganic As(III) and As(V) in phosphate-rich in vitro bioaccessible fractions of Ayurvedic formulations. *Spectrochim. Acta, Part B* **2019**, *153*, 1-9. https://doi.org/10.1016/j.sab.2019.01.002
(15) Resano, M.; García – Ruiz, E.; Mihucz, V. G.; Móricz, Á. M.; Záray, G.; Vanhaecke, F. Rapid screening method for arsenic speciation by combining thin layer chromatography and laser ablation-inductively coupled plasma-dynamic reaction cell-mass spectrometry. *J. Anal. At. Spectrom*. **2007**, *22*, 1158–1162. https://doi.org/10.1039/b704963c
(16) Meirer, F.; Pepponi, G.; Streli, C.; Wobrauschek, P.; Mihucz, V. G.; Záray, G.; Czech, V.; Broekaert, J. A. C.; Fittschen, U. E. A.; Falkenberg, G. Application of synchrotron-radiation-induced TXRF-XANES for arsenic speciation in cucumber (*Cucumis sativus* L.) xylem sap. *X-Ray Spectrom*. **2007**, *36*, 408–412. https://doi.org/10.1002/xrs.993
(17) Mihucz, V. G.; Bencs, L.; Koncz, K.; Tatár, E.; Weiszburg, T.; Záray, G. Fast arsenic speciation in water by on-site solid phase extraction and high-resolution continuum source graphite furnace atomic absorption spectrometry. *Spectrochim. Acta, Part B* **2017**, *128*, 30-35. https://doi.org/10.1016/j.sab.2016.12.010
(18) Mihucz, V. G.; Enesei, D.; Veszely, **Á.**; Bencs, L.; Pap-Balázs, T.; Óvári, M.; Streli, C.; Záray, G. A simple method for monitoring of removal of arsenic species from drinking water applying on-site separation with solid phase extraction and detection by atomic absorption and X-ray fluorescence based techniques. *Microchem. J.* **2017**, *135*, 105-113. https://doi.org/10.1016/j.microc.2017.08.006
(19) Sugár, É.; Tatár, E.; Záray, G.; Mihucz, V. G. Relationship between arsenic content of food and water applied for food processing. *Food Chem. Toxicol*. **2013**, *62*, 601–608. https://doi.org/10.1016/j.fct.2013.09.028
(20) Shraim, A.; Chiswell, B.; Olszowy, H. Speciation of arsenic by hydride generation–atomic absorption spectrometry (HG–AAS) in hydrochloric acid reaction medium. *Talanta* **1999**, *50*, 1109-1127. https://doi.org/10.1016/s0039-9140(99)00221-0

(21) Cerveira, C.; Pozebon, D.; de Moraes, D. P.; de Fraga, J. C. S. Speciation of inorganic arsenic in rice using hydride generation atomic absorption spectrometry (HG-AAS). *Anal. Methods* **2015**, *7*, 4528-4534. https://doi.org/10.1039/C5AY00563A
(22) Sugár, É.; Tatár, E.; Záray, G.; Mihucz, V. G. Field separation-based speciation analysis of inorganic arsenic in public well water in Hungary. *Microchem. J.* **2013**, *107*, 131–135. https://doi.org/10.1016/j.microc.2012.05.025
(23) Mihucz, V. G.; Tatár, E.; Virág, I.; Zang, C.; Jao, Y.; Záray, G. Arsenic removal from rice by washing and cooking with water. *Food Chem*. **2007**, *105*, 1718–1725. https://doi.org/10.1016/j.foodchem.2007.04.057
(24) Mihucz, V. G.; Tatár, E.; Virág, I.; Cseh, E.; Fodor, F.; Záray, G. Arsenic speciation in xylem sap of cucumber (*Cucumis sativus* L.). *Anal. Bioanal. Chem*. **2005**, *383*, 461–466. https://doi.org/10.1007/s00216-005-3325-y
(25) Mihucz, V. G.; Móricz, Á. M.; Kröpfl, K.; Szikora, S.; Tatár, E.; Parra, L. M. M.; Záray, G. Development of off-line layer chromatographic and total reflection X-ray fluorescence spectrometric methods for arsenic speciation. *Spectrochim. Acta, Part B* **2006**, *61*, 1124–1128. https://doi.org/10.1016/j.sab.2006.08.011
(26) Mihucz, V. G.; Silversmit, G.; Szalóki, I.; de Samber, B.; Schoonjans, T.; Tatár, E.; Vincze, L.; Virág, I.; Yao, J.; Záray, G. Removal of some elements from washed and cooked rice studied by inductively coupled plasma mass spectrometry and synchrotron based confocal micro-X-ray fluorescence. *Food Chem*. **2010**, *121*, 290–297. https://doi.org/10.1016/j.foodchem.2009.11.090
(27) Biswas, A.; Majumder, S.; Neidhardt, H.; Halder, D.; Bhowmick, S.; Mukherjee-Goswami, A.; Kundu, A.; Saha, D.; Berner, Z.; Chatterjee, D. Groundwater chemistry and redox processes: Depth dependent arsenic release mechanism. *Appl. Geochem*. **2011**, *26*, 516–525. https://doi.org/10.1016/j.apgeochem.2011.01.010
(28) Le, X. C.; Yalcin, S.; Ma, M. Speciation of Submicrogram per Liter Levels of Arsenic in Water: On-Site Species Separation Integrated with Sample Collection. *Environ. Sci. Technol*. **2000**, *34*, 2342–2347 https://doi.org/10.1021/es991203u
(29) Impellitteri, C. A. Effects of pH and competing anions on the speciation of arsenic in fixed ionic strength solutions by solid phase extraction cartridges. *Water Res*. **2004**, *38*, 1207–1214. https://doi.org/10.1016/j.watres.2003.11.023
(30) Ujević, M.; Duić, Ž.; Casiot, C.; Sipos, L.; Santo, V.; Dadić, Ž.; Halamić, J. Occurrence and geochemistry of arsenic in the groundwater of Eastern Croatia. *Appl. Geochem*. **2010**, *25*, 1017–1029. https://doi.org/10.1016/j.apgeochem.2010.04.008
(31) Issa, N. B.; Rajaković-Ognjanović, V. N.; Jovanović, B. M.; Rajaković, L. V. Determination of inorganic arsenic species in natural waters – Benefits of separation and preconcentration on ion exchange and hybrid resins. *Anal. Chim. Acta* **2010**, *673*, 185–193. https://doi.org/10.1016/j.aca.2010.05.027
(32) O'Reilly, J.; Watts, M. J.; Shaw, R. A.; Marcilla, A. L.; Ward, N. I. Arsenic contamination of natural waters in San Juan and La Pampa, Argentina. *Environ. Geochem. Health* **2010**, *32*, 491–515. https://doi.org/10.1007/s10653-010-9317-7
(33) Watts, M. J.; O'Reilly, J.; Marcilla, A. L.; Shaw, R. A.; Ward, N. I. Field based speciation of arsenic in UK and Argentinean water samples. *Environ. Geochem. Health* **2010**, *32*, 479–490. https://doi.org/10.1007/s10653-010-9321-y
(34) Jitmanee, K.; Oshima, M.; Motomizu, S. Speciation of arsenic(III) and arsenic(V) by inductively coupled plasma-atomic emission spectrometry coupled with preconcentration system. *Talanta* **2005**, *66*, 529–533. https://doi.org/10.1016/j.talanta.2004.09.024
(35) Piqué, À.; Grandia, F.; Canals, À. Processes releasing arsenic to groundwater in the Caldes de Malavella geothermal area, NE Spain. *Water Res*. **2010**, *44*, 5618–5630. https://doi.org/10.1016/j.watres.2010.07.012

(36) Meng, X.; Korfiatis, G. P.; Christodoulatos, C.; Bang, S. Treatment of arsenic in Bangladesh well water using a household co-precipitation and filtration system. *Water Res*. **2001**, *35*, 2805–2810. https://doi.org/10.1016/S0043-1354(01)00007-0
(37) Liang, P.; Liu, R. Speciation analysis of inorganic arsenic in water samples by immobilized nanometer titanium dioxide separation and graphite furnace atomic absorption spectrometric determination. *Anal. Chim. Acta* **2007**, *602*, 32–36. https://doi.org/10.1016/j.aca.2007.09.012
(38) Sperling, M.; Yin, X. F.; Welz, B. Differential determination of arsenic(III) and total arsenic using flow injection on-line separation and preconcentration for graphite furnace atomic absorption spectrometry. *Spectrochim. Acta, Part B* **1991**, *46*, 1789–1801. https://doi.org/10.1016/0584-8547(91)80206-I
(39) Koh, J.; Kwon, Y.; Pak, Y. N. Separation and sensitive determination of arsenic species (As3+/As5+) using the yeast-immobilized column and hydride generation in ICP–AES. *Microchem. J.* **2005**, *80*, 195–199. https://doi.org/10.1016/j.microc.2004.07.011
(40) Anthemidis, A. N.; Martavaltzoglou, E. K. Determination of arsenic(III) by flow injection solid phase extraction coupled with on-line hydride generation atomic absorption spectrometry using a PTFE turnings-packed micro-column. *Anal. Chim. Acta* **2006**, *573*, 413–418. https://doi.org/10.1016/j.aca.2005.12.055
(41) Xiong, C. M.; He, M.; Hu, B. On-line separation and preconcentration of inorganic arsenic and selenium species in natural water samples with CTAB-modified alkyl silica microcolumn and determination by inductively coupled plasma-optical emission spectrometry. *Talanta* **2008**, *76*, 772–779. https://doi.org/10.1016/j.talanta.2008.04.031
(42) Chen, D.; Huang, C.; He, M.; Hu, B. Separation and preconcentration of inorganic arsenic species in natural water samples with 3-(2-aminoethylamino) propyltrimethoxysilane modified ordered mesoporous silica micro-column and their determination by inductively coupled plasma optical emission spectrometry. *J. Hazard. Mater.*, **2009**, *164*, 1146–1151. https://doi.org/10.1016/j.jhazmat.2008.09.022
(43) Rahman, I. M. M.; Begum, Z. A.; Furusho, Y.; Mizutani, S.; Maki, T.; Hasegawa, H. Selective Separation of Tri- and Pentavalent Arsenic in Aqueous Matrix with a Macrocycle-Immobilized Solid-Phase Extraction System. *Water Air Soil Pollut*. **2013**, *224*, 1526-1537. https://doi.org/10.1007/s11270-013-1526-0
(44) Issa, N. B.; Rajaković-Ognjanović, V. N.; Marinković, A. D.; Rajaković, L. V. Separation and determination of arsenic species in water by selective exchange and hybrid resins. *Anal. Chim. Acta* **2011**, *706*, 191–198. https://doi.org/10.1016/j.aca.2011.08.015
(45) Chen, S. Z.; Zhan, X. L.; Lu, D. B.; Liu, C.; Zhu, L. Speciation analysis of inorganic arsenic in natural water by carbon nanofibers separation and inductively coupled plasma mass spectrometry determination. *Anal. Chim. Acta* **2009**, *634*, 192-196. https://doi.org/10.1016/j.aca.2008.12.018
(46) López-García, I.; Rivas, R. E.; Hernández-Córdoba, M. Use of carbon nanotubes and electrothermal atomic absorption spectrometry for the speciation of very low amounts of arsenic and antimony in waters. *Talanta* **2011**, *86*, 52-57. https://doi.org/10.1016/j.talanta.2011.07.105
(47) Zhang, Y.; Wang, W.; Li, L.; Huang, Y.; Cao, J. Eggshell membrane-based solid-phase extraction combined with hydride generation atomic fluorescence spectrometry for trace arsenic(V) in environmental water samples. *Talanta* **2010**, *80*, 1907–1912. https://doi.org/10.1016/j.talanta.2009.10.042
(48) Smedley, P. L.; Kinniburgh, D. G. A review of the source, behaviour and distribution of arsenic in natural waters. *Appl. Geochem*. **2002**, *17*, 517–568. https://doi.org/10.1016/S0883-2927(02)00018-5
(49) Abedin, M. J.; Feldmann, J.; Meharg, A. A. Uptake Kinetics of Arsenic Species in Rice Plants. *Plant Physiol*. **2002**, *128*, 1120–1128. https://doi.org/10.1104/pp.010733
(50) Takamatsu, T.; Aoki, H.; Yoshida, T. Determination of arsenate, arsenite, monomethylarsonate, and dimethylarsinate in soil polluted with arsenic. *Soil Sci*. **1982**, *133* (4), 239–246.

(51) Farnfield, H. R.; Marcilla, A. L.; Ward, N. I. Arsenic speciation and trace element analysis of the volcanic río Agrio and the geothermal waters of Copahue, Argentina. *Sci. Total Environ*. **2012**, *433*, 371–378. https://doi.org/10.1016/j.scitotenv.2012.05.098
(52) Wang, S.; Mulligan, C. N. Occurrence of arsenic contamination in Canada: Sources, behavior and distribution. *Sci. Total Environ*. **2006**, *366*, 701–721. https://doi.org/10.1016/j.scitotenv.2005.09.005
(53) Varsányi, I.; Matray, J. M.; Kovács, L. O. Hydrogeochemistry in two adjacent areas in the Pannonian Basin (Southeast-Hungary). *Chem. Geol*. **1999**, *156*, 25-39. https://doi.org/10.1016/S0009-2541(98)00178-8
(54) KvVM-EüM-FVM common order about the standard limits and measurement of contamination for the protection of underground water and geological medium. (In Hungarian). *Magyar Közlöny* **2009**, *51*, 14398-14414.
(55) Ódor, L.; Horváth, I.; Fügedi, U. J. Low-density geochemical mapping in Hungary. *Geochem. Explor*. **1997**, *60*, 55–66. https://doi.org/10.1016/S0375-6742(97)00025-3
(56) Szocs, T.; Horváth, I.; Bartha, A.; Bertalan, É.; Ballók, M.; Horváth, É. Speciation studies in understanding high As content in ground water. *Mineral. Mag*. **2008**, *72*, 107-111. https://doi.org/10.1180/minmag.2008.072.1.507
(57) Bezuglova, O. S.; Gorbov, S. N.; Tischenko, S. A.; Shimko, A. E. Use of brown coal as a detoxifier of soils contaminated with heavy metals. *J. Geochem. Explor*. **2018**, *184*, 232–238. https://doi.org/10.1016/j.gexplo.2016.11.004
(58) Pukalchik, M.; Panova, M.; Karpukhin, M.; Yakimenko, O.; Kydralieva, K.; Terekhova, V. J. Using humic products as amendments to restore Zn and Pb polluted soil: a case study using rapid screening phytotest endpoint. *Soils Sediments* **2018**, *18*, 750–761. https://doi.org/10.1007/s11368-017-1841-y
(59) Zhang, W. H.; Tong, L. Z.; Yuan, Y.; Liu, Z. Y.; Huang, H.; Tan, F. F.; Qiu, R. L. Influence of soil washing with a chelator on subsequent chemical immobilization of heavy metals in a contaminated soil. *J. Hazard. Mater*. **2010**, *178*, 578-587. https://doi.org/10.1016/j.jhazmat.2010.01.124
(60) Bolan, N.; Kunhikrishnan, A.; Thangarajan, R.; Kumpiene, J.; Park, J.; Makino, T.; Kirkham, M. B.; Scheckel, K. Remediation of heavy metal(loid)s contaminated soils – To mobilize or to immobilize? *J. Hazard. Mater*. **2014**, *266*, 141-166. https://doi.org/10.1016/j.jhazmat.2013.12.018
(61) Tsang, D. C. W.; Yip, A. C. K. Comparing chemical-enhanced washing and waste-based stabilisation approach for soil remediation. *J. Soils Sediments* **2014**, *14*, 936-947. https://doi.org/10.1007/s11368-013-0831-y
(62) Lee, S. H.; Lee, J. S.; Choi, Y. J.; Kim, J. G. In situ stabilization of cadmium-, lead-, and zinc-contaminated soil using various amendments. *Chemosphere* **2009**, *77*, 1069-1075. https://doi.org/10.1016/j.chemosphere.2009.08.056
(63) Komarek, M.; Vanek, A.; Ettler, V. Chemical stabilization of metals and arsenic in contaminated soils using oxides – A review. *Environ. Pollut*. **2013**, *172*, 9-22. https://doi.org/10.1016/j.envpol.2012.07.045
(64) Tsang, D. C. W.; Olds, W. E.; Weber, P. A.; Yip, A. C. K. Soil stabilisation using AMD sludge, compost and lignite: TCLP leachability and continuous acid leaching. *Chemosphere* **2013**, *93*, 2839-2847. https://doi.org/10.1016/j.chemosphere.2013.09.097
(65) Michalková, Z.; Komarek, M.; Sillerova, H.; Puppa, L. D.; Joussein, E.; Bordas, F.; Vanek, A.; Vanek, O.; Ettler, V. Evaluating the potential of three Fe- and Mn-(nano)oxides for the stabilization of Cd, Cu and Pb in contaminated soils. *J. Environ. Manage*. **2014**, *146*, 226-234. https://doi.org/10.1016/j.jenvman.2014.08.004
(66) Ahmad, M.; Rajapaksha, A. U.; Lim, J. E.; Zhang, M.; Bolan, N.; Mohan, D.; Vithanage, M.; Lee, S. S.; Ok, Y. S. Biochar as a sorbent for contaminant management in soil and water: A review. *Chemosphere* **2014**, *99*, 19-33. https://doi.org/10.1016/j.chemosphere.2013.10.071
(67) Bian, R.; Joseph, S.; Cui, L.; Pan, G.; Li, L.; Liu, X.; Zhang, A.; Rutlidge, H.; Wong, S.; Chia, C.; et al. A three-year experiment confirms continuous immobilization of cadmium and lead in contaminated paddy field with biochar amendment. *J. Hazard. Mater*. **2014**, *272*, 121-128. https://doi.org/10.1016/j.jhazmat.2014.03.017

(68) Tsang, D. C. W.; Yip, A. C. K.; Olds, W. E.; Weber, P. A. Arsenic and copper stabilisation in a contaminated soil by coal fly ash and green waste compost. *Environ. Sci. Pollut. Res*. **2014**, *21*, 10194-10204. https://doi.org/10.1007/s11356-014-3032-3
(69) Rajapaksha, A. U.; Ahmad, M.; Vithanage, M.; Kim, K. R.; Chang, J. Y.; Lee, S. S.; Ok, Y. S. The role of biochar, natural iron oxides, and nanomaterials as soil amendments for immobilizing metals in shooting range soil. *Environ. Geochem. Health* **2015**, *37*, 1-12. https://doi.org/10.1007/s10653-015-9694-z
(70) Mohan, D.; Singh, K. P.; Singh, V. K. Trivalent chromium removal from wastewater using low cost activated carbon derived from agricultural waste material and activated carbon fabric cloth. *J. Hazard. Mater*. **2006**, *135*, 280-295. https://doi.org/10.1016/j.jhazmat.2005.11.075
(71) Marris, E. Black is the new green. *Nature* **2006**, *442*, 624-626. https://doi.org/10.1038/442624a
(72) Glaser, B.; Birk, J. State of the scientific knowledge on properties and genesis of Anthropogenic Dark Earths in Central Amazonia (terra preta de Índio). *J. Geochim. Cosmochim. Acta*, **2012**, *82*, 39-51. https://doi.org/10.1016/j.gca.2010.11.029
(73) Yin, C. Y.; Aroua, M. K.; Daud, W. M. A. W. Review of modifications of activated carbon for enhancing contaminant uptakes from aqueous solutions. *Sep. Purif. Technol*. **2007**, *52*, 403-415. https://doi.org/10.1016/j.seppur.2006.06.009
(74) Lin, S. H.; Juang, R. S. Adsorption of phenol and its derivatives from water using synthetic resins and low-cost natural adsorbents: A review. *J. Environ. Manage*. **2009**, *90*, 1336-1349. https://doi.org/10.1016/j.jenvman.2008.09.003
(75) Dias, J. M.; Alvim-Ferraz, M. C.; Almeida, M. F.; Rivera-Utrillo, J.; Sánchez-Polo, M. Waste materials for activated carbon preparation and its use in aqueous-phase treatment: A review. *J. Environ. Manage*. **2007**, *85*, 833-846. https://doi.org/10.1016/j.jenvman.2007.07.031
(76) Samsuri, A. W.; Sadegh-Zadeh, F.; Seh-Bardan, B. J. Adsorption of As(III) and As(V) by Fe coated biochars and biochars produced from empty fruit bunch and rice husk. *J. Environ. Chem. Eng*. **2013**, *1*, 981-988. https://doi.org/10.1016/j.jece.2013.08.009
(77) Tavares, D.; Lopes, C.; Coelho, J.; Sánchez, M.; Garcia, A.; Duarte, A.; Otero, M.; Pereira, E. Removal of Arsenic from Aqueous Solutions by Sorption onto Sewage Sludge-Based Sorbent. *Water Air Soil Pollut*. **2012**, *223*, 2311-2321. https://doi.org/10.1007/s11270-011-1025-0
(78) Toor, M.; Jin, B. Adsorption characteristics, isotherm, kinetics, and diffusion of modified natural bentonite for removing diazo dye. *Chem. Eng. J*. **2012**, *187*, 79–88. https://doi.org/10.1016/j.cej.2012.01.089
(79) Kim, M. J.; Nriagu, J.; Haack, S. Arsenic species and chemistry in groundwater of southeast Michigan. *Environ. Pollut*. **2002**, *120*, 379–390. https://doi.org/10.1016/S0269-7491(02)00114-8
(80) Varsányi, I.; Kovács, L. Ó. Arsenic, iron and organic matter in sediments and groundwater in the Pannonian Basin, Hungary. *Appl. Geochem*. **2006**, *21*, 949-963. https://doi.org/10.1016/j.apgeochem.2006.03.006
(81) Rowland, H. A. L.; Omoregie, E. O.; Millot, R.; Jimenez, C.; Mertens, J.; Baciu, C.; Hug, S. J.; Berg, M. Geochemistry and arsenic behaviour in groundwater resources of the Pannonian Basin (Hungary and Romania). *Appl. Geochem*. **2011**, *26*, 1–17. https://doi.org/10.1016/j.apgeochem.2010.10.006
(82) Thundiyil, J. G.; Yuan, Y.; Smith, A. H.; Steinmaus, C. Seasonal variation of arsenic concentration in wells in Nevada. *Environ. Res*. **2007**, *104*, 367–373. https://doi.org/10.1016/j.envres.2007.02.007
(83) Kumar, P.; Kumar, M.; Ramanathan, A. L.; Tsujimura, M. Tracing the factors responsible for arsenic enrichment in groundwater of the middle Gangetic Plain, India: a source identification perspective *Environ. Geochem. Health* **2010**, *32*, 129–146. https://doi.org/10.1007/s10653-009-9270-5
(84) Nordstrom, D. K. Worldwide Occurrences of Arsenic in Ground Water. *Science* **2002**, *296*, 2143-2144. https://doi.org/10.1126/science.1072375
(85) Ajtony, Z.; Laczai, N.; Szoboszlai, N.; Bencs, L. Quantitation of Toxic Elements in Various Water Samples by Multi-element Graphite Furnace Atomic Absorption Spectrometry. *At. Spectrosc*. **2014**, *35*, 33-42.

(86) Lord, G.; Kim, N.; Ward, N. I. Arsenic speciation of geothermal waters in New Zealand. *J. Environ. Monit*. **2012**, *14*, 3192-3201. https://doi.org/10.1039/C2EM30486D
(87) Smichowski, P.; Valiente, L.; Ledesma, A. Simple Method for the Selective Determination of As(III) and As(V) by ETAAS After Separation With Anion Exchange Mini-column. *At. Spectrosc*. **2002**, *23*, 92-97.
(88) Yalçin, S.; Le, X. C. Speciation of arsenic using solid phase extraction cartridges. *J Environ Monit*. **2001**, *3*, 81-85. https://doi.org/10.1039/B007598L
(89) Sigrist, M.; Albertengo, A.; Beldoménico, H.; Tudino, M. Determination of As(III) and total inorganic As in water samples using an on-line solid phase extraction and flow injection hydride generation atomic absorption spectrometry. *J. Hazard. Mater*. **2011**, *188*, 311–318. https://doi.org/10.1016/j.jhazmat.2011.01.126
(90) Baranik, A.; Gagor, A.; Queralt, I.; Marguí, E.; Sitko, R.; Zawisza, B. Determination and speciation of ultratrace arsenic and chromium species using aluminium oxide supported on graphene oxide. *Talanta* **2018**, *185*, 264-275. https://doi.org/10.1016/j.talanta.2018.03.090
(91) Agrafioti, E.; Kalderis, D.; Diamadopoulos, E. Arsenic and chromium removal from water using biochars derived from rice husk, organic solid wastes and sewage sludge. *J. Environ. Manag*. **2014**, *133*, 309-314. https://doi.org/10.1016/j.jenvman.2013.12.007
(92) Mohan, D.; Pittman Jr., C. U. Arsenic removal from water/wastewater using adsorbents – A critical review. *J. Hazard. Mater*. **2007**, *142*, 1-53. https://doi.org/10.1016/j.jhazmat.2007.01.006
(93) Zhang, M.; Gao, B.; Varnoosfaderani, S.; Hebard, A.; Yao, Y.; Inyang, M. Preparation and characterization of a novel magnetic biochar for arsenic removal. *Bioresour. Technol*. **2013**, *130*, 457-462. https://doi.org/10.1016/j.biortech.2012.11.132
(94) Dombay, G. "Az arzéneltávolítás korszerű technológiai lehetőségei." *Vízmű Panoráma* **2002**, *10*, 38-40. (in Hungarian)
(95) Litter, M. I.; Morgada, M. E.; Bundschuh, J. Possible treatments for arsenic removal in Latin American waters for human consumption. *Environ. Pollut*. **2010**, *158*, 1105-1118. https://doi.org/10.1016/j.envpol.2010.01.028
(96) D'Amato, M.; Forte, G., Caroli, S. Identification and Quantification of Major Species of Arsenic in Rice. *J. AOAC Int*. **2004**, *87*, 238–243. https://doi.org/10.1093/jaoac/87.1.238
(97) Bohari, Y.; Lobos, G.; Pinochet, H., Pannier, F.; Astruc, A.; Potin-Gautier, M. Speciation of arsenic in plants by HPLC-HG-AFS: extraction optimisation on CRM materials and application to cultivated samples. *J. Environ. Monitor*. **2002**, *4*, 596–602. https://doi.org/10.1039/B203988P
(98) Rofkar, J. R.; Dwyer, D. F. Effects of Light Regime, Temperature, and Plant Age on Uptake of Arsenic by Spartina Pectinata and *Carex Stricta*. *Int. J. Phytoremediat*. **2011**, *13*, 528-537. https://doi.org/10.1080/15226514.2010.495151
(99) Rahman, M. A.; Kadohashi, K., Maki, T.; Hasegawa, H. Transport of DMAA and MMAA into rice (*Oryza sativa* L.) roots. *Environ. Exp. Bot*. **2011**, *72*, 41-46. https://doi.org/10.1016/j.envexpbot.2010.02.004
(100) Bravin, M. N.; Travassac, F.; Le Floch, M.; Hinsinger, P.; Garnier, J. M. Oxygen input controls the spatial and temporal dynamics of arsenic at the surface of a flooded paddy soil and in the rhizosphere of lowland rice (*Oryza sativa* L.): a microcosm study. *Plant Soil* **2008**, *312*, 207-218. https://doi.org/10.1007/s11104-007-9532-x
(101) Chen, T.; Yan, X.; Liao, X., Xiao, X.; Huang, Z.; Xie, H., Zhai, L. Subcellular distribution and compartmentalization of arsenic in *Pteris vittata* L. *Chin. Sci. Bull*. **2005**, *50*, 2843-2849. https://doi.org/10.1360/982005-943
(102) Dembitsky, V. M.; Rezanka, T. Natural occurrence of arseno compounds in plants, lichens, fungi, algal species, and microorganisms. *Plant. Sci*. **2003**, *165*, 1177–1192. https://doi.org/10.1016/j.plantsci.2003.08.007
(103) Meharg, A. A.; Hartley-Whitaker, J. Arsenic uptake and metabolism in arsenic resistant and nonresistant plant species. *New Phytol*. **2002**, *154*, 29–43. https://doi.org/10.1046/j.1469-8137.2002.00363.x

(104) Zhang, W.; Cai, Y.; Tu, C.; Ma, L. Q. Arsenic speciation and distribution in an arsenic hyperaccumulating plant. *Sci. Total Environ*. **2002**, *300*, 167–177. https://doi.org/10.1016/s0048-9697(02)00165-1
(105) Chen, R. X.; Smith, B. W.; Winefordner, J. D.; Tu, M. S.; Kertulis, G.; Ma, L. Q. Arsenic speciation in Chinese brake fern by ion-pair high-performance liquid chromatography–inductively coupled plasma mass spectroscopy. *Anal. Chim. Acta* **2004**, *504*, 199–207. https://doi.org/10.1016/j.aca.2003.10.042
(106) Kertulis, G. M.; Ma, L. Q.; MacDonald, G. E.; Chen, R.; Winefordner, J. D.; Cai, Y. Arsenic speciation and transport in *Pteris vittata* L. and the effects on phosphorus in the xylem sap. *Environ. Exp. Bot*. **2005**, *54*, 239-247. https://doi.org/10.1016/j.envexpbot.2004.09.001
(107) Cullen, W. R.; Reimer, K. J. Arsenic speciation in the environment. *Chem. Rev*. **1989**, *89*, 713–764. https://doi.org/10.1021/cr00094a002
(108) Unterbrunner, R.; Puschenreiter, M.; Sommer, P.; Wieshammer, G.; Tlustoš, P.; Zupan, M.; Wenzel, W. W. Heavy metal accumulation in trees growing on contaminated sites in Central Europe. *Environ. Pollut*. **2007**, *148*, 107–114. https://doi.org/10.1016/j.envpol.2006.10.035
(109) Mihucz, V. G.; Tatár, E.; Varga, A.; Záray, G.; Cseh, E. Application of total-reflection X-ray fluorescence spectrometry and high-performance liquid chromatography for the chemical characterization of xylem saps of nickel contaminated cucumber plants. *Spectrochim. Acta Part B* **2001**, *56*, 2235–2246. https://doi.org/10.1016/S0584-8547(01)00345-7
(110) Gasparics, T.; Mihucz, V. G.; Tatár, E.; Záray, G. Hyphenated technique for investigation of nickel complexation by citric acid in xylem sap of cucumber plants. *Microchem. J*. **2002**, *73*, 89–98. https://doi.org/10.1016/S0026-265X(02)00055-3
(111) Tatár, E.; Mihucz, V. G.; Varga, A.; Záray, G.; Cseh, E. Effect of lead, nickel and vanadium contamination on organic acid transport in xylem sap of cucumber. *J. Inorg. Biochem*. **1999**, *75*, 219–223. https://doi.org/10.1016/S0162-0134(99)00091-4
(112) Mihucz, V. G.; Tatár, E.; Kmethy, B.; Záray, G.; Cseh, E. Investigation of the transported heavy metal ions in xylem sap of cucumber plants by size exclusion chromatography and atomic absorption spectrometry. *J. Inorg. Biochem*. **2000**, *81*, 81-87. https://doi.org/10.1016/S0162-0134(00)00091-X
(113) Tatár, E.; Mihucz, V. G.; Kmethy, B.; Záray, G.; Fodor, F. Determination of organic acids and their role in nickel transport within cucumber plants. *Microchem. J*. **2000**, *67*, 73–81. https://doi.org/10.1016/S0026-265X(00)00101-6
(114) Pickering, I. J.; Prince, R. C.; George, M. J.; Smith, R. D.; George, G. N.; Salt, D. E. Reduction and Coordination of Arsenic in Indian Mustard. *Plant Physiol*. **2000**, *122*, 1171–1177. https://doi.org/10.1104/pp.122.4.1171
(115) Salgueiro, M. J.; Zubillaga, M. B.; Lysionek, A. E.; Caro, R. A.; Weill, R.; Boccio, J. R. The role of zinc in the growth and development of children. *Nutrition* **2002**, *18*, 510–519. https://doi.org/10.1016/S0899-9007(01)00812-7
(116) Untoro, J.; Karyadi, E.; Wibowo, L.; Erhardt, J.; Gross, R. Multiple Micronutrient Supplements Improve Micronutrient Status and Anemia but not Growth and Morbidity of Indonesian Infants: A Randomized, Double-Blind, Placebo-Controlled Trial. *The Journal of Nutrition* **2005**, *135*, 639S–645S. https://doi.org/10.1093/jn/135.3.639S
(117) Chan, S. S. L.; Ferguson, E. L.; Bailey, K.; Fahmida, U.; Harper, T. B.; Gibson, R. S. The concentrations of iron, calcium, zinc and phytate in cereals and legumes habitually consumed by infants living in East Lombok, Indonesia. *J. Food Compos. Anal.* **2007**, *20*, 609–617. https://doi.org/10.1016/j.jfca.2007.03.003
(118) Liang, J.; Han, B. Z.; Nout, M. J. R.; Hamer, R. J. Effects of soaking, germination and fermentation on phytic acid, total and in vitro soluble zinc in brown rice. *Food Chem*. **2008**, *110*, 821–828. https://doi.org/10.1016/j.foodchem.2008.02.064
(119) Zabłudowska, E.; Kowalska, J.; Jedynak, Ł.; Wojas, S.; Skłodowska, A.; Antosiewicz, D. M. Search for a plant for phytoremediation – What can we learn from field and hydroponic studies? *Chemosphere* **2009**, *77*, 301-307. https://doi.org/10.1016/j.chemosphere.2009.07.064

(120) Duan, G. L.; Zhou, Y.; Tong, Y. P.; Mukhopadhyay, R.; Rosen, B. P.; Zhu, Y. G. A CDC25 homologue from rice functions as an arsenate reductase. *New Phytol*. **2007**, *174*, 311–321. https://doi.org/10.1111/j.1469-8137.2007.02009.x
(121) Su, Y. H.; McGrath, S. P.; Zhu, Y. G.; Zhao, F. J. Highly efficient xylem transport of arsenite in the arsenic hyperaccumulator *Pteris vittata*. *New Phytol*. **2008**, *180*, 434–441. https://doi.org/10.1111/j.1469-8137.2008.02584.x
(122) Ellis, D. R.; Gumaelius, L.; Indriolo, E.; Pickering, I. J.; Banks, J. A.; Salt, D. E. A Novel Arsenate Reductase from the Arsenic Hyperaccumulating Fern *Pteris vittata*. *Plant Physiol*. **2006**, *141*, 1544–1554. https://doi.org/10.1104/pp.106.084079
(123) Xu, X. Y.; McGrath, S. P.; Zhao, F. J. Rapid reduction of arsenate in the medium mediated by plant roots. *New Phytol*. **2007**, *176*, 590–599. https://doi.org/10.1111/j.1469-8137.2007.02195.x
(124) Gonzaga, M. I. S.; Santos, J. A. G.; Ma, L. Q. Arsenic phytoextraction and hyperaccumulation by fern species. *Sci. Agric*. **2006**, *63*, 90–101. https://doi.org/10.1590/S0103-90162006000100015
(125) Ma, J. F.; Yamaji, N.; Mitani, N.; Xu, X. Y.; Su, Y. H.; McGrath, S. P.; Zhao, F. J. Transporters of arsenite in rice and their role in arsenic accumulation in rice grain. *Proc. Natl. Acad. Sci. U.S.A.* **2008**, *105*, 9931–9935. https://doi.org/10.1073/pnas.0802361105
(126) Su, Y. H.; McGrath, S. P.; Zhao, F. J. Rice is more efficient in arsenite uptake and translocation than wheat and barley. *Plant Soil* **2010**, *328*, 27–34. https://doi.org/10.1007/s11104-009-0074-2
(127) Zhao, F. J.; McGrath, S. P.; Meharg, A. A. Arsenic as a Food Chain Contaminant: Mechanisms of Plant Uptake and Metabolism and Mitigation Strategies. *Annu. Rev. Plant Biol*. **2010**, *61*, 535-559. https://doi.org/10.1146/annurev-arplant-042809-112152
(128) Quaghebeur, M.; Rengel, Z. The Distribution of Arsenate and Arsenite in Shoots and Roots of *Holcus lanatus* is Influenced by Arsenic Tolerance and Arsenate and Phosphate Supply. *Plant Physiol*. **2003**, *132*, 1600–1609. https://doi.org/10.1104/pp.103.021741
(129) Raab, A.; Williams, P. N.; Meharg, A.; Feldmann, J. Uptake and translocation of inorganic and methylated arsenic species by plants. *Environ. Chem*. **2007**, *4*, 197–203. https://doi.org/10.1071/EN06079
(130) LaFleur, J. P.; Salin, E. D. Speciation of Chromium by High-Performance Thin-Layer Chromatography with Direct Determination by Laser Ablation Inductively Coupled Plasma Mass Spectrometry. *Anal. Chem*. **2008**, *80*, 6821–6823. https://doi.org/10.1021/ac8010582
(131) Meharg, A. A.; Williams, P. N.; Adomako, E. E.; Lawgali, Y. Y.; Deacon, C.; Villada, A.; Cambell, R. C. J.; Sun, G.; Zhu, Y. G.; Feldmann, J.; et al. Geographical Variation in Total and Inorganic Arsenic Content of Polished (White) Rice. *Environ. Sci. Technol*. **2009**, *43*, 1612–1617. https://doi.org/10.1021/es802612a
(132) Yost, L. J.; Tao, S. H.; Egan, S. K.; Barraj, L. M.; Smith, K. M.; Tsuji, J. S.; Lowney, Y. W.; Schoof, R. A.; Rachman, N. J. Estimation of Dietary Intake of Inorganic Arsenic in U.S. Children. *Hum. Ecol. Risk Assess*. **2004**, *10*, 473–483. https://doi.org/10.1080/10807030490452151
(133) Ohno, K.; Yanase, T.; Matsuo, Y.; Kimura, T.; Rahman, M. H.; Magara, Y.; Matsui, Y. Arsenic intake via water and food by a population living in an arsenic-affected area of Bangladesh. *Sci. Total Environ*. **2007**, *381*, 68–76. https://doi.org/10.1016/j.scitotenv.2007.03.019
(134) Rahman, M. A.; Hasegawa, H. High levels of inorganic arsenic in rice in areas where arsenic-contaminated water is used for irrigation and cooking. *Sci. Total Environ*. **2011**, *409*, 4645–4655. https://doi.org/10.1016/j.scitotenv.2011.07.068
(135) Díaz, O. P.; Leyton, I.; Muñoz, O.; Nuñez, N.; Devesa, V.; Suner, M. A.; Velez, D.; Montoro, R. Contribution of Water, Bread, and Vegetables (Raw and Cooked) to Dietary Intake of Inorganic Arsenic in a Rural Village of Northern Chile. *J. Agric. Food Chem*. **2004**, *52*, 1773–1779. https://doi.org/10.1021/jf035168t
(136) Monroy-Torres, R.; Macias, A. E.; Gallaga-Solorzano, J. C.; Santiago-Garcia, E. J.; Hernandez, I. Arsenic in Mexican Children Exposed to Contaminated Well Water. *Ecol. Food Nutr*. **2009**, *48*, 59–75. https://doi.org/10.1080/03670240802575519

(137) Henden, E.; Cataloglu, R.; Aksuner, N. Determination of arsenic leaching from glazed and non-glazed Turkish traditional earthenware. *Sci. Total Environ*. **2011**, *409*, 2993–2996. https://doi.org/10.1016/j.scitotenv.2011.04.027

(138) Valentine, J. L.; Cebrian, M. E.; Garcia-Vargas, G. G.; Faraji, B.; Kuo, J.; Gibb, H. J.; Lachenbruch, P. A. Daily Selenium Intake Estimates for Residents of Arsenic-Endemic Areas. *Environ. Res*. **1994**, *64*, 1–9. https://doi.org/10.1006/enrs.1994.1001

(139) Bundschuh, J.; Nath, B.; Bhattacharya, P.; Liu, C. W.; Armienta, M. A.; Moreno López, M. V.; López, D. L.; Jean, J. S.; Cornejo, L.; Lauer Macedo, L. F.; et al. Arsenic in the human food chain: the Latin American perspective. *Sci. Tot. Environ*. **2012**, *429*, 92–106. https://doi.org/10.1016/j.scitotenv.2011.09.069

(140) Arnich, N.; Sirot, V.; Riviere, G.; Jean, J.; Noel, L.; Guerin, T.; Leblan, J. C. Dietary exposure to trace elements and health risk assessment in the 2nd French Total Diet Study. *Food Chem. Toxicol*. **2012**, *50*, 2432–2449. https://doi.org/10.1016/j.fct.2012.04.016

(141) Martorell, I.; Perelló, G.; Martí-Cid, R.; Llobet, J. M.; Castell, V.; Domingo, J. L. Human Exposure to Arsenic, Cadmium, Mercury, and Lead from Foods in Catalonia, Spain: Temporal Trend. *Biol. Trace Elem. Res*. **2011**, *142*, 309–322. https://doi.org/10.1007/s12011-010-8787-x

(142) Wong, W. W. K.; Chung, S. W. C.; Chan, B. T. P.; Ho, Y. Y.; Xiao, Y. Dietary exposure to inorganic arsenic of the Hong Kong population: Results of the first Hong Kong Total Diet Study. *Food Chem. Toxicol*. **2013**, *51*, 379–385. https://doi.org/10.1016/j.fct.2012.10.010

(143) Gallagher, P. A.; Wei, X. Y.; Shoemaker, J. A.; Brockhoff, C. A.; Creed, J. T. Detection of arsenosugars from kelp extracts via IC-electrospray ionization-MS-MS and IC membrane hydride generation ICP-MS. *J. Anal. At. Spectrom*. **1999**, *14*, 1829–1834. https://doi.org/10.1039/A906249A

(144) Tao, S. S. H.; Bolger, P. M. Dietary arsenic intakes in the United States: FDA Total Diet Study, September 1991 – December 1996. *Food Addit. Contam*. **1999**, *16*, 465–472. https://doi.org/10.1080/026520399283759

(145) Yost, L. J.; Schoof, R. A.; Aucoin, R. Intake of Inorganic Arsenic in the North American Diet. *Hum. Ecol. Risk Assess*. **1998**, *4*, 137–152. https://doi.org/10.1080/10807039891284244

(146) Schoof, R. A.; Yost, L. J.; Eickhoff, J.; Crecelius, E. A.; Cragin, D. W.; Meacher, D. M.; Menzel, D. B. A Market Basket Survey of Inorganic Arsenic in Food. *Food Chem. Toxicol*. **1999**, *37*, 839–846. https://doi.org/10.1016/S0278-6915(99)00073-3

(147) Davis, M. A.; Mackenzie, T. A.; Cottingham, K. L.; Gilbert-Diamond, D.; Punshon, T.; Karagas, M. R. Rice Consumption and Urinary Arsenic Concentrations in U.S. Children. *Environ. Health Perspect*. **2012**, *12*, 1418–1424. https://doi.org/10.1289/ehp.1205014

(148) Meacher, D. M.; Menzel, D. B.; Dillencourt, M. D.; Bic, L. F.; Schoof, R. A.; Yost, L. J.; Eickhoff, J. C.; Farr, C. H. Estimation of Multimedia Inorganic Arsenic Intake in the U.S. Population. *Hum. Ecol. Risk Assess*. **2002**, *8*, 1697–1721. https://doi.org/10.1080/20028091057565

(149) Meliker, J. R.; Franzblau, A.; Slotnick, M. J.; Nriagu, J. O. Major contributors to inorganic arsenic intake in southeastern Michigan. *Int. J. Hyg. Environ. Health* **2006**, *209*, 399–411. https://doi.org/10.1016/j.ijheh.2006.03.006

(150) Liang, J; Li, Z.; Tsuji, K.; Nakano, K.; Nout, M. J. R.; Hamer, R. J. Milling characteristics and distribution of phytic acid and zinc in long-, medium- and short-grain rice. *J. Cereal Sci*. **2008**, *48*, 83–91. https://doi.org/10.1016/j.jcs.2007.08.003

(151) Grant, C. A.; Clarke, J. M.; Duguid, S.; Chaney, R. L. Selection and breeding of plant cultivars to minimize cadmium accumulation. *Sci. Total Environ*. **2008**, *390*, 301–310. https://doi.org/10.1016/j.scitotenv.2007.10.038

(152) Liu, H.; Probst, A.; Liao, B. Metal contamination of soils and crops affected by the Chenzhou lead/zinc mine spill (Hunan, China). *Sci. Total Environ*. **2005**, *339*, 153–166. https://doi.org/10.1016/j.scitotenv.2004.07.030

(153) Liu, H. J.; Zhang, J. L.; Zhang, F. S. Role of iron plaque in Cd uptake by and translocation within rice (*Oryza sativa* L.) seedlings grown in solution culture. *Environ. Exp. Bot*. **2007**, *59*, 314–320. https://doi.org/10.1016/j.envexpbot.2006.04.001
(154) Rascio, N.; Vecchia, F. D.; La Rocca, N.; Barbato, R.; Pagliano, C.; Raviolo, M.; Gonnelli, C.; Gabbrielli, R. *Environ. Exp. Bot*., **2008**, *62*, 267–278. https://doi.org/10.1016/j.envexpbot.2007.09.002
(155) Heitkemper, D. T.; Vela, N. P.; Stewart, K. R.; Westphal, C. S. Determination of total and speciated arsenic in rice by ion chromatography and inductively coupled plasma mass spectrometry. *J. Anal. At. Spectrom*. **2001**, *16*, 299–306. https://doi.org/10.1039/B007241I
(156) Pizarro, I.; Gómez, M.; Palacios, M. A.; Cámara, C. Evaluation of stability of arsenic species in rice. *Anal. Bioanal. Chem*. **2003**, *376*, 102–109. https://doi.org/10.1007/s00216-003-1870-9
(157) Huang, J.-H.; Ilgen, G.; Fecher, P. Quantitative chemical extraction for arsenic speciation in rice grains. *J. Anal. At. Spectrom*. **2010**, *25*, 800-802. https://doi.org/10.1039/C002306J
(158) McKiernan, J. W.; Creed, J. T.; Brockhoff, C. A.; Caruso, J. A.; Lorenzana, R. M. A comparison of automated and traditional methods for the extraction of arsenicals from fish. *J. Anal. At. Spectrom.* **1999**, *14*, 607–613. https://doi.org/10.1039/A808824A
(159) Caruso, J. A.; Heitkemper, D. T.; B'Hymer, C. An evaluation of extraction techniques for arsenic species from freeze-dried apple samples. *Analyst* **2001**, *126*, 136–140. https://doi.org/10.1039/B009825F
(160) Pizarro, I.; Gómez, M.; Cámara, C.; Palacios, M. A. Arsenic speciation in environmental and biological samples: Extraction and stability studies. *Anal. Chim. Acta* **2003**, *495*, 85–98. https://doi.org/10.1016/j.aca.2003.08.009
(161) Sanz, E.; Muñoz-Olivas, R.; Cámara, C. A rapid and novel alternative to conventional sample treatment for arsenic speciation in rice using enzymatic ultrasonic probe. *Anal. Chim. Acta* **2005**, *535*, 227–235. https://doi.org/10.1016/j.aca.2004.12.021
(162) Sanz, E.; Muñoz-Olivas, R.; Cámara, C. Evaluation of a focused sonication probe for arsenic speciation in environmental and biological samples. *J. Chromatogr. A* **2005**, *1097*, 1–8. https://doi.org/10.1016/j.chroma.2005.08.012
(163) Abedin, M. J.; Cresser, M. S.; Meharg, A. A.; Feldmann, J.; Cotter-Howells, J. Arsenic Accumulation and Metabolism in Rice (*Oryza sativa* L.). *Environ. Sci. Technol*. **2002**, *36*, 962–968. https://doi.org/10.1021/es0101678
(164) European Commission Regulation (EU) 2015/1006 of 25 June 2015 amending Regulation (EC) No 1881/2006 as regards maximum levels of inorganic arsenic in foodstuffs. https://eur-lex.europa.eu/legal-content/EN/TXT/HTML/?uri=CELEX:32015R1006&from=EN [Accessed 28 November 2021].
(165) Williams, P. N.; Raab, A.; Feldmann, J.; Meharg, A. A. Market Basket Survey Shows Elevated Levels of As in South Central U.S. Processed Rice Compared to California: Consequences for Human Dietary Exposure. *Environ. Sci. Technol*. **2007**, *41*, 2178–2183. https://doi.org/10.1021/es061489k
(166) Zavala, Y. J.; Duxbury, J. M. Arsenic in Rice: I. Estimating Normal Levels of Total Arsenic in Rice Grain. *Environ. Sci. Technol*. **2008**, *42*, 3856–3860. https://doi.org/10.1021/es702747y
(167) Ackerman, A. H.; Creed, P. A.; Parks, A. N.; Fricke, M. W.; Schwegel, C. A.; Creed, J. T.; Heitkemper, D. T.; Vela, N. P. Comparison of a Chemical and Enzymatic Extraction of Arsenic from Rice and an Assessment of the Arsenic Absorption from Contaminated Water by Cooked Rice. *Environ. Sci. Technol*. **2005**, *39*, 5241–5246. https://doi.org/10.1021/es048150n
(168) Bae, M.; Watanabe, C.; Inaoka, T.; Sekiyama, M.; Sudo, N.; Bokul, M. H.; Ohtsuka, R. Arsenic in cooked rice in Bangladesh. *Lancet* **2002**, *360*, 1839–1840. https://doi.org/10.1016/S0140-6736(02)11738-7
(169) Kisomi, A. S.; Alizadeh, T.; Shakeri, A.; Nouri, A.; Farsadrooh, M.; Najafi, S.; Pashaki, A. Application of μ-TLC for speciation of inorganic arsenic by laser ablation inductively coupled plasma mass spectrometry. *Microchem. J*. **2020**, 105443. https://doi.org/10.1016/j.microc.2020.105443

(170) The Food and Agriculture Organization (FAO) Codex Alimentarius Commission - Geneva 14-18 July 2014. http://www.fao.org/news/story/en/item/238558/icode/SCOOP [Accessed 28 November 2021].
(171) Sharafi, K.; Yunesian, M.; Mahvi, A. H.; Pirsaheb, M.; Nazmara, S.; Nodehi, R. N. Advantages and disadvantages of different pre-cooking and cooking methods in removal of essential and toxic metals from various rice types- human health risk assessment in Tehran households, Iran. *Ecotoxicol. Environ. Saf.* **2019**, *175*, 128-137. https://doi.org/10.1016/j.ecoenv.2019.03.056
(172) Pal, A.; Chowdhury, U. K.; Mondal, D.; Das, B.; Nayak, B.; Ghosh, A.; Maity, S.; Chakraborti, D. Arsenic Burden from Cooked Rice in the Populations of Arsenic Affected and Nonaffected Areas and Kolkata City in West-Bengal, India. *Environ. Sci. Technol*. **2009**, *43*, 3349–3355. https://doi.org/10.1021/es803414j
(173) Isaac, C. P.; Sivakumar, A.; Kumar, C. R. Lead Levels in Breast Milk, Blood Plasma and Intelligence Quotient: A Health Hazard for Women and Infants. *Bull. Environ. Contam. Toxicol*. **2012**, *88*, 145-149. https://doi.org/10.1007/s00128-011-0475-9
(174) Oskarsson, A.; Hallén, I. P.; Sundberg, J.; Grawé, K. P. Risk assessment in relation to neonatal metal exposure. *Analyst* **1998**, 123, 19-23. https://doi.org/10.1039/A705136K
(175) Miklavčič, A.; Casetta, A.; Tratnik, J. S.; Mazej, D.; Krsnik, M.; Mariuz, M.; Sofianou, K.; Spiric, Z.; Barbone, F.; Horvat, M. Mercury, arsenic and selenium exposure levels in relation to fish consumption in the Mediterranean area. *Environ. Res*. **2013**, *120*, 7-17. https://doi.org/10.1016/j.envres.2012.08.010
(176) Concha, G.; Vogler, G.; Lezcano, D.; Nermell, B.; Vahter, M. Exposure to Inorganic Arsenic Metabolites during Early Human Development. *Toxicol. Sci*. **1998**, *44*, 185-190. https://doi.org/10.1006/toxs.1998.2486
(177) Joint FAO/WHO Expert Committee on Food Additives. Seventy-second meeting, Rome, 16–25 February 2010. http://www.who.int/foodsafety/chem/summary72_rev.pdf [Accessed 28 November 2021].
(178) Ballard, O.; Morrow, A. L. Human milk composition: nutrients and bioactive factors. *Pediatr. Clin. North Am*. **2013**, *60*, 49-74. https://doi.org/10.1016/j.pcl.2012.10.002
(179) Leotsinidis, M.; Alexopoulos, A.; Kostopoulou-Farri, E. Toxic and essential trace elements in human milk from Greek lactating women: Association with dietary habits and other factors. *Chemosphere* **2005**, *61*, 238-247. https://doi.org/10.1016/j.chemosphere.2005.01.084
(180) Letinić, J. G.; Sarić, M. M.; Piasek, M.; Jurasović, J.; Varnaic, V. M.; Grgec, A. S.; Orct, T. Use of human milk in the assessment of toxic metal exposure and essential element status in breastfeeding women and their infants in coastal Croatia. *J. Trace Elem. Med. Biol*. **2016**, *38*, 117-125. https://doi.org/10.1016/j.jtemb.2016.08.002
(181) Örün, E.; Yalçın, S. S.; Aykut, O.; Orhan, G.; Morgil, G. K.; Yurdakök, K.; Uzun, R. Breast milk lead and cadmium levels from suburban areas of Ankara. *Sci. Total Environ*. **2011**, *409*, 2467-2472. https://doi.org/10.1016/j.scitotenv.2011.02.035
(182) Coni, E.; Bocca, B.; Galoppi, B.; Alimonti, A.; Caroli, S. Identification of chemical species of some trace and minor elements in mature breast milk. *Microchem. J*. **2000**, *67*, 187-194. https://doi.org/10.1016/S0026-265X(00)00116-8
(183) Martino, F. A. R.; Sánchez, M. L. F.; Sanz-Medel, A. The potential of double focusing-ICP-MS for studying elemental distribution patterns in whole milk, skimmed milk and milk whey of different milks. *Anal. Chim. Acta* **2001**, *442*, 191-200. https://doi.org/10.1016/S0003-2670(01)01170-9
(184) Ecsedi-Angyal, M.; Tatár, E.; Óvári, M.; Kurin-Csörgei, K.; Záray, G.; Mihucz, V. G. Determination of low-level arsenic, lead, cadmium and mercury concentration in breast milk of Hungarian women. *Int. J. Environ. Anal. Chem*. **2020**, *100*, 549-566. https://doi.org/10.1080/03067319.2019.1637429
(185) Parr, R. M.; DeMaeyer, E. M.; Iyengar, V. G.; Byrne, A. R.; Kirkbright, G. F.; Schöch, G.; Ninistö, L.; Pineda, O.; Vis, H. L.; Hofvander, I.; Omololu, A. Minor and trace elements in human milk from Guatemala, Hungary, Nigeria, Philippines, Sweden, and Zaire. *Biol. Trace Elem. Res*. **1991**, *29*, 51-75. https://doi.org/10.1007/BF03032674

(186) Lovreglio, P.; D'Errico, M. N.; Gilberti, M. E.; Drago, I.; Basso, A.; Apostoli, P.; Soleo, L. The influence of diet on intra and inter-individual variability of urinary excretion of arsenic species in Italian healthy individuals. *Chemosphere* **2012**, *86*, 898-905. https://doi.org/10.1016/j.chemosphere.2011.10.050
(187) Chao, H. H.; Guo, C. H.; Huang, C. B.; Chen, P. C.; Li, H. C.; Hsiung, D. Y.; Chou, Y. K. Arsenic, Cadmium, Lead, and Aluminium Concentrations in Human Milk at Early Stages of Lactation. *Pediatr. Neonatol*. **2014**, *55*, 127-134. https://doi.org/10.1016/j.pedneo.2013.08.005
(188) Khan, S.; Ismail, A.; Gong, Y. Y.; Akhtar, S.; Hussain, M. Concentration of Aflatoxin M1 and selected heavy metals in mother milk samples from Pakistan. *Food Control* **2018**, 91, 344-348. https://doi.org/10.1016/j.foodcont.2018.04.015
(189) Samiee, F.; Vahidinia, A.; Javad, M. T.; Leili, M. Exposure to heavy metals released to the environment through breastfeeding: A probabilistic risk estimation. *Sci. Total Environ*. **2019**, *650*, 3075-3083. https://doi.org/10.1016/j.scitotenv.2018.10.059
(190) Kippler, M.; Hossain, M. B.; Lindh, C.; Moore, S. E.; Kabir, I.; Vahter, M.; Broberg, K. Early life low-level cadmium exposure is positively associated with increased oxidative stress. *Environ. Res*. **2012**, *112*, 164-170. https://doi.org/10.1016/j.envres.2011.11.012
(191) Sakamoto, M.; Chan, H. M.; Domingo, J. L.; Kubota, M.; Murata, K. Changes in body burden of mercury, lead, arsenic, cadmium and selenium in infants during early lactation in comparison with placental transfer. *Ecotoxicol. Environ. Saf*. **2012**, *84*, 179-184. https://doi.org/10.1016/j.ecoenv.2012.07.014
(192) Bassil, M.; Daou, F.; Hassan, H.; Yamani, O.; Kharma, J. A.; Attieh, Z.; Elaridi, J. Lead, cadmium and arsenic in human milk and their socio-demographic and lifestyle determinants in Lebanon. *Chemosphere* **2018**, *191*, 911-921. https://doi.org/10.1016/j.chemosphere.2017.10.111
(193) Almeida, A. A.; Lopes, C. M. P. V.; Silva, A. M. S.; Barrado, E. Trace elements in human milk: Correlation with blood levels, inter-element correlations and changes in concentration during the first month of lactation. *J. Trace Elem. Med. Biol*. **2008**, *22*, 196-205. https://doi.org/10.1016/j.jtemb.2008.03.007
(194) Rebelo, F. M.; Caldas, E. D. Arsenic, lead, mercury and cadmium: Toxicity, levels in breast milk and the risks for breastfed infants. *Environ. Res*. **2016**, *151*, 671-688. https://doi.org/10.1016/j.envres.2016.08.027
(195) Rebelo, F. M.; Cunha, L. R. D.; Andrade, P. D.; Costa Jr., W. A. D.; Bastos, W. R.; Caldas, E. D. Mercury in breast milk from women in the Federal District, Brazil and dietary risk assessment for breastfed infants. *J. Trace Elem. Med. Biol*. **2017**, *44*, 99-103. https://doi.org/10.1016/j.jtemb.2017.06.009
(196) European Food Safety Authority (EFSA). Opinion of the Scientific Committee on a request from EFSA related to A Harmonised Approach for Risk Assessment of Substances Which are both Genotoxic and Carcinogenic. Published: 27 October 2005. Adopted: 18 October 2005. https://doi.org/10.2903/j.efsa.2005.282
(197) Mieczan, A. W. Cadmium, Lead, Copper and Zinc in Breast Milk in Poland. *Biol. Trace Elem. Res*. **2014**, *157*, 36-44. https://doi.org/10.1007/s12011-013-9870-x
(198) Saper, R. B.; Phillips, R. S.; Sehgal, A.; Khouri, N.; Davis, R. B.; Paquin, J.; Thuppil, V.; Kales, S. N. Lead, Mercury, and Arsenic in US- and Indian-Manufactured Ayurvedic Medicines Sold via the Internet. *JAMA* **2008**, *300*, 915–923. https://doi.org/10.1001/jama.300.8.915
(199) Martena, M. J.; Van Der Wielen, J. C. A.; Rietjens, I. M. C. M.; Klerx, W. N. M.; de Groot, H. N. D.; Konings, E. J. M. Monitoring of mercury, arsenic, and lead in traditional Asian herbal preparations on the Dutch market and estimation of associated risks. *Food Addit. Contam. Part A* **2010**, *27*, 190-205. https://doi.org/10.1080/02652030903207235
(200) Kumar, A.; Nair, A. G. C.; Reddy, A. V. R.; Garg, A. N. Availability of essential elements in bhasmas: Analysis of Ayurvedic metallic preparations by INAA. *J. Radioanal. Nucl. Chem*. **2006**, *270*, 173–180. https://doi.org/10.1007/s10967-006-0326-z
(201) Sharma, S.; Dhingra, P.; Pandey, R. S. Trace determination of Pb, Cu, Cd and Zn in Ayurvedic, drug, "Mahayograj Guggulu" via polarographic technique. *J. Indian Chem. Soc*. **2008**, *85*, 962–965.

(202) Mahawatte, P.; Dissanayaka, K. R.; Hewamanna, R. Elemental concentrations of some Ayurvedic drugs using energy dispersive XRF. *J. Radioanal. Nucl. Chem*. **2006**, *270*, 657–660. https://doi.org/10.1007/s10967-006-0444-7

(203) Khandpur, S.; Malhotra, A. K.; Bhatia, V.; Gupta, S.; Sharma, V. K.; Mishra, R.; Arora, N. K. Chronic arsenic toxicity from Ayurvedic medicines. *Int. J. Dermatol.* **2008**, *47*, 618–621. https://doi.org/10.1111/j.1365-4632.2008.03475.x

(204) Saper, R. B.; Kales, S. N.; Paquin, J.; Burns, M. J.; Eisenberg, D. M.; Davis, R. B.; Phillips, R. S. Heavy Metal Content of Ayurvedic Herbal Medicine Products. *JAMA* **2004**, *292*, 2868–2873. https://doi.org/10.1001/jama.292.23.2868

(205) Giacomino, A.; Abollino, O.; Malandrino, M.; Karthik, M.; Murugesan, V. Determination and assessment of the contents of essential and potentially toxic elements in Ayurvedic medicine formulations by inductively coupled plasma-optical emission spectrometry. *Microchem. J*. **2011**, *99*, 2–6. https://doi.org/10.1016/j.microc.2011.01.002

(206) Oomen, A. G.; Hack, A.; Minekus, M.; Zeijdner, E.; Cornelis, C.; Schoeters, G.; Verstraete, W.; Van de Wiele, T.; Wragg, J.; Rompelberg, C. J. M. et al. Comparison of Five In Vitro Digestion Models To Study the Bioaccessibility of Soil Contaminants. *Environ. Sci. Technol*. **2002**, *36*, 3326–3334. https://doi.org/10.1021/es010204v

(207) Koch, I.; Moriarty, M.; House, K.; Sui, J.; Cullen, W. R.; Saper, R. B.; Reimer, K. J. Bioaccessibility of lead and arsenic in traditional Indian medicines. *Sci. Total Environ*. **2011**, *409*, 4545–4552. https://doi.org/10.1016/j.scitotenv.2011.07.059

(208) Koch, I.; Moriarty, M.; Sui, J.; Rutter, A.; Saper, R. B.; Reimer, K. J. Bioaccessibility of mercury in selected Ayurvedic medicines. *Sci. Total Environ*. **2013**, *454-455*, 9–15. https://doi.org/10.1016/j.scitotenv.2013.02.089

(209) Bolan, S.; Kunhikrishnan, A.; Chowdhury, S.; Seshadri, B.; Naidu, R.; Ok, Y. S. Comparative analysis of speciation and bioaccessibility of arsenic in rice grains and complementary medicines. *Chemosphere* **2017**, *182*, 433–440. https://doi.org/10.1016/j.chemosphere.2017.04.126

(210) Giacomino, A.; Abollino, O.; Casanova, C.; La Gioia, C.; Magi, E.; Malandrino, M. Determination of the total and bioaccessible contents of essential and potentially toxic elements in ayurvedic formulations purchased from different commercial channels. *Microchem. J.* **2015**, *120*, 6–17. https://doi.org/10.1016/j.microc.2014.12.005

(211) California Office of Environmental Health Hazard Assessment (OEHHA). Proposition 65 in Plain Language. https://oehha.ca.gov/proposition-65/general-info/proposition-65-plain-language [Accessed 28 November 2021].

(212) Tessier, A.; Campbell, P. G. C.; Bisson, M. Sequential extraction procedure for the speciation of particulate trace metals. *Anal. Chem*. **1979**, *51*, 844–851. https://doi.org/10.1021/ac50043a017

(213) Koch, I.; McPherson, K.; Smith, P.; Easton, L.; Doe, K. G.; Reimer, K. J. Arsenic bioaccessibility and speciation in clams and seaweed from a contaminated marine environment. *Mar. Pollut. Bull*. **2007**, *54*, 586–594. https://doi.org/10.1016/j.marpolbul.2006.12.004

(214) Vinas, P.; López-Garcia, I.; Merano, B.; Cempillo, N.; Hernández-Córdoba, M. Speciation of arsenic in baby foods and the raw fish ingredients using liquid chromatography-hydride generation-atomic absorption spectrometry. *Chromatographia* **2003**, *57*, 611–616. https://doi.org/10.1007/BF02491737

(215) Moreda-Pineiro, A.; Moreda-Pineiro, J.; Herbello-Hermelo, P.; Bermejo-Barrera, P.; Moniategui-Lorenzo, S.; López-Mahía, P.; Prada-Rodríguez, D. Application of fast ultrasound water-bath assisted enzymatic hydrolysis – High performance liquid chromatography–inductively coupled plasma-mass spectrometry procedures for arsenic speciation in seafood materials. *J. Chromatogr. A* **2011**, *1218*, 6970–6980. https://doi.org/10.1016/j.chroma.2011.07.101

(216) Almela, C.; Laparra, J. M.; Vélez, D.; Barberá, R.; Farré, R.; Montoro, R. Arsenosugars in Raw and Cooked Edible Seaweed: Characterization and Bioaccessibility. *J. Agric. Food Chem*. **2005**, *53*, 7344–7351. https://doi.org/10.1021/jf050503u

(217) Pardo-Martínez, M.; Vinas, P.; Fisher, A.; Hill, S. J. Comparison of enzymatic extraction procedures for use with directly coupled high performance liquid chromatography-inductively coupled plasma mass spectrometry for the speciation of arsenic in baby foods. *Anal. Chim. Acta* **2001**, *441*, 29–36. https://doi.org/10.1016/S0003-2670(01)01070-4

(218) Bhowmick, S.; Pramanik, S.; Singh, P.; Mondal, P.; Chatterjee, D.; Nriagu, J. Arsenic in groundwater of West Bengal, India: A review of human health risks and assessment of possible intervention options. *Sci. Total Environ*. **2018**, *612*, 148-169. https://doi.org/10.1016/j.scitotenv.2017.08.216

(219) Bolan, S.; Kunhikrishnan, A.; Seshadri, B.; Choppala, G.; Naidu, R.; Bolan, N. S.; Ok, Y. S.; Zhang, M.; Li, C.-G.; Li, F.; et al. Sources, distribution, bioavailability, toxicity, and risk assessment of heavy metal(loid)s in complementary medicines. *Environ. Int.* **2017**, *108*, 103–118. https://doi.org/10.1016/j.envint.2017.08.005

(220) Cubadda, F.; Jackson, B. P.; Cottingham, K. L.; Van Horne, Y. O.; Kurzius-Spencer, M. Human exposure to dietary inorganic arsenic and other arsenic species: State of knowledge, gaps and uncertainties. *Sci. Total Environ.* **2017**, *579*, 1228-1239. https://doi.org/10.1016/j.scitotenv.2016.11.108

(221) Arslan, B.; Djamgoz, M. B. A.; Akün, E. Arsenic: A Review on Exposure Pathways, Accumulation, Mobility and Transmission into the Human Food Chain. In: Gunther, F. A.; de Voogt, P. (Eds.) *Reviews of Environmental Contamination and Toxicology*, Vol. 243 of Springer Reviews of Environmental Contamination and Toxicology (Continuation of Residue Reviews). Springer, Cham, **2016**, 27-51. https://doi.org/10.1007/398_2016_18

(222) Ardini, F.; Dan, G.; Grotti, M. Arsenic speciation analysis of environmental samples. *J. Anal. At. Spectrom*. **2020**, *35*, 215-237. https://doi.org/10.1039/C9JA00333A

Brazilian Journal of Analytical Chemistry
2022, Volume 9, Issue 36, pp 52–77
doi: 10.30744/brjac.2179-3425.RV-123-2021

BrJAC

REVIEW

Ambient Ionization Mass Spectrometry: Applications and New Trends for Environmental Matrices Analysis

Andréa Rodrigues Chaves* ✉, **Rafael Oliveira Martins**, **Lanaia Ítala Louzeiro Maciel**, **Allyster Rodrigues Silva**, **Daniel Vieira Gondim**, **Júlia Martins Fortalo**, **Steffany de Souza Santos**, **Jussara Valente Roque**, **Boniek Gontijo Vaz**

Instituto de Química, Universidade Federal de Goiás, Avenida Esperança s/n, Câmpus Samambaia, 74690-900, Goiânia, GO, Brazil

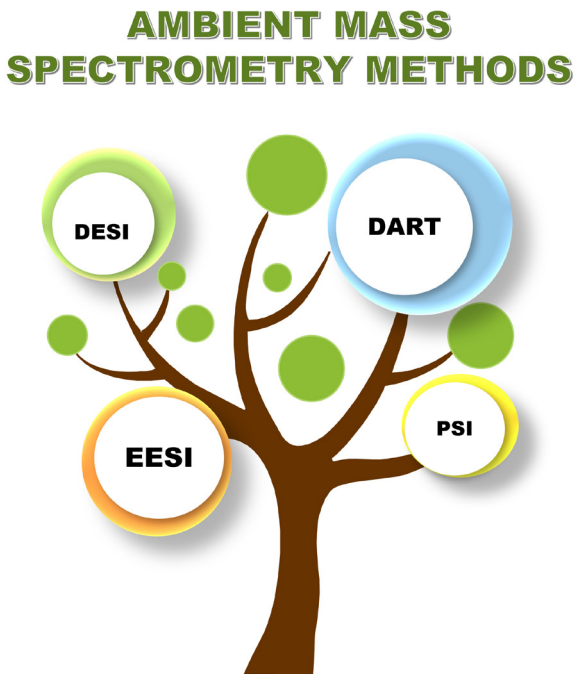

Since its introduction, ambient mass spectrometry methods have been demonstrated as potential approaches for a rapid and sensitive analysis of many compounds in complex matrices with a minimum or no sample preparation step performed. Some of these methods include low-cost devices and *in situ* methodologies that are included in the new trend of green analytical chemistry. The application of ambient methods for environmental analysis has been reported in the last decades for qualitative and quantitative analysis. This study aims to contribute with an overview of the 2016 to 2021 period of ambient mass spectrometry methods for applications in environmental analysis. In this context, this review reports especially applications for qualitative and quantitative analysis of contaminants using desorption electrospray ionization (DESI), direct analysis in real-time (DART), paper spray ionization (PSI), and extractive electrospray ionization (EESI) methods.

Keywords: Ambient mass spectrometry, Environmental, Green chemistry, Complex matrices, Environmental analysis

Cite: Chaves, A. R.; Martins, R. O.; Maciel, L. I. L.; Silva, A. R.; Gondim, D. V.; Fortalo, J. M.; Santos, S. S.; Roque, J. V.; Vaz, B. G. Ambient Ionization Mass Spectrometry: Applications and New Trends for Environmental Matrices Analysis. *Braz. J. Anal. Chem.* 2022, *9* (36), pp 52–77. http://dx.doi.org/10.30744/brjac.2179-3425.RV-123-2021

Submitted 29 Dec 2021, Resubmitted 1th time 04 March 2022, Resubmitted 2nd time 30 March 2022, Accepted 31 March 2022, Available online 07 April 2022.

INTRODUCTION

The constant and technological progress of the industrial and agricultural sectors in recent decades has brought with it improvements over the obtention of products related to these sectors.[1] However, at the same time, the anthropogenic activity of humans in the environment because of these advances has also increased.[2-4] Currently, anthropogenic activities represent the potential of humanity to interfere with the natural balance of the environment.[1]

The monitoring of some compounds, especially those harmful to the environment, is a requirement for the control of the contaminants in environmental matrices. However, this monitoring is a challenge for analytical methods due to these contaminants in many cases being found at trace concentration levels and in the presence of endogenous compounds that act as interferents.[5,6] Thus, the development of analytical methodologies for the analysis of contaminants represents a promising approach for the adequate monitoring of contaminants.

During the last decades, analytical methodologies such as ambient mass spectrometry (AIMS) methods have been introduced, these methodologies can overcome the use of laborious sample preparation steps which demands time and uses considerable solvent volume. The development of AIMS methodologies with high sensitivity and selectivity, and devices capable of performing *in situ* analysis helps to overcome the sample preparation methods drawbacks. These AIMS methodologies and devices can improve the qualitative and quantitative information on many samples, such as environmental matrices.[6]

AMBIENT MASS SPECTROMETRY (AIMS)

In general, electrospray ionization (ESI) represents an approach used to generate ions from the sample solution, especially for polar compounds.[7] Although ESI and other atmospheric pressure ionization (API) sources are capable to generate ions from many matrices, these traditional ionization methods still need an extensive sample preparation step before the analysis. These methods usually include the hyphenation of the mass spectrometer and a separation system, such as liquid chromatography (LC) and gas chromatography (GC).[6,8] On the other hand, AIMS methods allow the analysis of compounds in an open environment using minimal or no sample preparation, resulting in some devices that cover the trend of point-of-care (POC) analysis, which has been higher desirable by testing and diagnostics methods routine.[7] The literature methodologies reporting the use of techniques by AIMS have shown benefits in comparison with conventional ionization techniques, such as smaller sample volume requirement, little or no use of organic solvents, the elimination of the separation step by sample preparation, or chromatographic methods, and the improve of the method sensitivity and lower time of analysis.[6]

The AIMS concept was first introduced in 2004 by Cooks *et al*.[9] in which the use of desorption electrospray ionization (DESI) technique for the analysis of compounds present in tomato peel (*Lycopersicon esculentum*) and *Conium maculatum* seeds was reported. In this first application, it was proved to be an efficient approach for analysing the chemical profile and identifying the compounds present in the samples. In general, AIMS methods can be classified into two groups, that is spray-based (ESI-like) and plasma-based (APCI-like) methods. The spray-based approach includes the extractive electrospray ionization (EESI), easy ambient sonic-spray ionization (EASI), paper spray (PSI), probe electrospray ionization (PESI), and laser ablation electrospray ionization (LAESI) methods. In resume, this category involves momentum desorption, solvent extraction, and finally the ionization of the solution. The plasma-based methods include the direct analysis in real-time (DART), low-temperature plasma (LTP), dielectric barrier discharge ionization (DBDI), atmospheric pressure solids analysis probe (ASAP), and flowing atmospheric-pressure afterglow (FAPA). This category uses an electrical discharge between two electrodes in a gas flow to make the ionization of the target analyte (s).[6]

Since its introduction, AIMS techniques have brought great advances in the development of analytical methods, involving some fast and sensitive methodologies for a wide variety of analytes in different matrices, especially for environmental analysis (Figure 1) and (Table I).[8,9]

The upward trend in AIMS-related research can also be seen on platforms such as the Web of Science. The reports in such platforms have shown the increasing on the publications related with ambient mass spectrometry. Following this trend, applications of AIMS methods in environmental sciences has also been pointed out as an interesting field to the application of such methods and devices (Figure 2). Considering this, a discussion of the publications from the period of 2016-2021 on some AIMS methods for environmental matrices is presented in this revision study, as well as the trends for the future of the ambient methods for environmental analysis.

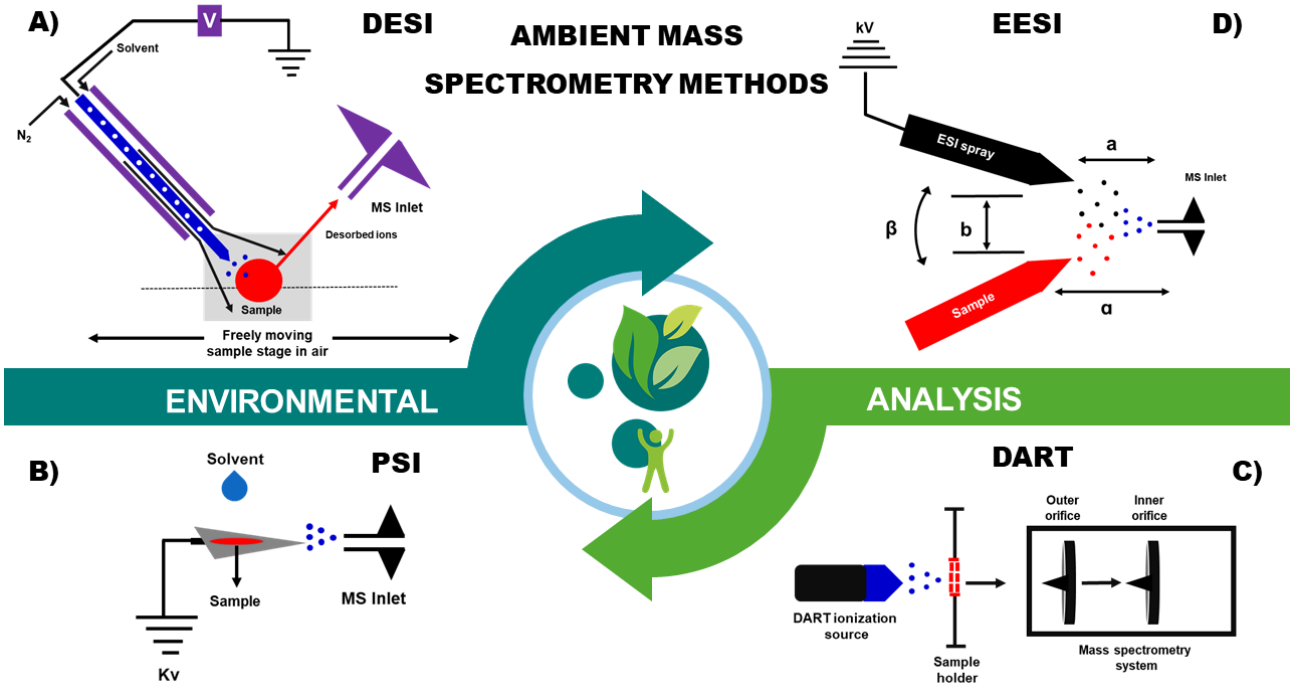

Figure 1. Ambient mass spectrometry techniques combined with environmental analysis.

Table I. Methods described in the literature using ambient mass spectrometry applied to environmental analysis

Analyte(s)	Sample	Analytical Methodology	LOQ	LOD	Recovery (%)	Ref
Perfluoroalkyls	Plants	DESI-MS HAS EDS	0.3-0.5 ng g^{-1}	0.09-0.15 ng g^{-1}	87.5-114.9	12
Dimethoate, trifloxystrobin, and tebuconazol	Olive and vine leaves	DESI-MS	50.0-150.0 ng g^{-1}	15.0-50.0 ng g^{-1}	-	13
32 pesticides	Fruit	DESI-MS	-	1.0 pg mm^2	88.0	14
Ionic liquids	Fish	DESI-MS	-	-	-	15
Duomeen O (n-oleyl-1,3-diaminopropane)	Industrial waters	PSI-MS/MS	-	< 0.1 pg	-	16
Acephate Cyazofamide Chlorpyrifos	Tomato peel	PSI-MS	0.03 mg g^{-1}	0.01 mg g^{-1}	90.4-96.4	17
Bisphenol A and S	Thermal paper	PSI-MS	87.0 ng g^{-1} / 13.0 ng g^{-1}	5.0 ng g^{-1} 1.9 ng g^{-1}	92.0 - 109.0	18
Metaldehyde	Water	PSI-MS/MS	-	0.05 ng mL^{-1}	-	19
Microcystins	Water	PSI-MS	3.0 μg L^{-1}	1.0μg L^{-1}	77.0 - 103.6	20
Tetrabromobisphenol A	Tap water Springwater Lake water	SPME-PSI-MS	0.001 μmol $^{-1}$	-	95.1 - 101.6	21
U, Bi, Pb, Cd, Fe and Zn	Cotton	PSI-MS	-	94.0 ng	-	22

(To be continued in the next page)

Table I. Methods described in the literature using ambient mass spectrometry applied to environmental analysis (Continuation)

Analyte(s)	Sample	Analytical Methodology	LOQ	LOD	Recovery (%)	Ref
Phenoxycarboxylic acids	Environmental waters	DART-MS	-	0.5-2.0 ng L^{-1}	79.9-119.1	23
Triazine Herbicides	Tap water, pool, and lake	DMSPE-DART-MS	-	1.6-152.1 ng L^{-1}	87.5-115.0	24
Phthalic Acid Esters	Environmental water	SSE-DART-MS	-	0.1-0.9 ng $^{-1}$	82.8–119.0	25
Microplastics and Nanoplastics	Natural waters	DART-MS	100.0 pg L^{-1}	30.0 pg L^{-1}	60.0-70.0	26
Pesticides	Surface water	SPME-TM-DART/MS	0.1-5.0 µg kg $^{-1}$	-	-	27
Pesticides	Lettuce and celery	QuPPe-DART-HRMS	50-190.0 µg kg 1	20.0-60.0 µg kg^{-1}	71.0-115.0	28
Steroid hormone	Residual water	DART-MS	-	2.5 ng L^{-1}	-	29
Trimethyl phosphate	Residual water	DART-MS/MS	50.0 pg mL^{-1}	0.05-100.0 ng mL^{-1}	88.0-107.6	30
Organic UV filters	Environmental water	DART-MS	-	40.0 ng L^{-1}	-	31
Glycosides	Tobacco Leaves	DART-MS	0.05-0.1 µg mL^{-1}	0.02-0.05 µg mL^{-1}	-	32
Tetrabromobisphenol A	Wastewater, river water and tap water	EESI-MS	-	0.05-4.6 µg L^{-1}	-	33

DESI-MS: Desorption electrospray ionization-mass spectrometry**; HAS-EDS:** transmission electron microscopy equipped with energy-dispersive spectroscopy**; PSI-MS:** Paper spray ionization mass spectrometry; **PSI-MS/MS:** Paper spray ionization-mass spectrometry tandem; **SPME-PSI-MS:** Solid-phase microextraction-paper spray ionization-mass spectrometry; **DART-MS**: Direct Analysis in Real-Time – Mass Spectrometry; **DMSPE-DART-MS:** Dispersive Magnetic Solid-phase Extraction - Direct Analysis in Real-Time - Mass Spectrometry; **SSE-DART-MS:** Sorbent and Solvent co-enhanced - Direct Analysis in Real-Time - Mass Spectrometry; **SPME-TM-DART-MS:** Solid Phase Micro Extraction - Transmission Mode - Direct Analysis in Real-Time - Mass Spectrometry; **QuPPe-DART-HRMS:** Quick Polar Pesticides Extraction - Direct Analysis in Real-Time - High-Resolution Mass Spectrometry; **DART-MS/MS:** Direct Analysis in Real-Time – Mass Spectrometry tandem; **EESI-MS:** extractive electrospray ionization mass spectrometry.

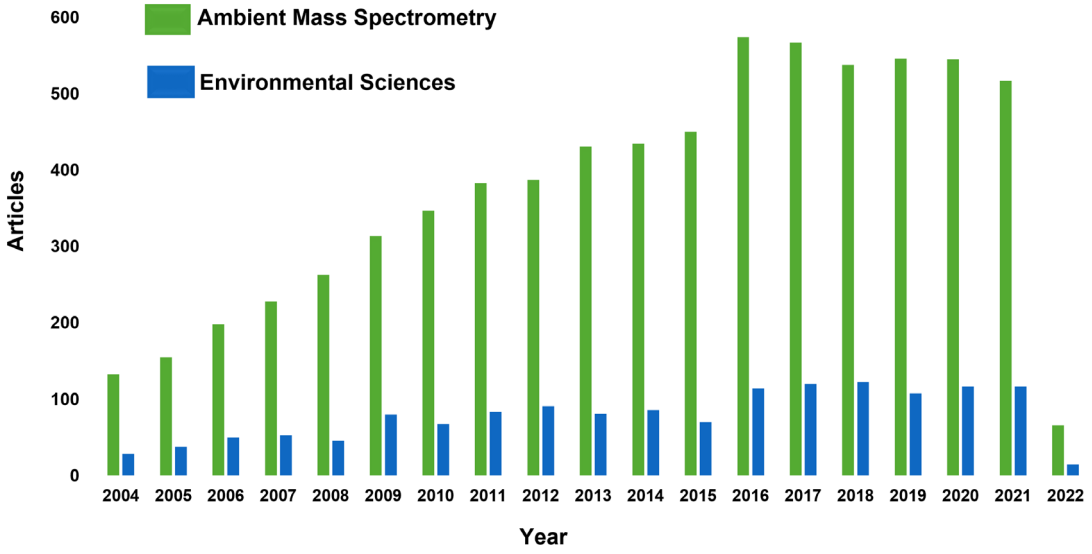

Figure 2. Publication numbers per year, using 'Ambient Mass Spectrometry' and 'Environmental sciences' as search words. Publication until Feb 2022. Source: www.webofscience.com

Desorption electrospray ionization desorption (DESI)

DESI technique was developed by Cooks *et al.* in 2004.[34] DESI belongs to the family of AIMS techniques and mass spectrometry imaging (MSI). In MSI analysis, chemical images are generated by plotting the signal intensities of the analyte of interest in a 2D or 3D space corresponding to the area of the sample that was analysed (Figure 1A). Through the application of DESI technique, it is possible to locate the spatial distribution of certain compounds in a sample of interest.[35] Because of the speed, sensitivity, and the possibility to perform *in situ* analysis, DESI technique has been highlighted as a potential approach to the development of surface analysis studies.[36]

In DESI ion desorption process, a primary spray is formed, with electrically charged solvent drops (less than 10 μm),[37] under high pressure of an inert gas jet in high-velocity (about 100 m s^{-1}) that reaches the sample on a glass slide.[38,39] This impact creates a thin layer of solvent that results in a solid-liquid extraction of the sample.[39] Then, the desorption of the analyte(s) occurs due to the shock of the primary spray. A secondary spray is formed containing the sample, and the analytes are then attracted to the mass spectrometer inlet.[40] The ionization of the technique creates single or multiple ions, in a mechanism exactly of what is observed in an ESI interface.[41] In this technique, changes in spray solvents are used to obtain good sample selectivity in a non-destructive way.[42]

The application of DESI in imaging analysis allows the visualization of biomolecules from a sample surface.[43] The MSI approach has been highlighted in literature to be manly performed in studied of the chemical profile of many biomolecules, such as metabolites,[44] lipids,[45] and proteins.[46] In DESI-imaging, an unidirectional scan on the x-axis of the sample is performed, in which each line on the x-axis results in a mass spectrum. The sample is located on a moving platform on the y-axis, enabling the next row to be parsed.[47] It is important to emphasize that this movement is repeated, the analytes of the next lines are not unduly removed, leading to the loss of information. The total area of the sample is divided into pixels. The distance between lines on the y-axis corresponds to 1 pixel and is the same distance on the x-axis. This distance corresponds to a spatial resolution that normally ranges from 150 μm to 250 μm. As desorption occurs continuously, it is necessary that the surface of the sample be smooth and flat, with no irregularities, after analysing the x and y axes, the generated spectra are merged to produce the images.[48,49]

The desorption efficiency of the analyte(s) is intrinsically linked to the optimization of some parameters in the geometric position of the DESI. The parameters that most influences the analysis are the angle of

incidence, which is the angle formed by the spray on the sample, the angle of ion collection, the distance between the sprayer and the surface, and the distance between the surface and the MS inlet, as shown in Figure 3.[50]

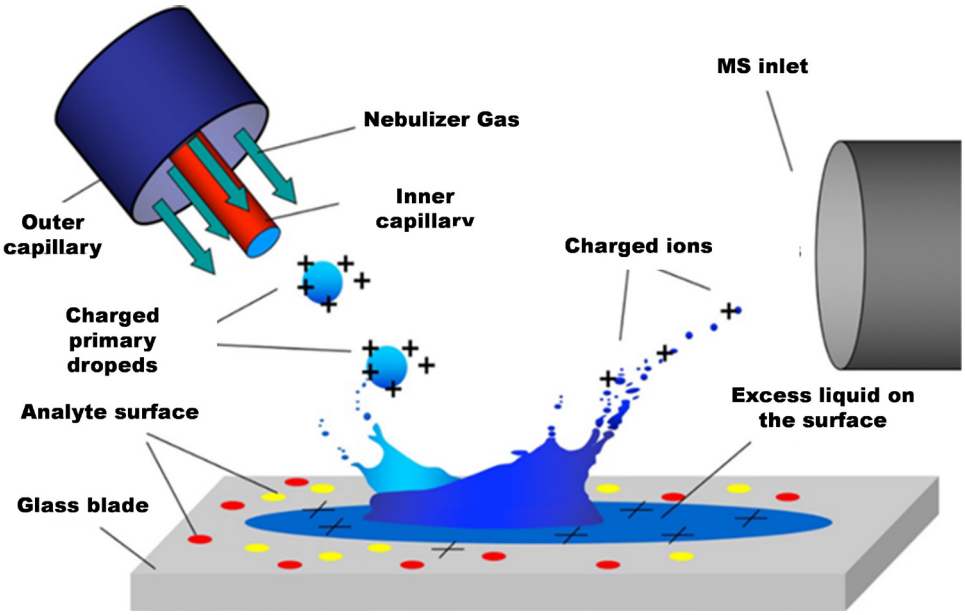

Figure 3. Scheme for geometric optimization of DESI.

Furthermore, the composition of the spray solvent is also a fundamental parameter for DESI desorption and ionization mechanism. The effect of the solvent on signal intensity and the resolution was extensively studied by Green *et al*.[51] The most used solvent composition is methanol and water, however, there are other solvent reported that include methanol (MeOH), acetonitrile (ACN), ethanol, dimethylformamide (DMF), among others.[52] Solvent optimization improves ionization efficiency and the method sensitivity.[51] Other parameters must be optimized for each sample, these parameters include the pressure of the nebulizing gas and the conditions in the mass spectrometer, all these parameters are directly linked to the obtained response.

DESI technique is widely used for biological samples, mainly for brain tissue in clinical case studies.[38,53–55] However, the literature points out the application in forensic chemistry,[56] metabolomics,[57] food,[14] and environmental analysis.[12]

Recently, Wang *et al.*[12] verified the absorption potential of perfluoroalkyl substances (PFASs) in plants using desorption electrospray ionization-mass spectrometry (DESI-MS) and transmission electron microscopy equipped with energy-dispersive spectroscopy (TEM-EDS). Within the PFASs group, perfluorooctanoic acid (perfluorooctanoic, PFOA) and perfluorooctane sulfonic acid (perfluorooctane sulfonic, PFOS) are the most representative substances, which present great risks of contamination to the environment and living beings. For the DESI-MS analysis, eight wet plants were submitted to hydroponic experiments (soilless cultivation technique) to visualize their distribution at tissue and cell levels. These plants were incubated for 1 month with PFOA and PFOS solutions washed with deionized water and divided into roots, stems, and leaves. The optimized DESI parameters were optimized, and results showed that the PFASs accumulated in the plants represented 1.67-6.7% of the total mass added to the hydroponic systems, and PFOS accumulated mostly in the roots (48.8-95.8%), while the PFOA was stored mainly in the aerial part (29.3-77.4%). DESI-MS and TEM-EDS analysis showed that PFASs were transported from the hydroponic root solution via both apoplastic (through cell walls and/or intercellular spaces) and symplastic pathways (through plasma membranes or via plasmodesma). Thus, DESI-MS and TEM-EDS

techniques demonstrated to be efficient approaches applied to visualization, tracking, absorption, and transport of PFOS and PFOA in plants.

DESI technique was also used as an interface in the analysis of the pesticides dimethoate, tebuconazol, and trifloxystrobin in olive and vine leaves by Rocca *et al*.[13] This study aimed to assess the exposure of workers during the application of these agrochemicals on crops, as evidence suggested serious adverse effects and chronic occupational exposure. The compositional mixture of the solvent used was methanol/water (80:20 v/v). This mixture showed great efficiency in the desorption of these analytes in the leaves of olive trees and vines. The three pesticides were analysed and validated using figures of merit. The validation showed weakness in intra-day precision, in which field analyses required more repetitions for reliability, which could suggest disadvantages in quantitative assays by DESI-MS. In addition, the actual monitoring of samples was close to the last point of the calibration curve, showing an excessive concentration of pesticides in the leaves. Although the DESI-MS methods had shown lower precision in the quantitative assay, the developed method showed advantages such as low solvent consumption (less environmental impact), absence in sample preparation, and reduced analysis time.

Gerbig *et al.*[14] applied DESI technique to detect 32 pesticides in nine different fruit samples. The surface of these fruits was pressed into glass slides to promote the passage of these pesticides onto a flat surface. The method showed great potential for quick and simple screening of food items. This was demonstrated using real samples taken from routine controls. Thus, it was also shown that DESI-MS could perform non-destructive actions in qualitative and semi-quantitative measurements. Although quantifying directly from the sample surface has limitations, the concentrations determined were in the same order of magnitude as the reference values and served as an indicator for deciding whether the product should be reanalyzed by another analytical method.

An approach to the toxicity of ionic liquids in zebrafish was reported by Perez *et al*.[15] The authors found after the images of these fish using DESI, that the liquid AMOENG 130 accumulated in the central and respiratory nervous system and could pass through the blood-brain barrier (“filter” formed by cells and nervous tissue). This was the first report on the use of the image produced by DESI to determine the distribution and metabolism of an ionic liquid in an aquatic vertebrate and demonstrated the potential of this technique to monitor other micropollutants in aquatic vertebrates.

Paper Spray ionization (PSI)

PSI technique was first introduced in 2010 by Cooks *et al*.[22] This AIMS method as the name suggest, uses a paper with a triangular shape connected to a macroscopic sharp tip.[58,59] The ionization of the analytes occurs after the application of the sample on the center of the paper’s surface with later application of a voltage (2 to 5kV),[60] finally the application of an acid or basic solvent onto the paper promotes the desorption of the analytes, this process leads to a generation of a Taylor cone spray which is taken towards the mass spectrometer inlet (Figure 1B).[61] The analysis is performed in two modes, positive and negative, according to the properties of the target analyte(s).[62,63] The ionization efficiency of the analyte(s) is intrinsically linked to its physicochemical characteristics, an effective interaction between the target analyte and the paper substrate, and the optimization of some fundamental parameters, promotes a more sensitive method and a better analytical performance.[64,65]

Among the main parameters to be evaluated, the paper substrate and the solvent must be considered to obtain a high sensitivity methodology.[61] The solvent must dissolve the compound of interest in the paper substrate to its greatest extent via capillarity, moving it to the tip of the triangular paper. The spray solvent has the function of extracting and solubilizing the analyte of interest. The choice of solvent is critical in the development of the method.[66] Due to the porous nature of the paper substrate, it can retain or not elute the analyte throughout the paper. Changing solvents can influence on method detection limits. Aqueous solvents improve surface tension and spray stability, while chlorinated solvents proved to be efficient in increasing the corona discharge voltage potential.[67]

Different substrates can offer specific results, as they can have different composition, thicknesses, and porosity, contributing to hindering the effectiveness of ionization and the flow of analyte throughout the paper. The chromatography paper and filter paper are the most commonly used materials; however, the modification of the paper can be performed according to the analysis objectives.[62] Thinner papers with smaller pore diameters, in general, tend to reduce the analyte flow throughout the paper, which could increase the ionization efficiency.[68]

Another important parameter to be evaluated for the efficiency of spray formation, but sometimes neglected, is the angle of the tip of the paper concerning the MS inlet source. Signal intensity, spray current and electric field are dependent on the paper angle. Based on the usually applied electric field, the literature pointed out that the most used angle has been 30°. In addition to this, paper substrates can be laser cut, with this approach it is possible to obtain correct angulation and reproducible construction.[62] To obtain good results with this technique, in addition to the mentioned factors, it is also necessary to evaluate other factors that may influence, such as the sample volume the distance between the spectrometer inlet capillary and the tip of the paper, which in general, will also depend on the ionization ratio of the analyte of interest.[58]

Since its introduction, the technique has been widely used in many fields, such as in the clinical,[69,70] forensics,[67] foods,[71] and environmental.[19]

Jjunju *et al*.[16] reported the analysis of aliphatic primary alkyl corrosion inhibitor amines in water samples reacting PSI experiments using an LTQ Orbitrap Exactive instrument. To prove the analytical performance of the method, the PSI-MS method was applied in three different water samples including feedwater, condensate water, and boiler water from large medium pressure. The method was capable to achieve a low limit of detection (LOD) of 0.1 pg with reproducibility less than 10%. The MS/MS of the Duomeen O molecule at the LOD concentration eliminated the matrix effect of the water samples providing to be a potential qualitative approach to corrosion inhibitor amines in water samples analysis.

The indirect contact with toxic substances is one of the most concerning about human health, especially those with the capacity of being retained in environmental compartments.[72] Concerning this, Bernardo *et al*.[18] described the use of PSI-MS for the detection and quantification of bisphenol S (BPS) in three different commercially brands of thermal papers. The analytical performance of the method showed a LOD as low as 5 ng g^{-1} with recovery values ranging from 92.2 to 109.04%. The quantification of BPS in the three papers showed values ranging from 1.36 to 6.77 μg L^{-1}. According to the authors the developed method was comparable to conventional analysis such as LC-MS and GC-MS reported in literature for BPS analysis. Due to this, the developed PSI-MS method was pointed out as a promising approach to replace some conventional methods of determination of BPS and without any sample preparation.

Rodrigues *et al*.[73] in 2020 reported a PSI-MS methodology for the steroid hormones (levonorgestrel and algestona) determination in wastewater samples analysis. The authors described the paper modification with a paraffin barrier on the triangular paper. This simple modification improved the analyte flow throughout the paper and resulted in a better spray stability, according to the authors. The ionization conditions of the analytes involved the use of a spray voltage of 3.5 kV and collision energy of 35 eV. The performance of the proposed methodology was evaluated through the figures of merit, reaching the low limit of quantification (LOQ) below to 2.3 μg mL^{-1} and LOD below to 0.7 μg mL^{-1}, in addition recovery values ranging from 82 to 102%. According to the obtained results, the modification with paraffin described led to an increase in the sensitivity of the technique.

Recently, PSI-MS soil analysis was reported by Dowling *et al*.[74] for the detection of pharmaceuticals, drugs, and hydrolysis products of chemical agents used in weapons. The voltage for both analytes was optimized separately, being used about 4.5 kV for drug analysis and 4.0 kV for hydrolysis products of chemical agents. As could be seen, the voltage is optimized according to the analyte structure and physicochemical proprieties, the better MS response is chosen considering not only the analyte response but also equipment integrity. According to the authors, the methodology reported an alteration for soil analysis, which is usually performed by obtaining the crude soil extract after many sample preparations steps.

Soil analysis by PSI-MS was also reported by Liu *et al*.[75] in which they described the quantification of tetrabromobisphenol A (TBBPA) in soils and sediments. The analysis was performed together with an internal standard enriched with a stable isotope (13C12-TBBPA) for the quantification of the target analyte. Better results were obtained by the voltage used of -2 kV, the vertex angle of 30°, base length 14 mm, and lateral length 29 mm. The chosen distance between the tip of the paper and the mass spectrometer inlet was 6 mm. Among the analysed solvents, methanol was chosen as the best for extracting and transporting solvents. This study demonstrated an alternative to improve the quantitative performance of the PSI-MS methods using an internal standard compound. Under these conditions, it was obtained a linear range of 0.1-100 mg L^{-1} (R^2 = 0.9975) and recoveries values between 90.4%-101.1%, being possible to compare with other conventional methods.

In 2017, Kotthoff *et al*.[76] also performed the analysis of TBBPA in sediment samples using liquid chromatography coupled with atmospheric pressure photoionization tandem mass spectrometry (LC-APPI-MS/MS) and obtained recoveries values ranging from 71.5 to112.5% for sediments. In comparison with methodologies applying separation steps such as chromatography, the methodology applied by Liu *et al*.[75] showed similar or higher recovery values, in addition to having presented an analysis time of 1 minute for each sample. Differences in results compared to other methods can be attributed to the correlation of the internal standard of the isotope method. Without sample purification and chromatographic separation, the method achieved high sensitivity and low analysis time, which was shown to have great potential for routine analysis of emerging contaminants in soil samples.

The analysis of samples from some animals is an alternative to identify the effect of bioaccumulation in the environment, in which some compounds with an accumulating potential are retained in animals, especially those of aquatic origins, such as fish and some vertebrates. Having this in mind, Chun Wei *et al*.[77] reported the modification of a paper with graphene oxide and nylon membrane for the analysis of malachite green and its metabolites in freshwater fish. The modification of the paper with graphene and the nylon membrane led to a strong interaction between the electrons of the π-π bond of graphene oxide with the conjugated in-plane π electrons of the rigid triphenylmethane backbone of the malachite green, in addition to the strong electrostatic interaction between the hydrogen bonds of the malachite green molecule and the graphene oxide, favoring the interaction between them. As a result, in tests with aqueous solutions, more than 98% malachite green was adsorbed onto the modified paper. The analysis of fish tissue samples showed that a concentration of 0.65 μg kg^{-1} was obtained, which met the minimum performance limit (2 mg kg^{-1}) proposed by the European Commission to determine the sum of malachite green and its metabolite green leucomalachite in food products.

Another paper modification was proposed in 2019 by Zargar *et al*.[78] in which the modification of a porous graphene paper with a molecularly imprinted polymer (MIP) was described for the analysis of the pesticide propoxur in samples of tap water and water from crops through the source by mobility spectrometry ionic (IMS). The application of MIP was intended to offer greater selectivity for the target analyte, thus the pesticide itself was used as a template during the synthesis of MIP and later electroplated on the surface of the graphene paper. The modification of the paper led to obtaining a LOD of 0.3 ng mL^{-1} and a recovery ranging from 94 to 102%. Through the proposed methodology, the authors stated that compared to other methods described in the literature, the PSI method proved to be fast and effective in analysing the target analyte. The modification with the polymer MIP generated greater selectivity for the pesticide propoxur, increasing the sensitivity of the analyte for the detection technique, which compensated the non-selectivity of the IMS analysis.

Direct real-time analysis (DART)

The AIMS method known as DART was introduced by Cooks *et al.* in 2005,[79] months after the introduction of DESI. The technique was introduced with the main focus on performing rapid analyses at ambient pressure, belonging to the class of AIMS techniques based on plasma ionization.[80] In DART the ion source can be used to analyse solid liquid, and gaseous samples.[81] In a few words, DART ionization uses heated

metastable gas atoms that are capable to desorb and then ionize the target analyte(s).[82] DART ionization process is performed in the presence of an inert gas (usually helium or nitrogen) in a discharge chamber leaving the species in an excited (metastable) state, resulting in a flow of plasma gas.[83] Upon leaving the chamber, the metastable species encounter the sample, and the desorption and ionization of the analyte(s) occur, which is directed to the mass spectrometer inlet (Figure 1C), the ionization of the sample can generate positive and negative ions. When applied in positive ion mode, metastable species collide with atmospheric water molecules producing hydronium (Penning ionization) and subsequently, the ionization of the analyte occurs. In contrast, in the negative ion mode, clusters of negative ions composing water and oxygen molecules react to form negative ions of the analyte.[80,83]

The optimization of the DART method involves the study of the ionization gas applied (He or N_2) and its temperature, the distance between the gas output of the ionization source and the sampling hole of the mass spectrometer, the electrical potential responsible for producing a glow discharge and the gas flow.[83]

According to Sisco and Forbes,[82] although nitrogen can also be used as the ionization gas, helium is the most commonly used in DART analysis. This preference of helium instead nitrogen is because of its energy to ionize water of the metastable atoms. In positive mode, the ionization mechanism is driven by the ionization of water in the atmosphere. The ionization mechanism can be seen in Equations 1–4 as follows:

$$He^{*} + H_2O \longrightarrow He + H_2O^{+\bullet} + e^{-} \quad (1)$$

$$H_2O^{+\bullet} + H_2O \longrightarrow H_3O^{+} + OH^{\bullet} \quad (2)$$

$$H_3O^{+} + nH_2O \longrightarrow [(H_2O)_{n+1} + H]^{+} \quad (3)$$

$$M + [(H_2O)_{n+1} + H]^{+} \longrightarrow [M+H]^{+} + (H_2O)_{n+1} \quad (4)$$

Robert *et al.* reported that the DART/orifice distance and the grid potential are parameters with significant influence on method efficiency, in which, the reduction of this distance and the increasing the potential from 250 V to 650 V, leads to an increase of the relative abundance of O2+• in the background mass spectrum of real-time direct analysis-mass spectrometry. Thus, these conditions benefit the formation of molecular ions, these parameters can be optimized and adjusted to the desirable conditions, in which the non-optimization of these parameters can lead to the two simultaneously ionization in the method (by proton transfer or by penning).[84]

Since the introduction of the DART technique in 2005, the literature has been reporting some applications in many scientific fields, such as food,[85] agriculture,[28] forensic,[86] clinical analysis,[87] and environmental analysis.[88]

In 2020, Nicolás Zabalegui *et al*.[89] reported the development of an analytical method based on a direct transmission mode analysis system in real-time quadrupole time-of-flight mass spectrometry (TM-DART-QTOF-MS) coupled with multivariate statistical analysis for the analysis of existing organic compounds in seawater samples in the surface microlayer (SML) and underlying water (ULW) collected on the Cape Verde Islands. The analysis involved the use of He as an ionizing gas at a temperature of 300 °C, in the negative ionization mode. The transmission mode geometry TM-DART was implemented as an optimization, which established a distance of 2.5 cm from the source, which allowed the analysis of samples in continuous flow and minimization of the risk of cross-contamination. From the methodology applied using DART, the authors found the possibility of differentiating the SLM and ULW samples through the chemical profile of both. In addition, the study pointed out that fatty acids, halogenated compounds, and organic compounds containing oxygenated boron were present in SML samples and could participate in photochemical reactions at the ocean air-water interface. According to the authors, one of the advantages of applying DART technique instead conventional electrospray methodologies for seawater analysis was to minimize the high salts concentration levels in the sample to MS analysis, not requiring desalination, which could result in a change of the matrix.

The analysis of microplastics in environmental water samples was recently described by Zhang *et al*.[88] For the analysis of microplastics, the samples were initially prepared, being heated by a ramp, starting at 50 °C and reaching 600 °C for 6 min. The products generated from this heating were taken to ionization by DART using helium as the reagent gas, a voltage of 350 V and heating of 300 °C, and analysis using the Orbitrap mass spectrometer. The application of the methodology for the analysis of microplastics led to the identification of plastics with different chemical profiles, and possibly from different origins, in which resulted in a mass spectrum exhibiting about ~ 10,000 discrete peaks, corresponding to plastic additives released by thermal desorption and degradation products of polymer generated by pyrolysis. Through the application of statistical data analysis, the chemical profile of plastics could be differentiated by creating a fingerprint for the analysis of each type of plastic.

Still on analysis of aquatic environments, Nei *et al*.[90] reported the use of DART-MS to estimate the concentration of histamine and 1,8-diaminooctane in fish fillets. The use of the DART-MS analysis method was applied to test the target analytes presented in 165 samples. According to the authors, the detection sensitivity was influenced by the temperature of the gas heater, and the temperatures between 350 and 450 °C resulted in larger and more defined peak areas. In addition, the matrix effect also affected and demonstrated by the recovery values of the developed method, (151.5 and 619.9%), in which, according to the authors, future studies would be necessary to reduce the matrix effect. However, the study proved to be a possible approach for analyzing mainly histamine, since it is a biogenic amine responsible for cases of food poisoning.

Emmons and Gionfriddo[91] reported a strategy to minimize one of the limitations of ambient mass spectrometry, which is the appearance of transient microenvironments (TME), that occur mainly in analyses that are carried out in variable and non-ideal conditions. For the study, the authors reported the use of solid-phase microextraction (SPME) with DART-MS coupled to a thermal desorption unit (TDU) for the analysis of pesticides and drugs from surface water. However, for more precise analysis, a new SPME geometry, SPME-Arrow shape, was used, which presented a greater improvement on extraction phase volume compared to conventional SPME fiber. This instrumentation used was an optimization of the conventional parameters of the DART technique. Furthermore, other parameters that were optimized regarding the ionization source were the localization of the TDU-DART device in the inlet of the mass spectrometer and the plasma temperature. During the analysis, three positions were tested: first in full contact, then a distance of 5mm, and finally 10mm. Meanwhile, for each position, the plasma was at different temperatures: 300, 350, and 450 °C, respectively, being capable to quantify the analytes in the range of μg L^{-1} with a time analysis of 5 minutes. The authors concluded that this study proved to be quite satisfactory, allowing further expansion of AIMS analysis into more complex samples and in unconventional environments, where the use of TDU-DART provided rapid and reliable on-site quantification.

Extractive electrospray ionization (EESI)

Before being known as extractive electrospray ionization, the EESI technique was first introduced as fused droplet electrospray ionization (FD-ESI) in 2002 by Shiea *et al*.[92] as an approach for the analysis of peptides and proteins. After this first introduction, the technique underwent extensive studies by other research groups, especially by Cooks *et al*.[93] In 2006 the technique was finally known as EESI, whose first application was in the analysis of biological matrices, reporting a methodology without any previous sample preparation.[94] The ionization mechanism involves the instrumental configuration using two sprays, one containing the solution for electrospray formation and connected to an energy source for the application of voltage, and the other spray with a neutral analyte solution. Then the two sprayers are placed in a certain position to form two converging streams (Figure 1D). In the gas phase, the particles containing the neutral analyte collide with the charged electrospray droplets, through this collision the analyte is extracted from the neutral drop to the charged electrospray drop forming the ions that are taken to the mass spectrometer inlet and then analyzed.[11,93,94]

As previously described, the system involves the use of two sprays that collide with each other. Thus, the parameters to be optimized for a better ionization efficiency involve the study of the formation of the two sprays.[95] In this context, the angles between the two nozzles (β) and between the nozzle containing the neutral analyte and the inlet of the mass spectrometer (α) should be optimized, being generally adjusted to 60° and 150° respectively. In addition to the angles, the distance between the two sprayers (b) and the inlet of the mass spectrometer (a) must be optimized to favor ionization, usually using distances of 0.5-20 mm and 3-15 mm respectively. In addition to these parameters, the flow of the sprayers must be controlled to favor an efficient collision between the charged spray and the neutral sample droplets.[6,81]

Despite having been introduced for the analysis of biological matrices, since its creation, the technique has been used in different scientific fields, such as cosmetic analysis,[96] drugs,[97] and also in the application in the environmental analysis.[6]

Recently, Giannoukos *et al*.[98] reported the use of the real-time detection of metals and trace elements in the production of biogas from the anaerobic digestion of manure and mixed organic sources, using an extractive electrospray ionization source coupled with time-of-flight mass spectrometry analysis (EESI-TOF-MS). The method optimization included the study of how the biogas interacted with the charged droplets of the spray. This study involved the evaluation of different proportions of N_2 (1/2, 1/5, and 1/10) as biogas diluent and N_2 flux. The optimization of the gas proportion and flow parameters led to the use of a 1:5 mixture of biogas: N_2 and a flow of 1.5 μL min^{-1}. Through the methodology, it was possible to compare the percentage of removal of 14 metals in installed adsorbent materials dedicated to the removal of organic contaminants. EESI quantification found that about 64% (for Cu), 60% (for Fe), 62% (for Zn), 36% (for Cd) and 100% (for Pb) were removed from the raw biogas. The application of the methodology proved to be an effective tool for monitoring the removal of metals in raw biogas, also assisting in the creation of cleaning and filtering protocols.

Although AIMS methods are not normally performed after some previous sample preparation, in some cases the application of a sample preparation step before the AIMS analysis can lead to an increase in the technique's sensitivity to achieve better analytical performance. In 2020, Liu *et al*.[99] described the use of internal extractive electrospray ionization (IESSI) ionization for the analysis of 15 organophosphate class pesticides (OPPs) in environmental water samples after enrichment by Fe_3O_4-ZrO_2 particles. The application of the material as a sample preparation step led to the removal of interfering agents present in the environmental samples and the concentration of OPPs. The proposed methodology showed LODs in the range of 0.14 to 16.39 ng L^{-1} and recovery values in the range of 85.4 to 105.9%. The application of EESI allowed the analysis of 15 pesticides in an analysis time of 1 min. The results showed that the application of a rapid pre-sample preparation can increase the sensitivity of the EESI technique, including high sensitivity, fast analysis, and selectivity for the detection of OPPs in environmental water samples.

Another application of previous sample preparation before analysis by EESI was described in 2018 by Kou *et al*.[100] in which the use of molecularly imprinted polymers and IEESI tandem analysis of fluoroquinolones (FQs) in environmental water samples was reported. The authors chose to use the MIP in a 0.22 μm filter, in which the water samples were eluted, and through a selective polymer interaction process, the FQ molecules were retained, and by applying electrospray as an elution solution, target analytes were eluted into the mass spectrometer inlet. Under the optimized conditions, the methodology offered LOD values ranging from 0.015 to 0.026 μg L^{-1} and recovery values from 91.14 to 103.60%. Although systems by AIMS do not normally use any previous sample preparation, the use of MIP's in this study allowed analyses by IESS in shorter times.

The analysis of pesticides in honey samples was described by Deng *et al*.[101] the authors reported the use of the neutral desorption-extractive electrospray ionization (ND-EESI) for the determination of organophosphate insecticides and two types of carbamate insecticides in commercial samples of honey without any previous sample preparation. The application of the methodology for the analysis of pesticides proved to be efficient for the determination of the analytes with LODs ranging from 1.16 to 4.18 ng g^{-1} and recovery values between 87 to 114.98%. The effect of the matrix on the analytes was the

parameter that most influenced the determination of pesticides. Of the five pesticides studied, only one (chlorpyriphos-methyl) had an average matrix effect on signal suppression, the others were not affected by the sample, this effect was attributed to the interaction of the pesticide with the sample. However, the proposed methodology using neutral desorption sampling gas to gently impact a surface led to a lower ion suppression which decreased the matrix effect observed for chlorpyriphos-methyl and improved real-time detection of other analytes in the sample without prior sample preparation.

In 2020, Gao *et al*.[102] applied EESI for the analysis of the chemical profile of nectar and honey samples from three citrus species. The analysis was performed by extractive electrospray ionization high-resolution mass spectrometry (EESI-HRMS), the results showed the presence of 12 polyphenols and 8 amino acids, while analysis by high-efficiency-detection liquid chromatography by ultraviolet (HPLC-UV) showed the presence of 9 polyphenols. Statistical analysis showed that the profile of the nectar samples was similar to each other, in the same way as the honey samples. However, through the results, it was possible to distinguish the nectar and honey samples by the differences between chemical composition. Compared to the HPLC-UV analysis, the EESI analysis showed greater detail in the presence of chemical components in the samples, without needing any separation step or previous sample preparation. According to the results, the EESI technique could not only be used for quantitative methods, but also for qualitative methods, especially for the differentiation of sample chemistry, through fast and sensitive methodologies.

NEW TRENDS FOR AIMS METHODS IN ENVIRONMENTAL ANALYSIS

Application of sample preparation methods for AIMS analysis

The combination of an adequate sample preparation with AIMS methodologies shown as an interesting tool either for sampling or to improve the selectivity and sensitivity of the MS analytical methods. In 2016, Fang *et al*.[103] reported on a review study, strategies, and applications of the SPME technique in association with AIMS methods. According to the authors, this combination can offer the opportunity for direct sampling and direct analysis of trace analytes in biological, environmental samples, forensics, food, small individual organisms, and even single-cell samples under open and environmental conditions.

The protective mask has become a reality for everyone, since 2019 due to an infection disease, known as COVID-19. Having this in mind, in 2020, Yuang *et al*.[104] reported the use of SPME fiber-containing different coatings (Polydimethylsiloxane, Polydimethylsiloxane /divinylbenzene, Carbon/ polydimethylsiloxane, and Carbon/polydimethylsiloxane/ divinylbenzene) into a face mask to *in vivo* sampling the aerosol of exhaled air by patients with the aim to screening the chemical profile of this aerosol by DART-MS. For this purpose, two SPME fibers were inserted into a face mask, after the sampling, one fiber was used for recording the full spectrum, the other was used to perform MS/MS analysis.

The related study showed a potential of sampling by SPME in the mask was appropriate to assess the chemical profile of breathed air. So, despite having been applied to the analysis of drugs, the authors point out that the methodology can be applied to other analyses that are directly linked to the respiratory quality of human beings. Thus, sampling by SPME and analysis by AIMS in an environmental context, can be used for the analysis of contaminants in the air, especially in large cities, to carry out the monitoring of these compounds in the daily life of large urban centers.

Another application of SPME containing a matrix-compatible coating together with DART-MS was reported in 2019 by Gómez-Rios *et al*.[27] for the analysis of pesticides in surface water. All the sampling processes of the SPME were performed in less than 3 min, after the sampling, the SPME fiber was placed at the DART inlet, and the analysis was performed in 4 min, showing the speed of the methodology. The applied methodology was capable to obtain LOQ's values of 0.1-5 μg Kg^{-1} for the 19 pesticides studied. The analysis offered the profile of pesticides in the samples, in addition to allowing their quantification in 2-minute per sample.

The application of the SPME technique directly to environmental samples was reported by Deng *et al*.[105] in which the authors described the coupling of SPME with ambient mass spectrometry ion source using a surface coated wood tip probe for ultra-trace perfluorinated compounds (PFCs) in water samples

analysis. The authors reported the modification with n-octadecyldimethyl[3-(trimethoxysilyl)propyl] ammonium chloride on the surface of a sharp wooden tip via silanization. The wooden tip is a desirable substrate for AIMS analysis due to its porous and hydrophilic properties. When applied some solvent and voltage, the material becomes conductive, and then an electrospray is generated. Furthermore, because of the of hydroxyl groups abundance, the material becomes an ideal candidate for the functionalization and modification of its surface. The optimized methodology presented LODs and LOQs values for PFCs analysis of 0.06-0.59 ng L^{-1} and 0.21-1.98 ng L^{-1} respectively. For last, quantification of real samples was performed by isotope internal standard calibration curve method or isotope dilution method, the results showed a range of PFCs from 0.95 to 15.95 ng L^{-1} for lake water, 0.55 to 20.1 ng L^{-1} for river water, 0.78 to 12.8 ng L^{-1} for whole blood, and 68.6 to 562.1 ng L^{-1} for milk samples showing its higher concentration of PFCs.

Electrospray laser ablation ionization (LAESI) applied for environmental analysis

The electrospray laser ablation ionization (LAESI) technique was introduced in 2007 by Nemes and Vertes.[106] The ionization consists in two-stage process.[107] In the first stage, it is created a fine mist of neutral droplets that is generated from the sample by contact with a pulsed mid-infrared (IR) laser, adjusted to the O-H stretch adsorption (2.94 μm). The ionization of the desorbed analytes from the sample is performed in the second stage, in which the interaction of the charged spray (ESI source) with the desorbed analytes promotes the ionization of the analyte(s) present in the sample (Figure 4A).[6,92,107,108] The eminent advantage of the technique is its ability to access more internal compounds in the sample and not just compounds present on the surface such as DESI. Thus, the LAESI technique brings the formation of chemical images as a function of depth (x, y, and z), due to IR laser ablation.[108] Since its introduction, the technique has been widely applied especially for cell and tissue analysis,[109,110] with few recent applications reported for analysis in environmental matrices.

In 2014, Beach *et al*.[110] described the analysis of the neurotoxin domoic acid (DA) in crustaceans by LAESI-MS/MS. The analysis of the muscle tissue of the crustacean samples compared with reference materials, led to the obtainment of a detection limit of 1 mg kg^{-1} and recovery values close to high-performance liquid chromatography-spectrometry methods of tandem masses (HPLC-MS/MS) (103-123%) in addition to analyses with times of up to 10 s for each sample. In the same year, Nielen and Beek[111] described the use of the Laser-ablation electrospray ionization-mass imaging (LAESI-IMS) to investigate the potential of the technique for obtaining macroscopic and microscopic images of pesticides, mycotoxins, and plant metabolites in rose leaves, orange and lemon fruits, ergot bodies, cherry tomatoes, and corn kernels. With the application of the technique, it was possible to quantify the analytes on the surface and inside the samples through laser penetration in contact with the different matrices, performing not only 2D images but also 3D images. The application of the technique in both studies showed the potential of the LAESI technique to carry out the mapping not only on the surface but also inside different samples with an environmental focus, in fast methodologies, and without sample preparation.

Recently, Vaz *et al*.[107] described the use of (LAESI imaging) to investigate the diffusion of the mycotoxin patulin from rotten to healthy areas of fruits. Although, this can be considered a food analysis, the environmental concerning of mycotoxins in food samples is due to its high toxicity in lower levels of concentration. Also, according with Escrivá *et al*.[112] due to the bioaccumulation of such secondary metabolites, they can cause their carry-over in animal fluid, organs and tissues, and consequently reach and affect human health. For the study, Vaz *et al*.[107] used slices of mold-infected and uninfected (control samples) apples and strawberries. The application of an infrared laser beam (2.94 μm) resulted in the ablation of the analytes. The application of LAESI as capable to achieve a LOD of 50 ng mL^{-1}. The visualization of the patulin was observed in all infected fruits in both diseased and healthy areas, these results suggested the diffusion of patulin from the mold-infected area.

Although there are not many works in the literature reporting the LAESI technique for environmental analysis, recently, Maloof *et al*.[113] described a literature review on the use of chemical imaging techniques

for environmental analysis, among them, the LAESI technique was discussed and showing possible trends for the technique that should be taken into account in this review.

The analysis of rocks and other environmental solids has always been considered a challenge, due to the difficulty of working with such matrices. However, imaging techniques such as LAESI have been proving to be an alternative to solve this problem. The analysis of rocks and other solid particles in the environment can provide important information, especially about where they were collected. Having this in mind, Gundlach-Graham *et al*.[114] reported the use of the low-dispersion laser ablation-inductively coupled plasma-mass spectrometry (LA-ICP-MS) for the analysis of metals in rock samples. The application of the technique showed a resolution of ~10 μm, proving to be effective for evaluating the chemical profile of environmental rocks.

The potential of this technique for environmental science lies in its functioning, allowing the analysis not only of the surface but also of the interior of the sample, which is a possible approach for the analysis of contaminants in difficult-to-work environmental matrices, such as rock samples. Furthermore, compared to other techniques based on electrospray, such as DESI, for example, the application of LAESI makes it possible to obtain 2D and 3D images, which makes it even more feasible to study the chemical profile of complex samples.

Perspectives in environmental analyses using the Nano-DESI technique

Another approach that has a few reports in the application in environmental analysis is Nano-DESI. This technique was first reported in 2010 by Roach *et al*.,[115] in which the conventional DESI resources are used, with some modified configurations. In summary, a solvent bridge is formed between two capillaries, and the surface is then analysed. One of the capillaries is responsible for providing the solvent for the extraction of analytes onto the surface. The second capillary promotes the transport of the solution containing the extracted analytes to the mass spectrometer inlet, through nano-spray self-aspiration (Figure 4B).[116,117] This technique has been constantly improving, showing until now high resolution and sensitivity, providing spatial distribution of surfaces analysed in great detail. The technique has been constantly improved showing resolutions of 200 μm and 20 μm for biological matrices and good sensitivity, providing adequate spatial distribution of surface analytes.[118]

Yin *et al*.[119] developed a Nano-DESI methodology, that happened the instrument fabrication to the processing of the obtained data, resulting in more sensitive and quantitative images of lipids and metabolites in biological matrices. A resolution better than 10 μm was possible by acquiring 104.400 pixels. The method for quantification was based on the use of internal standard and signal normalization to minimize the matrix effect, common in quantitative image analysis. The use of the internal standard and normalization requires special care, errors may represent inappropriate behavior of the analytes and may compromise the developed methodology. These advances show a great contribution to imaging via Nano-DESI, but the use of other complementary techniques such as HPLC may be necessary.

Like DESI, Nano-DESI can be applied in several areas, such as crude oil analysis,[120,121] analyses in biological matrices,[122,123] bacterial characterization,[124] pharmaceutical,[125] among others. Despite its wide application, its use in environmental matrices is few reported in the literature. In this context, approaches that integrate this area can be widely studied using this technique.

In 2014, Laskin *et al*.[126] analysed the molecular composition of organic matter in soil samples using the Nano-DESI technique. In this study, it was possible to molecularly characterize these samples without prior sample preparation, in short analysis time, high sensitivity, and low sample consumption. Nano-DESI made up the need for laborious extraction of organic matter from the soil, which usually uses large volume of organic solvents.[127] For these analyses, approximately 10 ng of organic mass was used, showing the effectiveness of this technique in an environmental matrix.

In summary, Nano-DESI is under constant development showing distinct applications to a wide range of analytes in different matrices. Having this in mind, the potential of application of this technique allows analyses with minimal or no sample preparation, low solvent consumption, low sample quantity, high

sensitivity, low analysis time, and better image resolution. Studies involving environmental matrices (ore, wood, rocks, pollutants, plants, among others) can help to unveil environmental states if better explored. Finally, the approximate ability to quantify analytes on a surface via Nano-DESI may open new doors for routine methods in the expression of pollutants in plants, for example.

As it was possible to observe, AIMS techniques also present the possibility of optimizing their resources, whether in the development of new approaches or the improvement of existing methodologies. However, there is still a lack of studies reporting the fabrication of devices capable of performing *in situ* analysis, in addition to the development of portable AIMS devices hyphenated to miniaturized mass spectrometers. Thus, studies are still needed, especially using consolidated techniques for biological samples, for their application in environmental matrices as a way of new approaches for rapid analysis of such complex matrices.

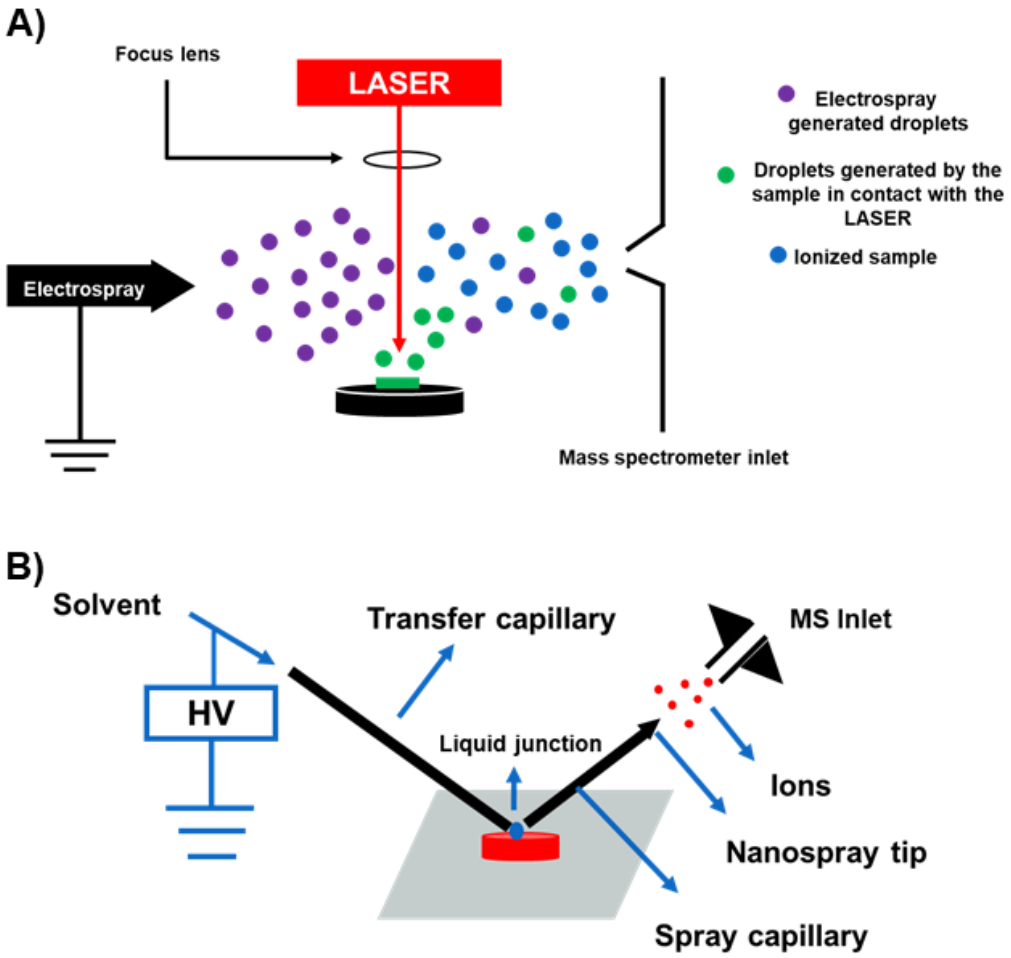

Figure 4. A) Schematic representation of the LAESI ionization mechanism, and B) Schematic representation of the Nano-DESI ionization mechanism

CONCLUSIONS

In this review, some of the main AIMS techniques that have been applied for the profile analysis and quantification of emerging contaminants in environmental matrices were discussed. Thus, it was possible to observe that the DESI, DART, PSI, and EESI techniques have wide application in environmental matrices, contributing to fast, sensitive, and high analytical performance analyses. Furthermore, when compared to existing conventional techniques, they show analytical capacity equal or superior in different analysis.

The techniques derived from the concepts established since the creation of DESI in 2004, bring with them advantages over conventional ionization techniques. The application of methodologies based on systems by AIMS shows analysis with a shorter analysis time than conventional techniques, lower consumption of organic solvents (highlighted in the concept of green chemistry). Advances in the development and optimization of systems by AIMS must meet the complexity of environmental matrices. Despite being techniques widely applied to biological matrices, imaging techniques such as DESI, Nano-DESI, and LAESI, which are few used in this scientific field, represent a new alternative for chemical monitoring of previously challenging matrices.

In general, the development of methodologies based on AIMS with a focus on environmental analysis still needs a more critical view, considering the development of *in situ* analysis systems, for quick and reliable analysis not only in large urban centers but also in remote locations, where the risk of contamination and lack of monitoring is greater.

Conflicts of interest

The authors declare no conflicts of interest.

Acknowledgements

This research was generously funded by CAPES, CNPq, and FAPEG.

REFERENCES

(1) Vieira Filho, J. E. R.; da Silveira, J. M. F. J. Mudança Tecnológica Na Agricultura: Uma Revisão Crítica Da Literatura e o Papel Das Economias de Aprendizado. *Rev. Econ. e Sociol. Rural* **2012**, *50* (4), 721–742. https://doi.org/10.1590/S0103-20032012000400008

(2) Wang, H.; Yang, Q.; Ma, H.; Liang, J. Chemical Compositions Evolution of Groundwater and Its Pollution Characterization Due to Agricultural Activities in Yinchuan Plain, Northwest China. *Environ. Res.* **2021**, *200*, 111449. https://doi.org/10.1016/J.ENVRES.2021.111449

(3) Zhang, R.; Ma, W.; Liu, J. Impact of Government Subsidy on Agricultural Production and Pollution: A Game-Theoretic Approach. *J. Clean. Prod.* **2021**, *285*, 124806. https://doi.org/10.1016/J.JCLEPRO.2020.124806

(4) Han, Q.; Liu, Y.; Feng, X.; Mao, P.; Sun, A.; Wang, M.; Wang, M. Pollution Effect Assessment of Industrial Activities on Potentially Toxic Metal Distribution in Windowsill Dust and Surface Soil in Central China. *Sci. Total Environ.* **2021**, *759*, 144023. https://doi.org/10.1016/J.SCITOTENV.2020.144023

(5) Ayala-Cabrera, J. F.; Santos, F. J.; Moyano, E. Recent Advances in Analytical Methodologies Based on Mass Spectrometry for the Environmental Analysis of Halogenated Organic Contaminants. *Trends Environ. Anal. Chem.* **2021**, *30*, e00122. https://doi.org/10.1016/J.TEAC.2021.E00122

(6) Chen, R.; Deng, J.; Fang, L.; Yao, Y.; Chen, B.; Wang, X.; Luan, T. Recent Applications of Ambient Ionization Mass Spectrometry in Environmental Analysis. *Trends Environ. Anal. Chem.* **2017**, *15*, 1–11. https://doi.org/10.1016/J.TEAC.2017.07.001

(7) Martins, R. O.; de Araújo, G. L.; de Freitas, C. S.; Silva, A. R.; Simas, R. C.; Vaz, B. G.; Chaves, A. R. Miniaturized Sample Preparation Techniques and Ambient Mass Spectrometry as Approaches for Food Residue Analysis. *J. Chromatogr. A* **2021**, *1640*, 461949. https://doi.org/10.1016/j.chroma.2021.461949

(8) Zhang, J.; Yu, W.; Suliburk, J.; Eberlin, L. S. Will Ambient Ionization Mass Spectrometry Become an Integral Technology in the Operating Room of the Future? *Clin. Chem.* **2016**, *62* (9), 1172–1174. https://doi.org/10.1373/clinchem.2016.258723

(9) Takáts, Z.; Wiseman, J. M.; Gologan, B.; Cooks, R. G. Mass Spectrometry Sampling under Ambient Conditions with Desorption Electrospray Ionization. *Science* **2004**, *306* (5695), 471–473. https://doi.org/10.1126/science.1104404

(10) GUO, X. Y.; HUANG, X. M.; ZHAI, J. F.; BAI, H.; LI, X. X.; MA, X. X.; MA, Q. Research Advances in Ambient Ionization and Miniature Mass Spectrometry. *Chinese J. Anal. Chem.* **2019**, *47* (3), 335–346. https://doi.org/10.1016/S1872-2040(19)61145-X
(11) ZHANG, X. L.; ZHANG, H.; WANG, X. C.; HUANG, K. K.; WANG, D.; CHEN, H. W. Advances in Ambient Ionization for Mass Spectrometry. *Chinese J. Anal. Chem.* **2018**, *46* (11), 1703–1713. https://doi.org/10.1016/S1872-2040(18)61122-3
(12) Wang, T. T.; Ying, G. G.; Shi, W. J.; Zhao, J. L.; Liu, Y. S.; Chen, J.; Ma, D. D.; Xiong, Q. Uptake and Translocation of Perfluorooctanoic Acid (PFOA) and Perfluorooctanesulfonic Acid (PFOS) by Wetland Plants: Tissue- A Nd Cell-Level Distribution Visualization with Desorption Electrospray Ionization Mass Spectrometry (DESI-MS) and Transmission Electron Microscopy Equipped with Energy-Dispersive Spectroscopy (TEM-EDS). *Environ. Sci. Technol.* **2020**, *54* (10), 6009–6020. https://doi.org/10.1021/ACS.EST.9B05160
(13) Mainero Rocca, L.; Cecca, J.; L'Episcopo, N.; Fabrizi, G. Ambient Mass Spectrometry: Direct Analysis of Dimethoate, Tebuconazole, and Trifloxystrobin on Olive and Vine Leaves by Desorption Electrospray Ionization Interface. *J. Mass Spectrom.* **2017**, *52* (11), 709–719. https://doi.org/10.1002/JMS.3978
(14) Gerbig, S.; Stern, G.; Brunn, H. E.; Düring, R.; Spengler, B.; Schulz, S. Method Development towards Qualitative and Semi-Quantitative Analysis of Multiple Pesticides from Food Surfaces and Extracts by Desorption Electrospray Ionization Mass Spectrometry as a Preselective Tool for Food Control. *Anal. Bioanal. Chem.* **2016**. https://doi.org/10.1007/s00216-016-0157-x
(15) Perez, C. J.; Tata, A.; de Campos, M. L.; Peng, C.; Ifa, D. R. Monitoring Toxic Ionic Liquids in Zebrafish (Danio Rerio) with Desorption Electrospray Ionization Mass Spectrometry Imaging (DESI-MSI). *J. Am. Soc. Mass Spectrom.* **2017**, *28* (6), 1136–1148. https://doi.org/10.1007/S13361-016-1515-9
(16) Jjunju, F. P. M.; Maher, S.; Damon, D. E.; Barrett, R. M.; Syed, S. U.; Heeren, R. M. A.; Taylor, S.; Badu-Tawiah, A. K. Screening and Quantification of Aliphatic Primary Alkyl Corrosion Inhibitor Amines in Water Samples by Paper Spray Mass Spectrometry. *Anal. Chem.* **2016**, *88* (2), 1391–1400. https://doi.org/10.1021/ACS.ANALCHEM.5B03992.
(17) Moura, A. C. M.; Lago, I. N.; Cardoso, C. F.; dos Reis Nascimento, A.; Pereira, I.; Vaz, B. G. Rapid Monitoring of Pesticides in Tomatoes (Solanum Lycopersicum L.) during Pre-Harvest Intervals by Paper Spray Ionization Mass Spectrometry. *Food Chem.* **2020**, *310*, 125938. https://doi.org/10.1016/j.foodchem.2019.125938
(18) Bernardo, R. A.; Sousa, J. C. P.; Gallimberti, M.; Junior, F. B.; Vaz, B. G.; Chaves, A. R. A Fast and Direct Determination of Bisphenol S in Thermal Paper Samples Using Paper Spray Ionization Mass Spectrometry. *Environ. Sci. Pollut. Res. 2021* **2021**, 1–9. https://doi.org/10.1007/S11356-021-14603-0
(19) Maher, S.; Jjunju, F. P. M.; Damon, D. E.; Gorton, H.; Maher, Y. S.; Syed, S. U.; Heeren, R. M. A.; Young, I. S.; Taylor, S.; Badu-Tawiah, A. K. Direct Analysis and Quantification of Metaldehyde in Water Using Reactive Paper Spray Mass Spectrometry. *Sci. Rep.* **2016**, *6*. https://doi.org/10.1038/SREP35643
(20) Zhu, X.; Huang, Z.; Gao, W.; Li, X.; Li, L.; Zhu, H.; Mo, T.; Huang, B.; Zhou, Z. Rapid Microcystin Determination Using a Paper Spray Ionization Method with a Time-of-Flight Mass Spectrometry System. *J. Agric. Food Chem.* **2016**, *64* (27), 5614–5619. https://doi.org/10.1021/ACS.JAFC.6B02101
(21) Zhang, G.; Ding, T.; Shi, Q.; Jiang, Z.; Niu, Y.; Zhang, M.; Tong, L.; Chen, Z.; Tang, B. Covalent Organic Frameworks-Based Paper Solid Phase Microextraction Combined with Paper Spray Mass Spectrometry for Highly Enhanced Analysis of Tetrabromobisphenol A. *Analyst* **2020**, *145* (19), 6357–6362. https://doi.org/10.1039/D0AN00759E
(22) Liu, J.; Wang, H.; Manicke, N. E.; Lin, J-M.; Cooks, R. G.; Ouyang, Z. Development, Characterization, and Application of Paper Spray Ionization. *Anal. Chem.* **2010**, *82* (6), 2463–2471. https://doi.org/10.1021/AC902854G

(23) Wang, J.; Zhu, J.; Si, L.; Du, Q.; Li, H.; Bi, W.; Chen, D. D. Y. High Throughput Screening of Phenoxy Carboxylic Acids with Dispersive Solid Phase Extraction Followed by Direct Analysis in Real Time Mass Spectrometry. *Anal. Chim. Acta* **2017**, *996*, 20–28. https://doi.org/10.1016/J.ACA.2017.10.007
(24) Jing, W.; Zhou, Y.; Wang, J.; Ni, M.; Bi, W.; Chen, D. D. Y. Dispersive Magnetic Solid-Phase Extraction Coupled to Direct Analysis in Real Time Mass Spectrometry for High-Throughput Analysis of Trace Environmental Contaminants. *Anal. Chem.* **2019**, *91* (17), 11240–11246. https://doi.org/10.1021/ACS.ANALCHEM.9B02197
(25) Jing, W.; Zhou, Y.; Wang, J.; Zhu, Y.; Lv, Y.; Bi, W.; Chen, D. D. Y. Sorbent and Solvent Co-Enhanced Direct Analysis in Real Time-Mass Spectrometry for High-Throughput Determination of Trace Pollutants in Water. *Talanta* **2020**, *208*, 120378. https://doi.org/10.1016/J.TALANTA.2019.120378
(26) Schirinzi, G. F.; Llorca, M.; Seró, R.; Moyano, E.; Barceló, D.; Abad, E.; Farré, M. Trace Analysis of Polystyrene Microplastics in Natural Waters. *Chemosphere* **2019**, *236*, 124321. https://doi.org/10.1016/J.CHEMOSPHERE.2019.07.052
(27) Gómez-Ríos, G. A.; Gionfriddo, E.; Poole, J.; Pawliszyn, J. Ultrafast Screening and Quantitation of Pesticides in Food and Environmental Matrices by Solid-Phase Microextraction–Transmission Mode (SPME-TM) and Direct Analysis in Real Time (DART). *Anal. Chem.* **2017**, *89* (13), 7240–7248. https://doi.org/10.1021/ACS.ANALCHEM.7B01553
(28) Lara, F. J.; Chan, D.; Dickinson, M.; Lloyd, A. S.; Adams, S. J. Evaluation of Direct Analysis in Real Time for the Determination of Highly Polar Pesticides in Lettuce and Celery Using Modified Quick Polar Pesticides Extraction Method. *J. Chromatogr. A* **2017**, *1496*, 37–44. https://doi.org/10.1016/J.CHROMA.2017.03.020
(29) Lei, Y. T.; Lu, Y.; Zhang, T. C.; Qi, Y.; Lu, Y. F. Rapid Screening of Testosterone in the Aquatic Environment Using Direct Analysis in Real-Time (DART) Mass Spectrometry. *Environ. Earth Sci. 2016 7512* **2016**, *75* (12), 1–7. https://doi.org/10.1007/S12665-016-5830-Z
(30) Wang, X.; Liu, J.; Liu, C. C.; Zhang, J.; Shao, B.; Liu, L.; Zhang, N. Rapid Quantification of Highly Polar Trimethyl Phosphate in Wastewater via Direct Analysis in Real-Time Mass Spectrometry. *J. Chromatogr. A* **2014**, *1333*, 134–137. https://doi.org/10.1016/J.CHROMA.2014.01.076
(31) Haunschmidt, M.; Klampfl, C. W.; Buchberger, W.; Hertsens, R. Determination of Organic UV Filters in Water by Stir Bar Sorptive Extraction and Direct Analysis in Real-Time Mass Spectrometry. *Anal. Bioanal. Chem. 2010 3971* **2010**, *397* (1), 269–275. https://doi.org/10.1007/S00216-009-3438-9
(32) Li, X.; Wang, X.; Ma, W.; Ai, W.; Bai, Y.; Ding, L.; Liu, H. Fast Analysis of Glycosides Based on HKUST-1-Coated Monolith Solid-Phase Microextraction and Direct Analysis in Real-Time Mass Spectrometry. *J. Sep. Sci.* **2017**, *40* (7), 1589–1596. https://doi.org/10.1002/JSSC.201601115
(33) Tian, Y.; Chen, J.; Ouyang, Y. zhong; Qu, G. bo; Liu, A. feng; Wang, X. mei; Liu, C. xiao; Shi, J. B.; Chen, H. wen; Jiang, G. bin. Reactive Extractive Electrospray Ionization Tandem Mass Spectrometry for Sensitive Detection of Tetrabromobisphenol A Derivatives. *Anal. Chim. Acta* **2014**, *814*, 49–54. https://doi.org/10.1016/J.ACA.2014.01.035
(34) Takáts, Z.; Wiseman, J. M.; Gologan, B.; Cooks, R. G. Mass Spectrometry Sampling under Ambient Conditions with Desorption Electrospray Ionization. *Science* **2004**, *306* (5695), 471–473. https://doi.org/10.1126/science.1104404
(35) McDonnell, L. A.; Heeren, R. M. A. Imaging Mass Spectrometry. *Mass Spectrom. Rev.* **2007**, *26* (4), 606–643. https://doi.org/10.1002/mas.20124
(36) Tang, C.; Guo, T.; Zhang, Z.; Yang, P.; Song, H. Rapid Visualized Characterization of Phenolic Taste Compounds in Tea Extract by High-Performance Thin-Layer Chromatography Coupled to Desorption Electrospray Ionization Mass Spectrometry. *Food Chem.* **2021**, *355*, 129555. https://doi.org/10.1016/J.FOODCHEM.2021.129555
(37) Gentili, A.; Fanali, S.; Mainero Rocca, L. Desorption Electrospray Ionization Mass Spectrometry for Food Analysis. *TrAC Trends Anal. Chem.* **2019**, *115*, 162–173. https://doi.org/10.1016/J.TRAC.2019.04.015

(38) Maciel, L. I. L.; Pereira, I.; Ramalho, R. R. F.; Ribeiro, R. I.; Pinto, M. C. X.; Vaz, B. G. A New Approach for the Analysis of Amino Acid Neurotransmitters in Mouse Brain Tissues Using DESI Imaging. *Int. J. Mass Spectrom.* **2022**, *471*, 116730. https://doi.org/10.1016/J.IJMS.2021.116730
(39) Cooks, R. G.; Ouyang, Z.; Takats, Z.; Wiseman, J. M. Ambient Mass Spectrometry. *Science* **2006**, pp 1566–1570. https://doi.org/10.1126/science.1119426
(40) Campbell, D. I.; Ferreira, C. R.; Eberlin, L. S.; Cooks, R. G. Improved Spatial Resolution in the Imaging of Biological Tissue Using Desorption Electrospray Ionization. *Anal. Bioanal. Chem.* **2012**, *404* (2), 389–398. https://doi.org/10.1007/s00216-012-6173-6
(41) Shrestha, S. A.; Cha, S. Ambient Desorption/Ionization Mass Spectrometry for Direct Solid Material Analysis. *TrAC Trends Anal. Chem.* **2021**, *144*, 116420. https://doi.org/10.1016/J.TRAC.2021.116420
(42) Zhang, J.; Rector, J.; Lin, J. Q.; Young, J. H.; Sans, M.; Katta, N.; Giese, N.; Yu, W.; Nagi, C.; Suliburk, J.; Liu, J.; Bensussan, A.; DeHoog, R. J.; Garza, K. Y.; Ludolph, B.; Sorace, A. G.; Syed, A.; Zahedivash, A.; Milner, T. E.; Eberlin, L. S. Nondestructive Tissue Analysis for Ex Vivo and in Vivo Cancer Diagnosis Using a Handheld Mass Spectrometry System. *Sci. Transl. Med.* **2017**, *9* (406), eaan3968. https://doi.org/10.1126/scitranslmed.aan3968
(43) Ishii, Y.; Nakamura, K.; Mitsumoto, T.; Takimoto, N.; Namiki, M.; Takasu, S.; Ogawa, K. Visualization of the Distribution of Anthraquinone Components from Madder Roots in Rat Kidneys by Desorption Electrospray Ionization-Time-of-Flight Mass Spectrometry Imaging. *Food Chem. Toxicol.* **2022**, *161*, 112851. https://doi.org/10.1016/J.FCT.2022.112851
(44) Yamamoto, E.; Taquahashi, Y.; Kuwagata, M.; Saito, H.; Matsushita, K.; Toyoda, T.; Sato, F.; Kitajima, S.; Ogawa, K.; Izutsu, K. ichi; Saito, Y.; Hirabayashi, Y.; Iimura, Y.; Honma, M.; Okuda, H.; Goda, Y. Visualizing the Spatial Localization of Ciclesonide and Its Metabolites in Rat Lungs after Inhalation of 1-Mm Aerosol of Ciclesonide by Desorption Electrospray Ionization-Time of Flight Mass Spectrometry Imaging. *Int. J. Pharm.* **2021**, *595*, 120241. https://doi.org/10.1016/J.IJPHARM.2021.120241
(45) Carson, R. H.; Lewis, C. R.; Erickson, M. N.; Zagieboylo, A. P.; Naylor, B. C.; Li, K. W.; Farnsworth, P. B.; Price, J. C. Imaging Regiospecific Lipid Turnover in Mouse Brain with Desorption Electrospray Ionization Mass Spectrometry. *J. Lipid Res.* **2017**, *58* (9), 1884–1892. https://doi.org/10.1194/JLR.M078170
(46) Shaw, J. B.; Brodbelt, J. S. Analysis of Protein Digests by Transmission-Mode Desorption Electrospray Ionization Mass Spectrometry with Ultraviolet Photodissociation. *Int. J. Mass Spectrom.* **2011**, *308* (2–3), 203–208. https://doi.org/10.1016/J.IJMS.2011.08.030
(47) Venter, A.; Sojka, P. E.; Cooks, R. G. Droplet Dynamics and Ionization Mechanisms in Desorption Electrospray Ionization Mass Spectrometry. *Anal. Chem.* **2006**, *78* (24), 8549–8555. https://doi.org/10.1021/AC0615807
(48) Francischini, D. S.; Arruda, M. A. Z. When a Picture Is Worth a Thousand Words: Molecular and Elemental Imaging Applied to Environmental Analysis – A Review. *Microchem. J.* **2021**, *169*, 106526. https://doi.org/10.1016/J.MICROC.2021.106526.
(49) Tillner, J.; McKenzie, J. S.; Jones, E. A.; Speller, A. V. M.; Walsh, J. L.; Veselkov, K. A.; Bunch, J.; Takats, Z.; Gilmore, I. S. Investigation of the Impact of Desorption Electrospray Ionization Sprayer Geometry on Its Performance in Imaging of Biological Tissue. *Anal. Chem.* **2016**, *88* (9), 4808–4816. https://doi.org/10.1021/acs.analchem.6b00345
(50) Wójtowicz, A., Wietecha-Posłuszny, R. DESI-MS Analysis of Human Fluids and Tissues for Forensic Applications. *Appl. Phys. A* **2019**, *125*, 312. https://doi.org/10.1007/s00339-019-2564-2
(51) Green, F. M.; Salter, T. L.; Gilmore, I. S.; Stokes, P.; O'Connor, G. The Effect of Electrospray Solvent Composition on Desorption Electrospray Ionisation (DESI) Efficiency and Spatial Resolution. *Analyst* **2010**, *135*, 731–737. https://doi.org/10.1039/B924208B
(52) Cooks, R. G.; Manicke, N. E.; Dill, A. L.; Ifa, D. R.; Eberlin, L. S.; Costa, A. B.; Wang, H.; Huang, G.; Ouyang, Z. New Ionization Methods and Miniature Mass Spectrometers for Biomedicine: DESI Imaging for Cancer Diagnostics and Paper Spray Ionization for Therapeutic Drug Monitoring. *Faraday Discuss.* **2011**, *149*, 247–267. https://doi.org/10.1039/c005327a

(53) Santoro, A. L.; Drummond, R. D.; Silva, I. T.; Ferreira, S. S.; Juliano, L.; Vendramini, P. H.; da Costa Lemos, M. B.; Eberlin, M. N.; Andrade, V. P. In Situ Desi-MSI Lipidomic Profiles of Breast Cancer Molecular Subtypes and Precursor Lesions. *Cancer Res.* **2020**, *80* (6), 1246–1257. https://doi.org/10.1158/0008-5472.CAN-18-3574

(54) Henderson, F.; Jones, E.; Denbigh, J.; Christie, L.; Chapman, R.; Hoyes, E.; Claude, E.; Williams, K. J.; Roncaroli, F.; McMahon, A. 3D DESI-MS Lipid Imaging in a Xenograft Model of Glioblastoma: A Proof of Principle. *Sci. Reports* **2020**, *10* (1), 1–7. https://doi.org/10.1038/s41598-020-73518-x

(55) Shariatgorji, R.; Nilsson, A.; Strittmatter, N.; Vallianatou, T.; Zhang, X.; Svenningsson, P.; Goodwin, R. J. A.; Andrén, P. E. Bromopyrylium Derivatization Facilitates Identification by Mass Spectrometry Imaging of Monoamine Neurotransmitters and Small Molecule Neuroactive Compounds. *J. Am. Soc. Mass Spectrom.* **2020**, *31* (12), 2553–2557. https://doi.org/10.1021/JASMS.0C00166

(56) Sugiura, Y.; Sugiyama, E.; Suematsu, M. Chapter 4 - DESI-Based Imaging Mass Spectrometry in Forensic Science and Clinical Diagnosis. In *Ambient Ionization Mass Spectrometry in Life Sciences*; Zaitsu, K., Ed.; Elsevier, **2020**; pp 107–118. https://doi.org/10.1016/B978-0-12-817220-9.00004-7

(57) Morse, N.; Jamaspishvili, T.; Simon, D.; Patel, P. G.; Ren, K. Y. M.; Wang, J.; Oleschuk, R.; Kaufmann, M.; Gooding, R. J.; Berman, D. M. Reliable Identification of Prostate Cancer Using Mass Spectrometry Metabolomic Imaging in Needle Core Biopsies. *Lab. Investig.* **2019**, *99* (10), 1561–1571. https://doi.org/10.1038/s41374-019-0265-2

(58) Zhi-Ping, Z.; Xiao-Ning, L.; Ya-Jun, Z. Ambient Ionization-Paper Spray Ionization and Its Application. *Chinese J. Anal. Chem.* **2014**, *42* (1), 145–152. https://doi.org/10.1016/S1872-2040(13)60706-9

(59) Smith, B. L.; Boisdon, C.; Romero-Perez, D.; Sham, T. T.; Bastani, B.; Zhou, Y.; McWilliam, S.; Badu-Tawiah, A. K.; Maher, S. Ambient Ion Focusing for Paper Spray Ionisation. *Int. J. Mass Spectrom.* **2022**, *471*, 116737. https://doi.org/10.1016/J.IJMS.2021.116737

(60) Fernandes, A. R.; Bernardo, R. A.; Sousa, J. C. P.; Georg, R. de C.; Vaz, B. G.; Chaves, A. R. Restrict Access Material for Paper Spray Ionization Mass Spectrometry: A Versatile Tool for Catecholamines and Antidepressants Determination in Plasma Samples. *Microchem. J.* **2020**, *158*, 105245. https://doi.org/10.1016/J.MICROC.2020.105245

(61) Da Silva, L. C.; Pereira, I.; De Carvalho, T. C.; Allochio Filho, J. F.; Romão, W.; Vaz, B. G. Paper Spray Ionization and Portable Mass Spectrometers: A Review. *Anal. Methods* **2019**, *11* (8), 999–1013. https://doi.org/10.1039/C8AY02270D

(62) McBride, E. M.; Mach, P. M.; Dhummakupt, E. S.; Dowling, S.; Carmany, D. O.; Demond, P. S.; Rizzo, G.; Manicke, N. E.; Glaros, T. Paper Spray Ionization: Applications and Perspectives. *TrAC Trends Anal. Chem.* **2019**, *118*, 722–730. https://doi.org/10.1016/j.trac.2019.06.028

(63) Espy, R. D.; Muliadi, A. R.; Ouyang, Z.; Cooks, R. G. Spray Mechanism in Paper Spray Ionization. *Int. J. Mass Spectrom.* **2012**, *325–327*, 167–171. https://doi.org/10.1016/J.IJMS.2012.06.017

(64) Frey, B. S.; Damon, D. E.; Badu-Tawiah, A. K. Emerging Trends in Paper Spray Mass Spectrometry: Microsampling, Storage, Direct Analysis, and Applications. *Mass Spectrom. Rev.* **2020**, *39* (4), 336–370. https://doi.org/10.1002/MAS.21601

(65) Ren, Y.; Wang, H.; Liu, J.; Zhang, Z.; McLuckey, M. N.; Ouyang, Z. Analysis of Biological Samples Using Paper Spray Mass Spectrometry: An Investigation of Impacts by the Substrates, Solvents and Elution Methods. *Chromatographia* **2013**, *76* (19–20), 1339–1346. https://doi.org/10.1007/S10337-013-2458-Y

(66) Liu, J.; Wang, H.; Manicke, N. E.; Lin, J. M.; Cooks, R. G.; Ouyang, Z. Development, Characterization, and Application of Paper Spray Ionization. *Anal. Chem.* **2010**, *82* (6), 2463–2471. https://doi.org/10.1021/AC902854G

(67) McKenna, J.; Dhummakupt, E. S.; Connell, T.; Demond, P. S.; Miller, D. B.; Nilles, J. M.; Manicke, N. E.; Glaros, T. Detection of Chemical Warfare Agent Simulants and Hydrolysis Products in Biological Samples by Paper Spray Mass Spectrometry. *Analyst* **2017**, *142* (9), 1442–1451. https://doi.org/10.1039/C7AN00144D

(68) Bills, B. J.; Kinkade, J.; Ren, G.; Manicke, N. E. The Impacts of Paper Properties on Matrix Effects during Paper Spray Mass Spectrometry Analysis of Prescription Drugs, Fentanyl and Synthetic Canabinoids. *Forensic Chem.* **2018**, *11*, 15–22. https://doi.org/10.1016/J.FORC.2018.08.002
(69) Jett, R.; Skaggs, C.; Manicke, N. E. Drug Screening Method Development for Paper Spray Coupled to a Triple Quadrupole Mass Spectrometer. *Anal. Methods* **2017**, *9* (34), 5037–5043. https://doi.org/10.1039/C7AY01009E
(70) Maciel, L. Í. L.; Ramalho, R. R. F.; Ribeiro, R. I.; Pinto, M. C. X.; Pereira, I.; Vaz, B. G. Combining the Katritzky Reaction and Paper Spray Ionization Mass Spectrometry for Enhanced Detection of Amino Acid Neurotransmitters in Mouse Brain Sections. *J. Am. Soc. Mass Spectrom.* **2021**, *32* (10), 2513–2518. https://doi.org/10.1021/JASMS.1C00153
(71) Su, Y.; Ma, X.; Ouyang, Z. Rapid Screening of Multi-Class Antimicrobial Residues in Food of Animal Origin by Paper Spray Mass Spectrometry. *Int. J. Mass Spectrom.* **2018**, *434*, 233–239. https://doi.org/10.1016/j.ijms.2018.10.003
(72) Jin, H.; Yang, D.; Wu, P.; Zhao, M. Environmental Occurrence and Ecological Risks of Psychoactive Substances. *Environ. Int.* **2022**, *158*, 106970. https://doi.org/10.1016/J.ENVINT.2021.106970
(73) Rodrigues, M. F.; Pereira, I.; Morais, R. L.; Lobón, G. S.; Gil, E. de S.; Vaz, B. G. A New Strategy for the Analysis of Steroid Hormones in Industrial Wastewaters by Paper Spray Ionization Mass Spectrometry. *J. Am. Soc. Mass Spectrom.* **2020**, *31* (11), 2250–2257. https://doi.org/10.1021/JASMS.0C00145
(74) Dowling, S.; McBride, E. M.; McKenna, J.; Glaros, T.; Manicke, N. E. Direct Soil Analysis by Paper Spray Mass Spectrometry: Detection of Drugs and Chemical Warfare Agent Hydrolysis Products. *Forensic Chem.* **2020**, *17*, 100206. https://doi.org/10.1016/J.FORC.2019.100206
(75) Liu, H.; Gao, W.; Tian, Y.; Liu, A.; Wang, Z.; Cai, Y.; Zhao, Z. Rapidly Detecting Tetrabromobisphenol A in Soils and Sediments by Paper Spray Ionization Mass Spectrometry Combined with Isotopic Internal Standard. *Talanta* **2019**, *191*, 272–276. https://doi.org/10.1016/J.TALANTA.2018.08.069
(76) Kotthoff, M.; Rüdel, H.; Jürling, H. Detection of Tetrabromobisphenol A and Its Mono- and Dimethyl Derivatives in Fish, Sediment and Suspended Particulate Matter from European Freshwaters and Estuaries. *Anal. Bioanal. Chem.* **2017**, *409* (14), 3685–3694. https://doi.org/10.1007/S00216-017-0312-Z
(77) Wei, S. C.; Fan, S.; Lien, C. W.; Unnikrishnan, B.; Wang, Y. S.; Chu, H. W.; Huang, C. C.; Hsu, P. H.; Chang, H. T. Graphene Oxide Membrane as an Efficient Extraction and Ionization Substrate for Spray-Mass Spectrometric Analysis of Malachite Green and Its Metabolite in Fish Samples. *Anal. Chim. Acta* **2018**, *1003*, 42–48. https://doi.org/10.1016/J.ACA.2017.11.076
(78) T, Z.; MT, J.; T, K. Molecularly Imprinted Graphite Spray Ionization-Ion Mobility Spectrometry: Application to Trace Analysis of the Pesticide Propoxur. *Mikrochim. Acta* **2019**, *186* (7). https://doi.org/10.1007/S00604-019-3467-9
(79) Cody, R. B.; Laramée, J. A.; Durst, H. D. Versatile New Ion Source for the Analysis of Materials in Open Air under Ambient Conditions. *Anal. Chem.* **2005**, *77* (8), 2297–2302. https://doi.org/10.1021/AC050162J
(80) Blokland, M. H.; Gerssen, A.; Zoontjes, P. W.; Pawliszyn, J.; Nielen, M. W. F. Potential of Recent Ambient Ionization Techniques for Future Food Contaminant Analysis Using (Trans)Portable Mass Spectrometry. *Food Anal. Methods* **2020**, *13* (3), 706–717. https://doi.org/10.1007/s12161-019-01666-6
(81) Domínguez-Rodríguez, G.; Marina, M. L.; Plaza, M. Rapid Fingerprinting of Extractable and Non-Extractable Polyphenols from Tropical Fruit Peels Using Direct Analysis in Real Time Coupled to Orbitrap Mass Spectrometry. *Food Chem.* **2022**, *371*, 131191. https://doi.org/10.1016/J.FOODCHEM.2021.131191
(82) Sisco, E.; Forbes, T. P. Forensic Applications of DART-MS: A Review of Recent Literature. *Forensic Chem.* **2021**, *22*, 100294. https://doi.org/10.1016/J.FORC.2020.100294

(83) Gross, J. H. Direct Analysis in Real Time-a Critical Review on DART-MS. *Anal. Bioanal. Chem.* **2014**, *406* (1), 63–80. https://doi.org/10.1007/s00216-013-7316-0
(84) Cody, R. B. Observation of Molecular Ions and Analysis of Nonpolar Compounds with the Direct Analysis in Real Time Ion Source. *Anal. Chem.* **2008**, *81* (3), 1101–1107. https://doi.org/10.1021/AC8022108
(85) Bee-DiGregorio, M. Y.; Feng, H.; Pan, B. S.; Dokoozlian, N. K.; Sacks, G. L. Polymeric Sorbent Sheets Coupled to Direct Analysis in Real Time Mass Spectrometry for Trace-Level Volatile Analysis—A Multi-Vineyard Evaluation Study. *Foods 2020, Vol. 9, Page 409* **2020**, *9* (4), 409. https://doi.org/10.3390/FOODS9040409
(86) Peace, M. R.; Smith, M. E.; Poklis, J. L. The Analysis of Commercially Available Natural Products Recommended for Use in Electronic Cigarettes. *Rapid Commun. Mass Spectrom.* **2020**, *34* (11), e8771. https://doi.org/10.1002/RCM.8771
(87) Gui, Y.; Lu, Y.; Li, S.; Zhang, M.; Duan, X.; Liu, C. C.; Jia, J.; Liu, G. Direct Analysis in Real Time-Mass Spectrometry for Rapid Quantification of Five Anti-Arrhythmic Drugs in Human Serum: Application to Therapeutic Drug Monitoring. *Sci. Reports 2020 101* **2020**, *10* (1), 1–10. https://doi.org/10.1038/S41598-020-72490-W
(88) Zhang, X.; Mell, A.; Li, F.; Thaysen, C.; Musselman, B.; Tice, J.; Vukovic, D.; Rochman, C.; Helm, P. A.; Jobst, K. J. Rapid Fingerprinting of Source and Environmental Microplastics Using Direct Analysis in Real Time-High Resolution Mass Spectrometry. *Anal. Chim. Acta* **2020**, *1100*, 107–117. https://doi.org/10.1016/J.ACA.2019.12.005
(89) Zabalegui, N.; Manzi, M.; Depoorter, A.; Hayeck, N.; Roveretto, M.; Li, C.; Van Pinxteren, M.; Herrmann, H.; George, C.; Monge, M. E. Seawater Analysis by Ambient Mass-Spectrometry-Based Seaomics. *Atmos. Chem. Phys.* **2020**, *20* (10), 6243–6257. https://doi.org/10.5194/ACP-20-6243-2020
(90) Nei, D.; Nakamura, N.; Ishihara, K.; Kimura, M.; Satomi, M. A Rapid Screening of Histamine Concentration in Fish Fillet by Direct Analysis in Real Time Mass Spectrometry (DART-MS). *Food Control* **2017**, *75*, 181–186. https://doi.org/10.1016/j.foodcont.2016.12.001
(91) Emmons, R. V.; Gionfriddo, E. Minimizing Transient Microenvironment-Associated Variability for Analysis of Environmental Anthropogenic Contaminants via Ambient Ionization. *Sci. Total Environ.* **2021**, *775*, 145789. https://doi.org/10.1016/J.SCITOTENV.2021.145789
(92) Chang, D-Y.; Lee, C-C.; Shiea, J. Detecting Large Biomolecules from High-Salt Solutions by Fused-Droplet Electrospray Ionization Mass Spectrometry. *Anal. Chem.* **2002**, *74* (11), 2465–2469. https://doi.org/10.1021/AC010788J
(93) Chen, H.; Venter, A.; Cooks, R. G. Extractive Electrospray Ionization for Direct Analysis of Undiluted Urine, Milk and Other Complex Mixtures without Sample Preparation. *Chem. Commun.* **2006**, No. 19, 2042–2044. https://doi.org/10.1039/B602614A
(94) Koyanagi, G. K.; Blagojevic, V.; Bohme, D. K. Applications of Extractive Electrospray Ionization (EESI) in Analytical Chemistry. *Int. J. Mass Spectrom.* **2015**, *379*, 146–150. https://doi.org/10.1016/J.IJMS.2015.01.011
(95) Law, W. S.; Wang, R.; Hu, B.; Berchtold, C.; Meier, L.; Chen, H.; Zenobi, R. On the Mechanism of Extractive Electrospray Ionization. *Anal. Chem.* **2010**, *82* (11), 4494–4500. https://doi.org/10.1021/AC100390T
(96) Zhang, X.; Wang, N.; Zhou, Y.; Liu, Y.; Zhang, J.; Chen, H. Extractive Electrospray Ionization Mass Spectrometry for Direct Characterization of Cosmetic Products. *Anal. Methods* **2012**, *5* (2), 311–315. https://doi.org/10.1039/C2AY25876E
(97) Berchtold, C.; Meier, L.; Zenobi, R. Evaluation of Extractive Electrospray Ionization and Atmospheric Pressure Chemical Ionization for the Detection of Narcotics in Breath. *Int. J. Mass Spectrom.* **2011**, *299* (2–3), 145–150. https://doi.org/10.1016/J.IJMS.2010.10.011

(98) Giannoukos, S.; Tarik, M.; Ludwig, C.; Biollaz, S.; Slowik, J.; Baltensperger, U.; Henry Prevot, A. S. Detection of Trace Metals in Biogas Using Extractive Electrospray Ionization High-Resolution Mass Spectrometry. *Renew. Energy* **2021**, *169*, 780–787. https://doi.org/10.1016/J.RENENE.2021.01.047
(99) Liu, A.; Kou, W.; Zhang, H.; Xu, J.; Zhu, L.; Kuang, S.; Huang, K.; Chen, H.; Jia, Q. Quantification of Trace Organophosphorus Pesticides in Environmental Water via Enrichment by Magnetic-Zirconia Nanocomposites and Online Extractive Electrospray Ionization Mass Spectrometry. *Anal. Chem.* **2020**, *92* (5), 4137–4145. https://doi.org/10.1021/ACS.ANALCHEM.0C00304
(100) Kou, W.; Zhang, H.; Bibi, A.; Ke, M.; Han, J.; Xiong, J.; Su, R.; Liang, D. Fast Quantification of Fluoroquinolones in Environmental Water Samples Using Molecularly Imprinted Polymers Coupled with Internal Extractive Electrospray Ionization Mass Spectrometry. *RSC Adv.* **2018**, *8* (31), 17293–17299. https://doi.org/10.1039/C8RA01837E
(101) Deng, M.; Yu, T.; Luo, H.; Zhu, T.; Huang, X.; Luo, L. Direct Detection of Multiple Pesticides in Honey by Neutral Desorption-Extractive Electrospray Ionization Mass Spectrometry. *Int. J. Mass Spectrom.* **2017**, *422*, 111–118. https://doi.org/10.1016/J.IJMS.2017.09.005
(102) Gao, Y.; Xue, A.; Li, X.; Huang, X.; Ning, F.; Zhang, X.; Liu, T.; Chen, H.; Luo, L. Analysis of Chemical Composition of Nectars and Honeys from Citrus by Extractive Electrospray Ionization High Resolution Mass Spectrometry. *LWT* **2020**, *131*, 109748. https://doi.org/10.1016/J.LWT.2020.109748
(103) Fang, L.; Deng, J.; Yang, Y.; Wang, X.; Chen, B.; Liu, H.; Zhou, H.; Ouyang, G.; Luan, T. Coupling Solid-Phase Microextraction with Ambient Mass Spectrometry: Strategies and Applications. *TrAC Trends Anal. Chem.* **2016**, *85*, 61–72. https://doi.org/10.1016/J.TRAC.2016.05.025
(104) Yuan, Z.-C.; Li, W.; Wu, L.; Huang, D.; Wu, M.; Hu, B. Solid-Phase Microextraction Fiber in Face Mask for in Vivo Sampling and Direct Mass Spectrometry Analysis of Exhaled Breath Aerosol. *Anal. Chem.* **2020**, *92* (17), 11543–11547. https://doi.org/10.1021/ACS.ANALCHEM.0C02118
(105) Deng, J.; Yang, Y.; Fang, L.; Lin, L.; Zhou, H.; Luan, T. Coupling Solid-Phase Microextraction with Ambient Mass Spectrometry Using Surface Coated Wooden-Tip Probe for Rapid Analysis of Ultra Trace Perfluorinated Compounds in Complex Samples. *Anal. Chem.* **2014**, *86* (22), 11159–11166. https://doi.org/10.1021/AC5034177
(106) Nemes, P.; Vertes, A. Laser Ablation Electrospray Ionization for Atmospheric Pressure, in Vivo, and Imaging Mass Spectrometry. *Anal. Chem.* **2007**, *79* (21), 8098–8106. https://doi.org/10.1021/AC071181R
(107) da Silva Lima, G.; Franco dos Santos, G.; Ramalho, R. R. F.; de Aguiar, D. V. A.; Roque, J. V.; Maciel, L. I. L.; Simas, R. C.; Pereira, I.; Vaz, B. G. Laser Ablation Electrospray Ionization Mass Spectrometry Imaging as a New Tool for Accessing Patulin Diffusion in Mold-Infected Fruits. *Food Chem.* **2022**, *373*, 131490. https://doi.org/10.1016/J.FOODCHEM.2021.131490
(108) Kiss, A.; Hopfgartner, G. Laser-Based Methods for the Analysis of Low Molecular Weight Compounds in Biological Matrices. *Methods* **2016**, *104*, 142–153. https://doi.org/10.1016/J.YMETH.2016.04.017
(109) Zhu, G.; Shao, Y.; Liu, Y.; Pei, T.; Li, L.; Zhang, D.; Guo, G.; Wang, X. Single-Cell Metabolite Analysis by Electrospray Ionization Mass Spectrometry. *TrAC Trends Anal. Chem.* **2021**, *143*, 116351. https://doi.org/10.1016/J.TRAC.2021.116351
(110) Beach, D. G.; Walsh, C. M.; McCarron, P. High-Throughput Quantitative Analysis of Domoic Acid Directly from Mussel Tissue Using Laser Ablation Electrospray Ionization – Tandem Mass Spectrometry. *Toxicon* **2014**, *92*, 75–80. https://doi.org/10.1016/J.TOXICON.2014.10.009
(111) Nielen, M. W. F.; Van Beek, T. A. Macroscopic and Microscopic Spatially-Resolved Analysis of Food Contaminants and Constituents Using Laser-Ablation Electrospray Ionization Mass Spectrometry Imaging. *Anal. Bioanal. Chem.* **2014**, *406* (27), 6805–6815. https://doi.org/10.1007/S00216-014-7948-8
(112) Escrivá, L.; Font, G.; Manyes, L.; Berrada, H. Studies on the Presence of Mycotoxins in Biological Samples: An Overview. *Toxins (Basel).* **2017**, *9* (8). https://doi.org/10.3390/TOXINS9080251

(113) Maloof, K. A.; Reinders, A. N.; Tucker, K. R. Applications of Mass Spectrometry Imaging in the Environmental Sciences. *Curr. Opin. Environ. Sci. Heal.* **2020**, *18*, 54–62. https://doi.org/10.1016/J.COESH.2020.07.005

(114) Gundlach-Graham, A.; Burger, M.; Allner, S.; Schwarz, G.; Wang, H. A. O.; Gyr, L.; Grolimund, D.; Hattendorf, B.; Günther, D. High-Speed, High-Resolution, Multielemental Laser Ablation-Inductively Coupled Plasma-Time-of-Flight Mass Spectrometry Imaging: Part I. Instrumentation and Two-Dimensional Imaging of Geological Samples. *Anal. Chem.* **2015**, *87* (16), 8250–8258. https://doi.org/10.1021/ACS.ANALCHEM.5B01196

(115) Roach, P. J.; Laskin, J.; Laskin, A. Nanospray Desorption Electrospray Ionization: An Ambient Method for Liquid-Extraction Surface Sampling in Mass Spectrometry. *Analyst* **2010**, *135* (9), 2233–2236. https://doi.org/10.1039/C0AN00312C

(116) Roach, P. J.; Laskin, J.; Laskin, A. Molecular Characterization of Organic Aerosols Using Nanospray-Desorption / Electrospray Ionization-Mass Spectrometry. *Anal. Chem*. **2010**, *82* (19), 7979–7986. https://doi.org/10.1021/ac101449p

(117) Lanekoff, I.; Heath, B. S.; Liyu, A.; Thomas, M.; Carson, J. P.; Laskin, J. Automated Platform for High-Resolution Tissue Imaging Using Nanospray Desorption Electrospray Ionization Mass Spectrometry. *Anal. Chem.* **2012**, *84* (19), 8351–8356. https://doi.org/10.1021/AC301909A

(118) Nguyen, S. N.; Sontag, R. L.; Carson, J. P.; Corley, R. A.; Ansong, C.; Laskin, J. Towards High-Resolution Tissue Imaging Using Nanospray Desorption Electrospray Ionization Mass Spectrometry Coupled to Shear Force Microscopy. *J. Am. Soc. Mass Spectrom.* **2018**, *29* (2), 316–322. https://doi.org/10.1007/S13361-017-1750-8

(119) Yin, R.; Burnum-Johnson, K. E.; Sun, X.; Dey, S. K.; Laskin, J. High Spatial Resolution Imaging of Biological Tissues Using Nanospray Desorption Electrospray Ionization Mass Spectrometry. *Nat. Protoc.* **2019**, *14* (12), 3445–3470. https://doi.org/10.1038/s41596-019-0237-4

(120) Laskin, J.; Eckert, P. A.; Roach, P. J.; Heath, B. S.; Nizkorodov, S. A.; Laskin, A. Chemical Analysis of Complex Organic Mixtures Using Reactive Nanospray Desorption Electrospray Ionization Mass Spectrometry. *Anal. Chem.* **2012**, *84* (16), 7179–7187. https://doi.org/10.1021/AC301533Z

(121) Eckert, P. A.; Roach, P. J.; Laskin, A.; Laskin, J. Chemical Characterization of Crude Petroleum Using Nanospray Desorption Electrospray Ionization Coupled with High-Resolution Mass Spectrometry. *Anal. Chem.* **2012**, *84* (3), 1517–1525. https://doi.org/10.1021/AC202801G

(122) Lanekoff, I.; Burnum-Johnson, K.; Thomas, M.; Cha, J.; Dey, S. K.; Yang, P.; Prieto Conaway, M. C.; Laskin, J. Three-Dimensional Imaging of Lipids and Metabolites in Tissues by Nanospray Desorption Electrospray Ionization Mass Spectrometry. *Anal. Bioanal. Chem.* **2015**, *407* (8), 2063–2071. https://doi.org/10.1007/s00216-014-8174-0

(123) Bergman, H. M.; Lundin, E.; Andersson, M.; Lanekoff, I. Quantitative Mass Spectrometry Imaging of Small-Molecule Neurotransmitters in Rat Brain Tissue Sections Using Nanospray Desorption Electrospray Ionization. *Analyst* **2016**, *141* (12), 3686–3695. https://doi.org/10.1039/C5AN02620B

(124) Watrous, J.; Roach, P.; Heath, B.; Alexandrov, T.; Laskin, J.; Dorrestein, P. C. Metabolic Profiling Directly from the Petri Dish Using Nanospray Desorption Electrospray Ionization Imaging Mass Spectrometry. *Anal. Chem.* **2013**, *85* (21), 10385–10391. https://doi.org/10.1021/AC4023154

(125) Cardoso-Palacios, C.; Lanekoff, I. Direct Analysis of Pharmaceutical Drugs Using Nano-DESI MS. *J. Anal. Methods Chem.* **2016**, *2016*. https://doi.org/10.1155/2016/3591908

(126) Laskin, A.; Laskin, J.; Nizkorodov, S. Probing Molecular Composition of Soil Organic Matter with Nanospray Desorption Electrospray Ionization (Nano-DESI) High-Resolution Mass Spectrometry. In *AGU Fall Meeting Abstracts* **2014**, Vol. 2014, B31L-06. [Available at: https://agu.confex.com/agu/fm14/meetingapp.cgi/Paper/5677]

(127) Akomeng, N.; Adusei, S. Organic Solvent Extraction and Spectrophotometric Quantification of Total Phenolic Content of Soil. *Heliyon* **2021**, *7* (11), e08388. https://doi.org/10.1016/J.HELIYON.2021.E08388

Brazilian Journal of Analytical Chemistry
2022, Volume 9, Issue 36, pp 78–97
doi: 10.30744/brjac.2179-3425.AR-112-2021

BrJAC

ARTICLE

Comparative Study Between Two Zeolitic Imidazolate Frameworks as Adsorbents for Removal of Organoarsenic, As(III) and As(V) Species from Water

Khalil Ahmad[1,2]*@ ✉, Habib-ur-Rehman Shah[1]@, Muhammad Ahmad[3], Muhammad Mahboob Ahmed[4], Khalida Naseem[5], Nagina Naveed Riaz[6,7], Ali Muhammad[1], Asif Ayub[1], Munir Ahmad[7], Zahoor Ahmad[8], Alisha Munwar[4], Abdul Rauf[1], Riaz Hussain[9], Muhammad Ashfaq[1]* ✉

[1]*Institute of Chemistry, Baghdad ul Jadeed Campus, The Islamia University of Bahawalpur, Bahawalpur, 63100, Pakistan*

[2]*Faculty of Science, Department of Chemistry, University of Central Punjab, Bahawalpur Campus, Bahawalpur, 63100, Pakistan*

[3]*Department of Chemistry, University of Sahiwal, Punjab, 57000, Pakistan*

[4]*Institute of Chemical Sciences, Bahauddin Zakariya University, Multan, Pakistan*

[5]*Faculty of Science, Department of Chemistry, University of Central Punjab, Lahore, Pakistan*

[6]*Department of Chemistry, Division of Science & Technology, University of Education, Lahore, Pakistan*

[7]*Department of Chemistry, Khawaja Fareed University of Engineering and Technology Rahim Yar Khan, Pakistan*

[8]*Faculty of Science, Department of Botany, University of Central Punjab, Bahawalpur Campus, Bahawalpur, 63100, Pakistan*

[9]*Department of Chemistry, Division of Science & Technology, University of Education, Dera Ghazi Khan Campus, Pakistan*

@ = Authors have equal contribution.

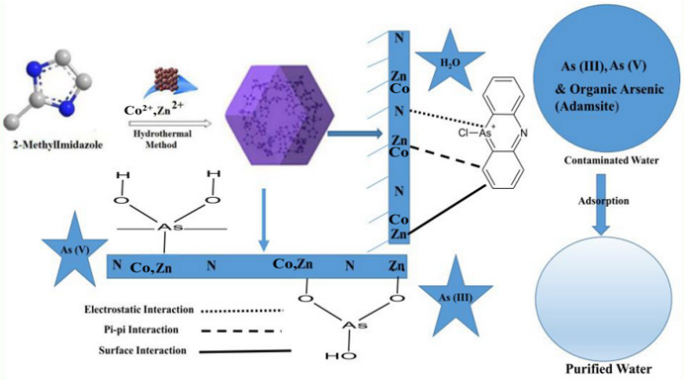

Water-stable zeolitic imidazolate frameworks (ZIF) with zinc and cobalt cations were synthesized to explore the effect of metal ions on arsenic adsorption. At room temperature (25 ± 2 ºC) and pH 7.8, maximum adsorption capacities of arsenic (As^{5+}) on the surface of ZIF-8 and ZIF-67 were 87.03 and 86.70 mg g^{-1} respectively, with encouraging results up to 95% reusability of the adsorbents. The results of this study revealed that electrostatic attraction and ion exchange were the major mechanisms responsible for better

Cite: Ahmad, K.; Shah, H-ur-R.; Ahmad, M.; Ahmed, M. M.; Naseem, K.; Riaz, N. N.; Muhammad, A.; Ayub, A.; Ahmad, M.; Ahmad, Z.; Munwar, A.; Rauf, A.; Hussain, R.; Ashfaq, M. Comparative Study Between Two Zeolitic Imidazolate Frameworks as Adsorbents for Removal of Organoarsenic, As(III) and As(V) Species from Water. *Braz. J. Anal. Chem.* 2022, *9* (36), pp 78–97. http://dx.doi.org/10.30744/brjac.2179-3425.AR-112-2021

Submitted 30 October 2021, Resubmitted 09 January 2022, Accepted 18 January 2022, Available online 04 May 2022.

efficiencies for adsorptive removal of arsenic. The evidence for the adsorption of arsenic contaminants was confirmed by FTIR analyses. The pseudo second order and Langmuir models were best suited to explain the adsorption of arsenic species on the surface of the as-synthesized metal-organic frameworks (MOFs). Based on the results, it was possible to conclude that the metal atoms in the synthesized MOFs had a minor impact on adsorption, since these MOFs presented identical results in the removal of arsenic species. This observation can be explained by the presence of a similar organic linker (2-methyl imidazole), which points to almost the same geometry and sponginess. However, there was a slight difference in the adamsite (organo-arsenic) removal achieved by the MOFs with different metal atoms.

Keywords: Arsenic removal, zeolitic imidazolate frameworks, metal organic frameworks, ZIF-MOFs, adsorption mechanism, adamsite removal, water purification

INTRODUCTION

Arsenic (As) is a metalloid element in nature that is highly toxic in its inorganic form. It is reported as one of the most significant chemical contaminants in groundwater. Unfortunately, arsenic impurities in ground and surface water have accumulated over time in the aqueous environment.[1,2] According to statistics, 226 million people from 105 countries worldwide are suffering due to arsenic pollution and toxicity. In Bangladesh, Taiwan, Myanmar, Lao, West Bengal (India), Japan, Mongolia (China), Cambodia and Pakistan, studies showed elevated concentrations of arsenic in water.[3,4] The existence of water pollution due to arsenic has been detected also in Chile, New Zealand, Hungary, Canada, USA, Poland, Mexico and Argentina,[5,6] but the highest and most severe level of arsenic was found in Bangladesh, West Bengal (India), and in some parts of eastern Pakistan as well. In Halifax County, Nova Scotia (CA) and British Columbia (CA) incidents related to arsenic pollution in water have occurred, and arsenic pollution exceeding 3 mg L^{-1} has been reported in the literature.[3,7–9]

Long-term exposure to arsenic polluted water causes various diseases like cancer (skin, bladder, eye, uterus and respiratory system), arsenicosis, arthritis, jaundice, liver problems, chronic and acute toxicity and even death as reported in many studies.[1,10] Arsenic species have high mobility and are easily accumulated in the aqueous environment as well as in the human body through the food chain, making arsenic a contaminant of concern worldwide. Uncontrolled anthropogenic activities, in addition to natural geochemical cycles, are the main conditions causing arsenic pollution. In the ground and wastewater, arsenic pollution occurs through natural processes such as the dissolution of rocks, ores, minerals and weathering or as a result of human activities such as gold and coal mining.[11–13] Other human activities that produce a huge amount of arsenic in the ecosystem are industrial, oil refining, metal extractions, agricultural waste and irrigation, metal smelting, poultry feed/medicines and mineral/ores mining with typical concentrations in water ranging from 0.5 ppm to 100 ppm.[14–16] WHO and USEPA have revised the permissible amount of arsenic in drinkable water, which is only 10 ppb (parts per billion). Arsenic naturally occurs in four different valences which are +5, +3, 0, and -3. However, in the ground and wastewater arsenic occurs mainly in two forms which are arsenite (+3) and arsenate (+5). According to the literature, the trivalent arsenic (arsenite) is the dominant form in groundwater due to the deficiency of oxygen while the pentavalent (arsenate) is the prevalent form in surface water due to excess of oxygen.[13,17,18] Because of the high toxicity and mobility of arsenite in the environment, it is considered more toxic than arsenate. When the trivalent arsenic enters through an intermediate, it accumulates in the body of fish and humans and has more chances of producing arsenicosis.

There are many organoarsenic compounds available in the market used as herbicides, insecticides and pesticides. Adamsite (i.e., diphenylaminechloroarsine), also a medicine containing arsenic (structure and some properties are shown in Figure 1), is used as herbicides, insecticides, pesticides and in candles. It is also used as emetic agents and in poultry diseases.[19–22]

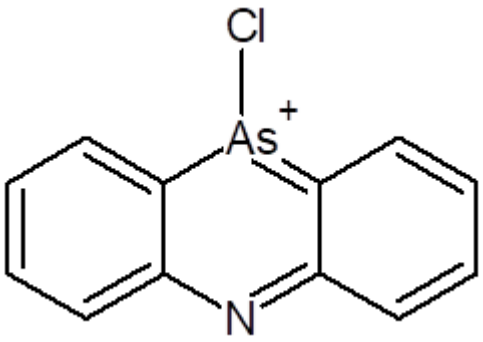

Figure 1. Structural formula of adamsite (diphenylaminechloroarsine) – organoarsenic having molar mass 277.58 g mol^{-1}, melting point 195 ºC, chemical formula $C_{12}H_9AsClN$, CAS number 578-94-9, and IUPAC name 10-chloro-5,10-dihydrophenarsazinine.

According to USEPA, many technologies are approved for the removal of arsenic species from water, such as i) precipitation, ii) adsorption, iii) ion exchange and iv) membrane separation. In addition to these, many other techniques are also applied, such as the use of zeolites, flocculation, chromatography, etc.[23] Among all these techniques, adsorption is recognized as one of the most popular and promising methods for removing pollutants, especially arsenic, due to its low cost, high specificity, ease of operation, non-toxicity and high efficiency, as also reported by Mohan and Pittman in their comprehensive review.[24]

The removal and uptake efficiency of the adsorbents are directly related to their porosity and surface-to-volume ratio.[25] According to these criteria, metal-organic frameworks (MOFs) are excellent porous materials for decontamination of arsenic and other pollutants, catalytic conversion, catalysis, gas separation, storage, etc., due to their unique mechanical and chemical features, flexible/versatile designs, excellent chemical and thermal stability, high surface area, tunable porosity, and highly active sites that are easily accessible. Omar M. Yaghi and colleagues accomplished many pioneer works for the designing and synthesis of MOFs.[26]

MOFs have proven to be excellent tools for the adsorption and separation of pollutants compared to traditional porous materials. Carbon-based materials and other porous materials are suitable for the decontamination caused by pollutants, but the cost of production and regeneration of these materials are very high, as reported by Mohan and Pittman.[24] On the other hand, MOF adsorbents, especially zinc and cobalt-based MOFs, are very cost-effective. In addition, zinc and cobalt-based MOFs have outstanding water stability, high pore size, ready availability, non-toxic metal source, and strong affinity to arsenic ions due to electrostatic interaction and π–π interaction, which make them very suitable as arsenic scavengers.[27–29] Highly durable and robust, zinc and cobalt-based MOFs will extend their use in the water purification field.[30]

In this paper, we report our as-synthesized zeolitic imidazolate frameworks, named ZIF-8 and ZIF-67, in which 2-methylimidazole binds to zinc and cobalt metal ions, respectively, which act as coordinately central metal atoms. ZIF-8 and ZIF-67 are structurally featured by high thermal and chemical stability, tunable porosity, high surface area and sufficient active sites, features that make them very suitable for their applications. Due to continuously increasing levels of arsenic in ground drinking water, there should be an urgent need to explore practical and effective technologies to remove arsenic species from aquatic environment. Moreover, ZIF-8 and ZIF-67 are hydrophobic materials widely used for the adsorption process. So, we synthesized these materials and compared them in terms of their adsorption capacity and removal efficiency to remove an organo-arsenic specie (adamsite) from water. In this study we also demonstrate adsorption mechanism for the adsorption of arsenic species from water as well as isothermal and kinetic studies. The adsorption mechanism includes electrostatic enhancement, and hydrophobic and π−π interactions.

MATERIALS AND METHODS

All the chemicals used were AR Grade. Zinc nitrate hexahydrate [$Zn(NO_3)_2 \cdot 6H_2O$], cobalt(II) nitrate hexahydrate [$Co(NO_3)_2 \cdot 6H_2O$], sodium arsenate [$Na_3AsO_4 \cdot 12H_2O$] for As(V), sodium arsenite [$NaAsO_2$]

for As(III), 2-methyl imidazole, methanol, HCl and NaOH were obtained from Merck, BDH, and used as received, without further purification. Adamsite was obtained from the local market of Bahawalpur, Punjab, Pakistan. For the washing and synthesis procedures, ultra-pure water was used.

Standard solutions with 1000 mg L^{-1} of adamsite, sodium arsenite and sodium arsenate were prepared and subsequently used for the preparation of solutions with 10, 15, and 20 mg L^{-1}, respectively.

Synthesis of Cobalt/Zinc MOFs

ZIF-8 and ZIF-67 materials were prepared according to reported literature,[30,31] with certain modifications. According to a typical method for the synthesis of ZIF-67 and ZIF-8, 1 mmol of metal salts (Zn/Co nitrate hexahydrate) was added in a minimal quantity of ultra-pure water in beakers. 4 mmol of 2-methyl imidazole was mixed in a minimal amount of methanolic solution and mixing was done using a stirrer. Then, these metal salt and imidazole solutions were mixed slowly under continuous stirring at ambient temperature (25 ± 2 ºC) for 30 minutes. After stirring, the mixture was left for 60 minutes to complete the processing of crystal aging. After aging, the crystals were washed 3 times with a mixture of water and methanol (1:1) and centrifuged at 6000 rpm for 10 minutes to remove unreacted reagents. These washed crystals were dried overnight in an oven at 100 ºC.

Characterization of Cobalt/Zinc MOFs

The synthesized ZIF-8 & ZIF-67 nanoparticles were characterized by the following advanced spectroscopic techniques: powder X-ray diffractometry (P-XRD), scanning electron microscopy (SEM), Brunauer-Emmett-Teller technique (BET) and Fourier transform infrared spectroscopy (FTIR). To obtain FTIR spectra, the attenuated total reflectance (ATR) technique and a Bruker FTIR instrument with a range of 400-4000 cm^{-1} were used. The surface morphology of the synthesized MOFs was studied using a JSM-7800F scanning electron microscope from JEOL. The crystalline nature of ZIF-8 was observed by the P-XRD technique. The surface area and porosity of the material were checked using the BET technique at 77.3 K using the Quadrasorb2MP, Quantachrome surface analyzer. The Perkin Elmer AAnalyst 100 AAS was used to determine arsenic species before and after the adsorption procedure.

Adsorption experiments

Adsorption experiments were performed by mixing a certain amount of adsorbent with a specific volume of the arsenic solution; the resulting mixture was stirred in constant rotation and at room temperature (25 ± 2 ºC). At the end of the experiments, the adsorbent was separated by filtration with syringe filter paper and the arsenic concentration in the filtrate was determined by atomic absorption spectroscopy (AAS).

The effect of pH on adsorption was studied by adding 10 mg of the adsorbent to 10 mL of arsenic solution (10 mg L^{-1}). The pH was adjusted using 0.1 M solutions of NaOH and HCl and the contact time was 2 h. The adsorbents showed maximum arsenic species removal efficiency (90.5%) at pH 7.8, so this optimized pH was used for further experiments.

In the following experiments, the concentration of the arsenic species was changed from 10 to 15 and 20 mg L^{-1}, and the solution volume was fixed at 250 mL with a contact time of 6 h.

Adsorption capacity q_e (mg g^{-1}) and removal efficacy were calculated by applying equations 1 and 2, respectively.

$$q_e = (C_o - C_e)V/W \quad (1)$$

$$\text{Removal efficiency (\%)} = (C_i - C_e)/ C_i*100 \quad (2)$$

where, C_i and C_o are the concentration of arsenic species (mg L^{-1}) before the adsorption process; C_e is the concentration of arsenic species after the adsorption process; W is the mass (g) of adsorbent (ZIF-8, ZIF-67) and V is the volume (L) of the solution.

The Langmuir and Freundlich models were also applied in the adsorption kinetics study to confirm the adsorption process. The pseudo second order and pseudo first order kinetics were also applied and they are expressed as linear functions using equations 3 and 4 respectively.

$$\ln Q_e - Q_t = \ln Q_e - K_1 t \quad (3)$$

$$t/Q_t = t/Q_e + 1/K_2 Q_e^2 \quad (4)$$

Q_e = quantity of arsenic adsorbed at equilibrium
Q_t = quantity of arsenic adsorbed in a time interval
t (h) = adsorption time in hours
K_1 (h^{-1}) = rate constant of pseudo 1st order
K_2 (g mg^{-1} h^{-1}) = rate constant of pseudo 2nd order
Values of K_1 and Q_e were determined from plotting ln ($Q_e - Q_t$) *vs* time (t). K_1 = slope and $\ln Q_e$ = intercept
K_2 value was determined by plotting the t/Q_t *vs* time

The initial adsorption rate (h = mg g^{-1} min^{-1}) can be calculated from equation 5 and the half adsorption time ($t_{0.5}$, h) from equation 6.

$$h = K_2 Q_e^2 \quad (5)$$

$$t_{0.5} = 1/K_2 Q_e \quad (6)$$

Evaluation of the reusability of the synthesized MOFs

To evaluate the regeneration of the adsorbent after a removal experiment of a solution containing 10 mg L^{-1} of arsenic, the adsorbent separated by filtration was washed with deionized water and added to 100 mL of an eluent solution containing NaOH (2 M), HCl (0.1 M) and NaCl (2 M) in a 2:7:1 ratio. This mixture of adsorbent and eluent was stirred for 120 minutes at 250 rpm at room temperature (25 ± 2 ºC) and the adsorption capacity as well as removal efficiency of the adsorbent was calculated using equations (1) & (2). This procedure was repeated 5 times.[32]

RESULTS AND DISCUSSION

FTIR spectra of the ZIF-8 and ZIF-67 MOFs are presented in Figures S1-S4 in which bands at 2817 cm^{-1} and 1566 cm^{-1} are observed. These bands correspond to stretching vibrations of -CH and -CN groups present in imidazole rings in ZIF-8 and ZIF-67 MOFs. Many other typical bands at about 3329 cm^{-1}, 684 cm^{-1}, 617 cm^{-1} and 432 cm^{-1} are also present, indicating the presence of -OH, Zn-O, Zn-N, and Co-N bonds, respectively in the MOFs. After the adsorption of arsenic species, FTIR spectra were also performed, and the results confirm that adsorption of arsenic species takes place successfully as indicated by the stretching vibrations at 832 cm^{-1}, 924 cm^{-1}, 3633 cm^{-1} and 3737 cm^{-1}. These vibrations are exhibited due to the interactions among the arsenic species and the ZIF-8 and ZIF-67 MOFs. From the FTIR study, it was concluded that the adsorption of arsenic species on the surface of MOFs takes place successfully, as vibrations in the FTIR spectrum at 832 cm^{-1} and 924 cm^{-1} are typically shown by As-O bonds present in MOFs after the adsorption process.[32]

From the powder XRD analysis, it was confirmed that the MOFs showed crystallinity, lattice structure and uniform morphology (Figure 2**).** The main peaks in Figure 2-b and 2-d closely matched with reported study.[30,33,34] From the scanning electron microscopy (SEM) results, it was shown that the ZIF-8 MOF have cubic and ZIF-67 have polyhedral geometry, which also gives a strong indication for the synthesis and purity of ZIF-8 & ZIF-67 nanoparticles (Figure 2).

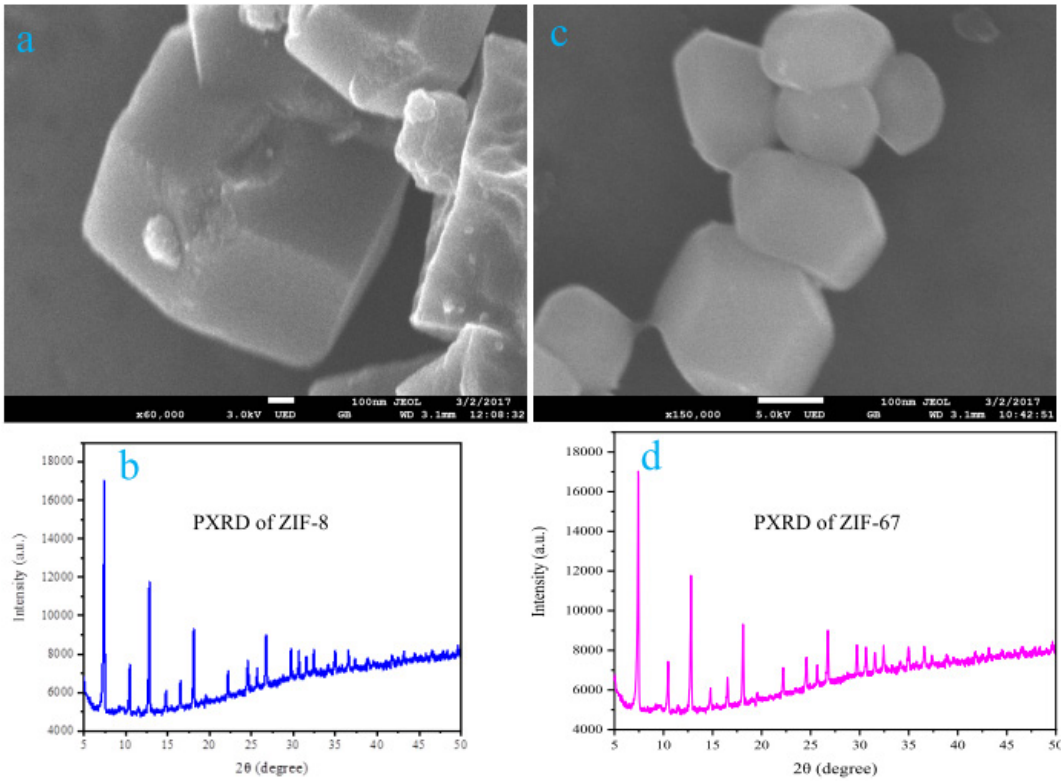

Figure 2. Morphology of ZIF-8 MOF which is cubic (a) and ZIF-67 MOF which is polyhedral (c) shown by SEM; Powder XRD pattern of ZIF-8 (b) and ZIF-67 (d). [Reprinted from *Food Chem. Toxicol*. **2021**, *149*, 112008. Ahmad, K.; Shah, H.-R.; Ashfaq, M.; Shah, S. S. A.; Hussain, E.; Naseem, H. A.; Parveen, S.; Ayub, A. Effect of metal atom in zeolitic imidazolate frameworks (ZIF-8 & 67) for removal of Pb^{2+} & Hg^{2+} from Water. https://doi.org/10.1016/j.fct.2021.112008 Copyright© (2022), with permission from Elsevier.]

From the Brunauer-Emmett-Teller (BET) analysis, the pore size ratio and porosity were calculated. The nitrogen adsorption/desorption curves in Figure 3 indicate that these MOFs have high surface area and are nanoparticles, which means that ZIF-8 & ZIF-67 are highly porous materials. The porosity is directly related to the separation and adsorption capacity of the material for the removal of contaminants.

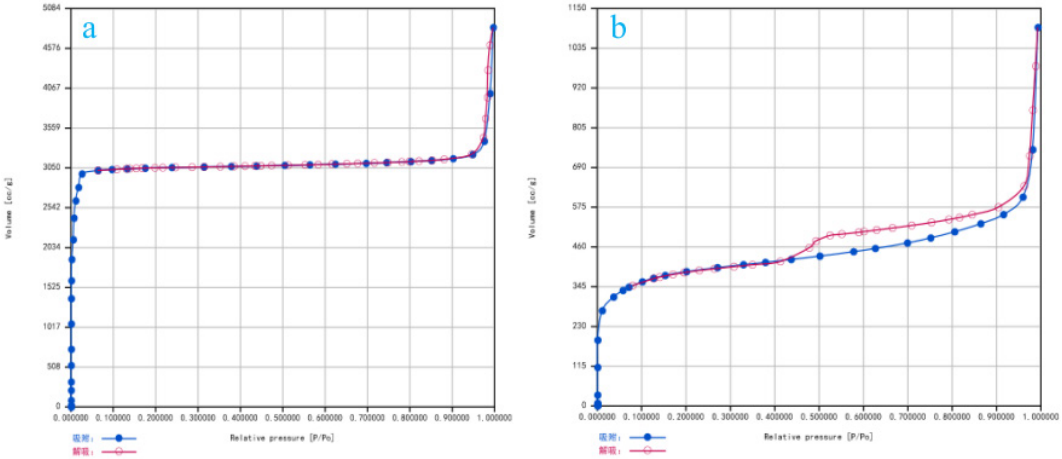

Figure 3. Nitrogen adsorption/desorption curves of ZIF-8 (a) and ZIF-67 (b).

Adsorption Studies

Effect of pH

The adsorption capacity of the synthesized MOFs was tested at different pH values. ZIF-8 & ZIF-67 showed maximum adsorption capacities for adamsite, As(III) and As(V) at pH 7.8, what can be explained by the negatively and positively charged sphere in ZIF-67 & ZIF-8 at pH 7.8. The maximum adsorption capacity was 70.29 & 62.01, 71.49 & 70.92, 87.03 & 86.70 mg g^{-1} for adamsite, arsenite and arsenate, respectively, at pH 7.8. From this experiment, it was supposed that π-π and electrostatic interactions are the main forces that operate between MOFs and arsenic species (Figures 4–5 and Figures S5–S8).

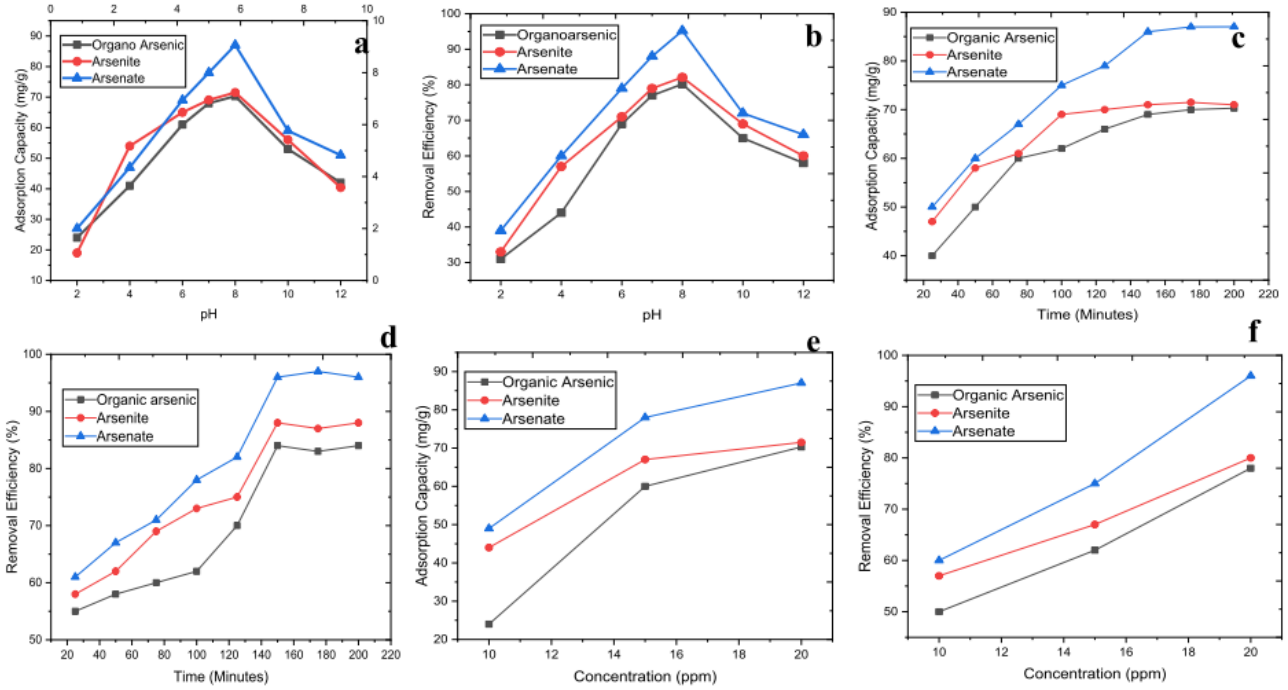

Figure 4. a) Adsorption capacity of ZIF-8 at acidic/basic and neutral pH; **b)** Removal efficiency of ZIF-8 at different pH values; **c)** Adsorption capacity of ZIF-8 *vs* time (minutes); **d)** Removal efficiency of ZIF-8 *vs* time (minutes); **e)** Adsorption capacity of ZIF-8 against different concentrations (10, 15 and 20 mg L^{-1}) of arsenic solutions in water; **f)** Removal efficiency of ZIF-8 against different concentrations (10, 15 and 20 mg L^{-1}) of arsenic solutions in water.

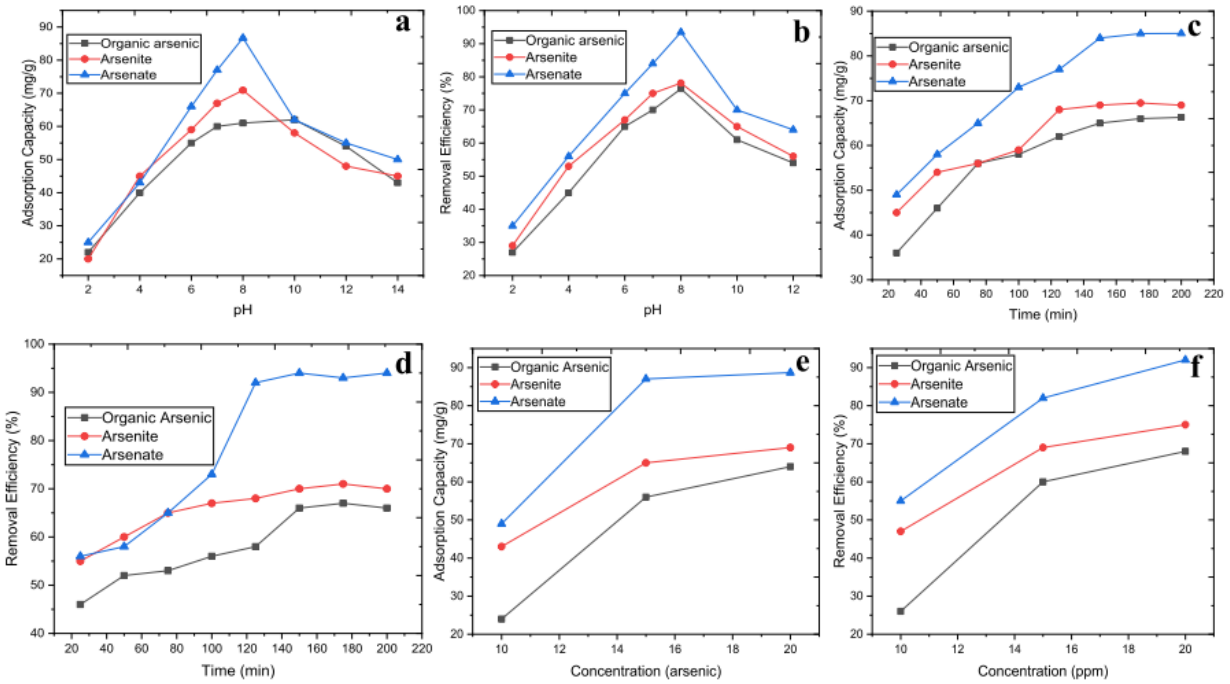

Figure 5. a) Adsorption capacity of ZIF-67 at acidic/basic and neutral pH. **b)** Removal efficiency of ZIF-67 at different pH. **c)** Adsorption capacity of ZIF-67 Vs time (minutes). **d)** Removal efficiency of ZIF-67 Vs time (minutes). **e)** Adsorption capacity of ZIF-67 against different concentrations (10, 15 and 20 mg L^{-1}) of arsenic solutions in water. **f)** Removal efficiency of ZIF-67 against different concentrations (10, 15 and 20 mg L^{-1}) of arsenic solutions in water.

To investigate the MOFs' stability and the ion exchange mechanism, 0.5 g of MOFs were added to 50 mL of ultra-pure water, sonicated for 30 minutes to form a suspension, and left for 6 hours. After that, filtration was done followed by centrifugation for 10 minutes. The amount of cobalt and zinc metal in the solutions were measured by atomic absorption spectrometry. The amount determined was 0.0003 g L^{-1}, which assumes that these MOFs are highly water stable and exchange their metal ions to a very low extent. To confirm the ion exchange mechanism, it was observed that at pH ≤ 5 these MOFs contain negative charge. As the arsenic species arsenite and arsenate exist in water in the anionic form and these MOFs at pH < 5 also contain negative sphere, these same charges should be repelled and there will be practically no adsorption at pH < 5. However, in the pH experiments, it was observed that at pH < 5 adsorption of arsenic also occurred. Consequently, from the results, it was concluded that in addition to the electrostatic interaction, the ion exchange interaction also occurs, which is responsible for this adsorption of arsenic species even with the same charges.[20,35]

Effect of contact time

The adsorption capacity of ZIF-8 & ZIF-67 was also studied at different time intervals to check the effect of removal efficiency with time. In the beginning, the removal of arsenic was very sharp and after 1 hour this process was slowed down and then reached equilibrium after 3 hours. Initially, the adsorption process was very fast due to the availability of maximum surface area and arsenic metal, but in the course of time, the availability of pores and arsenic metal ions decreased, hence the adsorption capacity also decreased.[36,37] The maximum adsorption capacity of ZIF-8 & ZIF-67 was 70.29 & 62.01, 71.49 & 70.92, 87.03 & 86.70 mg g^{-1} at equilibrium time of 3 hours with 20 mg L^{-1} solutions of adamsite, arsenite and arsenate, respectively. These results of removal efficiency and adsorption capacity *versus* time are shown in Figures 4–5 and Figures S9–S12.

Effect of initial concentration of arsenic species

The effect of the concentration of arsenic species on the adsorption capacity was also studied. For this purpose, solutions of varying concentrations were prepared, such as 10, 15, and 20 mg L^{-1} of adamsite, arsenite and arsenate, and an adsorbent dose of 1 g L^{-1} was used. From the concentration effect study, it was observed that as the concentration of arsenic species is increased from 10 – 20 mg L^{-1} the adsorption capacity of arsenic is also increased but removal efficiency decreased. The increase in the adsorption capacity was due to the availability of more and more arsenic ions in the solution which increases the adsorption of arsenic on the surface of MOFs (Figures 4–5 and Figures S13–S16).[38] Furthermore, it was observed that the adsorption capacity is directly proportional to the concentration of arsenic species, while the removal efficiency is inversely related to the concentration of these arsenic ions.[39]

Adsorption Kinetics

For explanation of the adsorption process with MOFs, pseudo 1st and 2nd order models were applied. It was observed that pseudo 2nd order is best fitted for adsorption of arsenic species, since the R^2 values for adamsite, arsenite and arsenate are high, namely: 0.9901 & 0.99087, 0.97013 & 0.9929, 0.9947 & 0.9975, respectively. As correlation coefficient value for pseudo 2nd order is maximum, it can be inferred that chemisorption or chemical adsorption of arsenic species takes place using MOFs. Chemical adsorption means that functional groups such as the amine group present in the MOFs are responsible for the adsorptive elimination of arsenic species from water. Besides chemical adsorption, the ion exchange process is also involved for the efficient removal of arsenic.[22] The graphical representation of kinetic models is given in Figure 6, Figures S17–S20 and Tables I–II.

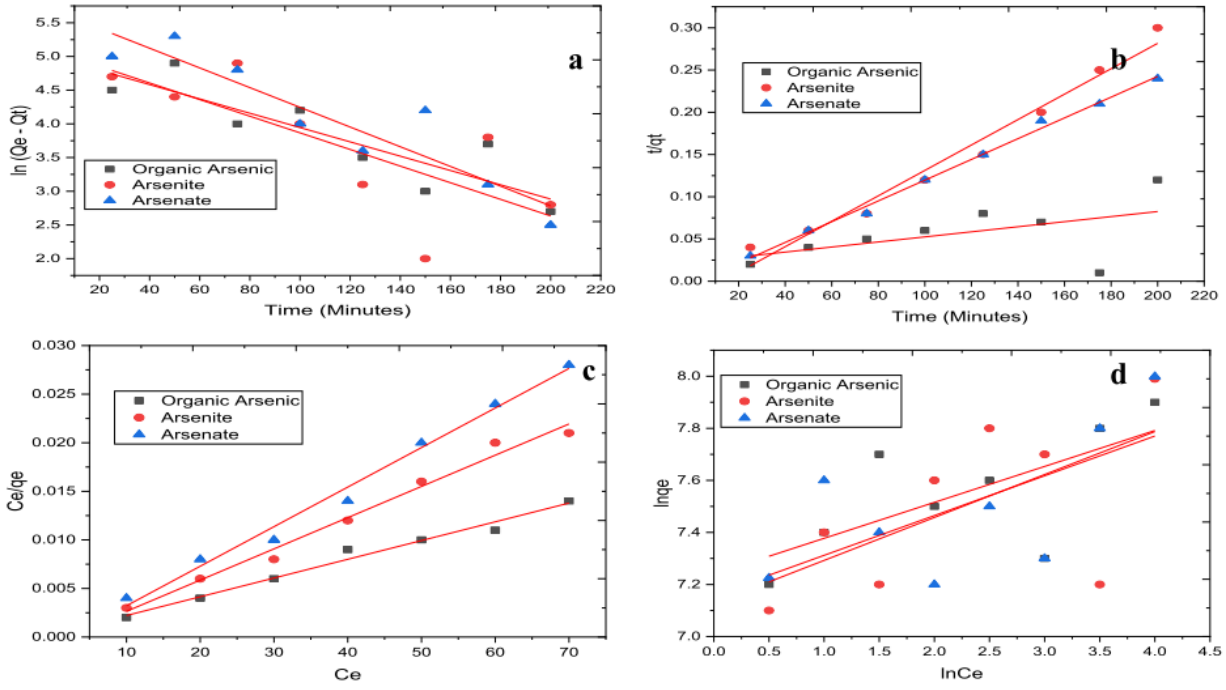

Figure 6. a) Kinetic parameters for the pseudo first order kinetics model for the removal of arsenic using ZIF-8, **b)** Kinetic parameters for the pseudo second order kinetics model for the removal of arsenic using ZIF-8, **c)** Adsorption isotherm fitted by Langmuir Model, **d)** Adsorption isotherm fitted by Freundlich Model.

Table I. Kinetic parameters (pseudo first order and second order equations) for adsorption process using ZIF-8

	Pseudo First Order				Pseudo Second Order				
Arsenic Species	**Q_e (mg g^{-1})**	**K_1 (h^{-1})**	**R^2**	**Pearson value**	**Q_e (mg g^{-1})**	**K_2 (g mg^{-1} h^{-1})**	**R^2**	**Qe exp (mg g^{-1})**	**Pearson value**
Organic Arsenic	58.66	2.3126	0.73081	0.70511	62.01	0.0577	0.99011	70.49	0.92451
As(III)	63.39	2.8932	0.49049	0.51472	68.78	0.0611	0.97013	71.29	0.98711
As(V)	71.10	3.0765	0.83125	0.85149	74.84	0.0687	0.99477	87.03	0.99775

Table II. Kinetic parameters (pseudo first order and second order equations) for adsorption process using ZIF-67

	Pseudo First Order				Pseudo Second Order				
Arsenic Species	**Q_e (mg g^{-1})**	**K_1 (h^{-1})**	**R^2**	**Pearson value**	**Q_e (mg g^{-1})**	**K_2 (g mg^{-1} h^{-1})**	**R^2**	**Q_e exp (mg g^{-1})**	**Pearson value**
Organic Arsenic	57.21	4.90714	0.73081	0.68521	62.01	0.0577	0.99011	76.21	0.99594
As(III)	62.01	5.009	0.56328	0.71421	70.92	0.0611	0.97013	78.12	0.99686
As(V)	86.70	5.60714	0.85535	0.80123	79.57	0.0687	0.99477	88.71	0.9989

Adsorption isotherm

To explain the isothermal adsorption, the Freundlich and Langmuir models were applied. The Langmuir model was best fitted having R^2 values for adamsite, arsenite and arsenate being 0.97898 & 0.98577, 0.98306 & 0.99356, 0.98577 & 0.99771, respectively. The linear plots of these models are presented in Figure 6, Figures S21–S24 and Tables III–IV**.** This experiment revealed that MOFs prescribe monolayer adsorptive removal of adamsite, arsenite and arsenate due to the higher surface area, large functionality,[40] open metal and pore sites, and exhibited maximum adsorption capacity in a very short time as compared to other MOFs, as given in Table V.

Table III. Langmuir and Freundlich model parameters using ZIF-8

	Langmuir Model				Freundlich Model		
Arsenic Species	**Q_e (mg g^{-1})**	**K_L (L mg^{-1})**	**R^2**	**Pearson Value**	**K_F (mg g^{-1})**	**R^2**	**Pearson value**
Organic Species	70.49	0.4258	0.97898	0.9912	59.23	0.38955	0.69048
As(III)	71.29	0.0292	0.98306	0.9929	61.12	0.29014	0.62574
As(V)	87.03	0.0337	0.98577	0.9941	74.70	0.34001	0.29014

Table IV. Langmuir and Freundlich model parameters using ZIF-67

	Langmuir Model				Freundlich Model		
Arsenic Species	**Q_e (mg g^{-1})**	**K_L (L mg^{-1})**	**R^2**	**Pearson Value**	**K_F (mg g^{-1})**	**R^2**	**Pearson value**
Organic Species	62.01	0.4101	0.98577	0.99405	57.11	0.11979	0.20045
As(III)	70.49	0.0287	0.99356	0.99731	60.58	0.15415	0.10356
As(V)	86.70	0.0371	0.99771	0.99904	78.19	0.14091	0.51345

Table V. Comparison of adsorption of As (III), As (V) and organic arsenic using ZIF-8 & ZIF-67 with other adsorbents reported in the literature

Adsorbent	**pH**	**Concentration (mg L^{-1})**	**Adsorption Capacity (mg g^{-1})**			**Ref.**
			As (III)	**As (V)**	**Organic As**	
Fe-Chitosan Flakes	7.0	1 – 10	16.15	22.47	-	41
Fe-Coated Zeolites	4.0	0 – 20	-	0.68	-	42
Activated Alumina	7.0	0 – 250	19.63	-	-	43
Fe-Zr Binary Oxide	7.0	0.5 – 15	-	9.36	-	44
Fe-Mn Binary Oxide	6.9	0 – 40	100.4	53.90	-	45
CuO Nanoparticles	8.0	0.1 – 100	26.9	22.60	-	46
Treated Laterite	7.0	0.2 – 20	9.4	21.60	-	47
$ZrO_2 \cdot xH_2O$	7.0	0.3 – 100	47.1	29.30	-	48
Fe_3O_4	7.0	0 – 100	5.68	4.78	-	49
ZIF-8	6.0-8.0	0 – 20	71.49	87.03	70.29	This Study
ZIF-67	6.0-8.0	0 – 20	70.92	86.70	62.01	This Study

Adsorption mechanism

Adsorption is a surface-based exothermic process in which molecules of a compound in the gaseous or liquid state are accumulated on an adsorbent surface. During adsorption, two main processes are involved, such as physical adsorption (physisorption or adsorptive adsorption) and chemical adsorption (chemisorption or reactive adsorption). Adsorption is caused by London dispersion forces, a type of van der Waals force that exists between molecules and acts in the same way as gravitational forces between planets. The adsorption process is always exothermic because surface particles of the adsorbent are unstable and when the adsorbate is adsorbed on the surface, the energy of the adsorbent decreases and this results in heat evolution.[41–46] For the explanation of the adsorption process for arsenic removal, FTIR analyses were also performed after the adsorption process. The spectra obtained show peaks in the range

of 832 cm^{-1}, 924 cm^{-1}, 3637 cm^{-1} and 3737 cm^{-1} which are exhibited due to interactions among arsenic species and MOFs (Figures S1–S4). Therefore, the FTIR results indicate that MOFs are successfully formed and adsorb arsenic species on their surfaces due to the presence of the NH group.[47–50] Furthermore, the bands in the FTIR spectrum at 832 cm^{-1} and 924 cm^{-1} are typically presented by MOFs due to As-O bonds after the adsorption of arsenic.[32] Figure 7 presents the proposed adsorption mechanism.

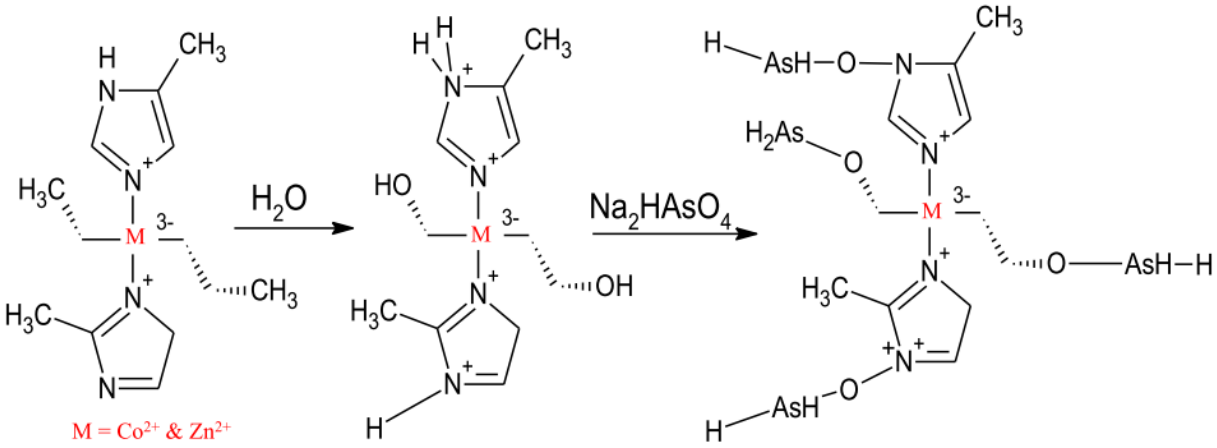

Figure 7. Proposed adsorption mechanism for the removal of arsenic species using ZIF-8 & ZIF-67.

Reusability of the synthesized MOFs

From the regeneration experiments, it was observed that the ZIF-67 and ZIF-8 MOFs exhibited regeneration up to 95% and 92% respectively (Figure S25), which indicates that these MOFs can be repeatedly applied for the removal of arsenic species present in water.[45,51,52]

CONCLUSION

In summary, the synthesis of ZIF-8 and ZIF-67 via hydrothermal technique was achieved and the MOFs obtained were considered suitable for the removal of arsenic metal ions from aqueous solution. The adsorption capacities of the synthesized MOFs were 70.29 & 62.01, 71.49 & 70.92, 87.03 & 86.70 mg g^{-1} for adamsite, arsenite and arsenate, respectively, which represent excellent adsorption capacities as compared to other adsorbents. This adsorption capacity is mainly due to three reasons: porosity of adsorbents which capture the arsenic species tightly to bind with ZIF-8 and ZIF-67, the MOFs' high surface area, and van der Waals forces. The ZIF-8 & ZIF-67 MOFs exhibited similar arsenic adsorption capacities due to the presence of the same organic ligand (2-methyl imidazole) and the same geometry, shape, pore size and porosity. There is a slight decrease in the adsorption capacity in the case of adamsite removal that can be explained due the presence of different central metal atoms, i.e. zinc in ZIF-8 and cobalt in ZIF-67. The regeneration procedures revealed that these MOFs can be applied repeatedly for arsenic removal from water. These results indicate that ZIF-8 and ZIF-67 are the most efficient MOFs for eliminating inorganic and organic arsenic from water solutions. From this work, it is suggested that future studies should be carried out for the applications of these MOFs for the removal of arsenic species in wastewater.

According to our information, this is the first study in which the assessment between ZIF-8 and ZIF-67 is explored for the removal of organic and inorganic arsenic species from water.

Conflict of interest

The authors declare no conflict of interest.

Acknowledgment

The authors are very thankful to the Institute of Chemistry, Baghdad ul Jadeed Campus, Islamia University of Bahawalpur, Punjab, Pakistan for making their facilities available, especially the atomic absorption spectrometer (AAS) to carry out this study.

REFERENCES

(1) Yazdani, M. R.; Tuutijärvi, T.; Bhatnagar, A.; Vahala, R. Adsorptive Removal of Arsenic(V) from Aqueous Phase by Feldspars: Kinetics, Mechanism, and Thermodynamic Aspects of Adsorption. *J. Mol. Liq.* **2016**, *214*, 149–156. https://doi.org/10.1016/j.molliq.2015.12.002

(2) Ahmad, K.; Shah, H.-R.; Ashfaq, M.; Shah, S. S. A.; Hussain, E.; Naseem, H. A.; Parveen, S.; Ayub, A. Effect of Metal Atom in Zeolitic Imidazolate Frameworks (ZIF-8 & 67) for Removal of Pb^{2+} & Hg^{2+} from Water. *Food Chem. Toxicol.* **2021**, *149*, 112008. https://doi.org/10.1016/j.fct.2021.112008

(3) Correll, R.; Huq, S. M. I.; Smith, E.; Owens. G.; Naidu, R. Dietary intake of arsenic from crops: Overview from the Bangladesh study. In R. Naidu, E. Smith, G. Owens, P. Bhattacharya, & P. Nadebaum (Eds.), *Managing Arsenic in the Environment: From soil to human health*, **2006**, 255–271. Melbourne, Australia: CSIRO Publishing.

(4) Naidu, R.; Bhattacharya, P. Arsenic in the Environment—Risks and Management Strategies. *Environ. Geochem. Health* **2009**, *31* (S1), 1–8. https://doi.org/10.1007/s10653-008-9243-0

(5) Zakhar, R.; Derco, J.; Čacho, F. An Overview of Main Arsenic Removal Technologies. *Acta Chim. Slovaca* **2018**, *11* (2), 107–113. https://doi.org/10.2478/acs-2018-0016

(6) Burkert, L. A. Geochemical controls on arsenic distribution and mobilization in groundwater of Southeastern Pennsylvania. A Thesis presented in 2006 to the Graduate and Research Committee of Lehigh University in candidacy for the Degree of Master of Science in the Department of Earth and Environmental Sciences, Lehigh University, PA, USA.

(7) Moore, J. W.; Ramamoorthy, S. *Heavy Metals in Natural Waters: Applied Monitoring and Impact Assessment.* Springer: New York, **2011**. https://doi.org/10.1016/0022-1694(85)90085-x

(8) Cebrian, M. E.; Albores, A.; Aguilar, M.; Blakely, E. Chronic Arsenic Poisoning in the North of Mexico. *Hum. Toxicol.* **1983**, *2* (1), 121–133. https://doi.org/10.1177/096032718300200110

(9) Brooks, R. R.; Fergusson, J. E.; Holzbecher, J.; Ryan, D. E.; Zhang, H. F.; Dale, J. M.; Freedman, B. Pollution by Arsenic in a Gold-Mining District in Nova Scotia. *Environ. Pollut. Ser. B, Chem. Phys.* **1982**, *4* (2), 109–117. https://doi.org/10.1016/0143-148X(82)90021-0

(10) Wang, G.; Zhao, X.; Han, S. Effect of MgO Addition on the Properties of Ni/Al_2O_3 and Its Catalytic Activity in Hydrogenation of N-(2`,3`-dimethoxy benzyl)-3,4-dioxy-methylene-phenylethylamine. *J. Chem. Soc. Pak.* **2019**, *41* (5), 796–804.

(11) Islam, S.; Shaikh, I. A.; Firdous, N.; Ali, A.; Sadef, Y. Performance Evaluation of Fenton Oxidation Treatment Method for the Reuse of Reactive Dyeing Effluent. *J. Chem. Soc. Pakistan* **2019**, *41* (6), 1138–1144.

(12) Mahmood, K.; Akhter, Z.; Liaqat, F.; Mirza, B. Synthesis, DNA Binding Affinity, Molecular Docking Study and Antitumor Activity of Cu(II), Pd(II) and Zn(II) Metal Complexes of Benzimidazole Schiff Base Ligand. *J. Chem. Soc. Pakistan* **2019**, *41* (5), 903–914.

(13) Khalid, I.; Ali, S.; Hussain, M. T.; Ashra, R.; Khan, A.; Ahmad, N. Investigating the Impact of Hard Water on Natural Dyeing of Cotton Fabric by *Tagetes erecta* Flowers. *J. Chem. Soc. Pakistan* **2019**, *41* (5), 788–795.

(14) Zheng, X.; Yi, M.; Chen, Z.; Zhang, Z.; Ye, L.; Cheng, G.; Xiao, Y. Efficient Removal of As(V) from Simulated Arsenic-contaminated Wastewater via a Novel Metal–Organic Framework Material: Synthesis, Structure, and Response Surface Methodology. *Appl. Organomet. Chem.* **2020**, *34* (5). https://doi.org/10.1002/aoc.5584

(15) Pang, D.; Wang, P.; Fu, H.; Zhao, C.; Wang, C.-C. Highly Efficient Removal of As(V) Using Metal–Organic Framework BUC-17. *SN Appl. Sci.* **2020**, *2* (2), 184. https://doi.org/10.1007/s42452-020-1981-3

(16) Ploychompoo, S.; Chen, J.; Luo, H.; Liang, Q. Fast and Efficient Aqueous Arsenic Removal by Functionalized MIL-100(Fe)/RGO/δ-MnO2 Ternary Composites: Adsorption Performance and Mechanism. *J. Environ. Sci.* **2020**, *91*, 22–34. https://doi.org/10.1016/j.jes.2019.12.014
(17) Haldar, D.; Duarah, P.; Purkait, M. K. MOFs for the Treatment of Arsenic, Fluoride and Iron Contaminated Drinking Water: A Review. *Chemosphere* **2020**, *251*, 126388. https://doi.org/10.1016/j.chemosphere.2020.126388
(18) Bessaies, H.; Iftekhar, S.; Doshi, B.; Kheriji, J.; Ncibi, M. C.; Srivastava, V.; Sillanpää, M.; Hamrouni, B. Synthesis of Novel Adsorbent by Intercalation of Biopolymer in LDH for the Removal of Arsenic from Synthetic and Natural Water. *J. Environ. Sci.* **2020**, *91*, 246–261. https://doi.org/10.1016/j.jes.2020.01.028
(19) Ahmad, K.; Naseem, H. A.; Parveen, S.; Shah, H.-R.; Shah, S. S. A.; Shaheen, S.; Ashfaq, A.; Jamil, J.; Ahmad, M. M.; Ashfaq, M. Synthesis and Spectroscopic Characterization of Medicinal Azo Derivatives and Metal Complexes of Indandion. *J. Mol. Struct.* **2019**, *1198*, 126885. https://doi.org/10.1016/j.molstruc.2019.126885
(20) Nasir, A. M.; Md Nordin, N. A. H.; Goh, P. S.; Ismail, A. F. Application of Two-Dimensional Leaf-Shaped Zeolitic Imidazolate Framework (2D ZIF-L) as Arsenite Adsorbent: Kinetic, Isotherm and Mechanism. *J. Mol. Liq.* **2018**, *250*, 269–277. https://doi.org/10.1016/j.molliq.2017.12.005
(21) Khan, N. A.; Najam, T.; Shah, S. S. A.; Hussain, E.; Ali, H.; Hussain, S.; Shaheen, A.; Ahmad, K.; Ashfaq, M. Development of Mn-PBA on GO Sheets for Adsorptive Removal of Ciprofloxacin from Water: Kinetics, Isothermal, Thermodynamic and Mechanistic Studies. *Mater. Chem. Phys.* **2020**, *245*, 122737. https://doi.org/10.1016/j.matchemphys.2020.122737
(22) Massoudinejad, M.; Mohammadi, A.; Sadeghi, S.; Ghaderpoori, M.; Sahebi, S.; Alinejad, A. Arsenic Adsorption over Dodecahedra ZIF-8 from Solution Aqueous: Modelling, Isotherms, Kinetics and Thermodynamics. *Int. J. Environ. Anal. Chem.* **2020**, 1–17. https://doi.org/10.1080/03067319.2020.1727458
(23) Younes, M. M.; Abdel-Rahman, H. A.; Hamed, E. Effect of gamma-irradiation on properties of polymer/fibrous/nanomaterials particleboard composites. *J. Chem. Soc. Pakistan* **2019**, *41* (6), 966–973.
(24) Mohan, D.; Pittman, C. U. Arsenic Removal from Water/Wastewater Using Adsorbents – A Critical Review. *J. Hazard. Mater.* **2007**, *142* (1–2), 1–53. https://doi.org/10.1016/j.jhazmat.2007.01.006
(25) Poyraz, M.; Sari, M.; Berber, H.; Karaca, N.; Demirci, F. Synthesis, characterization and X-Ray crystal structure of the new Schiff base and anticandidal evaluation. *J. Chem. Soc. Pakistan* **2019**, *41* (6), 1090–1096.
(26) Tranchemontagne, D. J.; Mendoza-Cortés, J. L.; O'Keeffe, M.; Yaghi, O. M. Secondary Building Units, Nets and Bonding in the Chemistry of Metal–Organic Frameworks. *Chem. Soc. Rev.* **2009**, *38* (5), 1257–1283. https://doi.org/10.1039/b817735j
(27) Xu, R.; Ji, Q.; Zhao, P.; Jian, M.; Xiang, C.; Hu, C.; Zhang, G.; Tang, C.; Liu, R.; Zhang, X.; Qu, J. Hierarchically Porous UiO-66 with Tunable Mesopores and Oxygen Vacancies for Enhanced Arsenic Removal. *J. Mater. Chem. A* **2020**, *8* (16), 7870–7879. https://doi.org/10.1039/C9TA13747E
(28) Ahmad, K.; Shah, H.-ur-R.; Ashfaq, A.; Ashfaq, M.; Kashif, M.; Naseem, H. A.; Aziz, T.; Parveen, S.; Hafsa, N. I. Synthesis of New Series of Phenyldiazene Based Metal Complexes for Designing Most Active Antibacterial and Antifungal Agents. *J. Chem. Soc. Pakistan* **2021**, *43* (5), 578–586. https://doi.org/10.52568/000599/JCSP/43.05.2021
(29) Peng, L.; Shah, S. S. A.; Wei, Z. Recent Developments in Metal Phosphide and Sulfide Electrocatalysts for Oxygen Evolution Reaction. *Chinese J. Catal.* **2018**, *39* (10), 1575–1593. https://doi.org/10.1016/S1872-2067(18)63130-4
(30) Nazir, M. A.; Yasar, A.; Bashir, M. A.; Siyal, S. H.; Najam, T.; Javed, M. S.; Ahmad, K.; Hussain, S.; Anjum, S.; Hussain, E.; Shah, S. S. A.; Rehman, A. U. Quality Assessment of the Noncarbonated-Bottled Drinking Water: Comparison of Their Treatment Techniques. *Int. J. Environ. Anal. Chem.* **2020**, 1–12. https://doi.org/10.1080/03067319.2020.1846732

(31) Qian, J.; Sun, F.; Qin, L. Hydrothermal Synthesis of Zeolitic Imidazolate Framework-67 (ZIF-67) Nanocrystals. *Mater. Lett.* **2012**, *82*, 220–223. https://doi.org/10.1016/j.matlet.2012.05.077
(32) Li, Z.; Liu, X.; Jin, W.; Hu, Q.; Zhao, Y. Adsorption Behavior of Arsenicals on MIL-101(Fe): The Role of Arsenic Chemical Structures. *J. Colloid Interface Sci.* **2019**, *554*, 692–704. https://doi.org/10.1016/j.jcis.2019.07.046
(33) Ayub, A.; Irfan, A.; Raza, Z. A.; Abbas, M.; Muhammad, A.; Ahmad, K.; Munwar, A. Development of Poly(1-Vinylimidazole)-Chitosan Composite Sorbent under Microwave Irradiation for Enhanced Uptake of Cd(II) Ions from Aqueous Media. *Polym. Bull.* **2022**, *79* (2), 807–827. https://doi.org/10.1007/s00289-020-03523-7
(34) Naseem, H. A.; Aziz, T.; Shah, H.-R.; Ahmad, K.; Parveen, S.; Ashfaq, M. Rational Synthesis and Characterization of Medicinal Phenyl Diazenyl-3-Hydroxy-1h-Inden-1-One Azo Derivatives and Their Metal Complexes. *J. Mol. Struct.* **2021**, *1227*, 129574. https://doi.org/10.1016/j.molstruc.2020.129574
(35) Huo, J.-B.; Xu, L.; Yang, J.-C. E.; Cui, H.-J.; Yuan, B.; Fu, M.-L. Magnetic Responsive Fe3O4-ZIF-8 Core-Shell Composites for Efficient Removal of As(III) from Water. *Colloids Surfaces A Physicochem. Eng. Asp.* **2018**, *539*, 59–68. https://doi.org/10.1016/j.colsurfa.2017.12.010
(36) Ahmad, K.; Shah, H.-U.-R.; Ashfaq, M.; Nawaz, H. Removal of Decidedly Lethal Metal Arsenic from Water Using Metal Organic Frameworks: A Critical Review. *Rev. Inorg. Chem.* **2021**. https://doi.org/10.1515/revic-2021-0005
(37) Meteku, B. E.; Huang, J.; Zeng, J.; Subhan, F.; Feng, F.; Zhang, Y.; Qiu, Z.; Aslam, S.; Li, G.; Yan, Z. Magnetic Metal–Organic Framework Composites for Environmental Monitoring and Remediation. *Coord. Chem. Rev.* **2020**, *413*, 213261. https://doi.org/10.1016/j.ccr.2020.213261
(38) Jian, M.; Liu, B.; Zhang, G.; Liu, R.; Zhang, X. Adsorptive Removal of Arsenic from Aqueous Solution by Zeolitic Imidazolate Framework-8 (ZIF-8) Nanoparticles. *Colloids Surfaces A Physicochem. Eng. Asp.* **2015**, *465*, 67–76. https://doi.org/10.1016/j.colsurfa.2014.10.023
(39) Parajuli, D.; Ponte, R.; Zhang, N.; Nakamura, T.; Kawamoto, T. Synthesis and Characterization of Mixed Co-Zn-ZIF for Arsenic(V) Adsorption. *Inorganica Chim. Acta* **2020**, *502*, 119311. https://doi.org/10.1016/j.ica.2019.119311
(40) Li, Y.; Li, J.; Soria, R. B.; Volodine, A.; Van der Bruggen, B. Aramid Nanofiber and Modified ZIF-8 Constructed Porous Nanocomposite Membrane for Organic Solvent Nanofiltration. *J. Memb. Sci.* **2020**, *603*, 118002. https://doi.org/10.1016/j.memsci.2020.118002
(41) Gupta, A.; Chauhan, V. S.; Sankararamakrishnan, N. Preparation and Evaluation of Iron–Chitosan Composites for Removal of As(III) and As(V) from Arsenic Contaminated Real Life Groundwater. *Water Res.* **2009**, *43* (15), 3862–3870. https://doi.org/10.1016/j.watres.2009.05.040
(42) Jeon, C.-S.; Baek, K.; Park, J.-K.; Oh, Y.-K.; Lee, S.-D. Adsorption characteristics of As(V) on iron-coated zeolite. *J. Hazard. Mater.* **2009**, *163* (2–3), 804–808. https://doi.org/10.1016/j.jhazmat.2008.07.052
(43) Maliyekkal, S. M.; Philip, L.; Pradeep, T. As(III) Removal from Drinking Water Using Manganese Oxide-Coated-Alumina: Performance Evaluation and Mechanistic Details of Surface Binding. *Chem. Eng. J.* **2009**, *153* (1–3), 101–107. https://doi.org/10.1016/j.cej.2009.06.026
(44) Gupta, K.; Basu, T.; Ghosh, U. C. Sorption Characteristics of Arsenic(V) for Removal from Water Using Agglomerated Nanostructure Iron(III)−Zirconium(IV) Bimetal Mixed Oxide. *J. Chem. Eng. Data* **2009**, *54* (8), 2222–2228. https://doi.org/10.1021/je900282m
(45) Zhang, G.-S.; Qu, J.-H.; Liu, H.-J.; Liu, R.-P.; Li, G.-T. Removal Mechanism of As(III) by a Novel Fe−Mn Binary Oxide Adsorbent: Oxidation and Sorption. *Environ. Sci. Technol.* **2007**, *41* (13), 4613–4619. https://doi.org/10.1021/es063010u
(46) Martinson, C. A.; Reddy, K. J. Adsorption of Arsenic(III) and Arsenic(V) by Cupric Oxide Nanoparticles. *J. Colloid Interface Sci.* **2009**, *336* (2), 406–411. https://doi.org/10.1016/j.jcis.2009.04.075
(47) Maiti, A.; Basu, J. K.; De, S. Experimental and Kinetic Modeling of As(V) and As(III) Adsorption on Treated Laterite Using Synthetic and Contaminated Groundwater: Effects of Phosphate, Silicate and Carbonate Ions. *Chem. Eng. J.* **2012**, *191*, 1–12. https://doi.org/10.1016/j.cej.2010.01.031

(48) Ren, Z.; Zhang, G.; Chen, J. P. Adsorptive Removal of Arsenic from Water by an Iron–Zirconium Binary Oxide Adsorbent. *J. Colloid Interface Sci.* **2011**, *358* (1), 230–237. https://doi.org/10.1016/j.jcis.2011.01.013

(49) Li, G.; Lan, J.; Liu, J.; Jiang, G. Synergistic Adsorption of As(V) from Aqueous Solution onto Mesoporous Silica Decorated Orderly with Al_2O_3 and Fe_2O_3 Nanoparticles. *J. Colloid Interface Sci.* **2013**, *405*, 164–170. https://doi.org/10.1016/j.jcis.2013.05.055

(50) Ahmad, K.; Rajpoot, S. R.; Shah, H. ur R.; Ashfaq, M.; Ahmad, Z. Assessment of Nutritional Status of Undergraduate Students of the Islamia University Bahawalpur. In Donmez, S. (Ed.) *Emerging Trends in Disease and Health Research,* Vol. 1; Book Publisher International (a part of SCIENCEDOMAIN International), **2021**, 32–43. https://doi.org/10.9734/bpi/etdhr/v1/15015D

(51) Shah, H. U. R.; Ahmad, K.; Naseem, H. A.; Parveen, S.; Ashfaq, M.; Aziz, T.; Shaheen, S.; Babras, A.; Shahzad, A. Synthetic Routes of Azo Derivatives: A Brief Overview. *J. Mol. Struct.* **2021**, *1244*, 131181. https://doi.org/10.1016/j.molstruc.2021.131181

(52) Shah, H. Ur R.; Ahmad, K.; Naseem, H. A.; Parveen, S.; Ashfaq, M.; Rauf, A.; Aziz, T. Water Stable Graphene Oxide Metal-Organic Frameworks Composite (ZIF-67@GO) for Efficient Removal of Malachite Green from Water. *Food Chem. Toxicol.* **2021**, *154*, 112312. https://doi.org/10.1016/j.fct.2021.112312

SUPPLEMENTARY MATERIAL

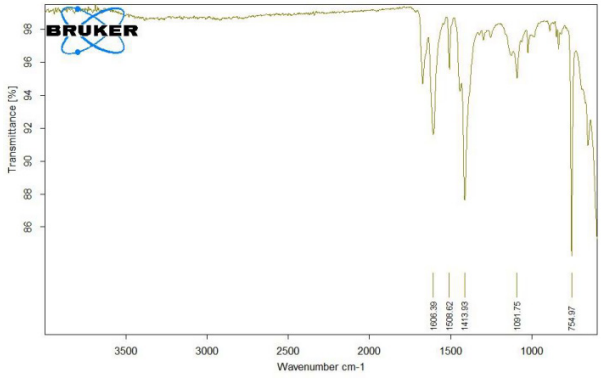

Figure S1. FTIR spectrum of ZIF-67 before the adsorption of Arsenic.

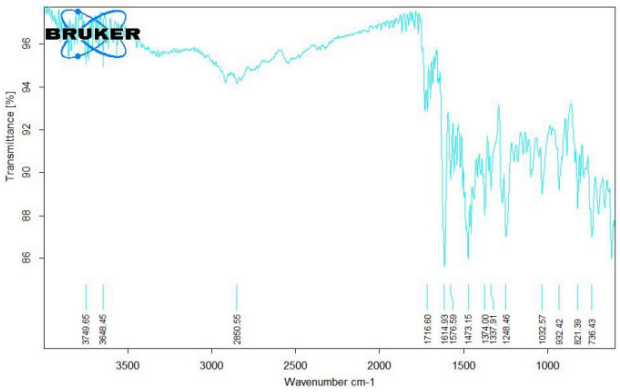

Figure S2. FTIR spectrum of ZIF-67 after the adsorption of Arsenic.

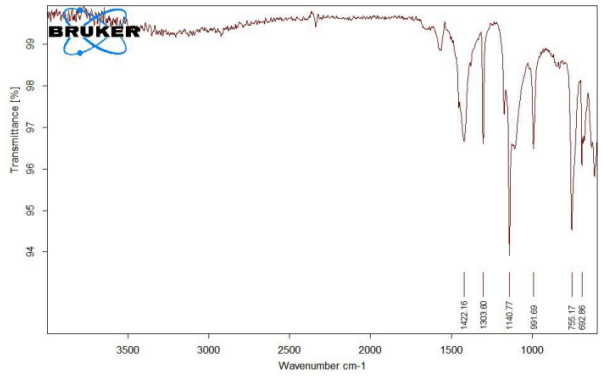

Figure S3. FTIR spectrum of ZIF-8 before the adsorption of arsenic.

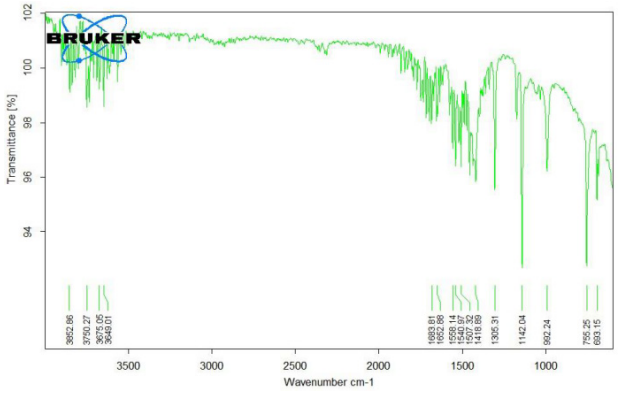

Figure S4. FTIR spectrum of ZIF-8 after the adsorption of arsenic.

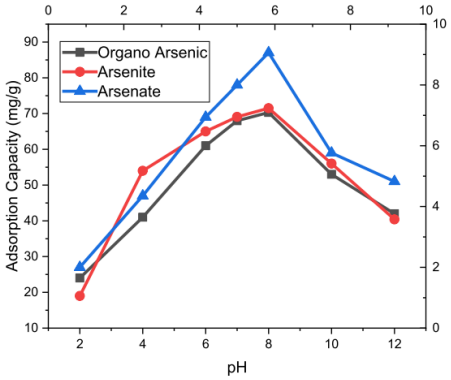

Figure S5. Adsorption capacity of organo arsenic, arsenite and arsenate using ZIF-8 at different pH.

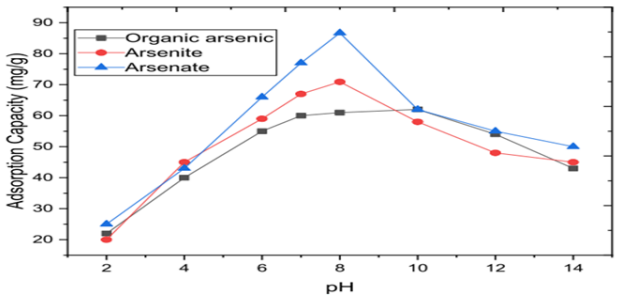

Figure S6. Adsorption capacity of organo arsenic, arsenite and arsenate using ZIF-67 at different pH.

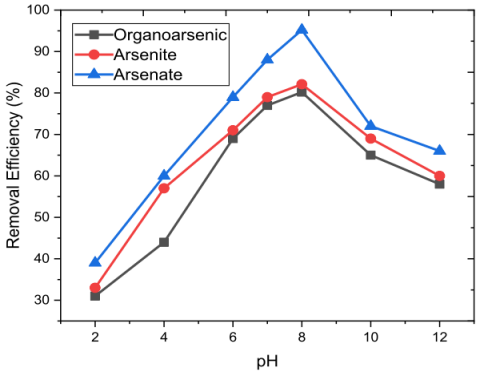

Figure S7. Removal efficiency of organo arsenic, arsenite and arsenate using ZIF-8 at different pH.

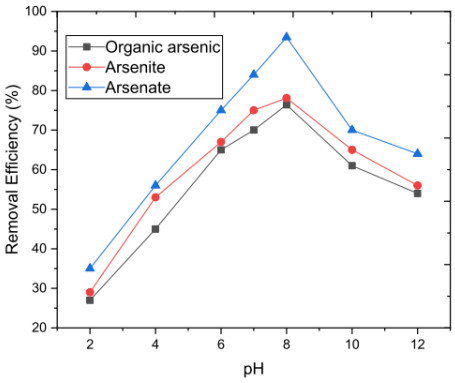

Figure S8. Removal efficiency of organo arsenic, arsenite and arsenate using ZIF-67 at different pH.

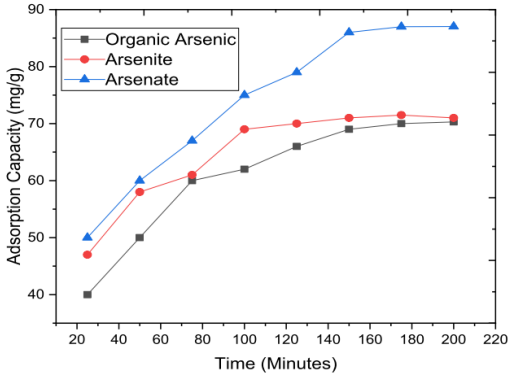

Figure S9. Adsorption capacity *vs* time for arsenic species using ZIF-8.

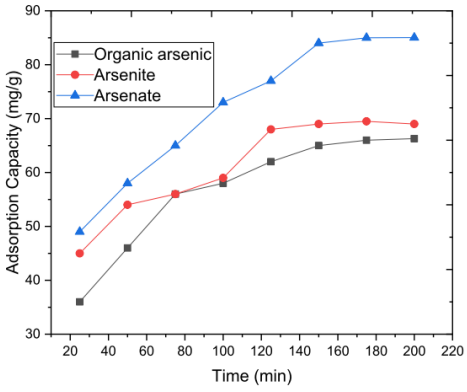

Figure S10. Adsorption capacity *vs* time for arsenic species using ZIF-67.

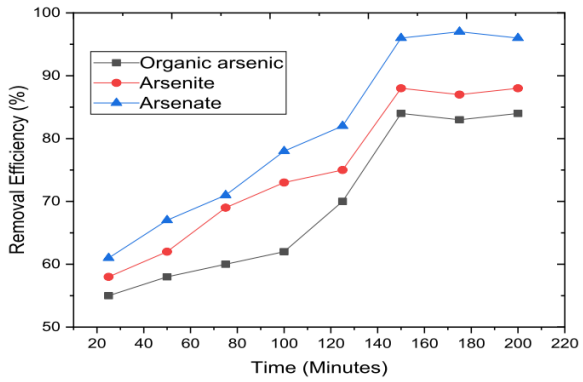

Figure S11. Removal efficiency *vs* time for arsenic species using ZIF-8.

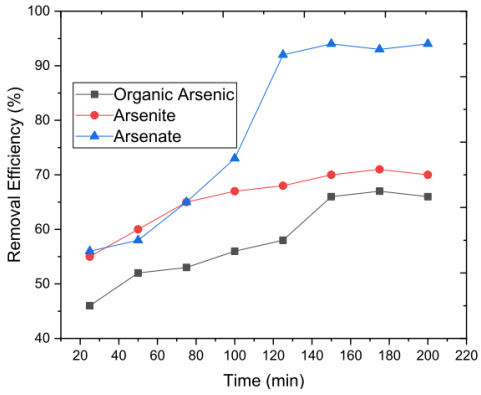

Figure S12. Removal efficiency *vs* time for arsenic species using ZIF-67.

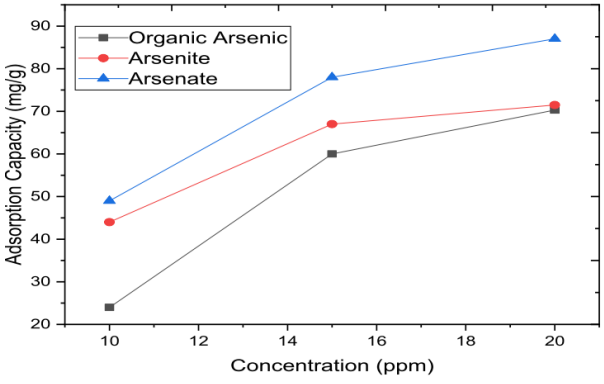

Figure S13. Adsorption capacity *vs* concentration for arsenic species using ZIF-8.

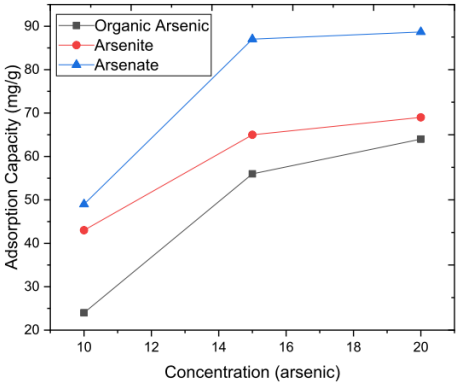

Figure S14. Adsorption capacity *vs* concentration for arsenic species using ZIF-67.

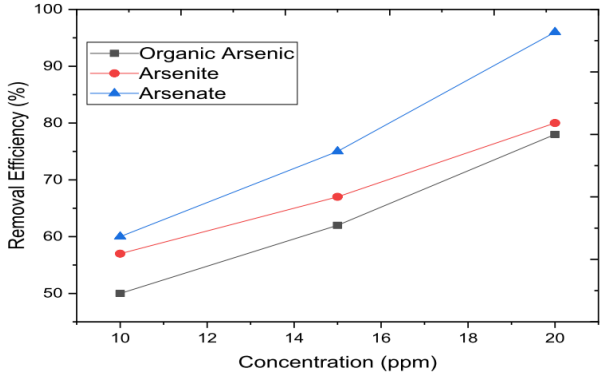

Figure S15. Removal Efficiency *vs* concentration for arsenic species using ZIF-8.

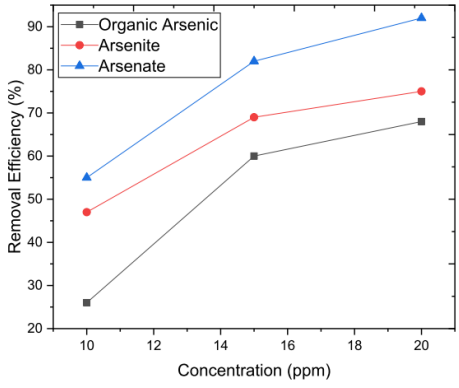

Figure S16. Removal Efficiency *vs* concentration for arsenic species using ZIF-67.

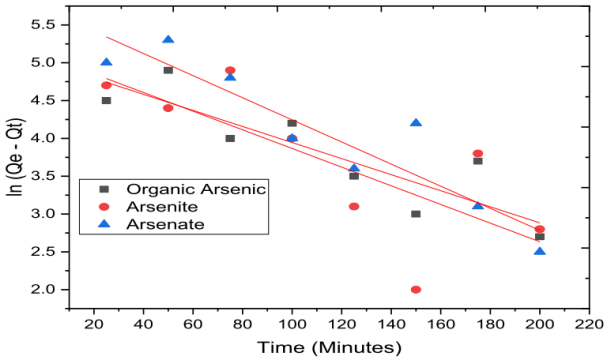

Figure S17. Kinetic parameters for the pseudo first order kinetics model for the removal of arsenic using ZIF-8.

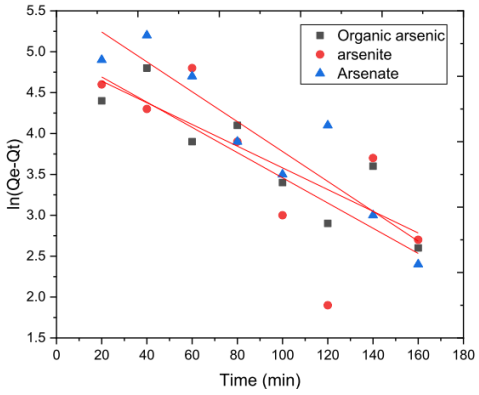

Figure S18. Kinetic parameters for the pseudo first order kinetics model for the removal of arsenic using ZIF-67.

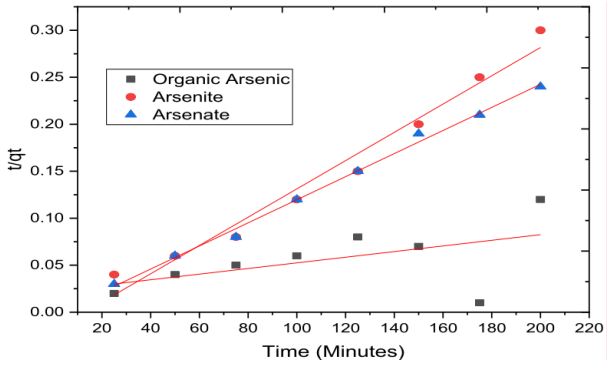

Figure S19. Kinetic parameters for the pseudo second order kinetics model for the removal of arsenic using ZIF-8.

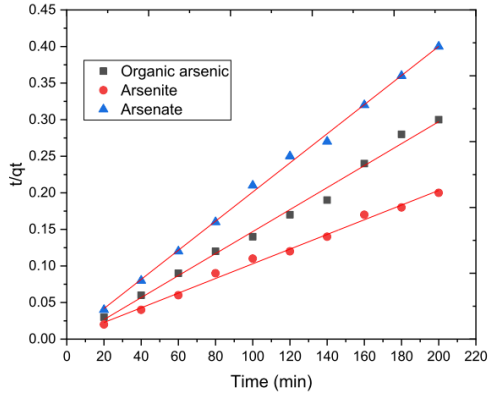

Figure S20. Kinetic parameters for the pseudo second order kinetics model for the removal of arsenic using ZIF-67.

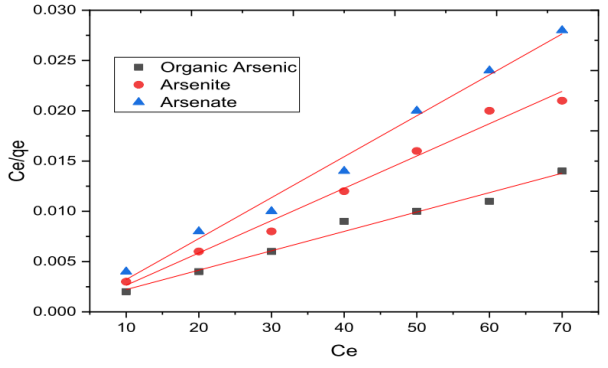

Figure S21. Adsorption isotherm fitted by Langmuir Model using ZIF-8.

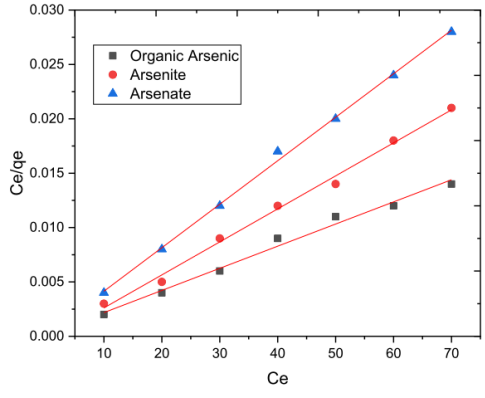

Figure S22. Adsorption isotherm fitted by Langmuir Model using ZIF-67.

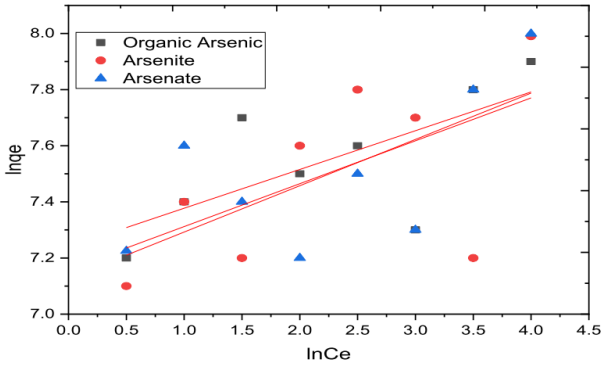

Figure S23. Adsorption isotherm fitted by Freundlich Model using ZIF-8.

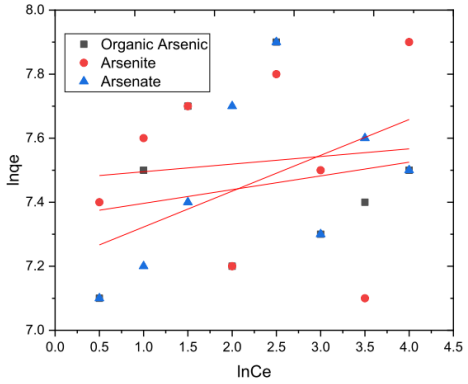

Figure S24. Adsorption isotherm fitted by Freundlich Model using ZIF-67.

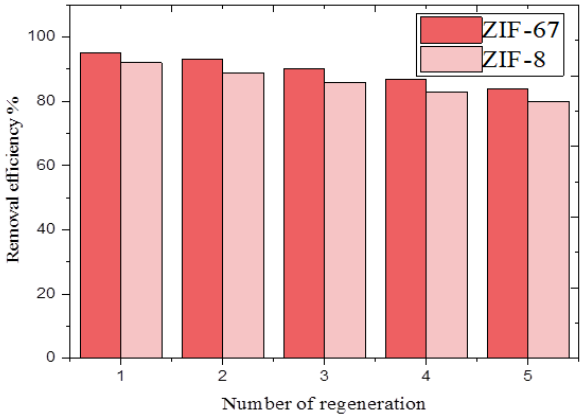

Figure S25. Regeneration of ZIF-67 & ZIF-8 up to five times and shows 95% removal efficiency.

Brazilian Journal of Analytical Chemistry
2022, Volume 9, Issue 36, pp 98–115
doi: 10.30744/brjac.2179-3425.AR-122-2021

BrJAC

ARTICLE

Evaluation of a Lignin Bio-alkyd Resin for the Selective Determination of Molybdenum in Biological, Pharmaceutical, Fertilizer and Water Samples

Elhossein A. Moawed*, **Sara M. Ragab**, **Amira R. El-Shobaky**, **Maha A. El Hagrasy**

Chemistry Department, Faculty of Science, Damietta University, P.O. Box: 34517, Damietta, Egypt

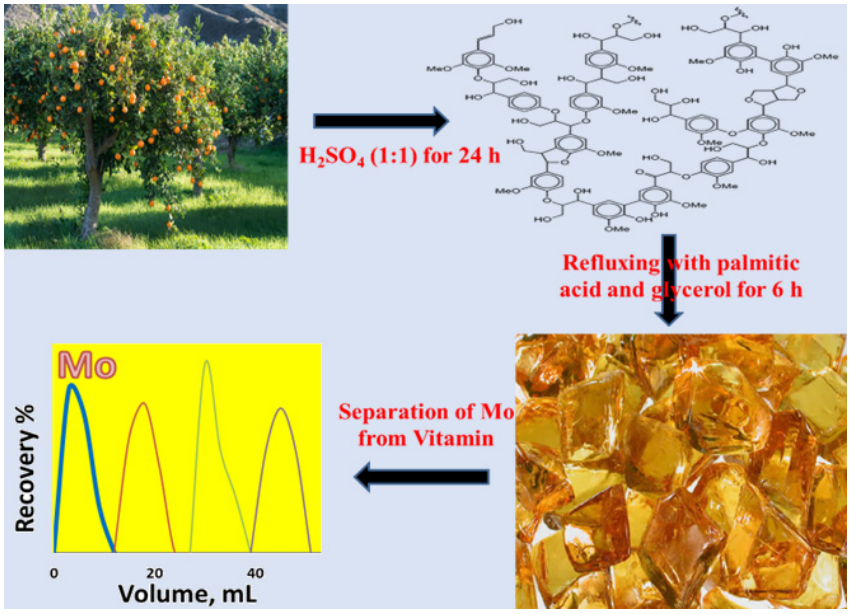

A lignin-based bio-alkyd resin (LA-Resin) was synthesized by the polycondensation reaction of lignin with a mixture of palmitic acid and glycerol. The LA-Resin was characterized using many techniques, including scanning electron microscopy, Fourier transform infrared spectroscopy, X-ray diffraction and thermal analysis. LA-Resin was proven to have graphitized structures with enhanced surface functional groups, showing a slightly basic character [pH of zero charge point (pH_{ZCP}) = 7.8]. It has a relatively better cation exchange capacity (0.70 mmol g^{-1}) in addition to the ability for physical adsorption. The performance of LA-Resin was assessed for the uptake of molybdenum (Mo), followed by spectrophotometric determination, applying both batch and column techniques. Elevated sorption percentages of Mo were observed in acidic medium H_2SO_4 (1.5 mol L^{-1}) in the presence of ascorbic acid (0.050 mol L^{-1}) and NH_4SCN (0.10 mol L^{-1}). The method was successfully applied to the separation and determination of Mo in mice liver, pharmaceuticals, water and fertilizer samples. Validation showed good recovery (96.6-99.6%), sensitivity (LOD, 0.9-4.0 µg L^{-1}), repeatability (RSD% ≤1.5%) and linearity (R^2 = 0.984), demonstrating a good quantitative performance of the method. Mo in all investigated samples regardless of different matrices were well-separated and detected, indicating that the method is sensitive enough to detect low concentrations of Mo even in small samples such as mice liver.

Keywords: Bio-alkyd resin, Molybdenum, Orange tree, Lignin, Pharmaceuticals

Cite: Moawed, E. A.; Ragab, S. M.; El-Shobaky, A. R.; El Hagrasy, M. A. Evaluation of a Lignin Bio-alkyd Resin for the Selective Determination of Molybdenum in Biological, Pharmaceutical, Fertilizer and Water Samples. *Braz. J. Anal. Chem.* 2022, *9* (36), pp 98–115. http://dx.doi.org/10.30744/brjac.2179-3425.AR-122-2021

Submitted 15 January 2022, Resubmitted 31 March 2022, 2nd time Resubmitted 18 April 2022, Accepted 18 April 2022, Available online 04 May 2022.

INTRODUCTION

Molybdenum (Mo) is an essential microelement for biological organisms due to its important role in maintaining several biological activities, enzymatic processes, and synthesis of proteins and nucleic acids.[1] Also, it is used for the regulation of body processes e.g., controlling digestion, eliminating harmful substances, reducing the activity of toxic compounds in the blood and suppressing cancer-causing agents.[2] Excess of Mo uptake results in severe gastroenteritis, decreased milk production, osteoporosis, and retarded growth. In addition, low Mo content affects adversely growth and may lead to neurological disorders and even early death. Mo also has a positive effect in the prevention of tooth decay.[3]

Mo was determined in various biological and pharmaceutical samples using different techniques.[4-7] The separation/spectrophotometric method is preferable, simple, inexpensive, and easy to handle.[8,9] In view of the very low concentration of Mo in environmental samples, it requires suitable methods for its preconcentration prior to its estimation.[10]

Adsorption is widely applied for the preconcentration and separation of diverse compounds including heavy metals. Bio-based sorbents are receiving great interest since they are environmentally friendly materials and have low to non-negative impact to environment. They, either in their pristine form or modified, have been extensively applied for the separation of different species regardless of their net charge.

Lignin is the most abundant natural aromatic biopolymer, it is produced as a waste product of the paper and pulp industry, and yet only a minute percentage is used for further refinement.[11] It contains various functional groups, such as ether linkages, aromatic hydroxyl, methoxy and aldehyde groups, making it appropriate for several modifications.[12] Functionalization of lignin would alter the chemical properties of the resulting material, which would offer enhanced sorption efficiency towards broader spectrum of pollutants. In addition, crosslinking of lignin can produce a more stable structure; hence, lignin would be a potential candidate for the preparation of different sorbents with distinctive characteristics.[13] The utilization of lignin not only provides potential sorbents, but also minimizes its impact, as a waste material, to the environment. Noteworthy drawbacks of lignin, however, are its brittle nature, along with its highly complex 3D structure, very low reactivity and its poor mechanical property. It is also a challenging task to recover lignin in a pure and clean form.[14] All of these would promote substantial challenges to its application. To overcome such drawbacks, lignin would be either incorporated into polymers, with relatively better properties, or chemically modified to produce materials with novel properties. Many studies have been performed to develop various lignin-based materials for different applications. Its composites were investigated for the removal cations and anions.[15] Also, it was produced in the form of microspheres and functionalized with amino groups for the removal of heavy metals.[16] In addition, the combination of lignin and surface-active layer was reported to be an effective approach for dye removal and heavy metal remediation as that found after the addition of reduced graphene oxide to lignin-poly(N-methylaniline).[17]

Alkyd resins (ARs) are eco-friendly highly branched polymers with a polyester backbone mainly developed for coating purposes[18] and recently were applied for the removal of contaminants.[19] They are prepared with abundant and bio-based resources by the polycondensation (esterification) of three types of monomers, which are polyhydric alcohols, polybasic acids and fatty acids.[20] ARs are inexpensive, thermally stable, soluble in organic solvents, have the ability to disperse pigments and fillers and have good adherence to different surfaces.[21] Having a molecular structure consists of hydroxyl groups, unsaturated double bonds, ester groups and carboxyl groups, enables its modification by the reaction with various materials, resulting in novel materials with enhanced properties.[22]

In this study, taking into consideration the necessity of green transition to address the global warming crisis, a simple, environmentally benign, and cost-effective sorbent was developed by the reaction of oxidized lignin, separated from orange tree wood, as a source of carboxylic groups, with a mixture of palmitic acid and glycerol to synthesis LA-Resin, via polycondensation reaction, for the purpose of selective separation of Mo. LA-Resin was characterized by scanning electron microscopy (SEM), Fourier transform infrared spectroscopy (FTIR), ultraviolet and visible spectroscopy (UV-Vis), X-ray diffraction analysis (XRD) and thermogravimetric analysis (TGA). LA-Resin was evaluated for the uptake of Mo from acidic solutions,

followed by spectrophotometric detection. In addition, adsorption isotherms, the corresponding kinetics, thermodynamic analysis, interference studies, column studies, stripping and reusability of the sorbent were also carried out. The developed quantitative method was validated in terms of addition and recovery, limits of detection and quantitation, linearity, repeatability, and selectivity. The method was applied for the preconcentration and separation of Mo from mice liver, pharmaceutical, water and fertilizer samples.

MATERIALS AND METHODS

Apparatus

The crystal structure of LA-Resin (XRD patterns) was investigated using an X-ray diffractometer (D8-Brucker Model) equipped with Cu Kα radiation (λ = 1.54 Å). The surface morphology of LA-Resin was analyzed using scanning electron microscope (SEM, JEOL model JSM-6510LV, USA). FTIR studies were carried out using a JASCO-410 spectrometer (JASCO, Easton, MD). A UV–Vis spectrophotometer (JASCO, V-630 UV-Vis Spectrophotometer, Japan) was employed for absorbance measurements. Thermogravimetric analysis (TGA), differential thermal analysis (DTA) and differential scanning calorimetry (DSC) were carried out by DSC-TGA device model (SDTQ 600, USA) under N_2 atmosphere with a heating rate of 10 °C/min (29-1000 °C).

Reagents and materials

All chemicals were of analytical grade reagents and used without further purification. Molybdenum (Mo) stock solution (1000 mg L^{-1}) was prepared by dissolving $(NH_4)_6Mo_7O_{24}.4H_2O$ (Merck) in doubly distilled water (DDW). Experimental solutions for adsorption and analysis were freshly prepared by diluting Mo stock solution with DDW. Nitric acid (65%, m/v), Sulfuric acid (98%, m/v) and ammonium hydroxide (29%, m/v) (Fluka) were used. Ascorbic acid (AA), ammonium thiocyanate, palmitic acid and glycerol were purchased from Sigma Aldrich.

Orange tree wood was obtained from local area in Damietta, Egypt. Wood samples were washed thoroughly with distilled water to remove dust and other impurities. These were cut into small pieces and dried in an oven at 105 °C, left to cool followed by grinding and sieving. For separating lignin, a 100 g sample of the powder was treated with a volume of 500 mL H_2SO_4 (1:1) for 24 h under stirring to remove the polysaccharide fraction. The acid-insoluble lignin residue was filtered, washed thoroughly with distilled water until a filtrate with a neutral pH value was obtained. For preparing oxidized lignin, solid lignin was treated with 100 mL of 0.1 mol L^{-1} $KMnO_4$ in 0.1 mol L^{-1} H_2SO_4 for 3 h at room temperature then filtered, washed thoroughly with distilled water and dried at 105 ºC. A 15 g of the as prepared material was refluxed with a mixture of 85 g of palmitic acid, and 30 g of glycerol for 6 h. The final product (LA-Resin) was separated, washed with distilled water, methanol and dried at 25 ºC.

Recommended procedures

Batch method was performed by mixing 0.10 g of LA-Resin with 25 mL of Mo(VI) solution (0.083 mmol L^{-1}) containing H_2SO_4 (0.1–2.0 mol L^{-1}), ascorbic acid (0.01–0.1 mol L^{-1}) and NH_4SCN (0.05–0.2 mol L^{-1}). The mixture solution was then shaken for 1 h at room temperature. After equilibrium, the solution samples were filtered and the concentration of the remaining and recovered Mo from the LA-Resin was determined spectrophotometrically as thiocyanate complex at λmax 457 nm (Figure 1S). Kinetic studies were conducted with a concentration of (0.083 mmol L^{-1}) molybdenum solution, and Mo uptake was carried out at different time intervals (1 - 120 min). The uptake percentage (E%) and equilibrium adsorption capacity of Mo (qe, mg/g) were calculated according to Equations (1) and (2).

$$E\% = 100\ ((C_0 - C_e)/C_0) \quad (1)$$

$$qe = V(C_0 - C_e)/m) \quad (2)$$

where, C_0 and C_e (mmol L^{-1}) are the initial and equilibrium Mo concentrations, respectively, V (L) is the solution volume, and m (g) is the dry mass of LA-Resin.

Dynamic method was performed using a 1.5 cm diameter glass column (35 cm length). The glass column was carefully loaded with a water slurry of LA-Resin material (10 g) to a bed height of 15 cm. Voids in the column bed were completely eliminated. Feed solutions of Mo, containing H_2SO_4 (1.5 mol L^{-1}), AA (0.050 mol L^{-1}) and NH_4SCN (0.10 mol L^{-1}) were passed through the column at a predetermined rate. Eluent solution contained 0.050 mol L^{-1} NH_4OH. The feed solution flow and elution rates were both set to 1–5 mL min^{-1}. Fractions of the solution (3 mL each) were collected then analyzed.

Pharmaceuticals used in this study are Ferrotron: Fe 15 mg; Cu 0.9 mg; Zn 11 mg and Mo 45 µg, Vitamix plus: Cu 2 mg; Fe 9 mg; Mn 5 mg and Mo 30 µg, Phara ferro 27 tablets: Cu 1 mg; Fe 30 mg; Zn: 2.5 mg; Mo: 15 µg (Nasr city, Egypt), and Octatron multivitamins capsules: Mo: 45 µg; Zn: 11 µg; Se: 55 µg; (Giza, Egypt). To prepare drug solutions. To prepare drug solutions, capsules or tablets, containing the desired Mo concentration, were dissolved in concentrated nitric acid and gently evaporated till dryness, then the solid residue was dissolved in DDW acidified with drops of nitric acid then quantitatively transferred into 25 mL measuring flasks, containing H_2SO_4 (1.5 mol L^{-1}), AA (0.050 mol L^{-1}) and NH_4SCN (0.10 mol L^{-1}) then completed to the mark with DDW.

Mice liver samples, containing pre-determined concentration of Mo, were kindly provided by Zoology Department, Faculty of Science, Damietta University. A 0.225 g sample of liver tissue was digested in a minimal volume of aqua regia and heated to ensure complete digestion. The digested was then dissolved with DDW and treated the same way as drug samples.

Water samples, collected from Damietta (Egypt), including River Nile, seawater, and industrial wastewater were filtered using a Millipore 0.45 µm pore-size membrane and kept in polyethylene bottles. The water sample was spiked with Mo(VI) solution (1 µg L^{-1}) and then determined as a molybdenum thiocyanate complex. Fertilizer sample (micro zein fertilizer), containing Zn: 2.4%; Fe: 2.4%; Mn: 2.4%; Cu: 0.6%; B: 0.6%; Mo: 0.06%; and S: 3.2% W/V (Unikim Tekstil Boyalarive, Turkey) was treated the same way as those of the pharmaceuticals.

The reusability of LA-Resin was explored for batch and continuous modes by following consecutive adsorption/desorption cycles. After each cycle, Mo was completely desorbed using 0.050 mol L^{-1} NH_4OH, followed by a through rinsing with distilled water until a neutral supernatant was acquired. Subsequently, after drying only for batch method, the same adsorbent mass was recycled under the aforementioned optimum adsorption experimental conditions.

RESULTS AND DISCUSSION

Characterization of LA-Resin

Of the advantages of LA-Resin, noticed during experimentation, is that it required very short time to dry and it was generally much easier to handle and to be separated. To assist the homogeneous dispersion of lignin into the alkyd resin matrix, lignin was oxidized to ensure the production of excess carboxylic groups to react with the alkyd formulation through a condensation reaction. SEM was used to compare between the surface morphology of lignin and that of LA-Resin. SEM micrographs, at magnifications of 3,000x and 5,000× of lignin show a bulk structure with wrinkled surface (Figure 1A, 1B). Whereas those of LA-Resin (Figure 1C, 1D) are completely different, they present prominent changes in the texture they show it has a multi-layered microstructure and contain many cavities with different sizes. Figures 1C and D illustrate interconnected well-organized sheets, with no visible boundaries between the mixture components and lignin could be no longer recognized, suggesting that lignin was completely well dispersed and integrated into the alkyd[23] formulation to produce LA-Resin. These observations demonstrate the successful preparation of LA-Resin

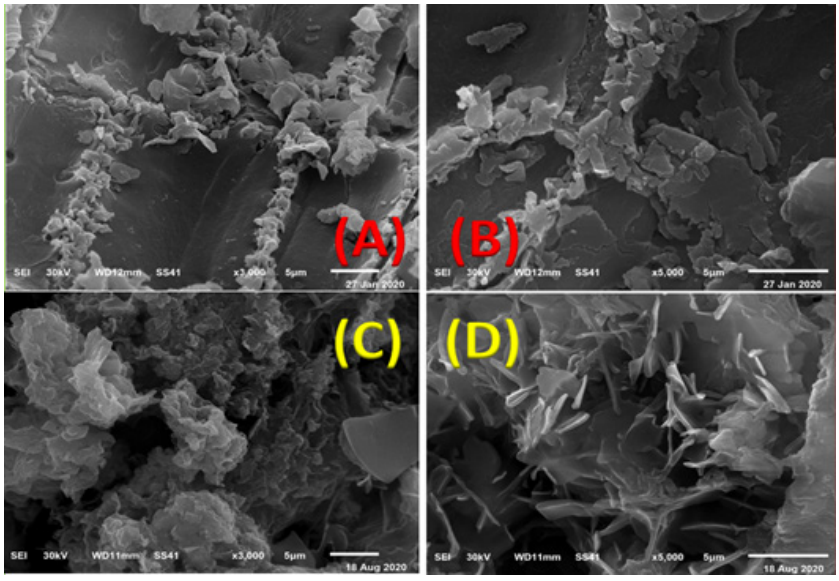

Figure 1. SEM micrographs of lignin (A, B) and LA-Resin (C, D) at magnifications of 3,000 and 5,000×.

FTIR was used to identify the chemical structure and functional groups of lignin, A-Resin and LA-Resin. The FTIR spectrum of lignin (Figure 2) shows a broad absorption band at 3729-2981 cm^{-1} which can be assigned to the stretching of phenolic and aliphatic -OH groups. Bands at 2923 cm^{-1} and 2855 cm^{-1} are ascribed to the C–H stretching of methylene and methyl groups, respectively. The characteristic bands located at 1511 and 1461 cm^{-1} correspond to the aromatic skeleton in lignin. These bands are nearly similar of the organosolv lignin.[24,25] The band at 1631 cm^{-1} is attributed to –C=O stretching of carboxyl groups conjugated with the aromatic ring. While the FTIR spectrum of A-Resin (Figure 2S), a broadband appeared from 3721 to 3103 cm^{-1} was assigned to OH group. Several sharp peaks were also observed at 2919, 2848 cm^{-1} (uCH), 1772-1565 cm^{-1} (uCO) and (uC=C) which characterize the matrix of A-Resin. All these band frequencies were shifted in the LA-resin spectrum (Figure 2) to 2797–3622, 2918, 2849, and 1556 cm^{-1}. In addition, two new sharp peaks developed at 1738 and 1268 cm^{-1}, which correspond to the –C=O and –COO stretching and the band at 1631 cm^{-1} was absent. It can be observed that most of the peaks of LA-resin are identical to those of alkyd resin. All these characteristic absorption bands support the formation of AR in the presence of lignin to obtain the LA-Resin.

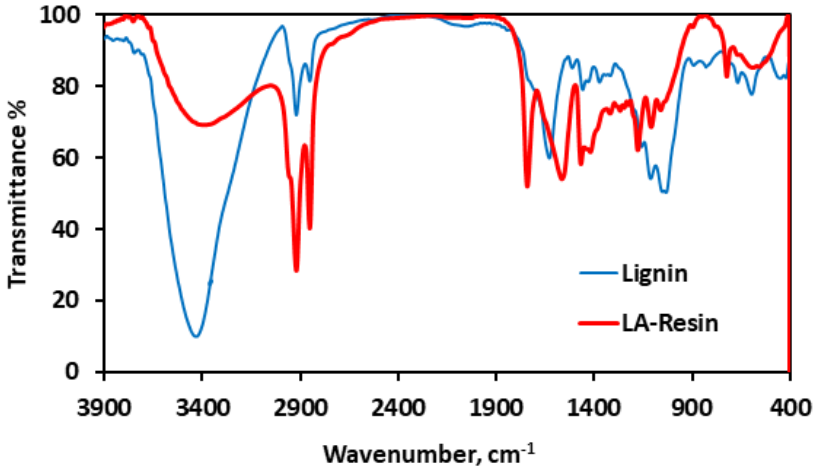

Figure 2. FTIR Spectra of lignin and LA-Resin.

Also, electronic spectra of solid-state lignin, A-Resin and LA-Resin, recorded in the range of ~ 200–400 nm (Figure 3S), reveal that lignin absorbs UV radiation very strongly below 215 nm and A-Resin at 373 nm. Whereas LA-Resin does not absorb below 290 nm and it has two distinctive sharp peaks at ~ 300 and 340 nm.

Of great importance to carbonaceous materials is the acid-base behavior of the surface functional groups and the value of pH_{zcp}, at which the net surface charge is zero. The surface acidic and basic functional groups of lignin and LA-Resin obtained from Boehm titration are reported in Table I. The results show that the total acidic and basic groups of LA-Resin are 1.48 and 1.62 mmol g^{-1}, respectively, which are greater than those of lignin (1.25 and 0.20 mmol g^{-1}, respectively). The decrease of the amount of carboxylic group from 0.63 to 25 mmol g^{-1} is due to it reacting with a glycerol molecule. The ratio of reacted lignin and incorporated lignin is the following 0.38: 0.25 (1.5:1). As evident, the value of basic functionalities of LA-Resin are relatively greater than that of the acidic one, rendering the surface slightly basic which was further indicated pHzcp measurements.

Figure 4S shows pH_{zcp} curves of lignin and LA-Resin. The estimated values are 3.0 and 7.8 for lignin and LA-Resin, respectively. These results are in accordance with the determined acidic and basic sites and supports the better performance of LA-Resin to remove different species regardless of their charge under any pH value. It is evident that the surface chemistry of LA-Resin is greatly altered compared to that of lignin in terms of enhanced acidic and basic functional groups.

Table I. Acidic and basic sites of sorbents

Sorbent	Basic Sites, mmol g^{-1}	Acidic Sites, mmol g^{-1}		
		Phenolic	Carboxylic	Lactonic
Lignin	0.20	0.15	0.63	0.47
LA-Resin	1.62	0.53	0.25	0.70

To investigate further the properties of the surface of LA-Resin, Iodine number (I_2 No) and methylene blue value (MB value) were determined. I_2 No would indicate the adsorption process of the sorbent while MB value implies the cation exchange ability. The I_2 No and MB value of lignin and LA-Resin are 1.6, 1.5, 0.6, and 0.7 mmol g^{-1}, respectively (Table II). In addition, electrical conductivity measurements were performed (σ). The values of σ of lignin and LA-Resin are 7×10^{-12} and 2×10^{-11} Ω^{-1} m^{-1}, respectively (Table II). This result signifies the very low electrical conductivities of both materials.

Table II. Iodine number and methylene value of sorbents

Sorbent	Iodine number mmol g^{-1}	Methylene blue value mmol g^{-1}	Electrical conductivity Ω^{-1} m^{-1}
Lignin	1.6	0.6	7×10^{-12}
LA-Resin	1.5	0.7	2×10^{-11}

Thermal properties of lignin and LA-Resin were evaluated using TGA, and DSC analysis (Figure 5S). These curves indicate two steps of thermal decomposition for both materials. The weight loss at initial stage until ~100 °C, due to loss of adsorbed water, for lignin and LA-Resin are 21.2, and 5.9%, respectively. At the second step, a weight loss of 39.0, and 74.1% is observed at 104-1000 °C, and 111-1000 °C for lignin and LA-Resin, respectively. The total weight loss of LA-Resin (80%) was higher than that of lignin (60.2%) which resulted from the decomposition of the alkyd polymer. While ≥ 90% of the weight loss for A-Resin was at 442 °C.[26]

A powder XRD study was performed to investigate the crystallographic nature of lignin (Figure 6S) and LA-Resin (Figure 3). The main characteristic feature noticed in both patterns is the presence of a broad diffraction peak at 2θ = 20–30° which, corresponds to the (002) plane of the graphitized structures.

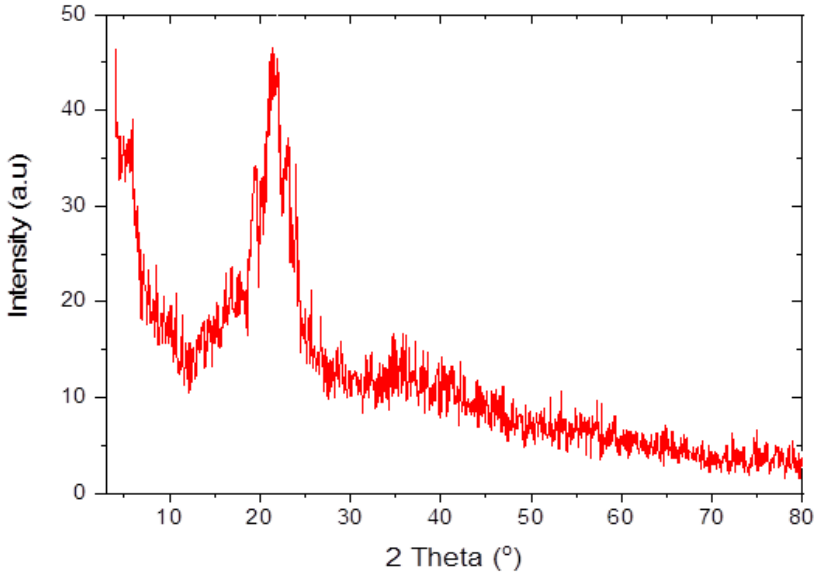

Figure 3. XRD pattern of LA-Resin.

Sorption of molybdenum ions

The sorption percentages of Mo from thiocyanate solution were investigated in an acidic medium (0.1–2.0 mol L^{-1} H_2SO_4), ascorbic acid (0.01–0.1 mol L^{-1}), ammonium thiocyanate (0.05–0.2 mol L^{-1}) and different weight of LA-Resin (0.05–0.2 g) (Figure 4). It was found that the optimum conditions for the sorption of Mo are 1.5 mol L^{-1} H_2SO_4, 0.06 mol L^{-1} ascorbic acid, 0.1 mol L^{-1} NH_4SCN and 0.1 g of LA-Resin.

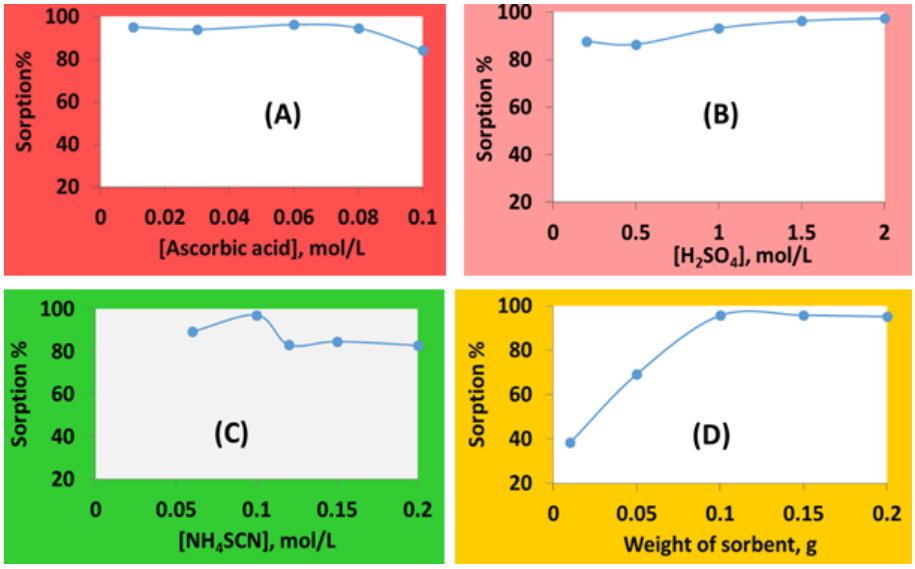

Figure 4. Conditions of the extraction of molybdenum from aqueous solution.

Mo adsorption onto LA-Resin occurred very rapidly within the first 5 min at which almost 75% of Mo was adsorbed. The adsorption rate decreased significantly after 30 min, which could be attributed to the decrease of adsorption reactive sites, available for Mo adsorption, then equilibrium was attained after 60 min. Consequently, 60 min was chosen as the optimum contact time. Pseudo-first-order (PFO) and pseudo-second-order (PSO) models were used to evaluate the adsorption kinetics. The results (Table 1S,

2S) suggest that Mo adsorption is better described by the PSO (R^2 = 0.997, Figure 7S), with a qe value almost equal to that of the experimental, kinetic model rather than PFO (R^2 = 0.750, Figure 7S). This result would indicate that Mo adsorption onto LA-Resin follows a chemisorption mechanism by sharing or replacing electrons between LA-Resin and Mo.

The adsorption capacity of LA-Resin was investigated by adsorption isotherms. As shown in Figure 8S, the uptake of Mo onto LA-Resin increases with the increase of concentration until a plateau is reached (q_{max} = 31.7 mg g^{-1}). The experimental data were then fitted by the Langmuir and Freundlich models to determine whether the adsorption process was a monolayer or a multilayer adsorption. The obtained results (Table S1) indicate that compared to Freundlich model (R^2 = 0.860, Figure 8S), Langmuir model (R^2 = 0.920, Figure 8S) is a good fit to the experimental data, suggesting a mono-molecular layer sorption, with a maximum monolayer sorption capacity of 39.20 mg g^{-1}, of Mo as well as a homogeneous distribution of active sites on the LA-Resin surface. Table 4S illustrates the adsorption capacities of some sorbents, revealing the good sorption capacity of LA-Resin.

The effect of temperature (25–60 °C) on the sorption of Mo ions using LA-Resin was studied. It was found that the sorption of Mo ions very slightly increased with increasing temperature. The calculated thermodynamic parameters are Gibbs's free energy (ΔG), enthalpy (ΔH), and entropy (ΔS) (Figure 9S, Table 5S, 6S). ΔH is 21.6 kJ mol^{-1}, the positive value reveals that the extraction of Mo ions by LA-Resin is endothermic. ΔG is -19.20 kJ mol^{-1}, indicating a spontaneous sorption process and ΔS is 137 J K^{-1} mol^{-1}.

Mechanism of Mo adsorption onto LA-Resin

LA-Resin has a relatively weak basic character, where the activity of total acidic and basic groups is 1.48 and 1.62 mmol g^{-1}, respectively, which was further indicated by a pH_{ZCP} value of 7.8. It has a good ability to accommodate Mo through different mechanisms since it has a cation exchange capacity of 0.70 mmol g^{-1} in addition to the ability for physical adsorption (I_2 No = 1.5 mmol g^{-1}) as also indicated from SEM images. Under the optimum conditions, Mo ions would be present as $[Mo(SCN)_6]^-$ and the surface of LA-Resin would be positively charged due to the protonation of the basic functional groups (solution pH < pH_{ZCP}). Accordingly, adsorption would firstly start as a result of the electrostatic attraction between the protonated LA-Resin surface and the negatively charged Mo thiocyanate complex and this would be the initial driving force to bind Mo to the sorbent surface. Afterwards, inner sphere complexation might have happened, as indicated by kinetic studies, which is the most important mechanism for Mo adsorption where it could be adsorbed into LA-Resin surfaces through coordination with functional groups (Figure 5).

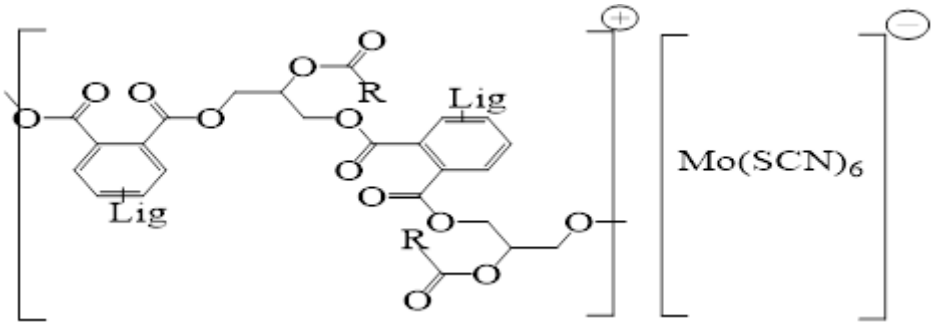

Figure 5. A mechanism scheme for the sorption of Mo onto LA-Resin.

Effect of foreign ions

The effect of the presence of different ions on the adsorption of molybdenum (200 µg) onto LA-Resin, using batch mode, was examined (Figure 10S). Ions such as Na^+, K^+, Mn^{2+}, Ni^{2+}, Pb^{2+}, Co^{2+}, Zn^{2+} and Ca^{2+} (1000 µg) had almost no interference (< 2%). However, Sb^{3+} and Fe^{3+} (1000 µg) caused noticeable interference (16-17%). The addition of either 1mL of 0.1 M citric acid or excess ascorbic acid solution eliminated such interference.

Column studies

The extraction and recovery of Mo ions were tested using a LA-Resin-loaded column (35 cm long and 1.5 cm in diameter contained 10 g of LA-Resin with bed height 15 cm). It was found that Mo ions were completely adsorbed under the optimized conditions and were eluted with 10-15 mL of 0.05 mol L^{-1} NH_4OH solutions at 1-5 mL min^{-1} (Figure 6). To investigate the effect of sample loading and eluent flow rates on Mo retention and recovery, either feed solutions of Mo, under the optimized experimental conditions, or eluent solutions (0.050 mol L^{-1} NH_4OH) were passed through the column at different flow rates varying from 1–5 mL min^{-1}. The flow rate of sample loading in the investigated range did not show any difference (data not shown) so, a flow rate of 1 mL min^{-1} was chosen for further experiments. According to the results shown in Figure 6, Mo species were eluted completely under the investigated range however, a better-resolved peak was obtained at eluent flow rate of 1 mL min^{-1}, accordingly, it was further applied for eluting Mo species. Preconcentration of Mo from water samples was investigated. Solutions of 100 µg of Mo ions in up to 500 mL of water samples were passed through the LA-Resin column (1 mL min^{-1}). The elution of Mo ions from the LA-Resin column was carried out by 10 mL NH_4OH (0.05 mol L^{-1}) solution then the eluates were determined.[27] The results show that the recovery percentages are about 100% with a preconcentration factor of up 50.

Capacity of the LA-Resin column was calculated by percolating it with Mo solution (0.10 mg mL^{-1}) at a flow rate of 1 mL min^{-1}. Breakthrough curves were obtained by measuring the content of Mo ions in 5 mL collected fractions from the effluent (Figure 11S). The breakthrough point is reached at a volume of 100-480 mL, the breakthrough capacity was 36.5 mg L^{-1}.

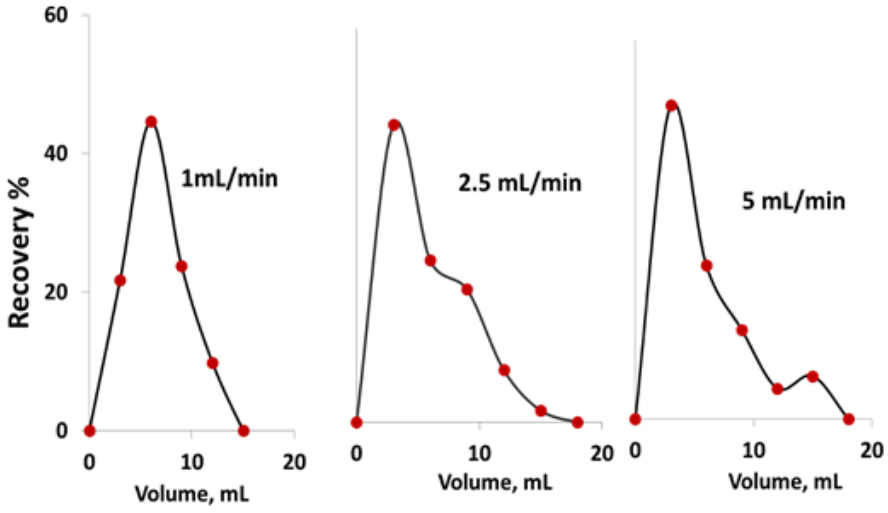

Figure 6. Effect of eluent flow rate on the recovery of molybdenum from LA-Resin column.

Regeneration of LA-Resin

The regeneration experiments were carried out to evaluate the reusability of AL-Resin. Based on the point that the adsorption of Mo onto LA-Resin took place in acidic medium, Mo desorption was tested in basic solution. The LA-resin material was affected at pH ≥ 12 using NaOH solution (Figure 12S) and not effect with ammonia solution. Therefore, the best eluent examined was NH_4OH with a concentration of 0.05 mol L^{-1} at 25 ºC for 12 h. After five cycles of regeneration, in batch mode, the adsorption capacity was unchanged as well as the removal efficiency. For column experiments, one column was conducted through the whole experiment for more than 10 cycles of sorption/desorption and it kept its performance unchanged. These results suggest that LA-Resin is not only a selective material for Mo at the investigated operating conditions but also could be an efficient adsorbent for the removal of Mo from different matrices.

Analytical performance of the proposed method

A calibration curve for Mo was obtained, applying the optimized preconcentration method. The linear range was obtained for a concentration range near the limit of quantification (LOQ) up to 15 mg L^{-1}, with R^2 value of 0.984. The analytical sensitivity was assessed by the limits of detection (LOD) and limits of quantitation (LOQ) for the extraction and recovery of Mo from the investigated biological and pharmaceutical samples using LA-Resin columns (Table III). The values of LOD and LOQ are in the range of 0.9-4.0 and 2.9-13.4 µg L^{-1}, respectively (n = 5) which indicate the higher sensitivity of Mo determination by LA-Resin columns compared to other reported results. The accuracy and precision for the determination of Mo using LA-Resin in real samples were investigated by analyzing spiked samples. Table IV shows the results of extraction and recovery of Mo from mice liver and pharmaceutical samples. The high recoveries (96.6–99.6%) of Mo along with their lower values of RSD% (0.3-1.5%, n = 5) reflect the good accuracy and precision of the proposed method.

Table III. Detection limit of molybdenum

Samples	LOD, µg L^{-1}	LOQ, µg L^{-1}
Liver mice tissue	2.5	8.4
Vitamix plus capsule	3.2	10.6
Octatron capsule	1.7	5.7
Ferrotron capsule	4.0	13.4
Phara ferro 27 tablet	0.9	2.9

Table IV. Determination of molybdenum in real samples

Samples	Added, µg	Found, µg	Recovery, %	RSD, %
Liver mice tissue	105	104.6	99.6	0.9
Vitamix plus capsule	90	88.8	98.7	1.2
Octatron capsule	90	89.5	99.5	0.5
Ferrotron capsule	90	86.9	96.6	1.5
Phara ferro 27 tablet	100	98.1	98.1	0.3

Preconcentration and recovery of Mo from real samples

Figure 7 shows chromatographic separation of Mo from other metals in Mo-containing pharmaceuticals, Ferrotron and Vitamix plus, on LA-Resin-packed columns. The elution of Mo was carried out at a flow rate of 1.0 mL min^{-1} using NH_4OH (0.05 mol L^{-1}), then the concentrations were determined spectrophotometrically. Mo ions were completely eluted from LA-Resin columns with a recovery percentage of 100% at the first 12 mL of NH_4OH solution. The resolution factors (Rs) for the separation of Mo from Cu ions in Vitamix plus and Ferrotron samples, calculated by the following equation: $Rs = 2(V_2 – V_1)/(W_1+W_2)$ are 1.1 and 1.4, respectively. These results considerably suggest that LA-Resin columns have the potential, under the operational conditions, for the separation of Mo from different matrices with good resolution and could be completely recovered from real samples.

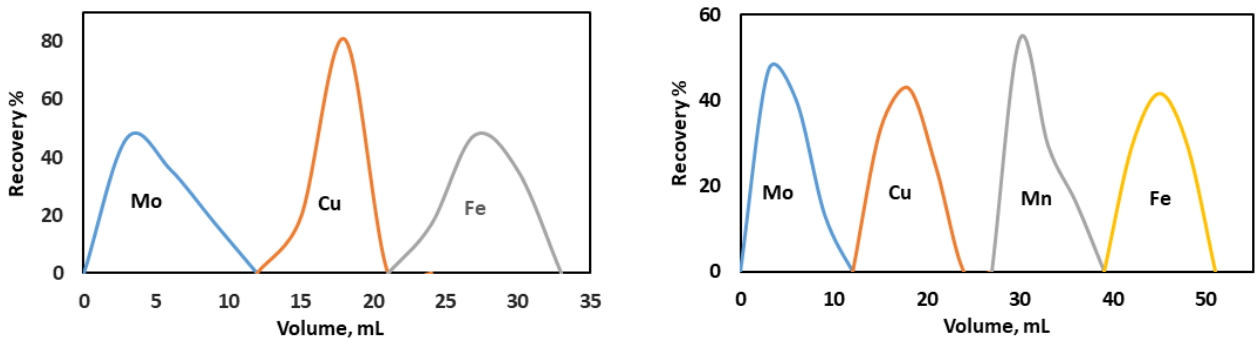

Figure 7. Chromatographic separation of molybdenum from pharmaceutical samples.

For the determination of Mo–bound in biological samples, using the mice liver as a model, the digest of mice liver samples, containing pre-determined concentration of Mo, were treated the same way as drug samples. The results (Table IV) show that the recovery percentage of Mo is 99.6% (RSD = 0.90%, n = 5).

LA-Resin column was applied for the extraction of Mo from water samples, namely, River Nile, seawater and industrial wastewater. Mo-spiked water samples, treated under the optimized conditions, were allowed to pass through the LA-Resin columns at a flow rate of 1 mL/min. The elution of Mo from the LA-Resin column was carried out by NH_4OH (0.05 mol L^{-1}) solution and the amount of Mo in the eluates were determined by the recommended method. The results show that the average recovery percentages of Mo are 100% (RSD = 0.00%, n = 5). Therefore, LA-Resin column could be applied for the recovery of Mo from different water samples. In addition, Mo content in micro zein fertilizer was assessed by LA-Resin column. The results show that the recovery percentage of Mo (60 µg) is 100% (RSD = 0.76%, n=5).

CONCLUSION

LA-Resin was synthesized and characterized by many techniques. The sorbent has a relatively weak basic character, where the total acidic and basic groups are 1.5 and 1.6 mmol g^{-1}, respectively. It has a good ability to accommodate sorbate species through different mechanisms since it has a cation exchange capacity of 0.7 mmol g^{-1} in addition to the ability for physical adsorption (I_2 No = 1.5 mmol g^{-1}). The sorbent showed, under the optimum conditions, that the uptake of $[Mo(SCN)_6]^-$ complex onto the positively charged LA-Resin most probably took place through the formation of ion-associate complex. Kinetic studies revealed that the removal of Mo follows a chemisorption mechanism by sharing or replacing electrons between LA-Resin and Mo. LA-Resin has a homogeneous distribution of active sites to accommodate a mono-molecular layer of Mo (q_{max} = 31.7 mg g^{-1}) as indicated by sorption isotherm studies. Mo ions were desorbed effectively using an aqueous solution of 0.05 mol L^{-1} NH_4OH. A LA-Resin-column was tested for the uptake and elution of the Mo and the recovery was almost 100% suggesting a good efficiency of LA-Resin to the chromatographic separation. The reusability experiment indicated that LA-Resin is not only a selective material for Mo at the investigated operating conditions but also is an efficient and cost-effective adsorbent for the removal of Mo from different matrices.

Conflicts of interest

The authors certify that they have NO affiliations with or involvement in any organization or entity with any financial interest (such as honoraria; educational grants; participation in speakers' bureaus; membership, employment, consultancies, stock ownership, or other equity interest; and expert testimony or patent-licensing arrangements), or non-financial interest (such as personal or professional relationships, affiliations, knowledge or beliefs) in the subject matter or materials discussed in this manuscript.

Acknowledgements

The authors gratefully acknowledge research support from Damietta University and the Chemistry Department, Faculty of Science, Damietta University, Egypt.

REFERENCES

(1) Janani, I.; Lakra, R.; Kiran, M. S.; Korrapati, P. S. Selectivity and sensitivity of molybdenum oxide-polycaprolactone nanofiber composites on skin cancer: Preliminary in-vitro and in-vivo implications. *J. Trace Elem. Med. Biol*. **2018**, *49*, 60–71. https://doi.org/10.1016/j.jtemb.2018.04.033

(2) Ellingsen, D. G.; Chashchin, M.; Berlinger, B.; Fedorov, V.; Chashchin, V.; Thomassen, Y. Biological monitoring of welders' exposure to chromium, molybdenum, tungsten and vanadium. *J. Trace Elem. Med. Biol*. **2017**, *41*, 99–106. https://doi.org/10.1016/j.jtemb.2017.03.002

(3) Li, W.; Dong, X.; Zhu, L.; Tang, H. Highly selective separation of Re(VII) from Mo(VI) by using biomaterial-based ionic gel adsorbents: Extractive adsorption enrichment of Re and surface blocking of Mo. *Chem. Eng. J*. **2020**, *387*, 124078. https://doi.org/10.1016/j.cej.2020.124078

(4) Dubascoux, S.; Andrey, D.; Vigo, M.; Kastenmayer, P.; Poitevin, E. Validation of a dilute and shoot method for quantification of 12 elements by inductively coupled plasma tandem mass spectrometry in human milk and in cow milk preparations. *J. Trace Elem. Med. Biol*. **2020**, *49*, 19–26. https://doi.org/10.1016/j.jtemb.2018.04.023

(5) Sun, W.; Roy, A.; Selim, H. M. Residence Time Effects on Molybdenum Adsorption on Soils: Elucidation by Multi-Reaction Modeling and XANES Analysis. *Soil Syst*. **2019**, *3*, 1–14. https://doi.org/10.3390/soilsystems3030055

(6) Krawczyk, M. Determination of macro and trace elements in multivitamin dietary supplements by high-resolution continuum source graphite furnace atomic absorption spectrometry with slurry sampling. *J. Pharm. Biomed. Anal*. **2014**, *88*, 377–384. https://doi.org/10.1016/j.jpba.2013.09.016

(7) Zhang, G.; Zhao, Y.; Liu, F.; Ling, J.; Lin, J.; Zhang, C. Determination of essential and toxic elements in Cordyceps kyushuensis Kawam by inductively coupled plasma mass spectrometry. *J. Pharm. Biomed. Anal*. **2013**, *72*, 172–176. https://doi.org/10.1016/j.jpba.2012.08.007

(8) Wei, Y.; Salih, K. A. M.; Rabie, K.; Elwakeel, K. Z.; Zayed, Y. E.; Hamza, M. F.; Guibal, E. Development of phosphoryl-functionalized algal-PEI beads for the sorption of Nd(III) and Mo(VI) from aqueous solutions – Application for rare earth recovery from acid leachates. *Chem. Eng. J*. **2021**, *412*, 127399. https://doi.org/10.1016/j.cej.2020.127399

(9) Gamal, R.; Rizk, S. E.; El-Hefny, N. E. The adsorptive removal of Mo(VI) from aqueous solution by a synthetic magnetic chromium ferrite nanocomposite using a nonionic surfactant. *J. Alloys Compd*. **2021**, *853*, 157039. https://doi.org/10.1016/j.jallcom.2020.157039

(10) Yadav, A. G.; Gujar, R. B.; Mohapatra, P. K.; Valsala, T. P.; Sathe, D. B.; Bhatt, R. B.; Verboom, W. Highly efficient uptake of tetravalent actinide ions from nitric acid feeds using an extraction chromatography material containing tetra-n-butyl diglycolamide and a room temperature ionic liquid. *J. Chromatogr. A* **2021**, *1655*, 462501. https://doi.org/10.1016/j.chroma.2021.462501

(11) Eriksson, K. E. L. Biotechnology in the pulp and paper industry. *Wood Sci Technol*. **1990**, *24*, 79−101. https://doi.org/10.1007/BF00225309

(12) Ge, Y.; Li, Z. L. Application of Lignin and Its Derivatives in Adsorption of Heavy Metal Ions in Water: A Review. *ACS Sustain. Chem. Eng.* **2018**, *6*, 7181–7192. https://doi.org/10.1021/acssuschemeng.8b01345

(13) Thakur, V. K.; Thakur, M. K.; Raghavan, P.; Kessler, M. R. Progress in Green Polymer Composites from Lignin for Multifunctional Applications: A Review. *ACS Sustain. Chem. Eng.* **2014**, *2*, 1072–1092. https://doi.org/10.1021/sc500087z

(14) Kubo, S.; Kadla, J. F. Lignin-based carbon fibers: Effect of synthetic polymer blending on fiber properties. *J. Polym. Environ*. **2005**, *13*, 97−105. https://doi.org/10.1007/s10924-005-2941-0

(15) Shi, X.; Qiao, Y.; An, X.; Tian, Y.; Zhou, H. High-capacity adsorption of Cr(VI) by lignin-based composite: Characterization, performance and mechanism *Int. J. Biol. Macromol*. **2020**, *159*, 839–849. https://doi.org/10.1016/j.ijbiomac.2020.05.130

(16) Popovic, A. L.; Rusmirovic, J. D.; Velickovic, Z.; Radovanovic, Z.; Ristic, M.; Pavlovic, V. P.; Marinkovic, A. D. Novel amino-functionalized lignin microspheres: High performance biosorbent with enhanced capacity for heavy metal ion removal. *Int. J. Biol. Macromol*. **2020**, *156*, 1160–1173. https://doi.org/10.1016/j.ijbiomac.2019.11.152
(17) Qian, H.; Wang, J.; Yan, L. Synthesis of lignin-poly(N-methylaniline)-reduced graphene oxide hydrogel for organic dye and lead ions removal. *J. Bioresour. Bioprod*. **2020**, *5*, 204–210. https://doi.org/10.1016/j.jobab.2020.07.006
(18) Das, P.; Sharma, N.; Puzari, A.; Kakati, D. K.; Devi, N. Synthesis and characterization of neem (*Azadirachta indica*) seed oil-based alkyd resins for efficient anticorrosive coating application. *Polym. Bull*. **2021**, *78*, 457–479. https://doi.org/10.1007/s00289-020-03120-8
(19) Moawed, E. A.; El-Hagrasy, M. A.; Senan, A. E. A. Application of bio-alkyd resin for the removal of crystal violet and methylene blue dyes from wastewater. *Int. J. Environ. Sci. Technol*. **2019**, *16*, 8495–8504. https://doi.org/10.1007/s13762-019-02343-1
(20) Ifijen, I. H.; Odi, H. D.; Maliki, M.; Omorogbe, S. O.; Aigbodion, A. I.; Ikhuoria, E. U. Correlative studies on the properties of rubber seed and soybean oil-based alkyd resins and their blends. *J. Coat. Technol. Res*. **2021**, *18*, 459–467. https://doi.org/10.1007/s11998-020-00416-2
(21) Wang, Z.; Huang, W.; Bin, P.; Zhang, X.; Yang, G. Preparation of quaternary amine-grafted organosolv lignin biosorbent and its application in the treatment of hexavalent chromium polluted water. *Int. J. Biol. Macromol*. **2019**, *126*, 1014-1022. https://doi.org/10.1016/j.ijbiomac.2018.12.087
(22) Zhang, D.; Xu, W.; Cai, J.; Cheng, S. Y.; Ding, W. P. Citric acid-incorporated cellulose nanofibrous mats as food materials-based biosorbent for removal of hexavalent chromium from aqueous solutions. *Int. J. Biol. Macromol*. **2020**, *149*, 459-466. https://doi.org/10.1016/j.ijbiomac.2020.01.199
(23) Khandelwal, H.; Ravi, B. Effect of molding parameters on chemically bonded sand mold properties. *Journal of Manufacturing Processes* **2016**, *22*, 127–133. https://doi.org/10.1016/j.jmapro.2016.03.007
(24) Galiwango, E.; Rahman, N. S. A.; Al-Marzouqi, A. H.; Abu-Omar, M. M.; Khaleel, A. A. Klason Method: An Effective Method for Isolation of Lignin Fractions from Date Palm Biomass Waste. *Chem. Process. Eng. Res*. **2018**, *57*, 46-58.
(25) Zhai. R.; Hu, J.; Chen, X.; Xu, Z.; Wen, Z.; Jin, M. Facile synthesis of manganese oxide modified lignin nanocomposites from lignocellulosic biorefinery wastes for dye removal. *Bioresour. Technol*. **2020**, *315*, 123846. https://doi.org/10.1016/j.biortech.2020.123846
(26) Xu, X.; Chen, L.; Guo, J.; Cao, X.; Wang, S. Synthesis and characteristics of tung oil-based acrylated-alkyd resin modified by isobornyl acrylate. *RSC Adv* **2017**, *7*, 30439-30445. https://doi.org/10.1039/C7RA02189E
(27) Moawed, E. A.; El-Hagrasy, M. A.; Embaby, N. E. M. Substitution influence of halo polyurethane foam on the removal of bismuth, cobalt, iron and molybdenum ions from environmental samples. *J. Taiwan Inst. Chem. Eng*. **2017**, *70*, 382-390. https://doi.org/10.1016/j.jtice.2016.10.037

SUPPLEMENTARY MATERIAL

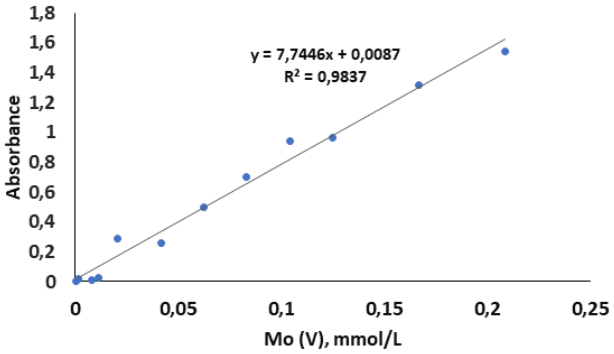

Figure 1S. Calibration curve for determination of molybdenum ions.

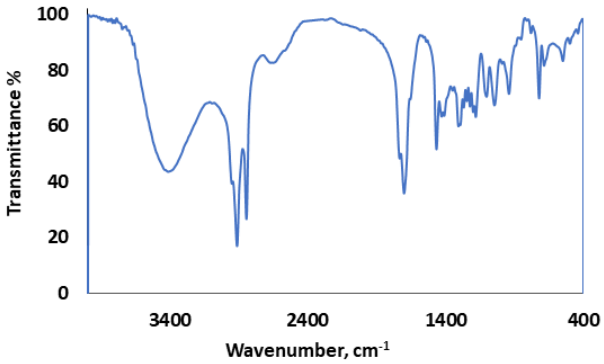

Figure 2S. FTIR spectrum of the A-Resin.

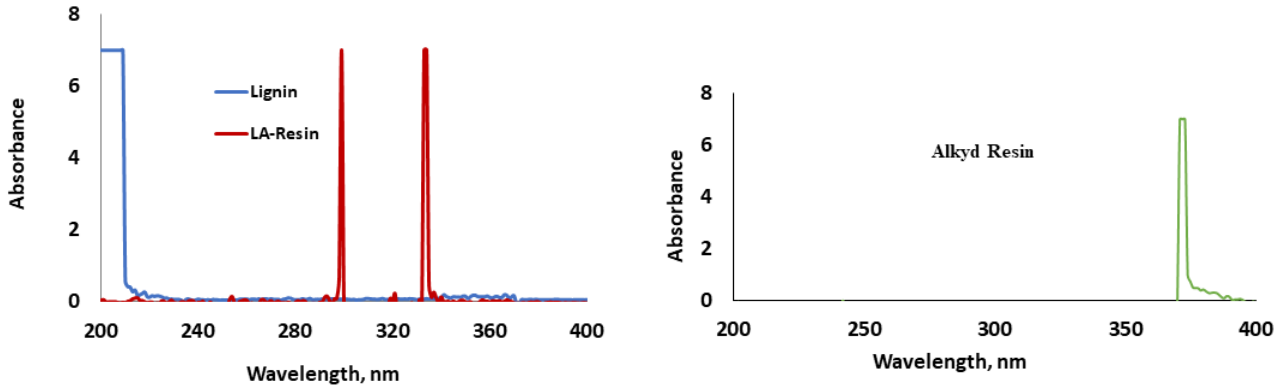

Figure 3S. Electronic spectra for lignin, and LA-Resin.

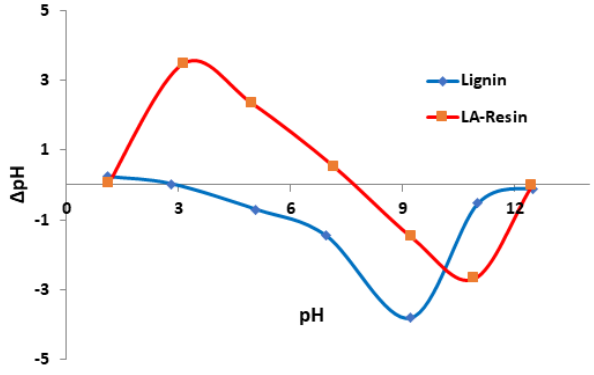

Figure 4S. The pH_{zpc} curves of lignin and LA-Resin.

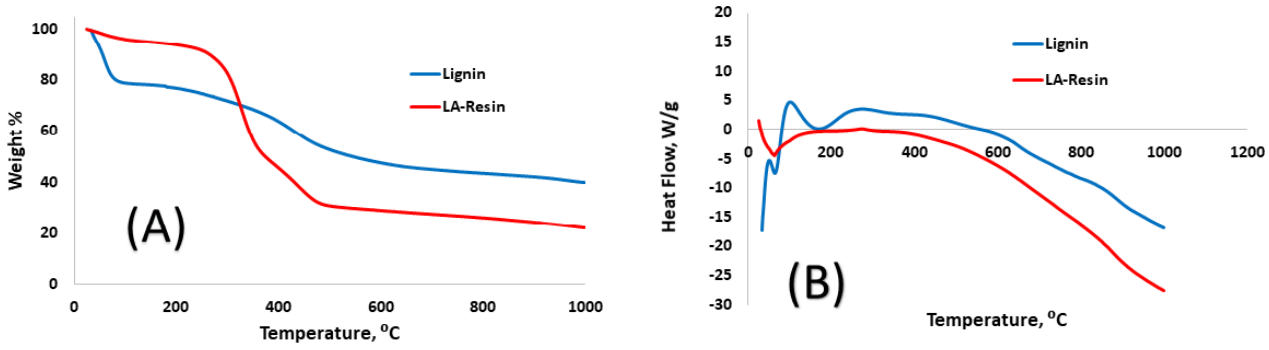

Figure 5S. TGA (A) and DTA (B) curves of lignin and LA-Resin.

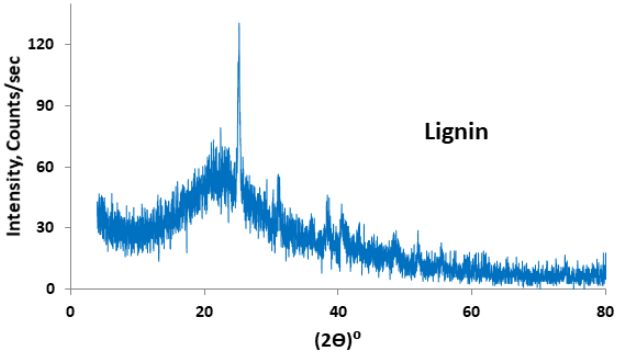

Figure 6S. XRD pattern of lignin.

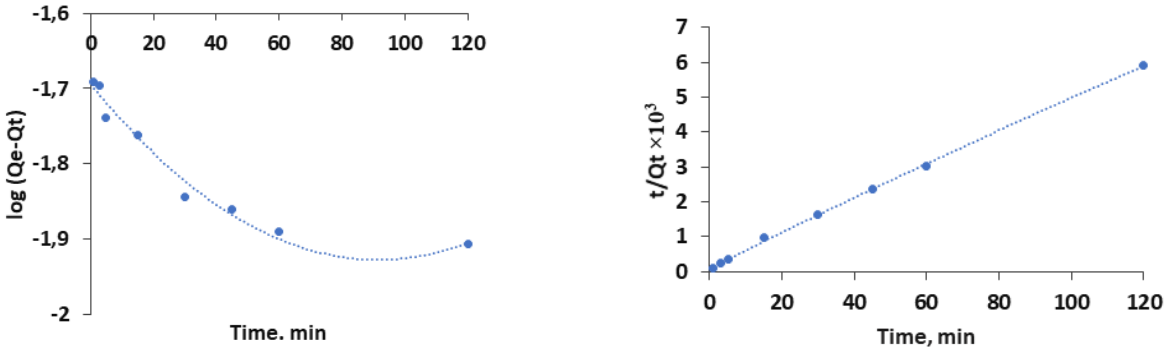

Figure 7S. Plots of non-linear kinetic models for the adsorption of Mo(VI) onto LA-Resin: Initial concentration of Mo(V) ions 5 to 200 mg L^{-1}; amount of LA-Resin 0.1 g; sample volume 25 mL; acidity 1.5 M.

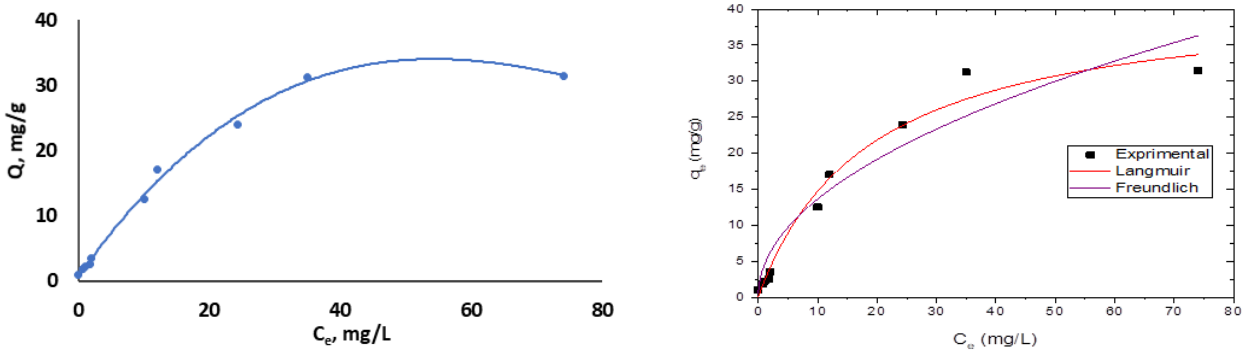

Figure 8S. Plots of non-linear isotherm models for the adsorption of Mo(VI) onto LA-Resin: Initial concentration of Mo(V) ions 5 to 200 mg L^{-1}; amount of LA-Resin 0.1 g; sample volume 25 mL; shaking time 60 min; acidity 1.5 M.

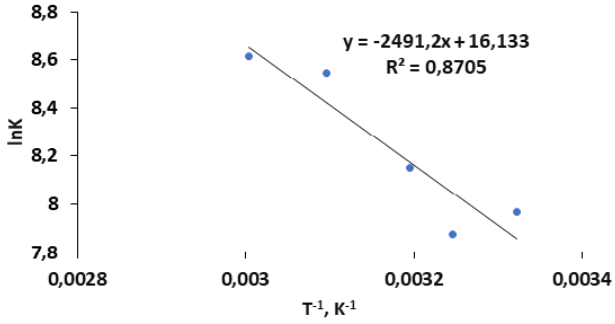

Figure 9S. Plots of thermodynamic model.

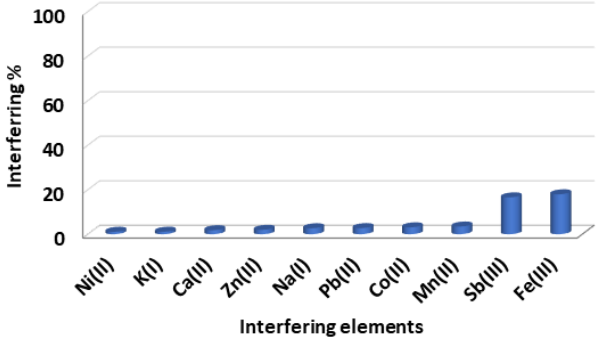

Figure 10S. Effect of the interfering ion on the extraction of Mo onto LA-Resin from aqueous solution.

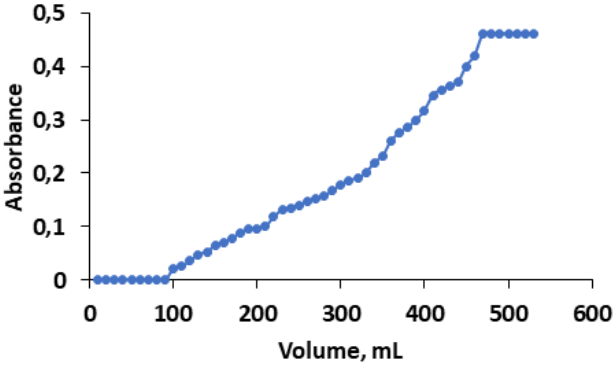

Figure 11S. Breakthrough curve for extraction of Mo from aqueous solution using LA-Resin column.

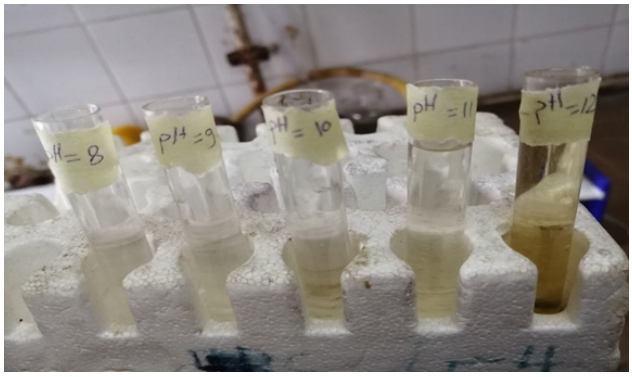

Figure 12S. Effect of alkaline solution on the stability of LA-Resin.

Table 1S. Kinetic and isotherm parameters for the sorption of Mo(V) onto LA-Resin

Kinetics	**Pseudo-first-order model**			**Pseudo-second-order model**		
Parameters	qe_1 (mg g^{-1})	k_1 (min^{-1})	R^2	qe_2 (mg g^{-1})	k_2 (g mg^{-1} min^{-1})	R^2
	1.77	0.043	0.75	1.98	2.01×10^{-5}	0.997
Isotherm	**Langmuir isotherm**			**Freundlich isotherm**		
Parameters	q_{max} (mg g^{-1})	b (L mg^{-1})	R^2	K_F	n	R^2
	39.2	0.026	0.92	0.356	2.01	0.86

*C_o = 8 mg L^{-1}, V = 25 mL, t = 0-120 min, q_{exp} = 1.94 mg g^{-1}

Table 2S. non-linear kinetic parameters for the adsorption of Mo(VI) onto LA-Resin: Initial concentration of Mo(V) ions 5 to 200 mg L^{-1}; amount of LA-Resin 0.1 g; sample volume 25 mL; acidity 1.5 M

Kinetics	**Pseudo-first-order model**			**Pseudo-second-order model**		
Parameters	qe_1 (mg/ g^{-1})	k_1 (min^{-1})	R^2	qe_2 (mg g^{-1})	k_2 (g mg^{-1} min^{-1})	R^2
	1.77	0.043	0.75	1.98	2.01×10^{-5}	0.997

Table 3S. Non-linear isotherm parameters for the adsorption of Mo(VI) onto LA-Resin: Initial concentration of Mo(V) ions 5 to 200 mg L^{-1}; amount of LA-Resin 0.1 g; sample volume 25 mL; shaking time 60 min; acidity 1.5 M

Isotherm	**Langmuir isotherm**			**Freundlich isotherm**		
Parameters	q_{max} (mg g^{-1})	b (L mg^{-1})	R^2	K_F	n	R^2
	42.1	0.053	0.98	4.4	2.2	0.92

Table 4S. Comparison between LA-Resin adsorption capacities of various adsorbents

Adsorbent	**Sorption capacity (mg g^{-1})**	**References**
Ch-NMA	29.7	(1)
Mn_3O_4-TiO_2 nanocomposite	20.6	(2)
WB1000	29.8	(3)
$CrFe_2O_4$ nanoparticles	17.03	(4)
SM-4 resin impregnated with CYANEX 923	8.2	(5)
TVEX- TOPO resin	17.6	(6)
TOA/perlite	7.2	(7)
Brown algae *Laminaria japonica* gel (CAG)	38.19	(8)

(continues on the next page)

Table 4S. Comparison between LA-Resin adsorption capacities of various adsorbents (continuation)

Adsorbent	Sorption capacity (mg g^{-1})	References
Silica gel/quercetin	8.54	(9)
Activated DWTRs	39.2	(10)
NaOCl-oxidized multiwalled carbon nanotubes	22.7	(11)
Di-(2-ethylhexyl) phosphoric acid	25.7	(12)
Carminic acid modified anion exchanger	13.5	(13)
Nano-magnetic $CuFe_2O_4$	30.6	(14)
Chitosan-modified magnetic nanoparticles	35.5	(15)

Table 5S. Thermodynamic parameters for the sorption Mo(V) onto LA-Resin

Thermodynamic parameters		
ΔG (kJ mol^{-1})	ΔH (kJ mol^{-1})	ΔS (J K^{-1} mol^{-1})
-19.2	21.6	137

Table 6S. The values of ΔG at different temperatures

Temperature, K	K	ln K	ΔG
298	2882.653	7.966466351	-19.73749397
308	2629.31	7.874476864	-20.1642674
313	3461.957	8.149589177	-21.20752922
323	5133.929	8.543626448	-22.94324242
333	5516.667	8.615529092	-23.85262645

Brazilian Journal of Analytical Chemistry
2022, Volume 9, Issue 36, pp 116–123
doi: 10.30744/brjac.2179-3425.TN-99-2021

BrJAC

TECHNICAL NOTE

How Sodiation Influences the Sucralose Behavior under Electrospray Ionization Mass Spectrometry

Paulo de Tarso Ferreira Sales[1], Katia Maria de Souza[2], Alyne Gonçalves Bezerra[1], Satu Anneli Ojala[3], Sérgio Botelho de Oliveira[2], Pierre Alexandre dos Santos[1], Maria Teresa Freitas Bara[3]*

[1]Universidade Federal de Goiás, Praça bloco B – R. 240, 406 – Setor Leste Universitário, CEP: 74605-170, Goiânia, GO, Brazil
[2]Instituto Federal de Goiás, R. 75, nº 46 – Centro, CEP: 74055-110, Goiânia, GO, Brazil
[3]Oulun Yliopisto, Faculty of Technology, Environmental and Chemical Engineering, University of Oulu, FI-90014, P.O. Box 4300, Oulu, Finland

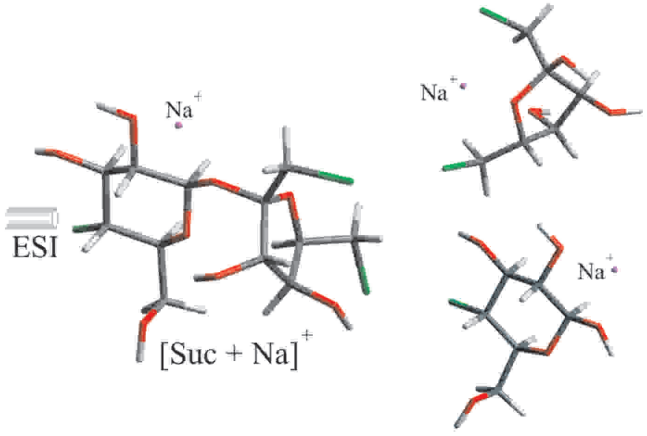

Nowadays, the detection of sucralose sodium adduct under electrospray ionization in mass spectrometry analysis is a common analysis method, but its high chemical stability is not fully understood. In this work, we use quantum chemistry calculations and mass spectrometry data to understand why sodiated sucralose presents this behavior in mass spectrometry conditions. The potential energy and the position of sodium ions were evaluated using different basis sets in order to comprehend the importance of sodiation in sucralose properties. Quantum-chemical calculations show higher reliability to explain the behavior of sucralose sodium adduct under mass spectrometry conditions, especially when its molecular geometry and potential energies are evaluated.

Keywords: DFT, Fukui functions, basis set, molecular geometry, potential energy.

INTRODUCTION

Sucralose ($C_{12}H_{19}Cl_3O_8$ – CAS 56038-13-2) is a synthetic organochlorine sweetener, sweeter than sucrose. Due to its wide use, and its environmental spreading, a higher sensitivity quantification method of sucralose sodium adduct was already reported,[1] that showed that it is interesting to evaluate sodiated compounds from different matrices in mass spectrometry (MS) studies. Nowadays, the use of MS for detection and quantitative analysis has been widely reported,[2–4] and today MS represents a conventional method for detecting several compounds. Although the detection of sodium adducts are reported for many pharmaceutical and organic compounds,[5–8] in studies using electrospray ionization (ESI) in mass

Cite: Sales, P. T. F.; de Souza, K. M.; Bezerra, A. G.; Ojala, S. A.; de Oliveira, S. B.; dos Santos, P. A. Bara, M. T. F. How Sodiation Influences the Sucralose Behavior under Electrospray Ionization Mass Spectrometry. *Braz. J. Anal. Chem.* 2022, *9* (36), pp 116–123. http://dx.doi.org/10.30744/brjac.2179-3425.TN-99-2021

Submitted 10 September 2021, Resubmitted 26 October 2021, Accepted 4 January 2022, Available online 7 March 2022.

spectrometry (ESI-MS) they are known to be difficult to fragment with tandem mass spectrometry (MS/MS) techniques.[9] However, it is unclear why some sodium adducts compounds presents higher chemical stability than the protonated ones in MS analysis. Moreover, Na^+ adduct formation is a quantitative and reproducible process which can be often used in ESI-MS.[10] In the present study, we evaluate the mass spectrum of sucralose sodium adduct in order to comprehend the position of the sodium ion, and why it is more stable ion in MS analysis, using quantum-chemical calculations (QCC).

A quantum-chemical theory was developed to investigate the structure of matter, and it is perceived as the density functional theory (DFT).[11] DFT is a worldwide accepted approach for modeling the ground state properties of molecules of interest,[12] and this function is a mixture of accurate (Hartree-Fock) exchange and local correction and gradient correction exchange and related terms, as first proposed by Becke (1996).[13] Thereby, this theory became a sophisticated tool for the semi-quantitative study of organic chemical reactivity.[14] To date, DFT has been used to calculate several reactive descriptors to predict molecular reactivity.[15] Exclusively B3LYP (Becke-3–Lee–Yang–Parr) has at present been used to show how halogenation of sucrose (sucralose) altered the electrostatic dipole moment of it,[16] and to calculate wavenumbers for the normal modes of vibration of sucralose.[17] Besides that, DFT calculations were used in MS studies to study the bond length, angle, and molecular geometry, which helps to understand their combination.[18]

MATERIALS AND METHODS

Reagents and Solvents

Sucralose was purchased from USP reference standard (Rockville, USA), acetic acid (Merck, Darmstadt, Germany), methanol (MeOH) was purchased from J.T Baker (USA). A Milli-Q-Plus ultrapure water system from Millipore (Milford, MA, USA) was used in stock solution of sucralose (1 μg mL^{-1}).

Sample Preparation

Acetic acid was added (0.1%) in 950 μL of methanol with 50 μL of a 1 mg mL^{-1} standard solution. After stirring during 1 min in a vortex, the samples were filtered in membrane 0.2 μm pore-size syringe filter, then they were injected into a mass spectrometer.

MS conditions

MS spectra were obtained either in the positive ion modes by direct infusion into Mass Spectrometer micrOTOF-QIII with Time-of-Flight and Electrospray Ionization (ESI-TOF) under the following conditions: Q-TOF (BrukerDaltonics, Massachusetts, USA); Electrospray positive mode; Scan Range (*m/z*): 50-600; Spray Voltage: 4.0 kV; Capillary temperature: 250 °C; Funnel: 200 Vpp. The samples were loaded into a 250 μL volume Hamilton gastight 7000 series syringe and introduced directly to the mass spectrometer, using Harvard Apparatus Pump 11 (Reno, NV) operating at a flow rate of 3 μL min^{-1}. Desolvation and nebuliser gas (N_2) flow rates were ~ 650 L h^{-1}.

Computational Details

The Gaussian 16 software revision A.03[19] used to perform the quantum chemical calculations. The molecular structures of all the species in-ground were optimized. Geometries were optimized to obtain local minimum energy. Molecular structures pictures were generated using Avogadro software, version 1.20.[20] The molecular 3D structure of transition states was visualized by using graphics software Molden 4. 2.[21] The descriptors based on the Fukui indices were generated by Multiwfn 3.2.1 program[22], which is a multifunctional program function analysis.

RESULTS AND DISCUSSION

Theoretical Molecular Ionization

Here, MS data from a quadrupole time-of-flight mass spectrometer operating in with Time-of-Flight (TOF) QTOF-ESI-MS are reported and QCC from correlation-consistent, Pople and minimum basis to understand how sodium ion affects sucralose in ESI conditions. First, the sucralose ionization was studied, and it is well known that the peak-based signal is related to cation stability of precursor ion.[23] In the theoretical ionization study, the sucralose molecular geometry was optimized from DFT/B3LYP/6-31G(d) level, then the dual Fukui function descriptor (FFD) was calculated (Figure 1), but the C3-Cl22 bond brokedown. Although a lack of a proper description of London dispersion effects in mere B3LYP/6-31G* calculations,[24] this level of calculation was chosen because of their popularity but deemed outdated in the theoretical community,[25] the intermolecular interactions of organic compounds,[26] and its cost effective factor.

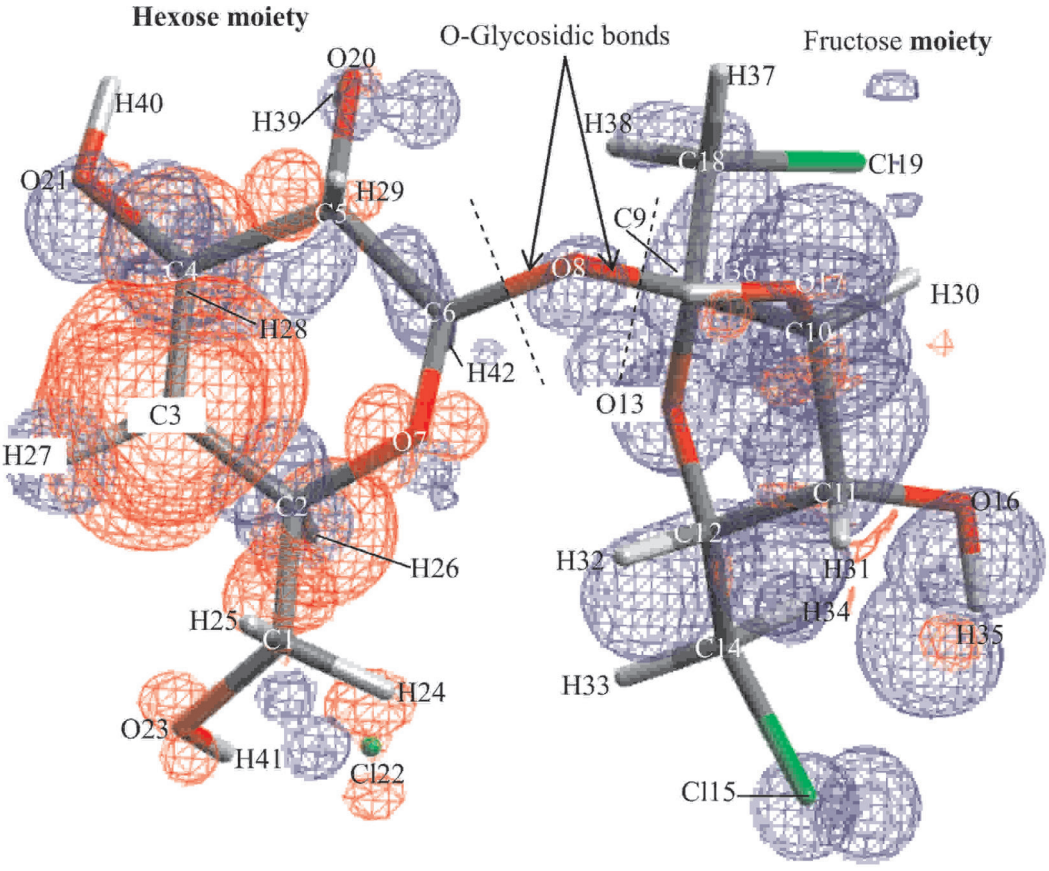

Figure 1. Map of the dual descriptor of the Fukui Function of the sucralose molecule from B3LYP/6-31G (d). Red and blue surfaces correspond to negative and positive regions, respectively. The atoms are numbered and labeled. The image was generated by the Avogadro program, and the descriptor was calculated by the Multiwfn program, from data generated by the Gaussian program 16.

According to the Figure 1, the FFD revealed that O17, O13, and O21 atoms presented the largest positive isosurfaces, as well the O20 atom. However, the O20, O8 and O17 atoms are able to coordinate the sodium ion, due to their spatial distribution. In order to study the potential energy involved in the molecular ionization, the theoretical protonation of sucralose molecule took place in oxygen atoms, and the sodium ion was added. After that, their molecular structures were optimized, and their potential ionization energies were calculated as the energy difference between the neutral molecule and its cation.

The equilibrium geometrical structures of sodium adduct of sucralose optimized from B3LYP/6-31G(d) presented the lowest potential energy (-2613,18 kcal mol^{-1}), while the protonated sucralose species presented the highest ones (average -2451,36 kcal mol^{-1}). Due to its lower potential energy, the base peak in the hypothetical mass spectra must be related to sucralose sodium adduct, even when an acidified solution is injected into a MS. The differences between ionization energies of protonated sucralose in O8, O13, and O21 atoms calculated from DFT/B3LYP/6-31G(d) were insignificant, which could not support us to certify the correct protonation site. In addition, the dual FFD indicates four nucleophilic groups with higher values, in both sites of the sucralose molecule and in O-glycosidic atom. We concluded that due to the exothermic nature of the sodium adduct formation, the dispersibility of sodium in the mobile phase, and the solubility in methanol, the ionization kinetics through the formation efficiency of the sodium adduct can be fully explained.[27]

Sucralose behavior under MS conditions

To verify if the QCC was able to predict which specie presented the base peak in the mass spectra, an acidified sample was directly injected into the high-resolution mass spectrometer with TOF mass analyzer via flow injection analysis mode and electrospray ionization ion source (ESI+) (Figure 2).

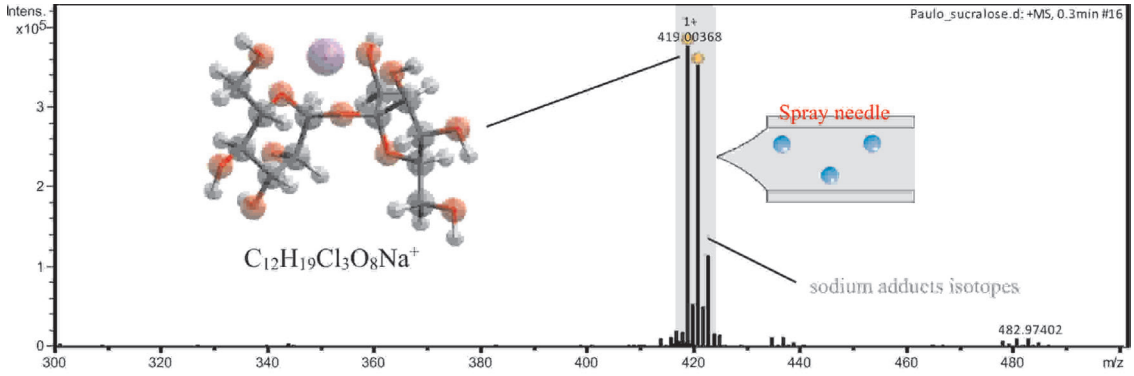

Figure 2. TOF-MS analysis of sucralose under positive ion mode, showing measured exact mass.

The mass spectra shows that sucralose sodium adduct at *m/z* 419.00368 ($C_{12}H_{19}Cl_3O_8Na^+$ – error 1.23 ppm) is the base peak, but the protonated sucralose was not observed. Furthermore, sucralose contains three chlorine atoms, and TOF analyses provided a valuable amount of isotopic accurate mass information for its detection of the sodium adducts isotopes (*m/z* 421.000112, 420.00651, 422.00445 Da) and mass defect (422.99829 and 422.00445 Da). Although the acidified sample was injected into the mass spectrometer, the sodium adduct was more stable than protonated sucralose, which spectral data confirmed that. Ferrer et al. (2013)[9] also concluded that sucralose forms a strong sodium adduct, most of which could be detected in MS. Complementarily, Nilsson et al. (2017)[29] and Zhou et al. (2016)[28] also reported that the signal intensity produced by sodiated adducts was higher than the produced by protonated precursor ions. Hence, the evaluation of potential energies of ionized sucralose is a reliable tool to study its molecular ionization that was confirmed in mass spectral data. Owing to this particularity, the sodiated sucralose was used as a precursor ion to quantify sucralose with an acute sensitivity[1,9,30] and this method was interesting due to its application in environmental studies.

Molecular geometry of sodiated sucralose

From a theoretical point of view, two different possible sites of sodium ion could take place to form the sodium adduct, and they are related to the interaction of O20, O8, and O17 and the sodium ion. Then, to study the interaction of sodium ion and the sucralose molecule, the sodiated sucralose structure was subjected to full QCC on different basis sets studies and a comparison of the bond lengths for the ion and

the potential energy were undertaken. Figure 3 shows the 3D molecular structure of $[Suc + Na]^+$ calculated from cc-pvdz , and 6-31G(d) basis sets.

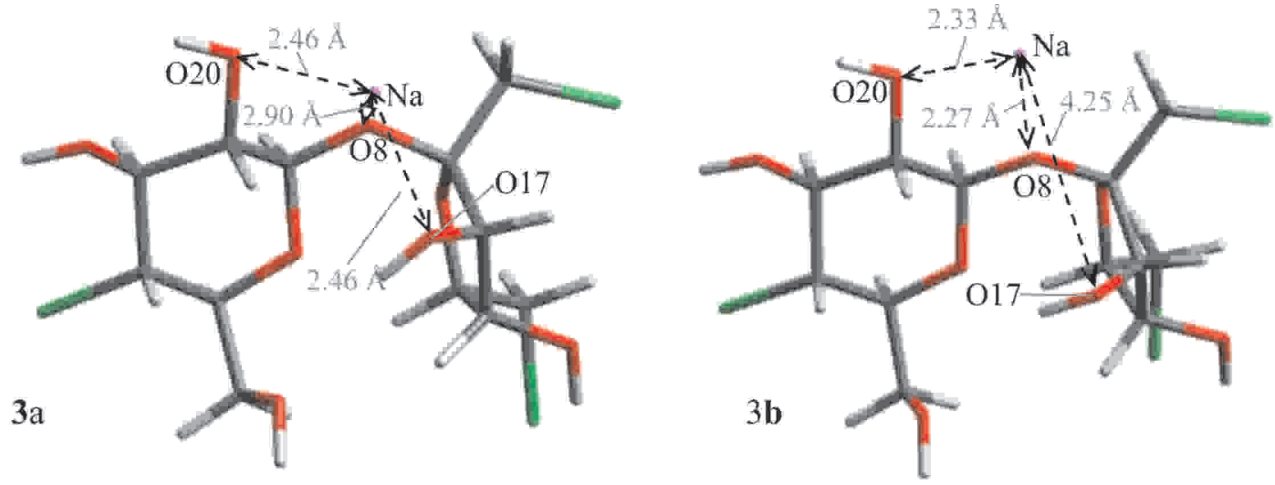

Figure 3. 3D optimized structure of the sodiated sucralose molecule, optimized from DFT level. The image was generated by the Avogadro program from data generated by the Gaussian program 16. Some atomic distances are shown. 3a - From RB3LYP/cc-pvdz. 3b - From B3LYP/6-31G(d).

Calculations from the thermodynamically most stable molecular structure of sodiated sucralose species were carried out, and the 3D models and the sodium ion position in a sodiated sucralose molecule are presented. According to the Figure 3, the oxygen atoms O20, O8 and O17 coordinated the approach of the sodium ion. The theoretical calculations using the basis sets 3-21G and cc-pvdz presented higher molecular geometry similarity, and they show an interaction of sodium ions and O8, O20 and O17 atoms. Otherwise, the basin sets LANL2DZ, 6-31G(d,p), 6-31G(d), STO-3G and cc-pvtz showed a specific interaction of the sodium ion and the O8 and O20 atoms. Analyzing the potential energy of sucralose sodium adducts, calculations from correlation-consistent basis sets presented lower values, while Pople and minimal basis sets revealed higher ones. Overall, the C9-O8 bond was longer than the C6-O8 one, but the addition of the sodium ion did not affect these bond lengths.

However, calculations from minimal basis sets presented longer bond lengths. The QCC from the basis set explored in this study showed that O8 atom presented highest negative atomic polat tensor (APT) charge in sodiated and neutral sucralose. Studying the electron density surfaces of molecules, Mohammad et al.[31] evaluated the equilibrium geometrical structures of sodium adducts optimized from pvdz basis, and observed higher accurancy of it which also explains our results. Moreover, evaluating different basis sets, the cc-pVDZ basis set was recommended as an acceptable balance between accuracy and computational cost.[32] Besides that, a deeper insight of non-covalent interactions were investigated and the cc-pVDZ basis set presented higher reliability to study the sodium coordination[33] due to its electron correlation level. However, augmented basis sets are computationally heavy, and outperformed by less computationally heavy options, but better results about energy are more significant.[34] Although Pople and minimal basis sets are a reasonable choice for exploration, they are not recommended when results require high accuracy or quantitative values. But the higher geometric correlation between 3-21G and cc-pvdz basis sets must be investigated. Differently, the basis sets LANL2DZ, 6-31G(d,p), 6-31G(d), STO-3G and cc-pvtz showed a specific interaction of the sodium ion and the O8 and O20 atoms.

To evaluate different basis sets, the cc-pvdz basis set is recommended as an acceptable balance between accuracy and computational cost,[32] and a deeper understanding of non-covalent interactions has also been studied, and due to its electronic correlation level, the cc-pvdz basis set has higher reliability

when studying sodium coordination[33] due to its electron correlation level. However, the enhanced basis set is computationally intensive, and the less computationally intensive option is better than the more computationally intensive one, but the better results regarding energy are more important.[34] Obviously, the position of Na^+ attachment is determined not only by the atomic charge, but also by spatial factors (the mutual position of the atomic interaction).[35]

CONCLUSIONS

Overall, sucralose exhibits a oxygen-rich structure and the combination of threshold QTOF-MS measurements and QCC allowed us to understand why the sodiated sucralose is more stable than the protonated one. Comparing theoretical potential energy of protonated and sodiated sucralose, the $[Suc + Na]^+$ presented an incomparable lowest one. These results certified the superior chemical stability of sodiated sucralose and as the base peak in the mass spectra. From these data, sucralose sodium adduct must improve the sensitivity of quantification in MS analysis. Moreover, sucralose isotopic distribution enhances the selectivity of precursor ion and TOF-MS or ESI-MS/MS that provides exact masses, improving the method accuracy. Consequently, the mass spectral data showed that the most stable ion was $[Suc + Na]^+$. Evaluating potential energy, bond lengths and sodium ion position of the sodiated sucralose from minimal (STO-3G), Pople (3-21G, 6-31G(d,p), and 6-31G(d)) and correlation-consistent (cc-pVDZ and cc-pVTZ) basis sets, the sodium position represented a remarkable difference. These basis sets did not present a more significant variance of APT charges and bond lengths, specially C9-O8 and C6-O8 bonds, but QCC presented that the oxygen atoms O20, O8 and O17 coordinated the approach of the sodium ion, and the basin sets 3-21G and cc-pvdz presented higher 3D geometry similarity due to the higher interaction of sodium ion and O8, O20 and O17 atoms.

Conflicts of interest

All authors declare no conflicts of interest.

Acknowledgements

To the Faculty of Pharmacy, and Institute of Chemistry at the Federal University of Goiás for the technical and laboratory support. To the Faculty of Technology, Chemical and Environmental Engineering of the University of Oulu, Finland. To the coordinators of the “No Waste” program in Brazil and Finland for the possibility of Exchange at the University of Oulu and the “Coordenação de Aperfeiçoamento de Pessoal de Nível Superior” (CAPES) for the award of the doctoral program.

REFERENCES

(1) Ferrer, I.; Thurman, E. M. Analysis of sucralose and other sweeteners in water and beverage samples by liquid chromatography/time-of-flight mass spectrometry. *J. Chromatogr. A* **2010**, *1217*, 4127–4134. https://doi.org/10.1016/j.chroma.2010.02.020

(2) Loos, R.; Gawlik, B. M.; Boettcher, K.; Locoro, G.; Contini, S.; Bidoglio, G. Sucralose screening in European surface waters using a solid-phase extraction-liquid chromatography–triple quadrupole mass spectrometry method. *J. Chromatogr. A* **2009**, *1216*, 1126–1131. https://doi.org/10.1016/j.chroma.2008.12.048

(3) Batchu, S. R.; Quinete, N.; Panditi, V. R.; Gardinali, P. R. Online solid phase extraction liquid chromatography tandem mass spectrometry (SPE-LC-MS/MS) method for the determination of sucralose in reclaimed and drinking waters and its photo degradation in natural waters from South Florida. *Chem. Cent. J.* **2013**, *7*, 141. https://doi.org/10.1186/1752-153X-7-141

(4) Arbeláez, P.; Borrull, F.; Pocurull, E.; Marcé, R. M. Determination of high-intensity sweeteners in river water and wastewater by solid-phase extraction and liquid chromatography–tandem mass spectrometry. *J. Chromatogr. A* **2015**, *1393*, 106–114. https://doi.org/10.1016/j.chroma.2015.03.035

(5) Clowers, B. H.; Dwivedi, P.; Steiner, W. E.; Hill, H. H.; Bendiak, B. Separation of sodiated isobaric disaccharides and trisaccharides using electrospray ionization-atmospheric pressure ion mobility-time of flight mass spectrometry. *J. Am. Soc. Mass Spectrom.* **2005**, *16*, 660–669. https://doi.org/10.1016/j.jasms.2005.01.010
(6) Chen, J.-L.; Nguan, H. S.; Hsu, P.-J.; Tsai, S.-T.; Liew, C. Y.; Kuo, J.-L.; Hu, W.-P.; Ni, C.-K. Collision-induced dissociation of sodiated glucose and identification of anomeric configuration. *Phys. Chem. Chem. Phys.* **2017**, *19*, 15454–15462. https://doi.org/10.1039/C7CP02393F
(7) Lepere, V.; Le Barbu-Debus, K.; Clavaguéra, C.; Scuderi, D.; Piani, G.; Simon, A.-L.; Chirot, F.; MacAleese, L.; Dugourd, P.; Zehnacker, A. Chirality-dependent structuration of protonated or sodiated polyphenylalanines: IRMPD and ion mobility studies. *Phys. Chem. Chem. Phys.* **2016**, *18*, 1807–1817. https://doi.org/10.1039/C5CP06768E
(8) Colsch, B.; Damont, A.; Junot, C.; Fenaille, F.; Tabet, J.-C. Experimental evidence that electrospray-produced sodiated lysophosphatidyl ester structures exist essentially as protonated salts. *Eur. J. Mass Spectrom.* **2019**, *25*, 333–338. https://doi.org/10.1177/1469066719838924
(9) Ferrer, I.; Zweigenbaum, J. A.; Thurman, E. M. Analytical Methodologies for the Detection of Sucralose in Water. *Anal. Chem.* **2013**, *85*, 9581–9587. https://doi.org/10.1021/ac4016984
(10) Kruve, A.; Kaupmees, K.; Liigand, J.; Oss, M.; Leito, I. Sodium adduct formation efficiency in ESI source. *J. Mass Spectrom.* **2013**, *48*, 695–702. https://doi.org/10.1002/jms.3218
(11) Hohenberg, P.; Kohn, W. Inhomogeneous Electron Gas. *Phys. Rev.* **1964**, *136*, B864–B871. https://doi.org/10.1103/PhysRev.136.B864
(12) Saha, S. K.; Banerjee, P. A theoretical approach to understand the inhibition mechanism of steel corrosion with two aminobenzonitrile inhibitors. *RSC Adv.* **2015**, *5*, 71120–71130. https://doi.org/10.1039/C5RA15173B
(13) Becke, A. D. Density-functional thermochemistry. IV. A new dynamical correlation functional and implications for exact-exchange mixing. *J. Chem. Phys.* **1996**, *104*, 1040–1046. https://doi.org/10.1063/1.470829
(14) Domingo, L.; Ríos-Gutiérrez, M.; Pérez, P. Applications of the Conceptual Density Functional Theory Indices to Organic Chemistry Reactivity. *Molecules* **2016**, *21*, 748. https://doi.org/10.3390/molecules21060748
(15) Huizar, L. H. M.; Rios-Reyes, C. H.; Olvera-Maturano, N. J.; Robles, J.; Rodriguez, J. A. Chemical reactivity of quinclorac employing the HSAB local principle - Fukui function. *Open Chem.* **2015**, *13*, 52–60. https://doi.org/10.1515/chem-2015-0008
(16) Chen, L.; Shukla, N.; Cho, I.; Cohn, E.; Taylor, E. A.; Othon, C. M. Sucralose Destabilization of Protein Structure. *J. Phys. Chem. Lett.* **2015**, *6*, 1441–1446. https://doi.org/10.1021/acs.jpclett.5b00442
(17) Brizuela, A. B.; Raschi, A. B.; Castillo, M. V.; Leyton, P.; Romano, E.; Brandán, S. A. Theoretical structural and vibrational properties of the artificial sweetener sucralose. *Comput. Theor. Chem.* **2013**, *1008*, 52–60. https://doi.org/10.1016/j.comptc.2012.12.017
(18) Ventura, G.; Abbattista, R.; Calvano, C. D.; De Ceglie, C.; Losito, I.; Palmisano, F.; Cataldi, T. R. I. Tandem mass spectrometry characterization of a conjugate between oleuropein and hydrated cis-diammineplatinum(II). *Rapid Commun. Mass Spectrom.* **2019**, *33*, 657–666. https://doi.org/10.1002/rcm.8394
(19) Gaussian 16, Revision A. 03. Frisch, M. J.; Trucks, G. W.; Schlegel, H. B.; Scuseria, G. E.; Robb, M. A.; Cheeseman, J. R.; Scalmani, G.; Barone, V.; Petersson, G. A.; Nakatsuji, H.; et al. Gaussian, Inc., Wallingford CT, **2016**.
(20) Hanwell, M. D.; Curtis, D. E.; Lonie, D. C.; Vandermeersch, T.; Zurek, E.; Hutchison, G. R. Avogadro: an advanced semantic chemical editor, visualization, and analysis platform. *J. Cheminform.* **2012**, *4*, 17. https://doi.org/10.1186/1758-2946-4-17
(21) Schaftenaar, G.; Noordik, J. H. Molden: a pre- and post-processing program for molecular and electronic structures*. *J. Comput. Aided. Mol. Des.* **2000**, *14*, 123–134. https://doi.org/10.1023/A:1008193805436

(22) Lu, T.; Chen, F. Multiwfn: A multifunctional wavefunction analyzer. *J. Comput. Chem.* **2012**, *33*, 580–592. https://doi.org/10.1002/jcc.22885
(23) Alsheikh, A. A.; Žídek, J.; Krčma, F.; Papp, P.; Lacko, M.; Matejčík, Š. Fragmentation of methylphenylsilane and trimethylphenylsilane: A combined theoretical and experimental study. *Int. J. Mass Spectrom.* **2015**, *385*, 1–12. https://doi.org/10.1016/j.ijms.2015.05.004
(24) Kruse, H.; Goerigk, L.; Grimme, S. Why the standard B3LYP/6-31G* model chemistry should not be used in DFT calculations of molecular thermochemistry: Understanding and correcting the problem. *J. Org. Chem.* **2012**, *77*, 10824–10834. https://doi.org/10.1021/jo302156p
(25) Zhao, Y.; Truhlar, D. G. Density functionals with broad applicability in chemistry. *Acc. Chem. Res.* **2008**, *41*, 157–167. https://doi.org/10.1021/ar700111a
(26) Freindorf, M.; Shao, Y.; Furlani, T. R.; Kong, J. Lennard–Jones parameters for the combined QM/MM method using the B3LYP/6-31G*/AMBER potential. *J. Comput. Chem.* **2005**, *26*, 1270–1278. https://doi.org/10.1002/jcc.20264
(27) Kruve, A.; Kaupmees, K. Adduct Formation in ESI/MS by Mobile Phase Additives. *J. Am. Soc. Mass Spectrom.* **2017**, *28*, 887–894. https://doi.org/10.1007/s13361-017-1626-y
(28) Zhou, S.; Hu, Y.; Veillon, L.; Snovida, S. I.; Rogers, J. C.; Saba, J.; Mechref, Y. Quantitative LC–MS/MS Glycomic Analysis of Biological Samples Using AminoxyTMT. *Anal. Chem.* **2016**, *88*, 7515–7522. https://doi.org/10.1021/acs.analchem.6b00465
(29) Nilsson, J.; Noborn, F.; Gomez Toledo, A.; Nasir, W.; Sihlbom, C.; Larson, G. Characterization of Glycan Structures of Chondroitin Sulfate-Glycopeptides Facilitated by Sodium Ion-Pairing and Positive Mode LC-MS/MS. *J. Am. Soc. Mass Spectrom.* **2017**, *28*, 229–241. https://doi.org/10.1007/s13361-016-1539-1
(30) Yan, W.; Wang, N.; Zhang, P.; Zhang, J.; Wu, S.; Zhu, Y. Simultaneous determination of sucralose and related compounds by high-performance liquid chromatography with evaporative light scattering detection. *Food Chem.* **2016**, *204*, 358–364. https://doi.org/10.1016/j.foodchem.2016.02.099
(31) Mohammad, R. K.; Madlol, R. A.; Umran, N. M.; Sharrad, F. I. Structure and electronic properties of substitutionally doped Cycloheptane molecule using DFT. *Results Phys.* **2016**, *6*, 1036–1043. https://doi.org/10.1016/j.rinp.2016.11.039
(32) Xin, D.; Sader, C. A.; Chaudhary, O.; Jones, P. J.; Wagner, K.; Tautermann, C. S.; Yang, Z.; Busacca, C. A.; Saraceno, R. A.; Fandrick, K. R.; et al. Development of a 13C NMR Chemical Shift Prediction Procedure Using B3LYP/cc-pVDZ and Empirically Derived Systematic Error Correction Terms: A Computational Small Molecule Structure Elucidation Method. *J. Org. Chem.* **2017**, *82*, 5135–5145. https://doi.org/10.1021/acs.joc.7b00321
(33) Wang, P.; Shi, R.; Su, Y.; Tang, L.; Huang, X.; Zhao, J. Hydrated Sodium Ion Clusters [Na+(H2O)n (n = 1–6)]: An ab initio Study on Structures and Non-covalent Interaction. *Front. Chem.* **2019**, *7*, 624. https://doi.org/10.3389/fchem.2019.00624
(34) Ferrari, B. C.; Bennett, C. J. A Comparison of Medium-Sized Basis Sets for the Prediction of Geometries, Vibrational Frequencies, Infrared Intensities and Raman Activities for Water. *J. Phys. Conf. Ser.* **2019**, *1290*. https://doi.org/10.1088/1742-6596/1290/1/012013
(35) Emmanuel, M. Interactions Between Sodium Ion and Constituents of Chitosan: DFT Study. *Int. J. Mater. Sci. Appl.* **2015**, *4*, 303. https://doi.org/10.11648/j.ijmsa.20150405.15

Brazilian Journal of Analytical Chemistry
2022, Volume 9, Issue 36, pp 124–145
doi: 10.30744/brjac.2179-3425.TN-108-2021

BrJAC

TECHNICAL NOTE

Chemical Characterization in the Production Chain of Permanent Magnets by Inductively Coupled Plasma Optical Emission Spectrometry (ICP OES)

Precise Quantification of Nd, Pr, Fe and B in Super-Magnets Samples

Rodrigo Papai*[1], Karina Torre da Fonseca[2], Gilmar Alves de Almeida[1,3], André Luiz Nunis da Silva[1], Thiago Pires Nagasima[1], Eduardo Gimenes Jabes[1,4], Célia Aparecida Lino dos Santos[1], Fernando José Gomes Landgraf[4], Maciel Santos Luz*[1]

[1]*Instituto de Pesquisas Tecnológicas do Estado de São Paulo (IPT), Avenida Professor Almeida Prado, 732, Cidade Universitária, 05508-901, São Paulo, SP, Brazil*
[2]*Instituto de Química da Universidade de São Paulo (IQ USP), Avenida Professor Lineu Prestes, 748, Cidade Universitária, 05508-000, São Paulo, SP, Brazil*
[3]*Instituto de Pesquisas Energéticas e Nucleares (IPEN), Avenida Professor Lineu Prestes, 2242, Cidade Universitária, 05508-000, São Paulo, SP, Brazil*
[4]*Escola Politécnica da Universidade de São Paulo (EP USP), Avenida Professor Luciano Gualberto, 380, Cidade Universitária, 05508-010, São Paulo, SP, Brazil*

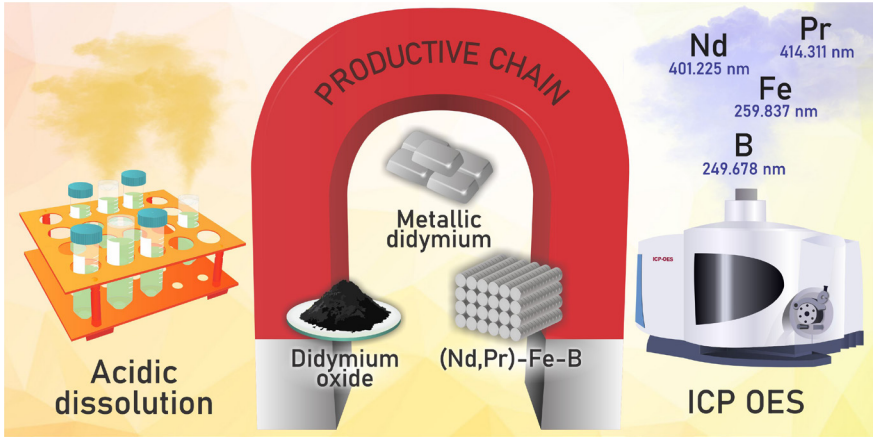

Super-magnets, materials whose strong magnetic activity is an attractive differential for the high-tech industry, may have their magnetic performance affected by small variations in their chemical composition. For example, the neodymium and praseodymium content can change the physicochemical properties of the permanent magnets. Aiming at a strict chemical quality control, this work developed an analytical method to quantify the major elements in the materials involved in the production process of didymium (the mixture of neodymium and praseodymium) super-magnets. The simultaneous determination of Nd (401.225 nm), Pr (414.311 nm), Fe (259.837 nm) and B (249.678 nm) in three different sample types (didymium oxide, metallic didymium and (Nd,Pr)-Fe-B alloy) was performed by sample dissolution in acidic media, followed by instrumental measurements using an Inductively Coupled Plasma Optical Emission

Cite: Papai, R; da Fonseca, K. T.; de Almeida, G. A.; da Silva, A. L. N.; Nagasima, T. P.; Jabes, E. G.; dos Santos, C. A. L.; Landgraf, F. J. G.; Luz, M. S. Chemical Characterization in the Production Chain of Permanent Magnets by Inductively Coupled Plasma Optical Emission Spectrometry (ICP OES) – Precise Quantification of Nd, Pr, Fe and B in Super-Magnets Samples. *Braz. J. Anal. Chem.* 2022, *9* (36), pp 124–145. http://dx.doi.org/10.30744/brjac.2179-3425.TN-108-2021

Submitted 21 October 2021, Resubmitted 01 April 2022 , Accepted 15 April 2022, Available online 17 May 2022.

Spectrometer. Linear calibration curves were obtained with high coefficient of determination ($0.9983 \leq R^2 \leq 0.9999$) and with appropriate limits for determining these elements at the percentage level, reaching detection limits less than 0.07 cg g^{-1}. The precision of the method was improved by weighing of the solutions during all the dilution steps and was evaluated by the coefficient of variation associated to instrumental precision (0.3 – 0.7%), method intermediate precision (1.9 – 3.1%) and also by the typical mass fraction provided as uncertainty (0.04 – 0.20 cg g^{-1}), reaching the pressing need to distinguish the content of the rare earth elements in less than 1 cg g^{-1}. The accuracy of the method was assessed by spiked and recovery test (96-104% for spikes equal to or greater than 0.50 cg g^{-1}) and also by the use of different analytical methods, involving the participation of other laboratories, obtaining an acceptable degree of agreement (85 – 107%).

Keywords: Didymium magnets, ICP OES, (Nd,Pr)-Fe-B

INTRODUCTION

Present in electric motors, wind turbines and data storage devices (hard disk), magnets are indispensable in the manufacture of computers, televisions, cell phones, smart watches and other various modern electronic devices.[1,2] The chemical composition of the magnet directly influences its magnetic performance with a consequent impact on the quality of the associated products.[3-6] In this context, knowing the major chemical composition of magnets contributes to a more efficient quality control in the act of production and also helps manufacturers in the high-tech industry to select magnets in order to keep the uniformity of these materials, valuing the isonomy of the final products with higher added value.

Although there are several magnet types, those that employ rare earth elements (REE) generally have strong magnetic activity,[1,7-11] and are often called permanent magnets or super-magnets.[2,3] Among the REE, the mixture of neodymium and praseodymium (called didymium[12,13]) is widely used in metal alloys together with the elements iron and boron to act as a super-magnet. Currently, the most powerful commercial magnets used in the world employ neodymium[14] or didymium.[15-18]

The production chain of metal alloy (Nd,Pr)-Fe-B is briefly summarized into the following steps: (i) in the production of didymium oxide (a mixture of neodymium and praseodymium oxides) through a process of separation of the ore that contains REE; (ii) the electrolytic reduction of didymium oxide, in order to obtain metallic didymium (a solid solution containing neodymium and praseodymium) and (iii) the incorporation of elemental iron and boron in the metallic didymium in liquid phase (process carried out under high temperatures) to finally obtain the metallic alloy (Nd,Pr)-Fe-B. The chemical composition of the super-magnets varies according to the application. In general, the typical contents of the elements in this alloy ranged around 25-35 cg g^{-1} of didymium, 0.5-2.0 cg g^{-1} of boron and 60-75 cg g^{-1} of iron. According to the need for the application, other minority elements can be added.[19]

After the production of the metal alloy, the magnet can be obtained by several processes that involve: hydrogen embrittlement (or also called hydrogen decrepitation[20-22]); milling;[23] magnetic particle alignment, which is induced by an intense magnetic field applied under the material; compaction; sintering and appropriate heat treatments, thus giving rise to the super-magnet.

In order to reduce cost, the chemical composition must minimize the use of REE. However, the reduction of REE content may cause alpha iron phase (an allotrope of iron with a body-centered cubic crystalline structure) to be present in magnets, which has a negative effect on the desired magnetic properties of the super-magnet and hinders further processing steps, such as the hydration and sintering of the alloy.[24]

Small variations in the Nd and Pr content strongly influence the physicochemical properties of the alloy, for this reason studies about alloy development involve minimal variations in the REE content. In this way, the chemical characterization of the alloy and the main materials involved in its production process are important to achieve the desired properties in these magnetic materials. Therefore, chemical analytical methods must be able to distinguish small variations in the concentration of their constituent elements.

Among the analytical techniques of elemental determination, those that allow direct solid analysis, would be ideal for analysing such materials, mainly due to: (i) high analytical frequency, which allows fast analysis of solid materials; (ii) the practicality of minimizing the sample treatment step or even eliminating it and (iii) the reduction of possible errors inherent in sample handling.[25] Currently, the main techniques for direct solids analysis include: Laser-Induced Breakdown Spectroscopy (LIBS),[26-30] X-ray Fluorescence (XRF),[31-33] Laser Ablation Inductively Coupled Plasma Mass Spectrometry (LA-ICP-MS),[34,35] Graphite Furnace Atomic Absorption Spectrometry (GF AAS),[36] among others.[25]

However, to quantify the analytes most of these techniques require calibrating materials, that is, solid standards whose chemical composition is well known with a suitable degree of accuracy and precision in a similar matrix to the sample. Unfortunately, to date, such solid standards for the materials involved in the production process of super-magnets are not available.

Considering the unavailability of calibrating materials for use in direct analysis of solids and aiming at a reliable analytical method to quantify Nd, Pr, Fe and B simultaneously in three different types of samples involved in production process of super-magnets (didymium oxide, metallic didymium and (Nd,Pr)-Fe-B alloy), this work reports the synthesis of these materials and a simple protocol for the dissolution of the sample in diluted acid solutions and subsequent quantification of analytes by Inductively Coupled Plasma Optical Emission Spectrometry (ICP OES), an instrumental technique with great potential for reliable determination of rare earth elements.[3,37-39]

The determination of chemical elements in samples of permanent magnets based on rare earths by ICP OES is not new, and it is possible to find old articles that mention having performed elemental analysis by ICP. However, the description of how to proceed with this chemical measurement task in these samples is scarce in the literature. In a world in which the reliability of the results is increasingly necessary, this work contributes with a detailed account of a robust method, which provides precise and accurate results. For the first time, a complete analytical method is reported to determine the main elements in the production chain of didymium permanent magnets. With the intention of establishing a standard method to be implemented routinely, the novelty of this work is centered on meeting the quality criteria necessary in the production chain of didymium magnets and it stands out for the: (i) high reliability of the results, (ii) high precision obtained, which allows to distinguish low contents of rare earth elements and (iii) in the evaluation of foreign elements that can be potential interfering species, making this paper act as a guide for the development of analytical applications in similar samples.

MATERIALS AND METHODS

Reagents and solutions

Standard solutions of neodymium 100,434 ± 450 mg L^{-1} (Specsol™), praseodymium 100,497 ± 450 mg L^{-1} (Specsol™), iron 10,027 ± 50 mg L^{-1} (SPEX CertiPrep™) and boron 1,002 ± 4 mg L^{-1} (SCP Science™) were used as reference solutions for calibration by external standardization.

Neodymium and praseodymium oxides were purchased from HEFA Rare Earth Canada Co.Ltd.™

Nitric acid solution 25% (v/v) was prepared by the slow addition of 25 mL of concentrated acid (65% w/w, Merck™) in 75 mL of deionized water.

Hydrochloric acid solution 27% (v/v) was prepared by the slow addition of 27 mL of concentrated acid (37% w/w, Merck™) in 73 mL of deionized water.

Samples and preparation

Three different sample types related to permanent magnets manufacturing process were evaluated in this study: (i) didymium oxide, obtained by mixing praseodymium and neodymium oxides; (ii) metallic didymium (solid solution containing Nd and Pr), produced in our laboratory by igneous electrolytic reduction, using molten lithium fluoride and didymium oxide concentrate and (iii) (Nd,Pr)-Fe-B alloy, prepared with the previously produced metallic didymium by the incorporation of iron and boron elements in liquid phase, followed by solidification and subsequent strip casting procedure. The samples were stored in an inert

atmosphere (argon gas) to prevent oxidation[40] and were exposed to atmospheric air only seconds before the sample treatment (acid dissolution).

The subsamples were divided in three different test portions (n = 3). Each test portion was weighed directly in a conical polypropylene tube (Falcon, Corning™) with a capacity of 50 mL until reaching a mass ideally close to the following values: 0.3, 0.4 and 0.5 g for didymium oxide, metallic didymium and (Nd,Pr)-Fe-B alloy sample, respectively. The real mass value was recorded (considering up to 4 decimal places) and then the samples dissolution was started.

In a fume hood, the dissolution of metallic didymium and (Nd,Pr)-Fe-B alloy samples was carried out in acidic solutions, containing 15 mL of nitric acid (25% v/v) and 5 mL of hydrochloric acid (27% v/v) for each test portion. Also in a fume hood, the didymium oxide was dissolved with 10 mL of concentrated hydrochloric acid (37% w/w) and 10 mL of concentrated nitric acid (65% w/w) until the dissolution reaction was completed (obtained visually when reaching a translucent colour).

When necessary, in exceptional cases, increments of up to 4 mL of concentrated nitric acid (65% w/w) were added, until the dissolution reaction was completed (obtained visually when reaching a translucent colour).

The initial mass of each tube was recorded and then after the dissolution step, the volume was completed to 50 mL with deionized water. Next, the final dissolved sample was weighed and its mass was recorded to calculate the real dilution factor. Using a micropipette and also weighing on the analytical balance, the resulting solution (sample dissolved) was diluted by factors of 150, 200 or 250-fold for (Nd,Pr)-Fe-B alloy, didymium oxide and metallic didymium, respectively, prior to analysis.

Blank solutions were prepared by adding all the reagents described previously without the samples. All solutions were produced in triplicate (n = 3).

ICP OES instrumentation and conditions

Inductively Coupled Plasma Optical Emission Spectrometer (iCap 7400 Duo, Thermo Scientific™) was used for chemical analysis. The main conditions used during the ICP OES analysis, such as: (i) nebulizer gas flow, (ii) RF generator power, (iii) peristaltic pump frequency and (iv) argon auxiliary gas flow were optimized, aiming to achieve the highest signal-to-background ratio, with 14 different parameters sets being evaluated. The optimal conditions are summarized in Table I.

Table I. Operational conditions optimized for ICP OES analysis

Parameter	Condition
RF generator power	27.12 MHz solid state, operated at 1150 W
Coolant gas flow rate (argon)	12 L min^{-1}
Auxiliary gas flow rate (argon)	0.50 L min^{-1}
Nebulizer type	Concentric (glass)
Spray chamber	Glass Cyclonic
Nebulizer gas flow	0.50 L min^{-1}
Sample flow rate	1.55 mL min^{-1} (50 rpm)
View mode	Axial
Exposure time	15 s for UV and 5 s for Visible measurements
Replicates	3
Monitored analytical lines	Nd II 401.225 nm Pr II 414.311 nm Fe II 259.837 nm B I 249.678 nm

Calibration

Calibration curves were constructed with 10 points by diluted standard solutions containing the analytes together in the range of 10.0 to 32.5 mg L^{-1} for neodymium, 0.10 to 10.00 mg L^{-1} for praseodymium, 30 to 57 mg L^{-1} for iron and 0.1 to 1.8 mg L^{-1} for boron. All dilutions were properly weighed using the analytical balance, recording the mass of each concentrated standard added to calculate the concentration of the solution accurately.

RESULTS AND DISCUSSION

The main results and the parameters that characterize an analytical method are discussed throughout the article, emphasizing: (i) Sample dissolution; (ii) Optical measurements and pixel selection; (iii) Calibration and limits of detection and quantitation; (iv) Precision; (v) Accuracy; (vi) Foreign elements and interference evaluation and (vii) Comparative analytical methods, advantages and drawbacks.

Sample dissolution

The complete dissolution of the sample was easily reached with the combination of nitric and hydrochloric acid, due to its oxidation strength. The concentrations reported in the experimental section were optimized to allow a quick and safe dissolution. Since both the metallic didymium and the (Nd,Pr)-Fe-B alloy can react violently with the acid mixture, the need to use diluted acids to prevent the release of particles was noticed. In contrast, didymium oxide exhibited less reactivity and therefore, its dissolution was affected with concentrated acids in a longer time (more than 1 hour). Visual observation indicated that heating in a water bath around 90 ºC can accelerate the sample dissolution time by up to 70%.

Although sample treatment is not such a difficult step, the analytes determination by optical spectrometry poses some challenges. For example, the high similarity in the electronic structure between the atoms of Nd and Pr can cause intense spectral interferences. This requires the use of a high resolution spectrometer, that is capable of resolving these interferences or the use of interference correction strategies.[3] The high amount of iron in the sample is also a challenge, as this is a chemical element known to emit at different wavelengths. Therefore, there is also a need to select appropriate wavelengths for measurement, as well as to control the content of Fe injected into ICP OES instrument.

Optical measurements and pixels selection

All optical emission measurements were performed in axial view. Although the instrument allows measurements in radial view, less sensitivity was obtained in this condition, making it difficult to distinguish between small concentrations of the analytes in solution. Tests performed with radial measurements required a lower sample dilution factor and, consequently, higher concentrations of the standards in the calibration curve to obtain appreciable emission intensities. However, in this condition, the greater number of chemical species introduced into ICP OES instrument caused wear of the torch, accumulating a thin metallic film on the quartz surface, that hinders the constancy of the plasma and consequently affected the long-term stability. Therefore, aiming to keep the analytical performance characteristics stable for a long time of operation and also aiming at a longer torch durability, the axial view measurement mode was chosen.

Different wavelengths were evaluated for quantitative measurements of Nd (378.425; 386.341; 401.225; 406.109; 415.608; 430.358 and 489.693 nm), Pr (390.844; 414.311; 417.939; 422.535 and 495.137 nm), Fe (233.280; 234.349; 238.204; 239.562; 240.488; 259.837; 261.187 and 371.994 nm) and B (181.837; 182.591; 182.641; 208.893; 208.959; 249.678 and 249.773 nm). Aiming at high precision quantifications, the best wavelengths were chosen based on: (i) greater intensity obtained in the central pixels; (ii) lower background observed to the right and left pixels of the emission peak and (iii) lower relative standard deviation of replicate measurements (n = 3). Thus, based on these criteria, the wavelengths selected for the quantification of Nd, Pr, Fe and B were 401.225, 414.311, 259.837 and 249.678 nm, respectively.

The emission spectra of the selected wavelengths are shown for a set of calibration solutions in the Figure 1. The spectra recorded for the dissolved samples exhibited the same peak shape.

To guarantee the absence of spectral interference mono-elemental standards were analysed independently. The results of the emission intensities allowed the calibration with multi-elemental solutions, without any spectral interference.

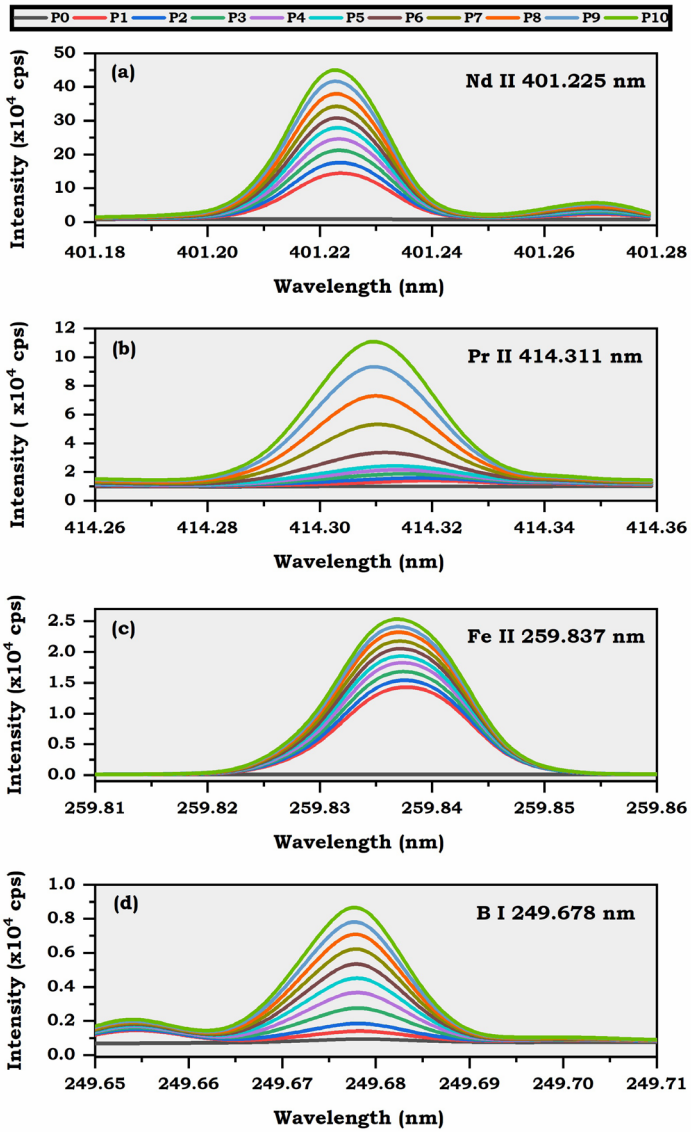

Figure 1. Fragment spectra obtained by ICP OES with standard solutions from blank (P0) to high calibration standard (P10), showing the peak emission for analytes.

According to Figure 1, for the Nd quantification, central pixels corresponding to the range of 401.217 – 401.233 nm were selected and lateral pixels for subtracting the background in the ranges of 401.176 – 401.183 nm (left) and 401.250 – 401.257 nm (right). For Pr quantification, central pixels located between 414.304 – 414.320 nm and lateral pixels at 414.262 – 414.269 nm (left) and 414.347 – 414.355 nm (right) were used. The quantification of Fe involved the pixels at 259.833 – 259.843 nm (central), 259.801 – 259.806 nm (left) and 259.865 – 259.870 nm (right). Boron utilized the following selected pixels: 249.672 –249.682 nm (central) and 249.708 – 249.713 nm (right), without pixels selected on the left, since residual emissions occur on the left side close to the emission peak, due to weak Fe I 249.653 nm emission line.

Calibration and limits

Linear responses between the emission intensity and the analyte concentration were obtained, according to linear regression by the method of least squares. The proper linear fit was confirmed by the high coefficient of determination ($0.9983 \leq R^2 \leq 0.9999$) and also by the random distribution in the residual plots, with less than 4% of bias at each calibration point, as seen in Figure 2. The main parameters, such as calibration sensitivity, coefficient of determination and explored linear range are shown in Table II.

Although new calibration approaches[41-44] are available, the external calibration with standard solutions was chosen in this work due to the high similarity of the aqueous standards with the diluted aqueous samples (whose composition is mostly Nd, Pr, Fe and B dissolved in acidic media). The acid concentration of the standards was matched with the final acid concentration of the sample (after dilution), to eliminate possible matrix differences.

The lower limit of detection (LLOD) was reported in two ways: Instrument detection limit (IDL) and method detection limit (MDL). The IDL refers to the smallest amount of analyte needed to obtain a signal significantly different from the blank in ICP OES, this limit was statistically estimated based on the standard deviation of 10 consecutive measurements from a blank solution (s_B) and considering the calibration sensitivity (m) at 98.3% confidence level[45], such that: $IDL = 3 \times s_B/m$. The IDL values ranged from 0.009 to 0.028 mg L^{-1} and were reported in Table II. Additionally, the MDL considers all dilution steps involved in the analytical sequence, providing the minimum detectable amount of analyte as a function of the sample mass. The BEC values reported in Table II are equivalent to the average value of nine points calculated at different levels of analyte concentration, ranging from 0.011 to 0.044 mg L^{-1}. For all analytes, the concentration required to exhibit the same intensity as the background proved to be below the instrumental quantitation limit (IQL), this rule out possible errors induced by the background in the instrumental measurements within the established limits.

Table II. Instrumental analytical performance characteristics in aqueous solution

Analyte	Calibration sensitivity[a] (cps L mg^{-1})	R^2	Exploited linear range (mg L^{-1})	IDL (mg L^{-1})	IQL (mg L^{-1})	BEC (mg L^{-1})
Nd	$1.4(\pm0.3)x10^{-4}$	0.9999	10.0 – 32.5	0.022	0.073	0.011
Pr	$9.3(\pm0.2)x10^{-3}$	0.9994	0.1 – 10.0	0.009	0.030	0.019
Fe	$4.0(\pm0.2)x10^{-3}$	0.9983	30.0 – 57.0	0.026	0.086	0.010
B	$3.1(\pm0.4)x10^{-3}$	0.9990	0.1 – 1.8	0.028	0.092	0.044

[a]Slope values with standard deviation for 10 calibration curves obtained on different days.

Table III shows MDL values for the three different sample types and these limits were below 0.07 cg g^{-1}, these values fully satisfy the conditions for quantitative chemical analysis of the samples evaluated in this study. Eventually, if necessary, lower MDL values can be achieved by decreasing the dilution factor of the samples employed by this method.

Analogously, the lower limit of quantitation (LLOQ) was reported by the instrumental quantitation limit (IQL), ranging from 0.030 to 0.092 mg L^{-1} and also by the practical quantitation limit (PQL), ranging from 0.03 to 0.25 cg g^{-1}. These limits refer to the lowest analyte concentration that can be measured with reasonable accuracy in aqueous solutions (IQL) and by the proposed method, covering all dilutions steps (PQL). Both, IQL and PQL, were estimated as 10/3 x IDL and MDL, respectively.

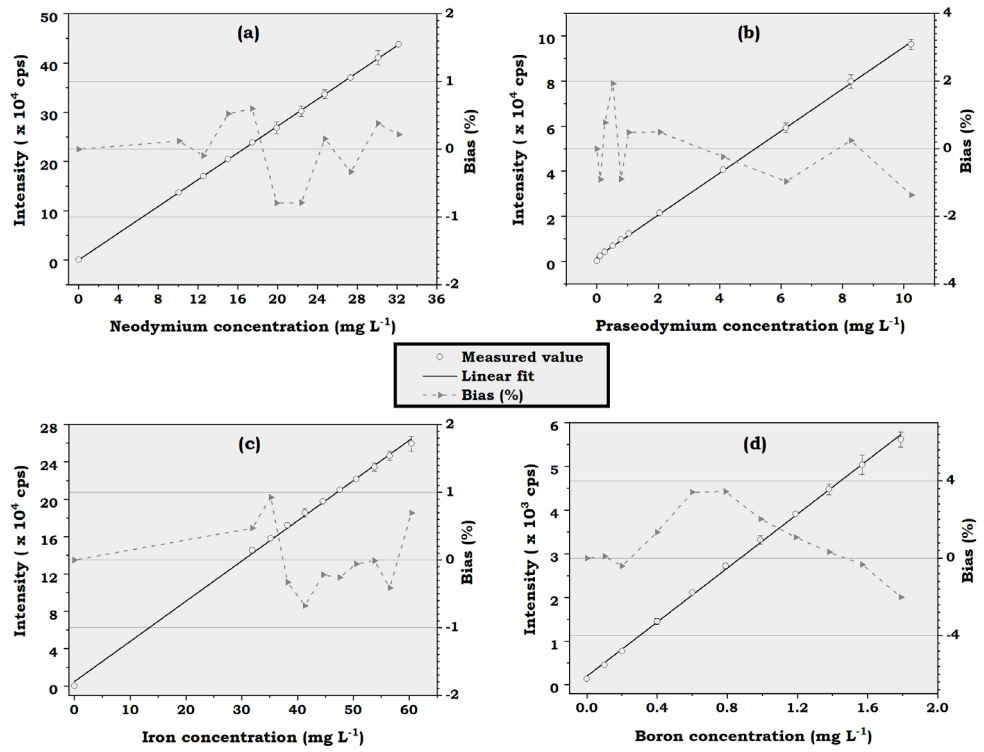

Figure 2. Calibration curves for (a) Neodymium, (b) Praseodymium, (c) Iron and (d) Boron obtained in ultrapure water containing 2% w/v of nitric acid. The graphs show the intensities in the left y-axis and the percentage bias in the right y-axis. Vertical error bars refer to ± 1 standard deviation of triplicate measurements (n = 3).

All analytical signals were measured in the presence of some degree of background, which can be originated from the emission from the plasma and also due to the detector and electronic characteristics. To assess the extent of this effect, the background equivalent concentration (BEC) was estimated for each wavelength used in analytical measurements by the following equation: $BEC = (C_{std} \times I_B)/(I_{std} - I_B)$, where C_{std} is the concentration of a standard solution, I_{std} is the emission intensity measured for the same standard solution and I_B is the intensity of the blank solution. The BEC values ranging from 0.011 to 0.044 mg L^{-1}, reported in Table III are equivalent to the average value of nine points calculated at different levels of analyte concentration. For all analytes, the concentration required to exhibit the same intensity as the background proved to be below the instrumental quantitation limit (IQL), this rule out possible errors induced by the background in the instrumental measurements within the established limits.

Table III. Figures of merit for different sample types

Sample type	Analyte	MDL (cg g^{-1})	PQL (cg g^{-1})	Mass fraction covered by calibration (cg g^{-1})
Didymium oxide	Nd	0.07	0.25	33.00 – 100.00
	Pr	0.03	0.09	0.33 – 33.00
Metallic Didymium	Nd	0.07	0.25	31.25 – 100.00
	Pr	0.03	0.09	0.31 – 31.25
(Nd,Pr)-Fe-B alloy	Nd	0.03	0.09	15.00 – 48.75
	Pr	0.01	0.03	0.15 – 15.00
	Fe	0.05	0.17	45.00 – 85.50
	B	0.04	0.13	0.15 – 2.70

Precision

The precision of the results provided by the proposed analytical method was evaluated and improved in order to obtain results with the least uncertainty possible. The samples related to the production chain of super-magnets requires precise quantifications, especially for the REE. Uncertainties greater than 1 cg g^{-1} in the mass fraction of the neodymium or the praseodymium can strongly impact the performance of permanent magnets.

Despite the instrumental precision of ICP OES (estimated by successive measurements of a standard solution performed in the same condition and on the same day) show a low relative standard deviation (RSD) ranging from 0.3 to 0.7% (as seen in Table IV), the precision of the method was initially out of the desirable, providing mass fraction results with more than 1 cg g^{-1} of uncertainty for the neodymium and praseodymium elements. Although this uncertainty is suitable for most analytical applications, it implies difficulties in the strict quality control of the super-magnets. In order to reduce this uncertainty, the sample dilution steps applied during the execution of the method were controlled by weighing.

Traditionally, the adjusting the volume in the solutions is a routine practice in chemistry laboratories, being performed visually by the analyst, who has the task of controlling the amount added until the liquid reaches the meniscus mark in precision glassware. In this practice, the volume adjustment is subject to intrinsic deviations, often insignificant for chemical analysis. However, the propagation of this uncertainty inevitably occurs in the method. To minimize the uncertainties arising from the dissolution and dilution of the samples, the solutions were weighed on an analytical balance and the recorded masses were used to calculate the dilution factor. Although the sample treatment procedure becomes slower, due to the additional step of registering all the masses added for each tube, the results were more precise.

The lower uncertainties in analytes mass fraction results were reached due to the fact that the analytical balance is one of the most precise and accurate instruments in a chemical laboratory, reaching legibility up to four decimal places. Next, the control of the dilution by weighing was applied for all samples and also for the calibration solutions.

After minimizing the uncertainty associated with the sample preparation by weighing strategy, the method intermediate precision[46,47] was assessed by the relative standard deviation (RSD) from the ten measurements of the emission intensity obtained with a specific standard solution, prepared and analysed on different days by different operators in different locations within the laboratory, using different calibration curves and the same instrument (ICP OES). The standard solution containing 42.0 mg L^{-1} of Nd, 1.0 mg L^{-1} of Pr, 42.0 mg L^{-1} of Fe and 0.8 mg L^{-1} of B was strategically selected to faithfully evaluate the method intermediate precision, since these concentrations are located in the middle of the linear ranges used for calibration curves of the proposed method. It is well known that precision is intrinsically associated with the level of analyte concentration,[48] with a systematic increase in the relative standard deviation occurring as the analyte concentration decreases.[49,50] For this reason, the evaluation of the method precision in its extreme conditions of the linear range may not reliably represent the expected precision for most samples, which ideally are located in the middle of the linear range, especially when the method is well delineated. The method intermediate precision values are shown in Table IV and range from 1.4 to 3.1%, showing acceptable RSD values, that indicate a relative ease of the method reproduction.

In addition to the method intermediate precision, the typical uncertainty obtained for each analyte in mass fraction results (cg g^{-1}) was estimated based on the average of the uncertainties obtained for a representative set of samples (n = 80), since it is an average value, eventually some samples may deviate from the typical uncertainty reported in Table IV.

So, the minimum and maximum values of uncertainty obtained with the proposed method for that same set of samples are also shown in Table IV. It is worth mentioning that the uncertainty values in mass fractions were expressed by the standard deviation obtained in triplicate (n = 3) and do not consider a confidence interval. Table IV summarizes the main parameters related to precision.

Table IV. Precision assessment to characterize the analytical method and typical values of uncertainty obtained when applying the proposed method in real samples

Analyte	Instrumental Precision[a]	Method intermediate precision[b]	Mass fraction typical uncertainty[c] (cg g^{-1})	Mass fraction range uncertainty[d] (cg g^{-1})
Nd	0.3%	2.0%	0.20	0.03 – 0.65
Pr	0.7%	3.1%	0.07	0.01 – 0.39
Fe	0.6%	1.4%	0.69	0.02 – 2.54
B	0.6%	1.9%	0.04	0.01 – 0.20

[a] Relative Standard Deviation (RSD) for 10 consecutive measurements of standard solution in the same day.
[b] RSD for 10 measurements of standard solution in different days, by different analysts.
[c] Average of mass fraction uncertainty for 80 samples. Typical uncertainty obtained for samples containing 16-80 cg g^{-1} of Nd, 1-26 cg g^{-1} of Pr, 63-70 cg g^{-1} of Fe and 0-2 cg g^{-1} of B.
[d] Minimum and maximum value of mass fraction uncertainty obtained in final results for 80 samples.

Accuracy

Due to the absence of super-magnet reference materials, the accuracy of the method was evaluated in two different ways: (i) by spike analyte and recovery test on the three different sample types and (ii) by the comparison of the mass fraction results obtained by proposed method with other laboratories results, that applied independent analytical methods to determination a same set of (Nd,Pr)-Fe-B alloy samples. The Table V shows the spiked value and recovery percentage of the analytes at six different concentration levels. As the spike was performed on the diluted sample, the sum of the analyte concentrations may eventually be greater than 100 cg g^{-1}. Spikes equal to or greater than 0.50 cg g^{-1} exhibited acceptable recovery values, ranging from 96 to 104% for all elements. This recovery values attests to the accuracy of the method when applied to these matrices. In smaller spikes concentrations (<0.50 cg g^{-1}), recovery values ranged from 90 to 140%, which indicates a difficulty of the method in distinguishing concentrations below 0.50 cg g^{-1}, especially for Nd, Pr and Fe. It should be noted that the quantification of boron was an exception, being able to distinguish contents on the order of 0.05 cg g^{-1}. Although some recovery values at 0.05 and 0.10 cg g^{-1} for Nd, Pr and Fe were suitable for chemical analysis, it is observed that the uncertainty obtained is equal to or greater than the spiked concentration value, making it impossible to distinguish between those levels. Better recoveries values (96 - 104%) were obtained when considering only spikes from 0.50 cg g^{-1}.

For comparison purposes, three samples of (Nd,Pr)-Fe-B alloy (labelled A, B and C) with distinct neodymium and praseodymium content, were selected, fractionated and sent to two different chemistry laboratories, located in different countries, which applied independent analytical methods to determine the main chemical elements. The mass fraction values reported by the invited laboratories were compared with the values obtained from the proposed method by a hypothesis test (student t-test) at 95% of confidence level. Table VI shows the statistical comparison that for most determinations there was no statistically significant difference, this indicates a good agreement between the results from the proposed method and those from the invited laboratories. Small differences exist only for the guest laboratory identified by the number two (2) that reported the boron element with values statistically different from the others for samples A and C, whose calculated t-values (3.56 and 3.55, respectively) were higher than the critical t-value (2.78) at 95% confidence level. This small statistical difference reveals a peculiar characteristic for boron, whose quantification requires some additional care in relation to the other analytes.

In our laboratory, during method development, we noticed oscillations in the blank intensities for boron. A fact that eventually impaired the good linear adjustment of the calibration curves and could influence inexact quantification for this element. The intensity oscillation was investigated and was shown to be linked to: (i) the purging time with argon required for measurements in the UV range in our ICP OES

equipment and (ii) the sample introduction system, including the nebulizer, nebulization chamber and the connection to the base of the torch, which are materials made of borosilicate glass that can eventually release the boron element and introduce it into the plasma, causing oscillations in the measurement steps (especially if the sample contains fluoride in an acid medium). Both situations were solved by adopting two simple procedures, which are strongly recommended if this method is implemented in the routine of other laboratories: (i) a minimum of four hours purging optics with argon gas prior to ICP OES measurements and (ii) washing the sample introduction system with nitric acid solution (10% v/v) followed by abundant rinsing with deionized water before instrumental analysis. Despite this small difference for boron, the other results are in full agreement and demonstrate a high level of accuracy achieved with the proposed method.

Table V. Analyte spike and recovery test in the three different sample types at six concentration levels

Sample type	Spiked (cg g^{-1})	Neodymium		Praseodymium		Iron		Boron	
		Found (cg g^{-1})	Rec (%)	Found (cg g^{-1})	Rec (%)	Found (cg g^{-1})	Rec (%)	Found (cg g^{-1})	Rec (%)
Didymium oxide	0.00	61.03 ± 0.23	***	25.04 ± 0.21	***	< MDL	***	< MDL	***
	0.05	61.08 ± 0.22	100	25.10 ± 0.18	120	< MDL	***	0.05 ± 0.03[a]	100
	0.10	61.13 ± 0.25	100	25.14 ± 0.15	100	0.09 ± 0.04[a]	90	0.10 ± 0.02	100
	0.50	61.52 ± 0.19	98	25.55 ± 0.12	102	0.49 ± 0.09	98	0.52 ± 0.04	104
	1.00	62.01 ± 0.31	98	26.08 ± 0.16	104	1.00 ± 0.15	100	0.99 ± 0.03	99
	1.50	62.55 ± 0.23	101	26.56 ± 0.22	101	1.49 ± 0.30	99	1.47 ± 0.12	98
	2.00	62.99 ± 0.26	98	27.05 ± 0.20	101	1.96 ± 0.48	98	2.02 ± 0.05	101
Metallic didymium	0.00	78.22 ± 0.33	***	22.41 ± 0.12	***	< MDL	***	< MDL	***
	0.05	78.28 ± 0.32	120	22.47 ± 0.11	120	< MDL	***	0.05 ± 0.02[a]	100
	0.10	78.33 ± 0.35	110	22.53 ± 0.11	120	0.09 ± 0.05[a]	90	0.10 ± 0.01	100
	0.50	78.74 ± 0.28	104	22.91 ± 0.16	100	0.48 ± 0.09	96	0.51 ± 0.03	102
	1.00	79.23 ± 0.22	101	23.44 ± 0.08	103	0.98 ± 0.12	98	1.01 ± 0.02	101
	1.50	79.75 ± 0.37	102	23.91 ± 0.22	100	1.53 ± 0.47	102	1.53 ± 0.07	102
	2.00	80.21 ± 0.34	99	24.43 ± 0.13	101	1.94 ± 0.57	97	1.98 ± 0.04	99
(Nd,Pr)-Fe-B alloy[b]	0.00	24.29 ± 0.07	***	6.59 ± 0.13	***	69.62 ± 0.83	***	1.07 ± 0.02	***
	0.05	24.34 ± 0.12	100	6.65 ± 0.03	120	69.69 ± 0.85	140	1.12 ± 0.01	100
	0.10	24.40 ± 0.10	110	6.70 ± 0.13	110	69.74 ± 0.94	120	1.17 ± 0.01	100
	0.50	24.78 ± 0.15	98	7.07 ± 0.14	96	70.14 ± 1.32	104	1.55 ± 0.09	96
	1.00	25.31 ± 0.13	102	7.62 ± 0.17	103	70.63 ± 0.97	101	2.06 ± 0.03	99
	1.50	25.77 ± 0.20	99	8.12 ± 0.16	102	71.16 ± 0.66	103	2.55 ± 0.02	99
	2.00	26.33 ± 0.16	102	8.63 ± 0.19	102	71.59 ± 1.05	98	3.11 ± 0.05	102

[a]Mass fraction value between MDL and PQL (MDL<x<PQL).
[b]Sample analysed by different laboratories, shown in Table VI as “Sample C”.

Table VI. Comparison of (Nd,Pr)-Fe-B alloy sample determinations and the conclusion of the student t-test at 95% confidence level

Sample	Element	Mass fraction (cg g^{-1})			Comparison					
		Guest Laboratory 1[a]	Guest Laboratory 2[b]	Proposed Method[c]	Student t-test		Statistically different[d] (t critical = 2.78)		Agreement[f] (%)	
					$t_{LAB\ 1}$	$t_{LAB\ 2}$	LAB 1	LAB 2	LAB 1	LAB 2
A	Nd	17.6 ± 0.9	17.2 ± 0.8	17.3 ± 0.3	0.55	0.20	Not	Not	102	99
	Pr	13.7 ± 0.7	14.0 ± 0.7	14.2 ± 0.4	1.07	0.43	Not	Not	96	99
	Fe	66.9 ± 3.3	not rated	67.0 ± 1.0	0.05	***	Not	***	100	***
	B	1.20 ± 0.06	1.04 ± 0.05	1.16 ± 0.03	1.03	3.56	Not	Yes	103	90
B	Nd	30.4 ± 1.5	30.4 ± 1.6	29.3 ± 0.3	1.25	1.17	Not	Not	104	104
	Pr	< 0.4[e]	0.08 ± 0.01	0.07 ± 0.02	1.43	0.77	Not	Not	***	114
	Fe	68.0 ± 3.4	not rated	68.4 ± 1.7	0.18	***	Not	***	99	***
	B	1.10 ± 0.06	1.03 ± 0.05	1.03 ± 0.02	1.92	0.00	Not	Not	107	100
C	Nd	24.5 ± 1.2	24.5 ± 1.2	24.3 ± 1.3	0.20	0.20	Not	Not	101	101
	Pr	6.4 ± 0.3	6.3 ± 0.3	6.6 ± 0.4	0.69	1.04	Not	Not	97	95
	Fe	67.5 ± 3.3	not rated	69.6 ± 5.1	0.60	***	Not	***	97	***
	B	1.10 ± 0.06	0.91 ± 0.05	1.07 ± 0.06	0.61	3.55	Not	Yes	103	85

[a]Reported values based on ICP OES measurements.
[b]Reported values based on ICP-MS measurements, employing quadrupole as mass analyser.
[c]Mass fraction values reported by proposed method include the confidence interval with 5% of significance level.
[d]Hypothesis test: If t calculated > t critical, values are statistically different.
[e]Reported values < x, were considered x ± x for the student t-test calculation, ranging from non-existent in the sample (zero concentration) up to double the reported minimum detectable concentration limit.
[f]Agreement calculated by (Guest laboratory result / Proposed method result) × 100

Foreign elements

Foreign chemical elements can be added to metal alloys to improve some specific characteristics for the application of permanent magnets,[51] for example: Dysprosium (Dy) is usually added to the alloy composition aiming to increases the intrinsic coercivity at higher temperatures.[33] Other chemical elements can be added to the super-magnets such as: Nb,[51] Ce,[52,53] Tb,[54] Ga,[55,56] Co,[57] Cu,[53,58] La,[52] Al,[58] among others. Usually, such elements have a low concentration, not exceeding 5 cg g^{-1}. As they have a different chemical nature from the analytes, it is possible that the foreign elements may interfere with the proposed analytical method. To assess the applicability of the proposed analytical method in the presence of foreign elements, mono-elemental standard solutions of 35 distinct chemical elements were analysed by ICP OES and the respective impacts on the analytical signals for the quantification of Nd, Pr, Fe and B were evaluated. The relative calibration sensitivity achieved for each foreign element at the monitored analytical lines (401.225, 414.311, 259.837 and 249.678 nm) is shown in Figure 3. The interference bias percentage values expressed in this figure correspond to the ratio between calibration sensitivity of foreign element and the calibration sensitivity of the analyte. As an example, a value of +10% interference bias caused by a foreign element in a given analyte makes each 1 cg g^{-1} of the foreign element in the sample induces an error of about +0.1 cg g^{-1} in the analyte quantification.

According to the results of Figure 3, the main interfering chemical elements in the neodymium quantification were: Cerium (+30.4%), europium (-6.4%), titanium (+2.9%), lutetium (+1.0 %) and samarium (-0.9%). In these specific cases of interference, alternative wavelengths can be used to quantify neodymium correctly, such as: 415.608 nm (good alternative to eliminate spectral interferences from Eu, Sm and Lu) or 406.109 nm (more suitable wavelength in the presence of cerium and titanium).

The determination of praseodymium was affected when present in the sample: Dysprosium (+13.5%), molybdenum (-6.3%), terbium (-2.5%) and niobium (+1.3%), with alternatives for a reliable measurement of praseodymium at 422.293 nm (aiming to eliminate the interferences from Dy and Mo) or at 422.535 nm (excellent to avoid spectral interference from Tb and Nb).

The iron characteristic wavelength (259.837 nm) can suffer interference from tantalum (+1.8%) and gold (+1.3%), a possible line free from these interferences corresponds to 238.204 nm. However, it is worth mentioning that in metallic alloys the impact of interference in the quantification of iron will be minimal, since iron is normally a component present in high concentrations in metallic alloys, being considered the “diluent” of the alloys, reaching concentrations of up to 70 cg g^{-1}, and in this concentration level the error induced by the spectral interference will not be significant.

In the interference evaluation, the quantification of boron was affected only by hafnium (-1.4%). In this case, a plausible alternative consists in measure boron at 182.641 nm. The other elements (Al, Ca, Co, Cr, Cu, Er, Ga, Gd, Ho, K, La, Li, Mg, Mn, Nb, Pb, Sc, Si, Sn, Tm, V, Yb, Zn and Zr) did not exhibit significant interference and therefore do not affect the applicability of this proposed analytical method.

Any spectral interferences that result in a negative bias are explained by optical emissions in regions close to those selected for the background calculation. Similarly, the interferences that result in a positive bias come from optical emissions that occur close to the central pixel.

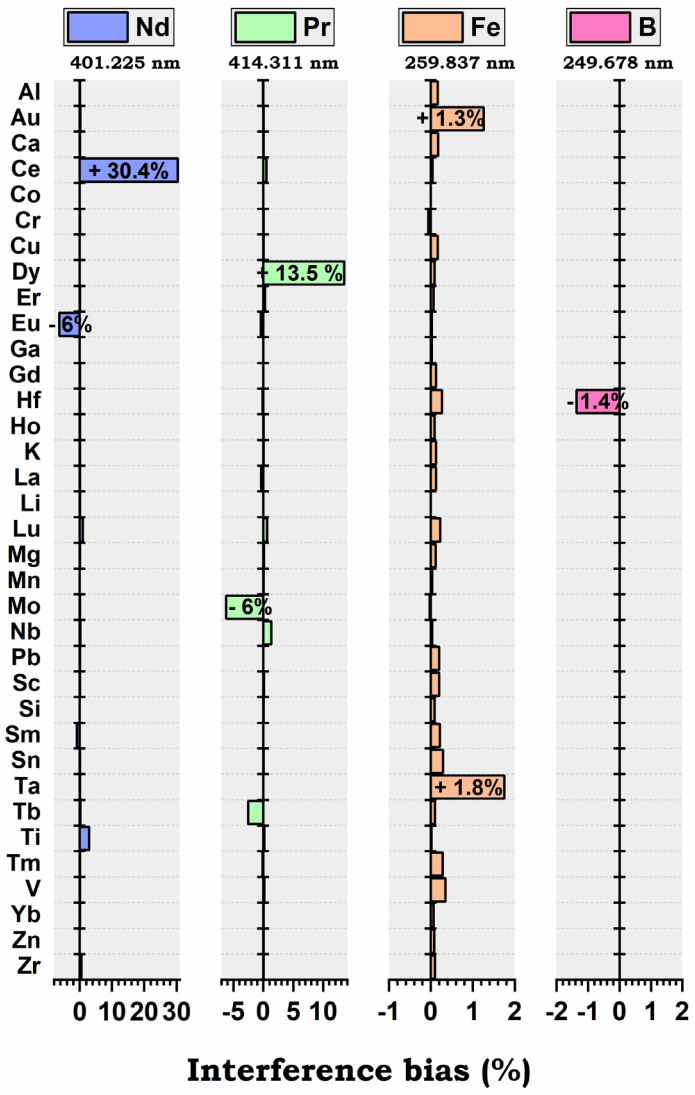

Figure 3. Interference chart showing the impact of foreign chemical elements in the calibration sensitivity of Nd, Pr, Fe and B in the proposed analytical method. The interference bias percentage value was calculated by the calibration sensitivity of the foreign element (estimated from two concentrations: 1 and 10 mg L^{-1}) divided by calibration sensitivity of the analyte.

Comparative analytical methods, advantages and drawbacks

Determinations of Nd, Pr, Fe and B in the samples related to the production chain of the permanent magnets have been explored by places that contain natural reserves of rare earth elements and that consequently dominate the production technology of super-magnets. The main publications related to this topic are concentrated in China, a country that exploits rare earth elements. Although many studies use chemical analysis to characterize samples related to the production process of super-magnets, few articles detail the methods and its figures of merit, parameters that are essential to compare and select an appropriate analytical method. Therefore, the scarcity of studies dedicated to the rigorous chemical analysis of these materials in the scientific literature hinders the comparison with other analytical methods. In this section, the proposed method was compared with another analytical methods that have at least one similar matrix or similar analytes that demonstrate a rigorous development. A summary comparison of the methods is shown in Table VII.

Two different studies stand out for minimizing sample preparation, proposing a direct analysis of magnets in hard disk devices (HD) by WD-XRF[59] and LIBS.[60] Although such methods have indisputable advantages when compared to the proposed method in this paper (that requires sample dissolution), the quantification of Nd by WD-XRF shown interference from Pr.[59] Such interference was not a problem in the

samples evaluated in the mentioned study, since the concentrations of Pr were lower than the 5 cg g^{-1},[59] but this is a different reality from that found in the samples related to the production process of didymium magnets, whose levels of Pr reached up to 25 cg g^{-1}. Therefore, the interference is a problem of that could lead to inadequate results when applied to didymium samples. In addition, both mentioned studies needed to know reference values of the analytes in samples for a suitable calibration, requiring to quantify the elements from the dissolved samples by ICP OES.[59,60]

The elemental analysis in HD magnets by ICP OES was proposed by Castro *et al*.[61] This important work reports, for the first time, a detailed method of chemical analysis of magnets by wet dissolution, with other conditions. When compared, the current work stands out: (i) for the application in different types of samples, (ii) for the rigorous studies of precision and accuracy and (iii) for the study of interference that allows a wide scope of application of this method. Differentials that highlight this work as an important reference in the scientific literature, establishing a standard method for the chemical analysis of magnets composed of neodymium and praseodymium.

Proposed by Papai *et al*. [3] the determination of Nd and Pr was successfully performed in samples of metallic didymium and (Nd, Pr)-Fe-B alloy, standing out for employing low resolution atomic emission spectrometry with a flame composed of acetylene/nitrous oxide and a mathematical approach to solve the spectral interferences. Although this method uses a more accessible spectrometer and less expensive cost of analysis when compared to the proposed method in this paper, it has a greater susceptibility to spectral interference from other elements, requiring mono-elemental calibrations and a suitable mathematical approach before providing the results. Furthermore, only the quantification of the elements Nd and Pr is performed, in contrast to the simultaneous quantification of four elements (Nd, Pr, Fe, B) in the proposed method.

Thus, the main advantages of the proposed method are: (i) simultaneous determination of Nd, Pr, Fe and B; (ii) versatility for application in different sample types related to the production process of super-magnets; (iii) high reliability of the results; (iv) low susceptibility to spectral interferences with alternatives to avoid them completely and (v) low uncertainties provided by triplicate (n = 3).

The main drawbacks to this method are: (i) the need to dissolve samples in an acid medium, whereas a faster quantification could be obtained by direct analysis of solids techniques; (ii) cost of analysis, since the consumption of argon has a significant impact on the laboratory's budget and (iii) the need to weigh all dilution steps, which requires more time from the analyst. Despite these drawbacks, the method clearly meets the needs for strict chemical quality control.

Table VII. Comparison of the current method with others reported in the scientific literature

Analytes	Sample type	Instrumental technique	Sample treatment	Advantages	Drawbacks	Ref.
Nd and Pr	(Nd,Pr)-Fe-B alloy Metallic Didymium	F AES[a]	Acidic dissolution (HNO_3 and HCl)	*Accessible spectrometer; *Low-cost; *Fast analysis	*Susceptibility to spectral interference; *Need unusual math approach to quantify	(3)
Nd	Hard Disk magnets	WD-XRF[b]	None or minimal	*Direct solid analysis; *Non-destructive; *Fast analysis;	*Subject to Pr interference;	(59)
Nd, Pr, Fe, B and others	Hard Disk magnets	LIBS[c]	None or minimal	*Direct solid analysis; *Fast acquisition of complete spectra;	*Calibration (need for samples with known reference values)	(60)
Nd, Pr, Fe, B and others	Hard Disk magnets	ICP OES	Acidic dissolution (HNO_3 and HCl)	*Simultaneous determination	*Need sample dissolution; *Cost of analysis;	(61)
Nd, Pr, Fe and B	(Nd,Pr)-Fe-B alloy Metallic Didymium Didymium oxide	ICP OES	Acidic dissolution (HNO_3 and HCl)	*Simultaneous determination; *High reliability; *Strict and high precision results guaranteed *Low susceptibility to spectral interferences; *Foreign elements evaluation;	*Need sample dissolution; *Cost of analysis;	This work

[a]Flame Atomic Emission Spectrometry
[b]Wavelength dispersive X-ray Fluorescence
[c]Laser-Induced Breakdown Spectrometry

CONCLUSIONS AND OUTLOOKS

The proposed method provided high precision results, with good accuracy and fulfilled the purpose of the strict quality control of the permanent magnets materials, solving the pressing need to distinguish neodymium and praseodymium concentrations in less than 1 cg g^{-1}.

The control of the dilution steps by weighing proved to be essential to achieve the low values of uncertainty reported in Table IV. Despite the weighing procedure adding an additional step in the proposed analytical method, that requires the most time from the analyst, this characteristic should not be considered a resistance to routine implementation, since there is a significant gain in improving precision and consequently reliability. This gain in reliability is associated with an improvement in the quality and performance of the final products since the chemical control throughout the production process impacts and guides the production routes to obtain materials within the required specifications.

The method was shown to be versatile, being easily applicable to at least three different sample types (didymium oxide, metallic didymium and (Nd,Pr)-Fe-B alloys).

The analytical method proved to be robust with few potentially interfering foreign elements. In the few verified cases of possible interference, alternative wavelengths have been suggested that eliminate spectral interferences.

As a perspective, this reported method paves the way for the production of standard materials to be applied in other instrumental techniques aimed at direct analysis of solids.

Conflicts of interest

The authors declare that they have no known competing financial interests or personal relationships that could have appeared to influence the work reported in this paper.

Acknowledgements

Funding sources: (i) “Conselho Nacional de Desenvolvimento Científico e Tecnológico” (CNPq) [465719/2014-7]; (ii) “Coordenação de Aperfeiçoamento de Pessoal de Nível Superior” (CAPES) [23038000776/2017-54]; (iii) “Fundação de Amparo à Pesquisa do Estado de São Paulo” (FAPESP) [2014/50887-4] and (iv) “Banco Nacional do Desenvolvimento” (BNDES FUNTEC).

Fellowships granted to: Rodrigo Papai (CNPq) [380490/2018-8] and [380939/2020-7], and Thiago Pires Nagasima (CNPq) [381315/2017-7].

The authors are also grateful to Bruno Menezes Siqueira (Product Manager and Application Scientist, M.Sc) for initial training in ICP OES instrument, Valeska Meirelles (Field Service Engineer and Application Scientist, Ph.D) for quick assistance, Tiago Finatte (Field Service Engineer) for technical support and Nova Analítica company for kindly granting an ICP OES instrument (iCap 7400) for use in our laboratory.

REFERENCES

(1) Dent, P. C. Rare earth elements and permanent magnets. *J. Appl. Phys*. **2012**, *111* (7), 07A721. https://doi.org/10.1063/1.3676616

(2) Nicola, J. Materials science: The pull of stronger magnets. *Nature* **2011**, *472* (7341), 22-23. https://doi.org/10.1038/472022a

(3) Papai, R.; de Freitas, M. A. S.; da Fonseca, K. T.; de Almeida, G. A.; da Silveira, J. R. F.; da Silva, A. L. N.; Ferreira Neto, J. B.; dos Santos, C. A. L.; Landgraf, F. J. G.; Luz, M. S. Additivity of optical emissions applied to neodymium and praseodymium quantification in metallic didymium and (Nd,Pr)-Fe-B alloy samples by low-resolution atomic emission spectrometry: An evaluation of the mathematical approach used to solve spectral interferences. *Anal. Chim. Acta* **2019**, *1085*, 21-28. https://doi.org/10.1016/j.aca.2019.07.049

(4) Li, J.; Huang, X.; Zeng, L.; Ouyang, B.; Yu, X.; Yang, M.; Yang, B.; Rawat, R. S.; Zhong, Z. Tuning magnetic properties, thermal stability and microstructure of NdFeB magnets with diffusing Pr-Zn films. *J. Mater. Sci. Technol*. **2020**, *41*, 81-87. https://doi.org/10.1016/j.jmst.2019.09.024

(5) Rehman, S. U.; Jiang, Q.; He, L.; Xiong, H.; Liu, K.; Wang, L.; Yang, M.; Zhong. Z. Microstructure and magnetic properties of NdFeB alloys by co-doping alnico elements. *Phys. Lett. A* **2019**, *383* (31), 125878. https://doi.org/10.1016/j.physleta.2019.125878

(6) Jiang, Q.; He, L.; Rehman, S. U.; Hu, Y.; Song, J.; Ouyang, H.; Yang, M.; Zhong. Z. Optimized composition and improved magnetic properties of Ce-Fe-B alloys. *J. Alloys Compd*. **2019**, *811*, 151998. https://doi.org/10.1016/j.jallcom.2019.151998

(7) Xu, X. D.; Dong, Z. J.; Sasaki, T. T.; Tang, X.; Sepehri-Amin, H.; Ohkubo, T.; Hono, K. Influence of Ti addition on microstructure and magnetic properties of a heavy-rare-earth-free Nd-Fe-B sintered magnet. *J. Alloys Compd*. **2019**, *806*, 1267-1275. https://doi.org/10.1016/j.jallcom.2019.07.289

(8) Mackie, A. J.; Dean, J. S.; Goodall, R. Material and magnetic properties of $Sm_2(Co, Fe, Cu, Zr)_{17}$ permanent magnets processed by Spark Plasma Sintering. *J. Alloys Compd*. **2019**, *770*, 765-770. https://doi.org/10.1016/j.jallcom.2018.08.186

(9) Jiang, Q.; Zhong, Z. Research and development of Ce-containing $Nd_2Fe_{14}B$-type alloys and permanent magnetic materials. *J. Mater. Sci. Technol*. **2017**, *33* (10), 1087-1096. https://doi.org/10.1016/j.jmst.2017.06.019

(10) Zeng, H. X.; Liu, Z. W.; Zhang, J. S.; Liao, X. F.; Yu, H. Y. Towards the diffusion source cost reduction for NdFeB grain boundary diffusion process. *J. Mater. Sci. Technol*. **2020**, *36*, 50-54. https://doi.org/10.1016/j.jmst.2019.08.009

(11) Engerroff, J. A. B.; Baldissera, A. B.; Magalhães, M. D.; Lamarão, P. H.; Wendhausen, P. A. P.; Ahrens, C. H.; Mascheroni, J. M. Additive manufacturing of Sm-Fe-N magnets. *J. Rare Earths* **2019**, *37* (10), 1078-1082. https://doi.org/10.1016/j.jre.2019.04.012

(12) Thornton, B. F.; Burdette, S. C. The neodymium neologism. *Nat. Chem*. **2017**, *9*, 194. https://doi.org/10.1038/nchem.2722

(13) Dingle, A. Praseodymium unpaired. *Nat. Chem*. **2018**, *10* (5), 576-576. https://doi.org/10.1038/s41557-018-0050-7

(14) Fim, R. G. T.; Mascheroni, A. A.; Antunes, L. F.; Engerroff, J. B. E.; Ahrens, C. H.; Wendhausen, P. A. P. Increasing packing density of Additively Manufactured Nd-Fe-B bonded magnets. *Addit. Manuf*. **2020**, *35*,101353. https://doi.org/10.1016/j.addma.2020.101353

(15) Liu, Y.; Xia, W.; Liu, J. P.; Du, J.; Yan, A.; Guan, D.; Liu, Y.; Zhang, J. Coercivity enhancement and mechanism in a high Ce-containing Nd–Ce–Fe–B film by the design of a diffusion layer. *J. Mater. Chem. C* **2019**, *7* (24), 7318-7326. https://doi.org/10.1039/C9TC01279F

(16) Rollat, A.; Guyonnet, D.; Planchon, M.; Tuduri, J. Prospective analysis of the flows of certain rare earths in Europe at the 2020 horizon. *Waste Management* **2016**, *49*, 427-436. https://doi.org/10.1016/j.wasman.2016.01.011

(17) München, D. D.; Veit, H. M. Neodymium as the main feature of permanent magnets from hard disk drives (HDDs). *Waste Management* **2017**, *61*, 372-376. https://doi.org/10.1016/j.wasman.2017.01.032

(18) Pathak, A. K.; Gschneidner, K. A.; Khan, M.; McCallum, R. W.; Pecharsky, V. K. High performance Nd-Fe-B permanent magnets without critical elements. *J. Alloys Compd*. **2016**, *668*, 80-86, https://doi.org/10.1016/j.jallcom.2016.01.194

(19) Yang, F.; Zhang, X.; Guo, Z.; Ye, S.; Sui, Y.; Volinsky, A. A. 3D printing of NdFeB bonded magnets with $SrFe_{12}O_{19}$ addition. *J. Alloys Compd*. **2019**, *779*, 900-907. https://doi.org/10.1016/j.jallcom.2018.11.335

(20) Yuping, L.; Mengling, W.; Jiayu, L. Sintered Nd-Fe-B magnet with core–shell structures fabricated through the intergranular addition of ultra-fine as-disproportionated (Nd,Dy)–Fe–B–Cu powder. *J. Mater. Sci.: Mater. Electron*. **2020**, *31* (9), 7211-7218. https://doi.org/10.1007/s10854-020-03293-y

(21) Ma, B.; Bao, X.; Sun, A.; Li, J.; Cao, S.; Gao, X.-x. Normal and Abnormal Grain Growth in Hydrogenation-Disproportionation-Desorption-Recombination Processed Nd–Fe–B Strip-Cast Alloys. *Cryst. Growth Des*. **2020**, *20* (5), 3119-3130. https://doi.org/10.1021/acs.cgd.0c00006

(22) Ikram, A.; Mehmood, F.; Sheridan, R. S.; Awais, M.; Walton, A.; Eldosouky, A.; Sturm, S.; Kobe, S.; Rozman, K. Z. Particle size dependent sinterability and magnetic properties of recycled HDDR Nd–Fe–B powders consolidated with spark plasma sintering. *J. Rare Earths* **2020**, *38* (1), 90-99. https://doi.org/10.1016/j.jre.2019.02.010

(23) Fim, R. G. T.; Silva, M. R. M.; Silva, S. C.; Casini, J. C. S.; Wendhausen, P. A. P.; Takiishi, H. Influence of Milling Time on Magnetic Properties and Microstructure of Sintered Nd-Fe-B Based Permanent Magnets. *Mater. Sci. Forum* **2018**, *930* 445-448. https://doi.org/10.4028/www.scientific.net/MSF.930.445

(24) Kianvash, A.; Harris, I. R. The influence of free iron on the hydrogen decrepitation capability of some Nd(Pr)–Fe–B alloys. *J. Alloys Compd*. **1998**, *279* (2), 245-251. https://doi.org/10.1016/S0925-8388(98)00652-5

(25) Machado, R. C.; Andrade, D. F.; Babos, D. V.; Castro, J. P.; Costa, V. C.; Sperança, M. A.; Garcia, J. A.; Gamela, R. R.; Pereira-Filho, E. R. Solid sampling: advantages and challenges for chemical element determination—a critical review. *J. Anal. At. Spectrom*. **2020**, *35*, 54-77. https://doi.org/10.1039/C9JA00306A

(26) Costa, V. C.; Castro, J. P.; Andrade, D. F.; Babos, D. V.; Garcia, J. A.; Sperança, M. A.; Catelani, T. A.; Pereira-Filho, E. R. Laser-induced breakdown spectroscopy (LIBS) applications in the chemical analysis of waste electrical and electronic equipment (WEEE). *TrAC, Trends Anal. Chem*. **2018**, *108*, 65-73. https://doi.org/10.1016/j.trac.2018.08.003

(27) Papai, R.; Mariano, C. S.; Pereira, C. V.; da Costa, P. V. F.; Leme, F. O.; Nomura, C. S.; Gaubeur, I. Matte photographic paper as a low-cost material for metal ion retention and elemental measurements with laser-induced breakdown spectroscopy. *Talanta* **2019**, *205*, 120167. https://doi.org/10.1016/j.talanta.2019.120167

(28) Noll, R.; Fricke-Begemann, C.; Connemann, S.; Meinhardt, C.; Sturm, V. LIBS analyses for industrial applications – an overview of developments from 2014 to 2018. *J. Anal. At. Spectrom*. **2018**, *33* (6), 945-956. https://doi.org/10.1039/C8JA00076J

(29) Papai, R.; Sato, R. H.; Nunes, L. C.; Krug, F. J.; Gaubeur, I. Melted Paraffin Wax as an Innovative Liquid and Solid Extractant for Elemental Analysis by Laser-Induced Breakdown Spectroscopy. *Anal. Chem*. **2017**, *89* (5), 2807-2815. https://doi.org/10.1021/acs.analchem.6b03766

(30) Fortes, F. J.; Moros, J.; Lucena, P.; Cabalín, L. M.; Laserna, J. J. Laser-Induced Breakdown Spectroscopy. *Anal. Chem*. **2013**, *85* (2), 640-669. https://doi.org/10.1021/ac303220r

(31) Vanhoof, C.; Bacon, J. R.; Ellis, A. T.; Vincze, L.; Wobrauschek, P. 2018 atomic spectrometry update – a review of advances in X-ray fluorescence spectrometry and its special applications. *J. Anal. At. Spectrom*. **2018**, *33* (9), 1413-1431. https://doi.org/10.1039/C8JA90030B

(32) Vanhoof, C.; Bacon, J. R.; Ellis, A. T.; Fittschen, U. E. A.; Vincze, L. 2019 atomic spectrometry update – a review of advances in X-ray fluorescence spectrometry and its special applications. *J. Anal. At. Spectrom.* **2019**, *34* (9), 1750-1767. https://doi.org/10.1039/C9JA90042J

(33) Imashuku, S.; Takahashi, J.; Kunimura, S.; Wagatsuma, K. Application of Portable Total-Reflection X-Ray Fluorescence Spectrometer to Analysis of Dysprosium in Neodymium-Iron-Boron Magnet. *ISIJ Int*., **2016**, *56* (12), 2224-2227. https://doi.org/10.2355/isijinternational.ISIJINT-2016-349

(34) Russo, R. E.; Mao, X.; Gonzalez, J. J.; Zorba, V.; Yoo, J. Laser Ablation in Analytical Chemistry. *Anal. Chem*. **2013**, *85* (13), 6162-6177. https://doi.org/10.1021/ac4005327

(35) Augusto, A. S.; Sperança, M. A.; Andrade, D. F.; Pereira-Filho, E. R. Nutrient and Contaminant Quantification in Solid and Liquid Food Samples Using Laser-Ablation Inductively Coupled Plasma-Mass Spectrometry (LA-ICP-MS): Discussion of Calibration Strategies. *Food Analytical Methods* **2017**, *10* (5), 1515-1522. https://doi.org/10.1007/s12161-016-0703-3

(36) Alonso, E. V.; Guerrero, M. M. L.; Cordero, M. T. S.; Pavón, J. M. C.; de Torres, A. G. Characterization of solid magnetic nanoparticles by means of solid sampling high resolution continuum source electrothermal atomic absorption spectrometry. *J. Anal. At. Spectrom*. **2016**, *31* (12), 2391-2398. https://doi.org/10.1039/C6JA00225K

(37) Leme, F. O.; Lima, L. C.; Papai, R.; Akiba, N.; Batista, B. L.; Gaubeur, I. A novel vortex-assisted dispersive liquid-phase microextraction procedure for preconcentration of europium, gadolinium, lanthanum, neodymium, and ytterbium from water combined with ICP techniques. *J. Anal. At. Spectrom*. **2018**, *33* (11), 2000-2007. https://doi.org/10.1039/C8JA00252E

(38) Zawisza, B.; Pytlakowska, K.; Feist, B.; Polowniak, M.; Kita, A.; Sitko, R. Determination of rare earth elements by spectroscopic techniques: a review. *J. Anal. At. Spectrom*. **2011**, *26* (12), 2373-2390. https://doi.org/10.1039/C1JA10140D

(39) Renko, M.; Osojnik, A.; Hudnik, V. ICP emission spectrometric analysis of rare earth elements in permanent magnet alloys. *Fresenius' Journal of Analytical Chemistry* **1995**, *351* (7), 610-613. https://doi.org/10.1007/BF00323334

(40) Santos, C. A.; Panossian, Z. Permanent Rare-Earth Magnets – The need to protect them against corrosion. *Materials Sciences and Applications* **2019**, *10*, 317-327. https://doi.org/10.4236/msa.2019.104024

(41) Carter, J. A.; Barros, A. I.; Nóbrega, J. A.; Donati, G. L. Traditional Calibration Methods in Atomic Spectrometry and New Calibration Strategies for Inductively Coupled Plasma Mass Spectrometry. *Frontiers in Chemistry* **2018**, *6* (504). https://doi.org/10.3389/fchem.2018.00504

(42) Virgilio, A.; Gonçalves, D. A.; McSweeney, T.; Gomes Neto, J. A.; Nóbrega, J. A.; Donati, G. L. Multi-energy calibration applied to atomic spectrometry. *Anal. Chim. Acta* **2017**, *982*, 31-36. https://doi.org/10.1016/j.aca.2017.06.040

(43) Williams, C. B.; Jones, B. T.; Donati, G. L. Multi-flow calibration applied to microwave-induced plasma optical emission spectrometry. *J. Anal. At. Spectrom*. **2019**, *34* (6), 1191-1197. https://doi.org/10.1039/C9JA00091G

(44) Donati, G. L.; Amais, R. S. Fundamentals and new approaches to calibration in atomic spectrometry. *J. Anal. At. Spectrom*. **2019**, *34*, 2353-2369. https://doi.org/10.1039/C9JA00273A

(45) Ingle Jr, J. D.; Crouch, S. R. *Spectrochemical Analysis*, Prentice Hall, Upper Saddle River, New Jersey, United States, **1988**.

(46) ASTM E456-13ae4 *Standard Terminology Relating to Quality and Statistics*, ASTM International, West Conshohocken, PA, **2013**.

(47) ASTM E177-14 *Standard Practice for Use of the Terms Precision and Bias in ASTM Test Methods*, ASTM International, West Conshohocken, PA, **2014**.

(48) Thompson, M. Variation of precision with concentration in an analytical system. *Analyst* **1988**, *113* (10), 1579-1587. https://doi.org/10.1039/AN9881301579

(49) Horwitz, W. Evaluation of analytical methods used for regulation of foods and drugs. *Anal. Chem*. **1982**, *54* (1), 67-76. https://doi.org/10.1021/ac00238a002

(50) Horwitz, W.; Albert, R. Precision in analytical measurements: Expected values and consequences in geochemical analyses. *Fresenius' Journal of Analytical Chemistry*, **1995**, *351* (6), 507-513. https://doi.org/10.1007/bf00322724

(51) da Silva, M. R. M.; Fim, R. G. T.; Silva, S. C.; Casini, J. C. S.; Wendhausen, P. A. P.; Takiishi, H. Influence of Alloying Elements Zr, Nb and Mo on the Microstructure and Magnetic Properties of Sintered Pr-Fe-Co-B Based Permanent Magnets. *Mater. Sci. Forum*, **2018**, *930*, 440-444. https://doi.org/10.4028/www.scientific.net/MSF.930.440

(52) Jin, J.; Yan, M.; Ma, T.; Li, W.; Liu, Y.; Zhang, Z.; Fu, S. Balancing the microstructure and chemical heterogeneity of multi-main-phase Nd-Ce-La-Fe-B sintered magnets by tailoring the liquid-phase-sintering. *Materials & Design* **2020**, *186*, 108308. https://doi.org/10.1016/j.matdes.2019.108308

(53) Cui, X. G.; Zhang, H. J.; Pan, J. X.; Cui, C. Y.; Cheng, L. L.; Ma, T. Y.; Zhang, J.; Wang, C.; Chen, T. H.; Xu, X. J. Magnetic properties, thermal stability, and microstructure of spark plasma sintered multi-main-phase Nd-Ce-Fe-B magnet with PrCu addition. *J. Alloys Compd*. **2020**, *822*, 153612. https://doi.org/10.1016/j.jallcom.2019.153612

(54) Skotnicova, K.; Burkhanov, G. S.; Kolchugina, N. B.; Kursa, M.; Cegan, T.; Lukin, A. A.; Zivotsky, O.; Prokofev, P. A.; Jurica, J.; Li, Y. Structural and magnetic engineering of (Nd, Pr, Dy, Tb)–Fe–B sintered magnets with Tb3Co0.6Cu0.4Hx composition in the powder mixture. *J. Magn. Magn. Mater*. **2020**, *498*, 166220. https://doi.org/10.1016/j.jmmm.2019.166220

(55) Li, J.; Tang, X.; Sepehri-Amin, H.; Sasaki, T. T.; Ohkubo, T.; Hono, K. Angular dependence and thermal stability of coercivity of Nd-rich Ga-doped Nd–Fe–B sintered magnet. *Acta Mater*. **2020**, *187*, 66-72. https://doi.org/10.1016/j.actamat.2020.01.035

(56) Cho, Y.; Sasaki, T.; Harada, K.; Sato, A.; Tamaoka, T.; Shindo, D.; Ohkubo, T.; Hono, K.; Murakami, Y. Magnetic flux density measurements from grain boundary phase in 0.1 at% Ga-doped Nd–Fe–B sintered magnet. *Scr. Mater*. **2020**, *178*, 533-538. https://doi.org/10.1016/j.scriptamat.2019.12.030

(57) Rezchikova, I. I.; Moiseeva, N. S.; Valeev, R. A.; Morgunov, R. B.; Piskorskii, V. P. Change in the Magnetization of Sintered Pr–Dy–Fe–Co–B Magnets in Time. *Russ. Metall*. **2020**, 66-70. https://doi.org/10.1134/S0036029520010097

(58) Lu, K.; Bao, X.; Zhou, Y.; Lv, X.; Ding, Y.; Zhang, M.; Wang, C.; Gao, X. Effect of Al/Cu on the magnetic properties and microstructure of Nd-Fe-B sintered magnet by diffusing Pr-Tb-(Cu, Al) alloys. *J. Magn. Magn. Mater*. **2020**, *500*, 166384. https://doi.org/10.1016/j.jmmm.2019.166384

(59) Castro, J. P.; Sperança, M. A.; Babos, D. V.; Andrade, D. F.; Pereira-Filho, E. R. Neodymium determination in hard drive disks magnets using different calibration approaches for wavelength dispersive X-ray fluorescence. *Spectrochim Acta B* **2020**, *164*, 105763. https://doi.org/10.1016/j.sab.2019.105763

(60) Castro, J. P.; Babos, D. V.; Pereira-Filho E. R., Calibration strategies for the direct determination of rare earth elements in hard disk magnets using laser-induced breakdown spectroscopy. *Talanta* **2020**, *208*, 120443. https://doi.org/10.1016/j.talanta.2019.120443

(61) Castro, J. P.; Pereira-Filho, E. R. Spectroanalytical method for evaluating the technological elements composition of magnets from computer hard disks. *Talanta* **2018**, *189*, 205-210. https://doi.org/10.1016/j.talanta.2018.06.062

JOINT FORENSIC SCIENCE MEETING

8° ENQFOR
NATIONAL MEETING OF FORENSIC CHEMISTRY

5° SBCF
MEETING OF THE BRAZILIAN SOCIETY OF FORENSIC SCIENCE

Connecting Science and Justice

September 05-08 | 2022

Ribeirão Preto Convention Center
Ribeirão Preto/SP - Brazil

THEMATIC SESSIONS

SHORT COURSES

CRIME SCENE

The universe of FORENSIC SCIENCES

AWARDS

SPONSOR EXPOSURE

Take part!

SBCF Sociedade Brasileira de Ciências Forenses

USP

USP QUÍMICA RIBEIRÃO PRETO

For more information:
www.enqfor.org.br

Brazilian Journal of Analytical Chemistry
2022, Volume 9, Issue 36, pp 147–149

FEATURE

The 45th Annual Meeting of the Brazilian Chemical Society had "Chemistry for Sustainable and Sovereign Development" as its Theme

Held from May 31 to June 3, 2022, in Maceió, AL, Brazil, the 45th edition of the Annual Meeting of the Brazilian Chemical Society (45th RASBQ) received an audience of 1,100 people. The theme of the 45th RASBQ was the culmination of the movement "Chemistry Post 2022 – Sustainability and Sovereignty", which aims to promote reflections on how chemistry can contribute to Brazil's sustainability and sovereignty. To learn more about this interesting movement and watch a video, visit: http://www.sbq.org.br/mqp2022/.

The opening conference entitled "From Fossil to Renewable: Chemistry for Sustainable Development" was held by Dr. Claudio José de Araujo Mota, full professor and director of the Institute of Chemistry of the Federal University of Rio de Janeiro (IQ-UFRJ), RJ, Brazil.

45th RASBQ opening conference held by Dr. Claudio J. A. Mota (IQ-UFRJ).
(Photo: Facebook SBQ)

The opening conference addressed how chemistry can contribute to the sustainable development of planet Earth from the industrial revolution, when the use of coal and oil had a positive impact on nature, to the environmental issues caused by the increasing use of these sources, which gives rise to research on renewable energy sources and inputs for the chemical industry.

People from Brazil and abroad, including students, professors, and researchers in the field of chemistry and related areas, had the opportunity to discuss and exchange ideas through lectures, symposia, thematic sessions, and work discussions. Important researchers from all areas of Brazilian and international chemistry were invited to compose the program schedule.

The event took place at the Ruth Cardoso Cultural and Exhibition Center, which has a total area of 48 thousand square miles, a theater on two levels with 1,251 seats, a parking lot with 600 parking spaces, and a pavilion with almost 5 thousand square miles. Due to the health insecurity scenario resulting from the COVID-19 pandemic, the last two meetings of the Brazilian Chemical Society (SBQ) were held virtually. Upon returning to in person events, the 45th RASBQ returned to the Northeast region of Brazil and was held in the city of Maceió, AL for the first time.

“The choice of the Northeast was made because of the great importance of this region for SBQ, as it is home to many chemists who work in educational and research institutions, in addition to the dense representation of SBQ members”, explained Fernando de Carvalho da Silva, associate professor at the Institute of Chemistry of the Fluminense Federal University, RJ, Brazil, secretary general of the SBQ, and chairman of the organizing committee of the 45th RASBQ.

SBQ at Secondary School

One of the important events taking place within RASBQ is “SBQ at Secondary School”, which provides participants from secondary schools with scientific knowledge and experiments that demonstrate how important chemistry is for sustainable development and how much it continuously contributes to improving people’s lives.

SBQ at Secondary School. (Photo: Facebook SBQ)

Tribute Session

During the 45th RASBQ, the science personalities in Brazil who stood out in 2020, 2021, and 2022 received awards at the tribute session. The awards given were: the Simão Mathias Medal, the Journal of the Brazilian Chemical Society Medal, the Virtual Journal of Chemistry Award, the Fernando Galembeck–SBQ Innovation Award, the Royal Society of Chemistry–SBQ Young Researcher Award, the Vanderlan da Silva Bolzani Award, and the Oswaldo Luiz Alves Award. The winners of the National Writing Competition, an initiative aimed at students in basic education with the intention of involving a significant part of the Brazilian school community, including chemistry teachers, were also announced.

Another award given was the American Chemical Society (ACS)–SBQ Brazilian Women in Chemistry Award, 2022 edition, which is sponsored by the Chemical Abstracts Service (CAS), a division of ACS, and the journal Chemical & Engineering News (C&EN).

To learn more about the honorees and winners, visit: http://www.sbq.org.br/45ra/pagina/sessao-homenagens.php/.

Award Session. (Photo: Facebook SBQ)

Exhibition Area

In addition to all of the knowledge, experiences, and information exchanged, participants also had the opportunity to attend the exhibition held by the sponsoring companies. Some of the companies present included: Agilent, Allcrom, Bruker, dpUnion, MBRAUN, Metrohm, Nova Analítica, PerkinElmer, Quantum Design, Shimadzu, Sigma-Aldrich, and Tescan.

Exhibition Area. (Photo: Lilian Freitas)

Brazilian Journal of Analytical Chemistry
2022, Volume 9, Issue 36, pp 150–154

BrJAC

SPONSOR REPORT

PDF

This section is dedicated for sponsor responsibility articles.

Tackling sample preparation for elemental analysis in the lithium-ion battery industry

Joaquim A. Nóbrega[1], Diego Carnaroglio[2], Matteo Volpi[2], Gianpaolo Rota[2]

[1]Department of Chemistry, Federal University of São Carlos, São Paulo, Brazil
[2]Milestone Srl., Bergamo, Italy

This report was extracted from a Milestone eBook of the same title and available for download here

Over the last years, there has been a growing awareness to stop global warming and to keep our planet healthy. It is clear that we need changes in our way of life and in our technology. We need ideas to use energy in a better way. A clear step is the move from combustion engines to electric vehicles. Batteries are evolving and Li-ion battery is the chosen technology so far. Consequently, we must understand how to improve batteries performance, and the chemical analysis of their components is a necessary step.
Materials for anodes, cathodes and electrolytes should be fully characterized. Microwave-assisted digestion has become an essential ally for sample preparation of battery materials before measurements by inductively coupled plasma optical emission spectrometry. We are going to demonstrate how the use of microwave-assisted closed vessel digestions makes feasible the metal analysis of several components used in the Li-ion battery industry. Moreover, this approach led to shorter digestion cycles, using lower volumes of reagents and higher temperatures without compromising safety aspects. The implementation of Li-ion battery technology aims to a more sustainable world, so a green approach should be taken to address this new analytical challenge. The developed procedures are fully compatible with green technologies and incorporate green chemistry attributes to improve our environment.

Keywords: Li-ion battery, Microwave-assisted digestion

INTRODUCTION

Battery is an electrochemical device to store energy and all batteries are composed of two electrodes connected by an electrolyte. According to Armand and Tarascon[1] “when these electrodes are connected by means of an external device, electrons spontaneously flow from the more negative to the more positive potential. Ions are transported through the electrolyte, maintaining the charge balance, and electrical energy can be taped by the external circuit. In secondary, or rechargeable, batteries, a larger voltage applied in the opposite direction can cause the battery to recharge”. Nowadays, Li-ion batteries are the choice to power portable electronics and hybrid/full electric vehicles. Nitta et al. stated that “Li-ion batteries have an unmatchable combination of high energy and power density”. These authors also listed fundamental advantages of Li-ion batteries: Li has the lowest reduction potential of any element and, consequently, Li-based batteries have the highest possible cell potential.[2] They also highlighted that Li is the third lightest element and has one of the smallest ionic radii of any single charged ion. These factors are related to the high power density of Li-ion batteries.

Processes of charge or discharge of Li-ion battery are based on electrochemical processes involving Li ions between these electrodes. Li-ion battery is composed by two electrodes, anode and cathode, and a polyolefin-based separator soaked with an electrolyte.

The performance of anode and cathode materials affects Li-ion batteries energy density, safety, and lifespan. One important aspect about the performance and lifecycle of these materials is related to their

composition and formed decomposition products along their lifetime. It is important to know the chemical composition of all components of batteries to better understand aging effects and expand their lifecycle. Consequently, chemical analysis is a must for determining stoichiometries of the active materials, their changes along charge/discharge cycles and impurities. Nowadays, elemental analysis is frequently based on plasma methods. Inductively coupled plasma optical emission spectrometry (ICP-OES) and inductively coupled plasma mass spectrometry (ICP-MS) are used depending on the required sensitivity. However, despite instrumental alternatives for direct solid analysis, both instrumental methods generally involve analysis of solutions introduced by pneumatic nebulization. It means that solid samples, i.e., anode, cathode and separator materials of batteries, should be converted in representative solutions before instrumental analysis. The sample preparation step exerts a pronounced effect on the quality of analytical results and inorganic materials used as electrodes in Li-ion batteries are hardly decomposed. Mixed oxides and carbon-containing materials are resistant to chemical attack and special procedures should be developed for efficient conversion of these materials in representative solutions.

Nowak and Winter[3] emphasized that considering the huge volume of publications it is astonishing that the research field of elemental analysis of batteries is in a so-early stage. They also stated that: "… it is clear already today, that the continuous improvement and adaptation of advanced analysis methods will be the key for the accurate chemical analysis of batteries and its components, thus unraveling the unanswered degradation mechanisms and those to come.".

Microwave-assisted digestion methods are applicable and less aggressive reagents can be used at high temperatures in closed vessels. Adopting this technology, green digestion procedures can be developed for sample preparation and these are fully compatible with the advent of a greener technology for powering devices and vehicles.

MATERIALS AND METHODS

Microwave-assisted Acid Digestion

Sample acid digestion was performed with two types of system based on different microwave technologies.

The ETHOS UP is a flexible and high performing platform used for elemental analysis. Equipped with easyTEMP contactless sensor, it directly controls the temperature of all samples and solutions, providing accurate temperature feedback to ensure complete digestion in all vessels and high safety. ETHOS UP works with SK-15 rotor capable of high temperature (up to 300 °C) and pressure (up to 100 bar). The SK-15 also features Milestone's patented "vent-andreseal" technology for controlling the internal pressure of each vessel. This ensures complete, safe and reproducible digestions of even the most difficult samples.

The ultraWAVE, developed and patented by Milestone, with Single Reaction Chamber (SRC) technology utilizes high-performance stainless steel, allowing to reach higher pressures and temperatures (up to 199 bar and 300 °C respectively) and to use any type of acids. Disposable vessels eliminate the need to assemble, disassemble or clean between processing. Just as important, dissimilar samples can be processed simultaneously using any mixture of disposable glass, quartz or TFM vials, thus saving time and money. The ultraWAVE is simply the fastest, easiest and most efficient digestion system ever made.

Digestion methods for Spodumene sample

ETHOS UP					ultraWAVE				
Sample mass	100 mg				100 mg				
Final volume	50 mL				50 mL				
Reagents	3 mL of H_3PO_4, 3 mL of H_2SO_4 and 2 mL of HF (dil 1:3)				1.5 mL of H_3PO_4, 1.5 mL of H_2SO_4 and 2 mL of HF (dil 1:3)				
	Microwave heating program				**Microwave heating program**				
		Time	Temp	Power		Time	T1	T2	Power
	1	25 min	230°C	1800 W	1	15 min	280 °C	60 °C	1500 W
	2	30 min	230°C	1800 W	2	20 min	280 °C	60 °C	1500 W

Digestion methods for $LiFePO_4$ (LFP) sample

ETHOS UP					ultraWAVE				
Sample mass	500 mg				500 mg				
Final volume	50 mL				50 mL				
Reagents	2 mL of HNO_3 + 6 mL of HCl				1 mL of HNO_3 + 3 mL of HCl				
	Microwave heating program				**Microwave heating program**				
		Time	Temp	Power		Time	T1	T2	Power
	1	25 min	230°C	1800 W	1	15 min	250 °C	60 °C	1500 W
	2	15 min	230°C	1800 W	2	20 min	250 °C	60 °C	1500 W

Determination of Metals

The instrument used for metals and trace metals determination was an inductively-coupled plasma optical emission spectrometer (ICP OES), with axial view and equipped with automatic sampler. The instrument setup and the operating conditions are reported in Table 1.

Table 1. ICP OES operating parameters

Parameter	Setting
RF applied power (kW)	1.3
Plasma gas flow rate (L/min)	15
Auxiliary gas flow rate (L/min)	1.5
Nebulizer gas flow rate (L/min)	0.75
Replicate read time (s)	5
Stabilization delay (s)	30
Sample uptake delay (s)	30
Pump rate (rpm)	15
Rinse time (s)	15
Replicates	3
Emission lines (nm)	Indicated in each table of data

Spike recoveries and Internal standard Spike standard

Three replicates out of six were spiked with 1000 µL of periodic table mix 1 (solution h) and 2 (solution i) for ICP standards respectively, immediately after sample weighing and prior to reagent addition. These worked as recovery studies for elemental impurities. The concentration of the spiked elements in the final digested solution was 200 µg/L. Internal standard. 10 µg/mL of Yttrium standard (d) was added to calibration standards, blanks, digested solutions and, where appropriate, to their dilutions (e.g.: 500 µL of Y std added to 50 mL of digested solution). This was used as internal standard to correct matrix effects.

RESULTS AND DISCUSSION

Spodumene is a pyroxene mineral consisting of lithium aluminum inosilicate ($LiAlSi_2O_6$). It is the most widely exploited mineral source of lithium (theoretical lithium content = 3.73%). Other lithium-bearing pegmatite silicates include lepidolite and petalite. Although in the past industry transitioned to extracting lithium from brines, nowadays the exploding demand for lithium has made the exploration for and development of spodumene deposits a highly attractive endeavor.

ETHOS UP and UW led to efficient digestions and results using ICP OES did not present any statistical difference. Consequently, we have decided not to specify for each set of results the used system because both led to accurate data.

Table 2. Major elements in Spodumene sample

	Determined concentration (%)	RSD% (n = 6)
Al 396.152	12.9	1.67
Li 670.783	2.95	0.92
Si 251.611	27.9	1.12

Lithium iron phosphate, $LiFePO_4$ (LFP), is extensively used in the lithium-ion battery field as cathode material. The main advantages of LFP are its flat voltage profile, low material cost, abundant material supply and better environmental compatibility compared to other cathode materials. In fact, LFP contains neither nickel nor cobalt, both of which are supply-constrained and expensive. The use of phosphates avoids cobalt's cost and environmental concerns. The purposes of LFP analysis are 1) to determine the composition of the main elements (QC/Production) and 2) to evaluate the purity of the raw material (QC/R&D).

Table 3. Major elements in $LiFePO_4$ (LFP) sample

	Determined concentration (%)	RSD% (n = 6)
Li 670.783	4.81	1.38
Fe 238.204	33.9	1.65
P 213.618	20.2	4.01
Ca 396.847	0.47	4.55
K 766.491	0.00844	3.54
Mg 279.553	0.000829	5.80
Na 589.592	0.00557	4.32

Table 4. Impurities and spike recoveries in $LiFePO_4$ (LFP) sample

	Determined concentration (µg/L)	RSD% (n = 3)	Spiked determined concentration (µg/L)	RSD% (n=3)	Spike recovery (%)
Ag 328.068	26.5	21.3	120	7.94	93
Al 237.312	16.6	2.45	121	1.34	105
As 193.696	72.1	10.4	179	1.79	106
Ba 455.403	<MDL		95.8	1.81	96
Be 313.107	<MDL		93.3	3.67	93
Cd 214.439	45.7	11.4	144	2.48	98
Co 238.892	<MDL		94.4	0.86	94
Cr 206.158	38.5	16.2	144	1.78	105
Cu 324.754	<MDL		95.0	0.56	95
Mo 202.032	<MDL		98.4	1.61	98
Ni 231.604	<MDL		91.9	0.68	92
Nb 313.078	<MDL		94.4	1.71	94
Pb 182.143	<MDL		97.3	0.84	97
Ru 240.272	76.9	7.4	169	3.70	93
Sb 206.834	<MDL		93.8	1.30	94
Sr 407.771	<MDL		95.6	3.35	96
Ti 336.122	<MDL		93.1	2.77	93
V 292.401	92.4	2.83	210	4.15	118
Zn 206.200	263	8.35	359	4.63	97

REFERENCES

1. M. Armand, J. M. Tarascon, Building better batteries. *Nature*, *451* (2008) 652-657.
2. N. Nitta, F. Wu, J. T. Lee, G. Yushin, Li-Ion battery materials: present and future. *Materials Today*, *18* (2015) 252-264.
3. A. Yoshino, The birth of the lithium-ion battery. *Angewandte Chemie International Edition*, *51* (2012) 5798- 5800.
4. Nowak, S.; Winter, M. Elemental analysis of lithium ion batteries. *Journal of Analytical Atomic Spectrometry*, *32* (2017) 1833-1847. https://doi.org/10.1039/C7JA00073A

This sponsor report is the responsibility of Milestone SRL.

Brazilian Journal of Analytical Chemistry
2022, Volume 9, Issue 36, pp 155–160

BrJAC

SPONSOR REPORT

PDF

This section is dedicated for sponsor responsibility articles.

Sensitive determination of elements in lithium batteries using the Thermo Scientific iCAP PRO XP ICP OES

Jingfang He[1], Xiaobo Li[1], Fei Wang[1], Miao Jing[1], and Jianfeng Cui[2]

[1]Thermo Fisher Scientific, Shanghai, China
[2]Thermo Fisher Scientific, Bremen, Germany

This report was extracted from the Thermo Scientific Application Note 73872

Keywords: Lithium battery, iCAP PRO XP ICP OES, cathode material, ternary materials, fast detection, robust analysis, quantification

GOAL

This note demonstrates a fast analytical method for the determination of major and trace elements in the ternary cathode material of lithium batteries using the Thermo Scientific™ iCAP™ PRO Series ICP-OES.

INTRODUCTION

The continuous development of lithium-ion batteries and the research into their materials is at the forefront of the energy sector as it moves away from fossil fuels. To regulate the quality of production, the Chinese national standard method YS/T 798-2012 was established. All new lithium battery developments must meet the requirements of these standards. The ternary material of lithium batteries typically contains lithium, nickel, cobalt, and manganese, and potassium aluminate as its cathode material. In recent years, lithium batteries using ternary materials as cathode materials have gradually replaced nickel-metal hydride batteries, lithium cobalt batteries and lithium-ion phosphate batteries. This is due to the high capacity, good cycle stability (battery life), and moderate cost of the new battery type. The proportion and content of the main elements in the ternary cathode material can affect the performance and cost of the lithium battery significantly and the content of impurities in the ternary material alters the safety of the battery. Therefore, the accurate determination and quantification of the main elements, as well as trace impurities in the ternary cathode material, becomes particularly important.

EXPERIMENTAL

Standards and sample preparation

A series of calibration standards were prepared to determine the elemental impurities and major elements within the lithium battery material. Multi-element standard solutions were prepared by diluting single-element stock standards with 2% hydrochloric acid (elements in this solution are listed in Table 2). The standard concentrations of analytes defined as impurities were 0, 0.05, 0.10, 0.50, 1.0, and 5.0 mg L^{-1} in a mixed standard solution. To determine the concentration of major elements, calibration standards containing lithium at 0, 2, 5, and 10 mg L^{-1} and Co, Ni, and Mn at 0, 10, 20, and 50 mg L^{-1} were prepared.

To prepare the sample, an aliquot of 0.25 g of ternary cathode material was weighed into a polytetrafluoroethylene beaker. A volume of 10 mL hydrochloric acid (37%, Sinopharm) was added, and the mixture was heated on a hot plate for digestion at just below the boiling point of the acid until all

the sample powder dissolved to a clear solution. After the sample cooled, it was transferred to a 50 mL volumetric flask and filled to volume with ultrapure water with a resistivity of 18.2 MΩ·cm (Barnstead™ water purification system, Thermo Scientific™) A preparation blank was also prepared using the same method. For the analysis of elemental impurities, the sample solution was analyzed undiluted, while for the analysis of major elements, the sample solution was diluted 50-fold.

Instrument parameters and method optimization

The iCAP PRO XP ICP OES Radial system was selected for the application, the lower detection limits offered by the axial view of a dual view system were not required for this application. The system utilizes intelligent Full Range (iFR) mode and captures the complete spectrum in the range of 167 to 852 nm in one exposure. This not only reduces the overall analysis time, but also the operational cost as the argon gas consumption is also reduced. The parameters used for the analysis are shown in Table 1. The standard and the sample solutions were introduced into the plasma to collect the spectral data information of all elemental impurities. After data collection was completed, each spectrum was displayed by the subarray spectrum overlay functionality of the Thermo Scientific™ Qtegra™ Intelligent Scientific Data Solution™ (ISDS) Software (Figure 1). Using the wavelength library in the Qtegra ISDS Software, potential interferences can be avoided. The adjustment and optimization of the array position allows for more reasonable data collection points.

Table 1. Instrument parameters used for the analysis

Parameter	Setting
Peristaltic pump speed	50 rpm
RF power	1150 W
Nebulizer gas	0.6 L min^{-1}
Auxiliary gas	0.5 L min^{-1}
Cooling gas	12 L min^{-1}
Viewing mode	Radial
Nebulizer	Glass concentric nebulizer
Torch	EMT quartz torch
Injector	2.0 mm quartz injector
Spraychamber	Glass cyclonic spraychamber
Radial viewing height	10 mm
Exposure time	10 s
Analysis mode	iFR

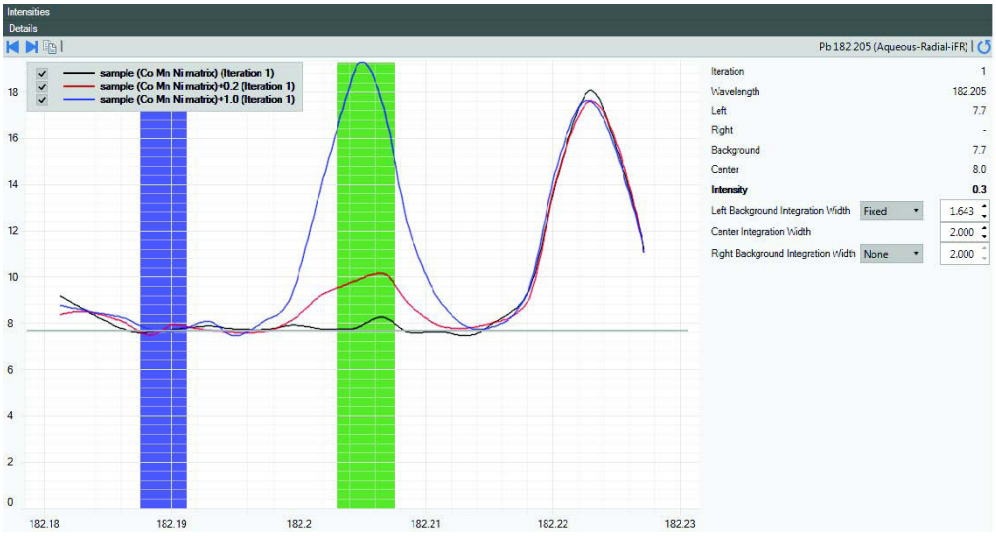

Figure 1. Spectrum of Pb at 182.205 nm, showing no interference in the central observation area.

RESULTS AND DISCUSSION

The correlation coefficients R^2 of the obtained calibration curves were higher than 0.9995 for all analytes, indicating excellent linearity of the wavelengths selected (Table 2).

Table 2. Correlation coefficients (R^2) determined from calibration curves of each analyte and concentration range

Element and wavelength (nm)	Correlation coefficient R^2	Concentration range (mg L^{-1})
Al 396.152	0.9997	0–5
As 189.042	>0.9999	0–5
Ba 455.403	>0.9999	0–5
Ca 393.366	>0.9999	0–5
Cd 214.438	>0.9999	0–5
Cr 206.157	>0.9999	0–5
Cu 324.754	>0.9999	0–5
Fe 259.940	>0.9999	0–5
K 766.490	0.9995	0–5
Mg 285.213	>0.9999	0–5
Mo 204.598	>0.9999	0–5
Na 589.592	0.9995	0–5
P 213.618	>0.9999	0–5
Pb 182.205	0.9995	0–5
S 180.731	>0.9999	0–5
Sb 206.833	>0.9999	0–5

Table 2 continued. Correlation coefficients (R^2) determined from calibration curves of each analyte and concentration range

Element and wavelength (nm)	Correlation coefficient R^2	Concentration range (mg L^{-1})
Si 212.412	0.9995	0–5
Sn 189.989	>0.9999	0–5
Ti 334.941	>0.9999	0–5
V 309.311	>0.9999	0–5
Zn 206.200	>0.9999	0–5
Li 670.791	>0.9999	0–10
Mn 191.510	>0.9999	0–50
Ni 221.647	>0.9999	0–50
Co 228.616	>0.9999	0–50

The unspiked ternary cathode material sample was analyzed for impurities and the results are shown in Table 3.

Table 3. Quantification of detected elemental impurities in an unspiked ternary cathode sample as well as instrument and method detection limits. <LOD stands for values below the detection limit.

Element and wavelength (nm)	Concentration in the solid sample (mg kg^{-1})	Instrument detection limit in solution (mg L^{-1})	Method detection limit in solid (mg kg^{-1})
Al 396.152	1067	0.0098	1.959
As 189.042	2.06	0.0082	1.631
Ba 455.403	19.16	0.0001	0.020
Ca 393.366	62.13	0.0001	0.010
Cd 214.438	0.37	0.0003	0.064
Cr 206.157	1.26	0.0015	0.304
Cu 324.754	1.64	0.0025	0.500
Fe 259.940	18.62	0.0012	0.243
K 766.490	30.85	0.0090	1.808
Mg 285.213	103	0.0006	0.124
Mo 204.598	<LOD	0.0052	1.035
Na 589.592	102	0.0052	1.030
P 213.618	<LOD	0.0054	1.088
Pb 182.205	7.02	0.0142	2.838
S 180.731	805.39	0.0073	1.461
Sb 206.833	<LOD	0.0192	3.835

Table 3 continued. Quantification of detected elemental impurities in an unspiked ternary cathode sample as well as instrument and method detection limits. <LOD stands for values below the detection limit.

Element and wavelength (nm)	Concentration in the solid sample (mg kg^{-1})	Instrument detection limit in solution (mg L^{-1})	Method detection limit in solid (mg kg^{-1})
Si 212.412	65.39	0.0102	2.039
Sn 189.989	2.41	0.0065	1.296
Ti 334.941	4.54	0.0008	0.166
V 309.311	<LOD	0.0014	0.275
Zn 206.200	1.19	0.0007	0.147

The sample was spiked with 1.0 mg L^{-1} of Al and S and 0.2 mg L^{-1} of all other elements. The recoveries are all in the range of 90% to 110% as shown in Figure 2.

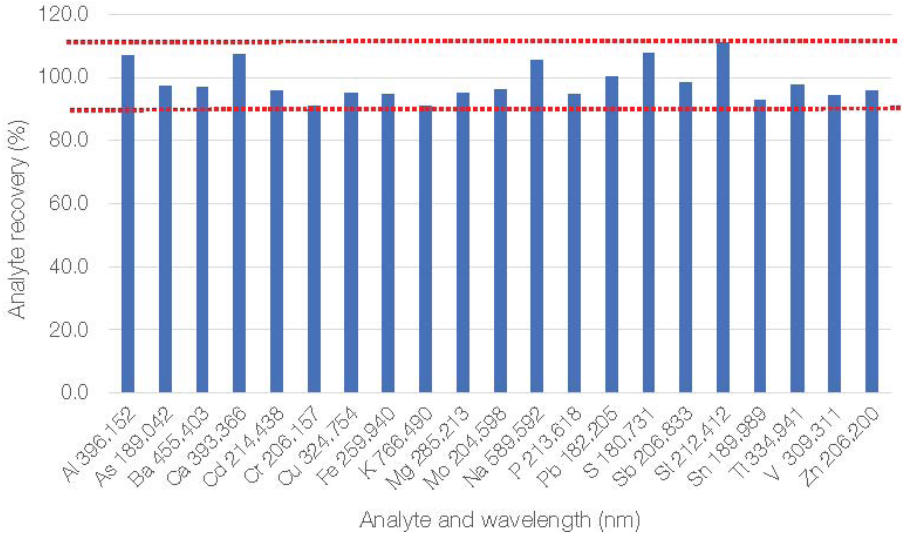

Figure 2. Calculated recoveries (%) for target analytes in the spiked ternary material samples. Spiked at 1.0 mg L^{-1} for Al and S and with 0.2 mg L^{-1} for all other elements.

A stability test was conducted on the major elements in the sample by analyzing the stability test sample every 20 minutes over a period of 2 hours. The RSDs are well below 1% for all analytes and no drift is observed (Table 4).

Table 4. Major element concentration (in mg kg^{-1}), average values, standard deviation (SD) values as well as repeatability data as % RSD (n=7) of the test sample

Measurement Nr/Element	Li 670.791	Mn 191.510	Ni 221.647	Co 228.616
1	6.99	11.06	34.56	12.33
2	7.01	11.08	34.07	12.16
3	6.95	11.24	34.54	12.34
4	7.06	11.20	34.66	12.34

Table 4 continued. Major element concentration (in mg kg^{-1}), average values, standard deviation (SD) values as well as repeatability data as % RSD (n=7) of the test sample

Measurement Nr/Element	Li 670.791	Mn 191.510	Ni 221.647	Co 228.616
5	7.05	11.17	34.62	12.29
6	7.03	11.11	34.43	12.34
7	6.98	11.21	34.81	12.46
Average	7.01	11.15	34.53	12.32
SD	0.040	0.068	0.234	0.089
RSD%	0.574	0.613	0.677	0.721

CONCLUSION

In this application note, a Thermo Scientific iCAP PRO XP ICP-OES Radial system was used to establish a rapid detection method for the determination of major elements and trace impurities in a ternary cathode material used in lithium batteries.

For the impurity elements, recovery values of between 90% and 110% were achieved, as calculated from the spiked samples. For interferences from complex matrices, such as cobalt-nickel-manganese-lithium matrix and the spectral interference of elements, such as nickel and manganese, the iCAP PRO XP ICP-OES system uses a high-resolution optical system that can obtain accurate test results for each element.

All performance specifications meet the testing requirements specified by the national standard method YS/T 798-2012.[1] The iCAP PRO XP ICP-OES system has an ultra-high sensitivity and stability for the detection of elements with characteristic wavelengths in the far ultraviolet region (e.g., S 180.731 nm, Pb 182.205 nm).

The iCAP-PRO XP ICP-OES system performance for major elements, such as nickel, cobalt, manganese, and lithium, demonstrated excellent levels of precision (with % RSD <1%) and accuracy (spike recoveries with the range 90% to 110%).

Overall, the analytical solution employed in this study with the iCAP PRO XP ICP-OES system meets all analytical requirements for routine or research laboratories that aim to analyze elements in ternary materials of lithium batteries.

REFERENCE

1. YS/T 798-2012: China National non-ferrous metal industry standards, Lithium nickel cobalt manganese oxide, Ministry of Industry and Information Technology of the People's Republic of China.

Find out more at thermofisher.com/ICP-OES

This sponsor report is the responsibility of Thermo Fisher Scientific.

Brazilian Journal of Analytical Chemistry
2022, Volume 9, Issue 36, pp 161–172

BrJAC

SPONSOR REPORT

PDF

This section is dedicated for sponsor responsibility articles.

Low-level consistent analysis of PBDEs in environmental and food matrices using triple quadrupole GC-MS/MS

Kjell Hope[1], Giulia Riccardino[2], Adam Ladak[3], and Paul Silcock[3]

[1]Pacific Rim Laboratories Inc., Canada
[2]Thermo Fisher Scientific, Milan, IT
[3]Thermo Fisher Scientific, Hemel Hempstead, UK

This report was extracted from the Thermo Scientific Application Note 000493

Keywords: Polybrominated diphenyl ethers (PBDEs), food, environment, gas chromatography-mass spectrometry, GC-MS, triple quadrupole, TSQ 9610 mass spectrometer, NeverVent Advanced Ionization ion source (AEI), TRACE 1610 GC, programmable temperature vaporizing injector, PTV, AI/AS 1610

GOAL

The aim of this application note is to demonstrate the performance of the Thermo Scientific™ TSQ™ 9610 triple quadrupole mass spectrometer coupled to the Thermo Scientific™ TRACE™ 1610 GC for the determination of polybrominated diphenyl ethers (PBDEs) in environmental and food samples.

INTRODUCTION

PBDEs are classes of polybrominated hydrocarbons existing as mixtures of congeners with similar molecular structures but different chemical and physical properties (e.g., congeners with lower numbers of bromine atoms tend to be more volatile and to bioaccumulate more than higher brominated congeners).[1] Historically these compounds were widely used as flame retardants in a variety of products, such as plastics, furniture, upholstery, electrical equipment, electronic devices, textiles, and other household products, because of their capability to release bromine radicals that reduce both the rate of combustion and dispersion of fire when exposed at high temperatures.[1] These compounds enter the environment through emissions from manufacturing processes, volatilization from various products that contain PBDEs, recycling wastes, and leachate from waste disposal sites. They are considered ubiquitous persistent pollutants as they have been detected in the airborne particulate matter, bonded to sediments, surface water, fish, and other marine animals, and therefore represent a risk to human health. As a consequence, the use of certain toxic PBDEs with links to cancer and endocrine disruption (including penta-, tetra-, and deca-PBDE) have been prohibited, and are currently listed in the Stockholm Convention inventory of persistent organic pollutants.[2]

There are several challenges associated with the analysis of PBDEs in food and environmental samples. Firstly, confident low level of detection must be achieved consistently. This can be difficult due to the complexity of the matrices being analyzed. Secondly, as the PBDE congeners have similar structures and are isobaric compounds, separating these compounds chromatographically can be difficult without extended run times. Analytical laboratories must deliver results to their customers in a timely manner and instrument downtime is not acceptable. Traditionally, gas chromatography coupled to either electron capture detection (GC-ECD), mass spectrometry (GC-MS), or high-resolution accurate mass mass spectrometry

(GC-HRMS) is the technique of choice for analysis of PBDEs. Combining with triple quadrupole mass spectrometry (GC-MS/MS), with its high selectivity in removing interferences from the matrix that can lead to false positive erroneous results, yields sensitivity for detection of PBDEs at ultra-trace levels.

In this study, the TSQ 9610 triple quadrupole GC-MS/MS was used for the determination of PBDEs in fish oil and environmental (water and soil) samples. The Thermo Scientific™ TraceGOLD™ PDBE column was tested for chromatographic separation of the isobaric congeners; whereas selected reaction monitoring (SRM) acquisition mode ensured appropriate selectivity and sensitivity when matrix samples were analyzed. Linearity and instrument detection limits (IDLs) were assessed in the experiments for all compounds as well as an extended robustness study over n=100 injections of matrix samples to assess the reproducibility of the detection of trace levels of PDBEs.

EXPERIMENTAL

In the experiments described here, a TSQ 9610 triple quadrupole mass spectrometer equipped with a Thermo Scientific™ NeverVent™ Advanced Electron Ionization (AEI) ion source was coupled to a TRACE 1610 gas chromatograph equipped with a Thermo Scientific™ iConnect™ programmable temperature vaporizing (iConnect-PTV) injector and a Thermo Scientific™ AI/AS 1610 autosampler. The TRACE 1610 GC with its instant connect injector and detector modules allows for the reconfiguration of the instrument to adapt to different workflows in minutes. The NeverVent technology allows for ion source cleaning, filament replacement, and column exchange without breaking instrument vacuum, therefore ensuring minimum downtime to the laboratory workflow. The AI/AS 1610 GC ensures ease-of-use and cost-effectiveness for high-throughput laboratory work.

Chromatographic separation was achieved on a TraceGOLD TG-PBDE capillary column, 15 m × 0.25 mm × 0.10 µm (P/N 26061-0350). The TraceGOLD PDBE column has been developed to ensure fast analysis of PBDE with excellent separation of isobaric congeners (PBDE-49 and PBDE-71), exceeding the U.S. EPA Method 16143 resolution criteria, coupled to a thin film phase and high thermal stability (maximum temperatures up to 360 ˚C) for faster elution of high boiling point PBDEs (e.g., PBDE-209) with improved peak shapes.

Additional GC-MS/MS and autosampler parameters as well as a complete list of the target compounds are detailed in Table 1 and Appendix 1, respectively.

Table 1. GC-MS/MS and autosampler experimental conditions for the analysis of PBDEs

AI/AS 1610 Autosampler parameters		**iConnect-PTV parameters**	
Injection type	Standard	Injection temperature (˚C)	65
Sample mode	Standard	Liner	PTV 6 baffle Siltek™ liner
Fill strokes	10	Inlet module and mode	PTV, splitless
Sample depth	Bottom	Injection time (min)	0.1
Injection mode	Fast	Transfer rate (˚C/s)	5.0
Pre-injection delay time (s)	0	Transfer temperature (˚C)	330
Post-injection delay time (s)	0	Transfer time (min)	1.50
Pre-injection wash cycles	0	Cleaning rate (˚C/s)	14.5
Pre-injection solvent wash vol. (µL)	6.0	Cleaning temperature (˚C)	330
Post-injection wash cycles	4	Cleaning time (time)	5.00
Pre-injection solvent wash vol. (µL)	6.0	Cleaning split flow (mL/min)	75

Table 1 continued. GC-MS/MS and autosampler experimental conditions for the analysis of PBDEs

AI/AS 1610 Autosampler parameters		**iConnect-PTV parameters**	
Sample wash cycles	1	Post cycle temperature	Maintain
Sample wash volume (µL)	1.0	Split flow (mL/min)	50
Injection volume (µL)	1.0	Septum purge flow (mL/min)	5, constant
		Carrier gas, flow (mL/min)	He, 1.5
TRACE 1610 GC parameters		**TSQ 9610 Mass Spectrometer parameters**	
Oven temperature program		Transfer line temperature (˚C)	300
Temperature (˚C)	100	Ion source type and temp. (˚C)	NeverVent AEI, 300
Hold time (min)	2.00	Ionization type	EI
Rate (˚C/min)	30	Emission current (µA)	50
Temperature 2 (˚C)	330	Aquisition mode	timed-SRM
Hold time (min)	3	Q1 and Q3 resolution	Mono-hepta BDE normal (0.7 amu); Octa-deca BDE wide (1.2 amu)
GC run time (min)	12.67	Tuning parameters	AEI Smart Tune
Column TraceGOLD TG-PBDE	15 m, 0.25 mm, 1.0 µm (P/N 26061-0350)	Collision gas and pressure (psi)	Argon at 70

Data acquisition, processing, and reporting

Data was acquired, processed, and reported using the Thermo Scientific™ Chromeleon™ Chromatography Data System (CDS) software, version 7.3. Integrated instrument control ensures full automation of the analytical workflow combined with an intuitive user interface for data analysis, customizable reporting, and storage in compliance with the Federal Drug Administration Title 21 Code of Federal Regulations Part 11 (Title 21 CFR Part 11). In particular, PBDE quantitative analysis requires the use of use of isotope dilution, this feature is available in Chromeleon CDS from software version 7.2.9 onwards.

Standard and sample preparation

Standard preparation

A calibration solution kit at five calibration levels (CS1 to CS5) containing native as well as ^{13}C mass-labeled PBDE congeners and mass-labeled PBDE internal standards was purchased from Wellington Laboratories, Inc. (P/N BDE-CVS-G). The lowest calibration level (CS1) was furtherly diluted 1:2 and 1:4 in nonane to expand the calibration curve from 0.25 to 2,000 ng/mL. For the calculation of IDLs, standard solutions ranging from 0.03 to 1.25 ng/mL were prepared by serially diluting the 1:4 CS1 calibration standard.

Sample preparation

Water, soil, and fish oil samples were extracted and provided by Pacific Rim Laboratories Inc., Canada. A schematic of the sample preparation workflow is reported in Figure 1. Samples were dried before shipment and reconstituted with 50 µL of nonane, sonicated in the ultra-sonic bath for few minutes and vortexed before injection into the chromatographic system.

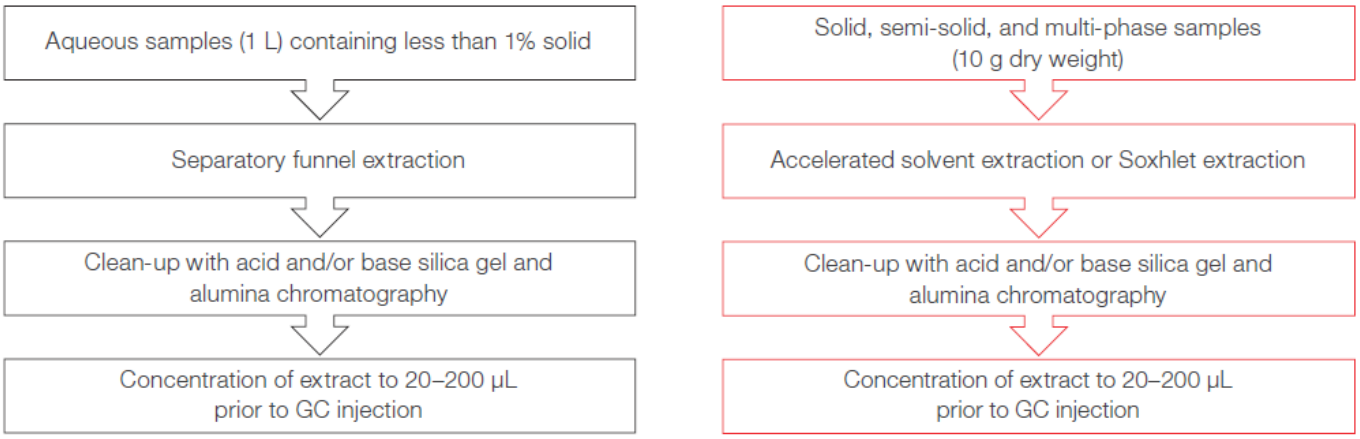

Figure 1. Sample preparation procedure for aqueous, solid, semi-solid and multi-phase samples

RESULTS AND DISCUSSION

Chromatography

The high selectivity of the TraceGOLD TG-PBDE capillary column ensured the chromatographic resolution of the target analytes in less than 13 minutes, including the isobaric congeners PBDE-49/PBDE-71 for which the calculated resolution was 5% at the valley height, therefore exceeding the U.S. EPA Method 1614 requirement of less than 40%.3 Moreover, Gaussian peak shape was achieved for the high molecular weight compounds PBDE-209 (MW=952.2) with a calculated asymmetry factor of 1.1 as shown in Figure 2.

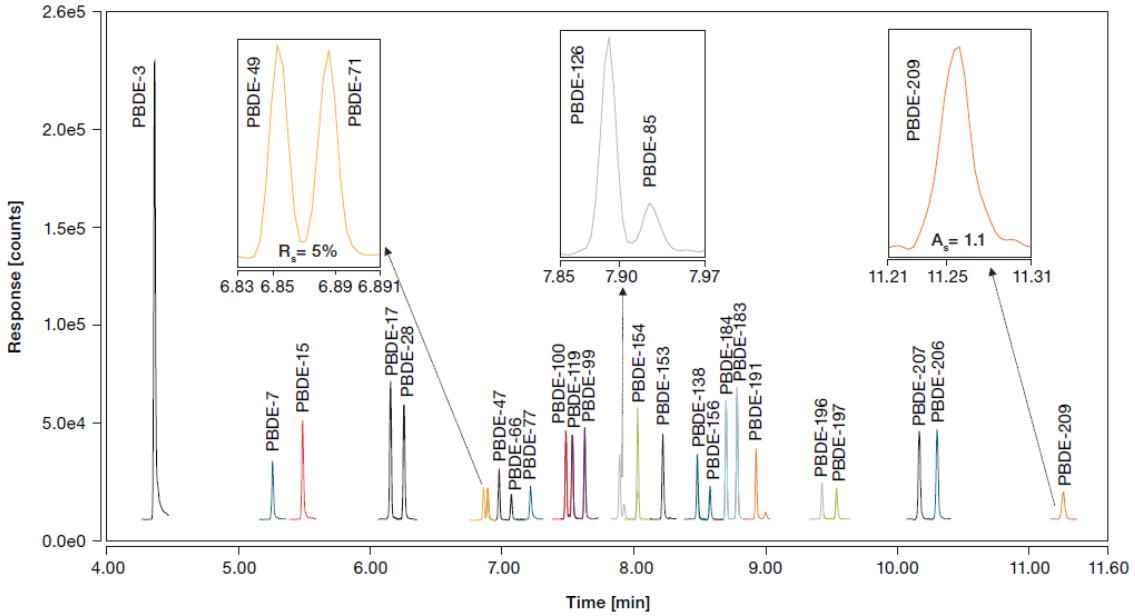

Figure 2. t-SRM acquisition showing baseline chromatographic separation for the investigated compounds in CS1 solvent standard (1.0–5.0 ng/mL). The insets highlight the resolution on the critical pairs and the calculated asymmetry factor for the high boiling point congeners (PBDE-209).

The timed-selected reaction monitoring (t-SRM) acquisition method allowed high selectivity to discriminate between the target compounds and the complex matrix, thus ensuring a confident and selective identification of analytes. As an example, environmental and fish oil samples total ion chromatograms (TIC) acquired in EI, full-scan (FS, *m/z* 40–1,000) showing the complexity of the matrices and the selectivity of the SRM acquisition are reported in Figure 3.

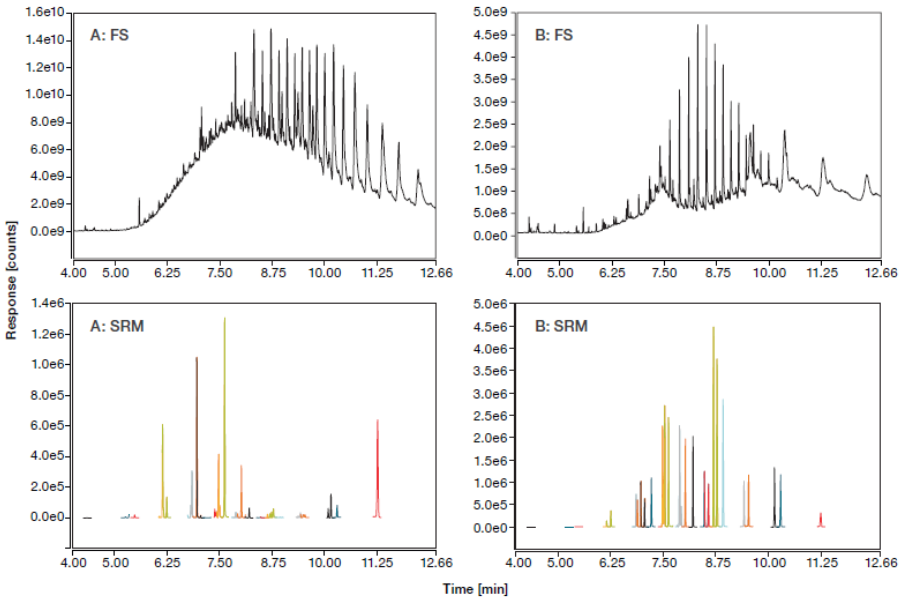

Figure 3. TIC (FS: *m/z* 40–1,000) and SRM acquisitions for environmental (A-left traces) and fish oil (B-right traces) sample extracts containing PBDEs showing the complexity of the matrices (FS acquisition) and the selectivity of the SRM acquisition.

Linearity, instrument detection limit (IDL), and limitof quantitation (LOQ)

The TSQ 9610 NeverVent AEI is equipped with theThermo Scientific™ XLXR™ detector, which is an electronmultiplier that offers extended detector lifetime and dynamic range. Calibration curves ranging from 0.25 to 2,000 ng/mLwere prepared as detailed in the Standard preparation section. Each calibration level was injected in triplicate. Native PBDE congeners were quantified using their corresponding isotopes using isotope dilution quantitation. The target analytes showed a linear trend with coefficient of determination (R2)>0.990 and residual values (measured as %RSD of average response factors, AvCF %RSD) <15%, thus confirming a wider linear range canbe easily achieved as reported in Appendix 2. Full range calibration curves for PBDE-47 (0.25–400 ng/mL), PBDE-183(0.5–800 ng/mL) and PBDE-209 (1.25–2,000 ng/mL) as wellas zoomed detail (0.25–5.0 ng/mL, 0.5–10.0 ng/mL, and 1.25–25.0 ng/mL, respectively) are shown as an example in Figure 4.

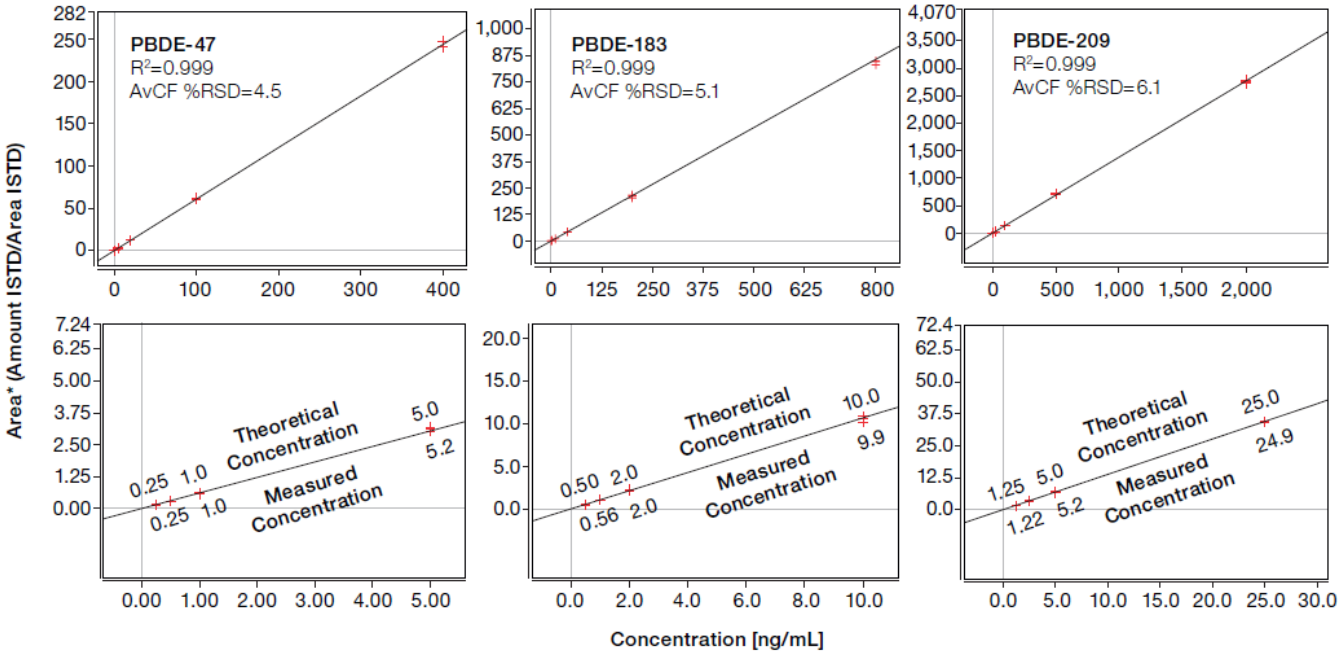

Figure 4. Example of solvent (nonane) calibration curves for PBDE-47 (full range: 0.25–400 ng/mL, zoomed detail: 0.25–5.0 ng/mL), PBDE-183 (full range: 0.5–800 ng/mL, zoomed detail: 0.5–10.0 ng/mL) and PBDE-209 (full range: 1.25–2,000 ng/mL, zoomed detail: 1.25–25.0 ng/mL). Each calibration level was injected in triplicate. Coefficient of determination (R2) and AvCF %RSD are annotated.

The instrument detection limit was determined for all the target compounds by injecting (n=10) solvent standards ranging from 0.03 to 1.25 ng/mL, corresponding to 1.5 pg/L to 62.5 pg/L in water samples and 0.15 to 6.25 ng/kg in soil and fish oil samples. IDLs were calculated taking into account the one-tailed Student's t-test values for the corresponding n-1 degrees of freedom at 99% confidence, the concentration, and the absolute peak area %RSD (<15%) for each analyte. Calculated IDLs ranged from 5 fg to 122 fg on column (OC) corresponding to 0.25 pg/L to 6.10 pg/L for water samples and 0.025 to 0.61 ng/kg for soil and fish oil samples (Figure 5).

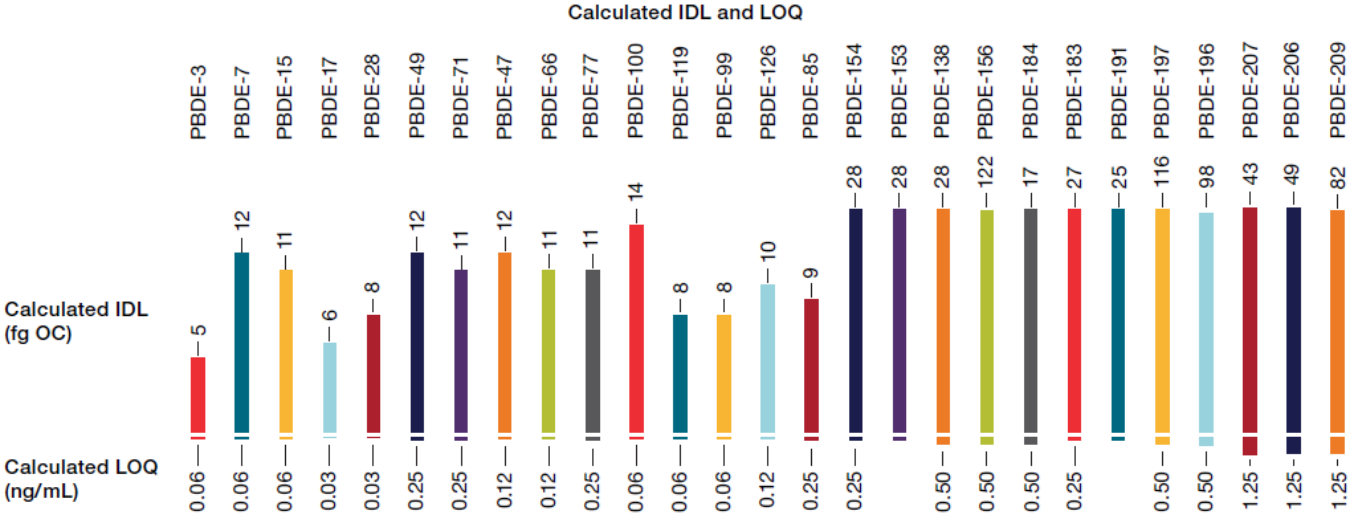

Figure 5. Calculated IDLs and LOQs for all investigated PBDEs. Calculated IDLs ranged from 5 fg to 122 fg on column (OC), corresponding to 0.25 pg/L to 6.10 pg/L for water samples and 0.025 to 0.61 ng/kg for soil and fish oil samples. Calculated LOQs ranged from 0.03 to 1.25 ng/mL, corresponding to 1.5 pg/L to 62.5 pg/L in water samples and 0.15 to 6.25 ng/kg in soil and fish oil samples.

The standard concentration for which (i) the ion ratios were within ±30% of the expected values calculated as an average across a calibration curve ranging from 0.25 to 2,000 ng/mL, (ii) the absolute peak area repeatability was <15 %RSD, and (iii) the relative response factor (RRF) was within ±30% of that calculated from the average of the calibration was chosen as the LOD for individual PBDEs. The calculated LOQ, as well as ion ratios, peak area %RSD, and RRF for the investigated compounds are detailed in Appendix 3. Examples of the consistency of the RRF for some selected PBDEs are shown in Figure 6.

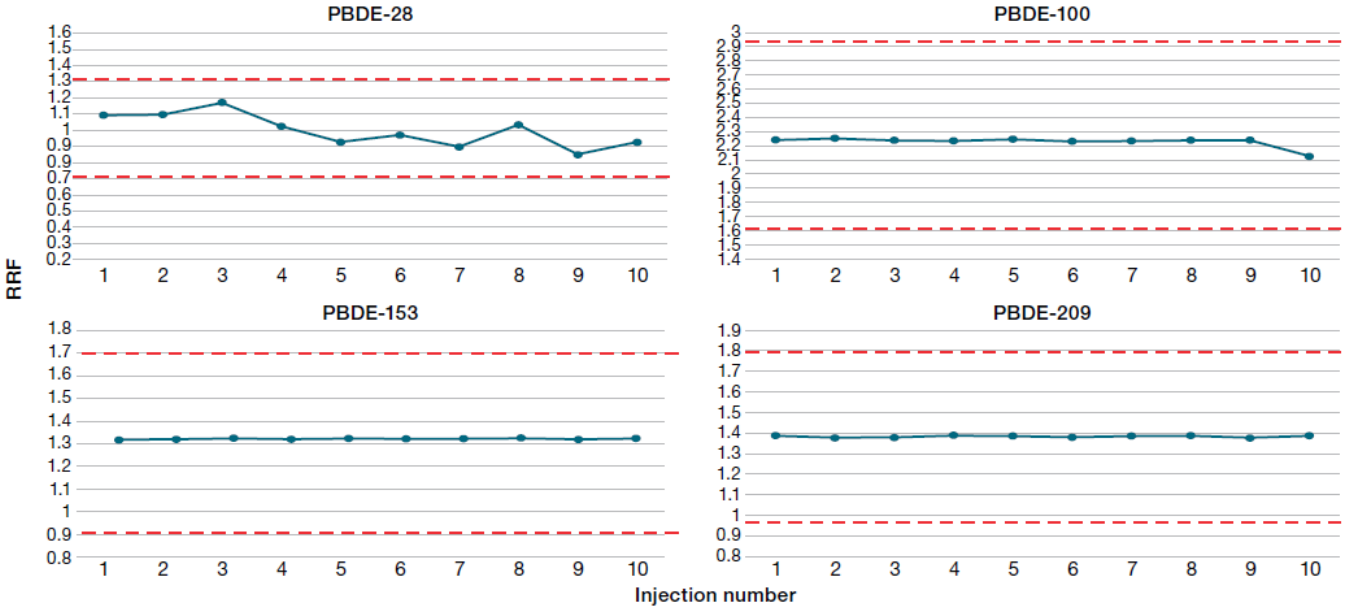

Figure 6. Examples of the consistency of the RRF for some selected PBDEs. The RRF was within ±30% of that calculated from the average of the calibration. The amber dotted lines represents the acceptance limits.

Robustness

Analytical testing laboratories need to process a high number of samples every day; therefore, it is critical that the instrument performs consistently. Mass calibration and resolution tuning are two of the most important aspects ensuring system performance. The Thermo Scientific™ SmartTune™ feature allows the user to check the tune status of the system with a few mouse clicks in an easy and quick fashion. Instrument robustness for everyday analysis and quantitative performance was evaluated by repeatedly injecting various environmental and fish oil extracts (n=100). A quality control standard in nonane (QC) at a concentration of 5.0–25.0 ng/mL was injected in duplicate every 10 samples to monitor the system stability. The SmartTune feature was used to check the instrument status at the beginning, middle, and end of the sequence. It uses the MS parameters established during the initial tuning with a clean source and intelligently assesses the performance of the system, only re-tuning when MS performance has been compromised. No inlet or MS maintenance or any re-tuning was required during the robustness evaluation. The QC showed stable response across the injections with ion ratios consistently within 30% of the calculated average from the calibration curve and QC normalized peak area %RSD <20% (Figure 7).

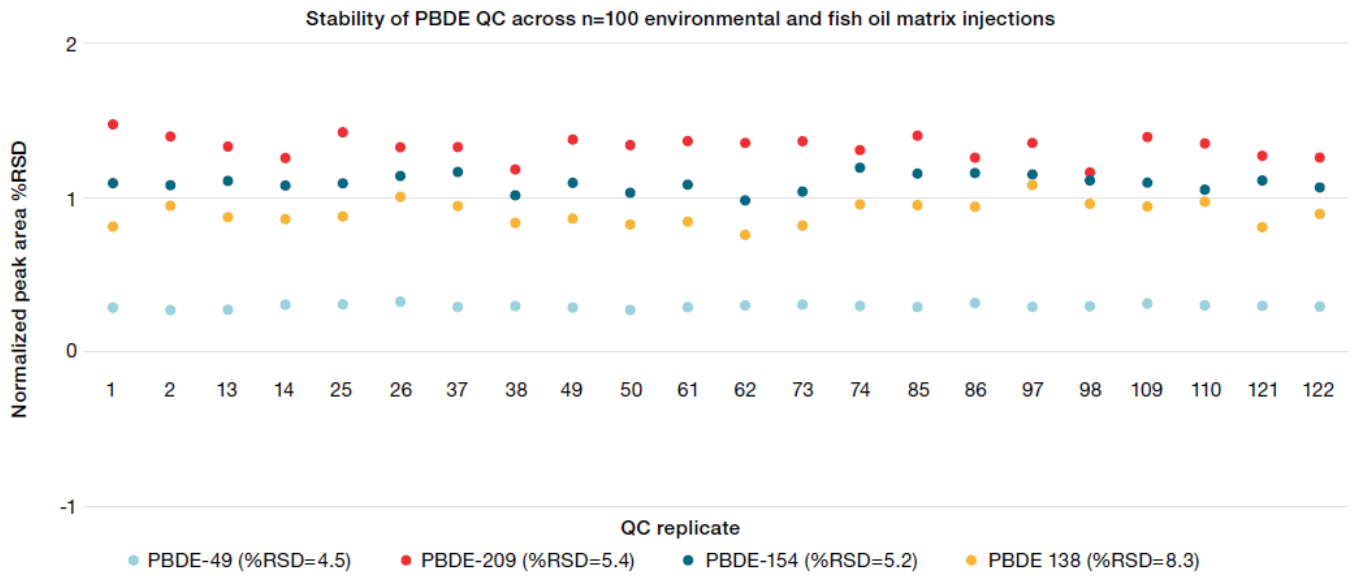

Figure 7. QC normalized peak area %RSD across a sequence of n=100 injections of various environmental and fish oil extracts.

CONCLUSION

The results obtained in these experiments demonstrate that the TSQ 9610 mass spectrometer equipped with the NeverVent AEI ion source in combination with the TRACE 1610 GC and the AI/AS 1610 liquid autosampler delivers consistent and reliable analytical performance for analysis of PBDEs in environmental and food samples.

- The high selectivity of the TraceGOLD TG-PBDE column ensured chromatographic separation of the target analytes in less than 12 minutes. Calculated resolution of the isobaric congeners PBDE-49 / PBDE-71 was 5% at the valley height, therefore exceeding the U.S EPA Method 1614 requirement of less than 40%. Furthermore, the thin film phase and high thermal stability (maximum temperatures of 360 ˚C) of the capillary column ensured elution of the high boiling point PBDEs (e.g., PBDE-209) with improved peak shapes.
- The XLXR detector allowed for extended linearity over a concentration range of 0.25 to 2,000 ng/mL with coefficient of determination of R2>0.99 and AvCF %RSDs <20. Moreover, the Chromeleon CDS advanced reprocessing capability allowed for isotope dilution quantitative analysis.
- The engineered design and the improved sensitivity of the NeverVent AEI ion source allowed for low instrument detection limits ranging from 5 fg to 122 fg OC, corresponding to 0.25 pg/L to 6.10 pg/L for water samples and 0.025 to 0.61 ng/kg for soil and fish oil samples, with calculated LOQ ranging from 1.5 pg/L to 62.5 pg/L in water samples and 0.15 to 6.25 ng/kg in soil and fish oil samples. Ion ratios and RRF were within ±30% of the expected values calculated as an average across a calibration curve even at such low analyte concentrations.
- The enhanced robustness and reliability of the AI/AS 1610 liquid autosampler combined with the efficient transfer of the analyte through the PTV injector, the inertness of the flow path, and the stability of the NeverVent AEI ion source allowed for n=100 matrix injections without requiring any system re-tuning or maintenance of the MS or inlet.

REFERENCES

1. United States Environmental Protection Agency, U.S. EPA, Technical Fact Sheet – Polybrominated Diphenyl Ethers (PBDEs), November 2017. https://www.epa.gov/sites/default/files/2014-03/documents/ffrrofactsheet_contaminant_perchlorate_january2014_final_0.pdf

2. Guidance for the inventory of polybrominated diphenyl ethers (PBDEs) listed under the Stockholm Convention on POPs. http://chm.pops.int/Implementation/NationalImplementationPlans/Guidance/GuidancefortheinventoryofPBDEs/tabid/3171/Default.aspx
3. United States Environmental Protection Agency, U.S. EPA, Method 1614A Brominated Diphenyl Ethers in Water, Soil, Sediment, and Tissue by HRGC/HRMS, May 2010. https://www.epa.gov/sites/default/files/2015-08/documents/method_1614a_2010.pdf

Appendix 1. List of target analytes, retention times (RT, min), and quantifier and qualifier ions (*m/z*)

Compound	RT (min)	Quantifier ion (*m/z*)	Qualifier 1 ion (*m/z*)	Qualifier 2 ion (*m/z*)
PBDE-3	4.37	248.00/141.20	250.00/115.10	250.00/141.10
PBDE-3L C13	4.37	260.00/124.20	260.00/152.20	262.00/152.20
PBDE-7	5.26	325.90/139.20	325.90/168.20	327.90/168.20
PBDE-15	5.49	325.90/139.20	325.90/168.20	327.90/168.20
PBDE-15L C13	5.49	337.90/180.20	339.90/150.20	339.90/180.20
PBDE-17	6.16	405.80/139.20	405.80/246.10	407.80/248.10
PBDE-28	6.25	405.80/139.20	405.80/246.10	407.80/248.10
PBDE-28L C13	6.25	417.80/150.20	417.80/258.10	419.80/260.10
PBDE-49	6.85	483.70/217.10	483.70/326.00	485.70/325.90
PBDE-71	6.88	483.70/217.10	483.70/326.00	485.70/325.90
PBDE-47	6.97	483.70/217.10	483.70/326.00	485.70/325.90
PBDE-47L C13	6.97	495.70/336.00	495.70/338.00	497.70/338.00
PBDE-79L C13	7.02	495.80/228.10	497.80/230.10	497.80/338.00
PBDE-66	7.07	483.70/217.10	483.70/326.00	485.70/325.90
PBDE-77	7.21	483.70/217.10	483.70/326.00	485.70/325.90
PBDE-100	7.48	403.80/137.10	563.60/403.80	565.60/405.90
PBDE-100L C13	7.48	575.70/307.90	575.70/415.50	577.70/415.90
PBDE-119	7.54	403.80/137.10	563.60/403.80	565.60/405.90
PBDE-99	7.63	403.80/137.10	563.60/403.80	565.60/405.90
PBDE-99L C13	7.63	575.70/307.90	575.70/415.50	577.70/415.90
PBDE-85	7.89	403.80/137.10	563.60/403.80	565.60/405.90
PBDE-126	7.93	403.80/137.10	563.60/403.80	565.60/405.90
PBDE-126L C13	7.93	575.70/307.90	575.70/415.50	577.70/415.90
PBDE-154	8.03	641.50/481.70	641.50/483.70	643.50/483.70
PBDE-154L C13	8.03	653.60/493.80	653.60/495.80	655.60/495.80
PBDE-153	8.22	483.70/323.90	641.50/481.70	641.50/483.70
PBDE-153L C13	8.22	653.60/493.80	653.60/495.80	655.60/495.80
PBDE 138L C13	8.48	495.70/336.00	653.60/493.80	653.60/495.80
PBDE-138	8.48	641.50/481.70	641.50/483.70	643.50/483.70

Appendix 1 continued. List of target analytes, retention times (RT, min), and quantifier and qualifier ions (*m/z*)

Compound	RT (min)	Quantifier ion (*m/z*)	Qualifier 1 ion (*m/z*)	Qualifier 2 ion (*m/z*)
PBDE-156	8.58	641.50/481.70	641.50/483.70	643.50/483.70
PBDE-184	8.7	721.40/561.60	721.40/563.60	723.40/563.50
PBDE-183	8.78	721.40/561.60	721.40/563.60	723.40/563.50
PBDE-183L C13	8.78	733.50/573.70	733.50/575.70	735.50/575.70
PBDE-191	8.93	721.40/561.60	721.40/563.60	723.40/563.50
PBDE-197	9.43	641.50/481.70	799.30/639.40	801.30/641.50
PBDE-197L C13	9.43	811.40/651.40	813.40/653.70	813.40/655.20
PBDE-196	9.54	641.50/481.70	799.30/639.40	801.30/641.50
PBDE-207L C13	10.17	733.50/573.60	891.30/731.20	893.30/733.20
PBDE-207	10.17	879.30/719.20	879.30/721.30	881.30/721.30
PBDE-206L C13	10.3	733.50/573.60	891.30/731.20	893.30/733.20
PBDE-206	10.3	879.30/719.20	879.30/721.30	881.30/721.30
PBDE-209	11.26	797.30/637.30	797.30/639.40	799.50/639.20
PBDE-209L C13	11.26	809.40/649.80	811.40/651.30	971.20/811.30

Appendix 2. List of target analytes, calibration ranges, calculated coefficient of determination (R^2), and residual values (measured as %RSD of average response factors, AvCF %RSD)

Peak name	Retention time (min)	Calibration range (ng/mL)	Coefficient of determination (R^2)	AvCF %RSD
PBDE-3	4.37	0.25–400	0.9974	9.9
PBDE-7	5.26	0.25–400	0.9968	6.9
PBDE-15	5.49	0.25–400	0.9977	7.0
PBDE-17	6.15	0.24–384	0.9990	5.0
PBDE-28	6.25	0.25–400	0.9990	3.5
PBDE-49	6.85	0.25–400	0.9946	7.4
PBDE-71	6.88	0.25–400	0.9984	7.0
PBDE-47	6.97	0.25–400	0.9990	4.5
PBDE-66	7.07	0.25–400	0.9965	7.1
PBDE-77	7.22	0.25–400	0.9920	8.9
PBDE-100	7.48	0.25–400	0.9986	5.4
PBDE-119	7.54	0.25–400	0.9963	7.2
PBDE-99	7.63	0.25–400	0.9990	4.4
PBDE-126	7.89	0.25–400	0.9913	8.6
PBDE-85	7.93	0.25–400	0.9943	14.4
PBDE-154	8.03	0.50–800	0.9903	8.9
PBDE-153	8.22	0.50–800	0.9974	4.4

Appendix 2 continued. List of target analytes, calibration ranges, calculated coefficient of determination (R^2), and residual values (measured as %RSD of average response factors, AvCF %RSD)

Peak name	Retention time (min)	Calibration range (ng/mL)	Coefficient of determination (R^2)	AvCF %RSD
PBDE-138	8.48	0.50–800	0.9991	5.1
PBDE-156	8.58	0.50–800	0.9984	7.1
PBDE-184	8.70	0.50–800	0.9953	8.6
PBDE-183	8.78	0.50–800	0.9994	5.1
PBDE-191	8.93	0.50–800	0.9924	7.3
PBDE-197	9.43	0.50–800	0.9925	7.3
PBDE-196	9.54	0.50–800	0.9993	4.7
PBDE-207	10.17	1.25–2,000	0.9930	5.9
PBDE-206	10.30	1.25–2,000	0.9949	6.2
PBDE-209	11.26	1.25–2,000	0.9990	6.1

Appendix 3. Calculated IDLs (fg OC), LOQs (ng/mL), as well as ion ratios (IR, expected and measured), peak area %RSD, and RRF at calculated LOQ for the investigated compounds

Peak name	Quantification ion	Injected amount (pg OC)	Peak area %RSD (n=10)	Expected IR	Average measured IR	Calculated IDL (fg OC)	Calculated LOQ (ng/mL)
PBDE-3	248.00/141.20	0.06	6.1	46	44	5	0.06
PBDE-7	325.90/139.20	0.06	9.6	430	444	12	0.06
PBDE-15	325.90/139.20	0.06	13.5	120	115	11	0.06
PBDE-17	405.80/139.20	0.03	10.9	133	139	6	0.03
PBDE-28	405.80/139.20	0.03	9.0	158	156	8	0.03
PBDE-49	483.70/217.10	0.25	5.9	178	174	12	0.25
PBDE-71	483.70/217.10	0.25	7.1	182	193	11	0.25
PBDE-47	483.70/217.10	0.12	9.6	160	160	12	0.12
PBDE-66	483.70/217.10	0.12	12.4	197	184	11	0.12
PBDE-77	483.70/217.10	0.25	8.2	43	44	11	0.25
PBDE-100	403.80/137.10	0.06	13.6	116	122	14	0.06
PBDE-119	403.80/137.10	0.06	10.1	75	70	8	0.06
PBDE-99	403.80/137.10	0.06	13.1	92	91	8	0.06
PBDE-126	403.80/137.10	0.12	11.3	85	85	10	0.12
PBDE-85	403.80/137.10	0.25	6.4	183	168	9	0.25
PBDE-154	641.50/481.70	0.25	11.5	75	78	28	0.25
PBDE-153	483.70/323.90	0.25	7.0	86	86	28	0.25

Appendix 3 continued. Calculated IDLs (fg OC), LOQs (ng/mL), as well as ion ratios (IR, expected and measured), peak area %RSD, and RRF at calculated LOQ for the investigated compounds

Peak name	Quantification ion	Injected amount (pg OC)	Peak area %RSD (n=10)	Expected IR	Average measured IR	Calculated IDL (fg OC)	Calculated LOQ (ng/mL)
PBDE-138	641.50/481.70	0.50	6.2	77	75	88	0.50
PBDE-156	641.50/481.70	0.50	7.4	81	79	122	0.50
PBDE-184	721.40/561.60	0.50	6.1	50	51	17	0.50
PBDE-183	721.40/561.60	0.25	9.2	49	51	27	0.25
PBDE-191	721.40/561.60	0.25	10.8	50	53	25	0.25
PBDE-197	641.50/481.70	0.50	8.2	172	138	116	0.50
PBDE-196	641.50/481.70	0.50	7.1	139	115	98	0.50
PBDE-207	879.30/719.20	1.25	7.5	50	48	43	1.25
PBDE-206	879.30/719.20	1.25	7.3	48	46	49	1.25
PBDE-209	797.30/637.30	1.25	7.3	57	58	82	1.25

This sponsor report is the responsibility of Thermo Fisher Scientific.

20ºENQA | 8ºCIAQA

Encontro Nacional de Química Analítica
20th Brazilian Meeting on Analytical Chemistry

Congresso Ibero-Americano de Química Analítica

September • 25 to 28, 2022 • Dall'Onder Grande Hotel • Bento Gonçalves • RS • Brazil

These events are organized with short courses, conferences, oral and poster sessions, workshops, awards and commercial exhibitions.

Event topics

- Electrochemistry and Electroanalysis
- Atomic Spectrometry
- Mass Spectrometry
- Analytical Instrumentation
- Separation methods
- Sample preparation
- Environmental Chemistry
- Chemometrics
- Other topics in Analytical Chemistry

For more information: www.enqa.com.br

Held by: Sociedade Brasileira de Química | UFSM

Sponsorship – Diamond: Anton Paar, ThermoFisher Scientific

Sponsorship - Gold: Agilent, Astro 34, União, Metrohm, analítica

Sponsorship – Silver: HORIBA, Waters

Sponsorship - Bronze: ALLCROM, SHIMADZU

Organized by: acontece

RELEASE

Ethos UP High Performance Microwave Digestion Systems

The new ETHOS UP™ is simply the most advanced yet easy to use system for microwave sample preparation we have ever manufactured. It offers a perfect integration between microwave hardware, user interface, digestion sensors and pressure vessels.

The Largest Stainless-Steel Microwave Cavity

The microwave cavity has a volume of over 70 liters, the largest currently available. Therefore, digestion rotors with more sample places can be accommodated, incresing both productivity and sample throughput. Secondly, it improves the inherently safety because a larger cavity contains gases escaping from vessels in a more efficient way, in case of a sudden over pressurization.

Pressure-Responsive Door for Max Safety

For additional safety, the ETHOS UP features a full stainless steel door with an innovative opening and self-resealing mechanism. Should there be a sudden over pressurization of the cavity, the door slightly opens for rapid and safe pressure release and the microwave power is instantaneously cut off. Immediately afterwards, the door is pulled back, resealing the microwave cavity.

The Most Powerful Microwave Digester

The ETHOS UP is equipped with two 950 Watt magnetrons for a total of 1900 Watt. The system additionally employs a rotating diffuser that evenly distributes the microwaves throughout the cavity. High power coupled with this diffuser enable very fast heating of high throughput rotors and the complete digestion of the most difficult samples.

Live Monitoring with Milestone Safeview

The ETHOS UP integrates the Milestone safeVIEW, a high definition digital camera interfaced with the instrument terminal. It allows the chemist to monitor the progress of the digestion whilst being fully protected by the instrument's all-stainless steel door. A video of the entire run is shown in real time.

Sensors for Unparalleled Digestion Control

In a digestion process, the temperature controls the sample decomposition and directly affects digestion quality. Milestone pioneered the use of infrared sensors combined with an in-situ temperature sensor. Today, Milestone innovates again by combining all the benefits of in-situ and infrared sensors into the Milestone easyTEMP, a direct contactless temperature sensor.

Rugged, reliable microwave platform

While other manufacturers use molded plastic, Milestone uses 316 stainless steel construction throughout which creates the most durable, reliable, and safe microwave system available.

Find out more at milestonesrl.com

Productivity UP.
Simplicity UP.
Safety UP.
Ethos UP.

HIGHEST THROUGHPUT ROTORS

NO METHOD DEVELOPMENT

REMOTE SYSTEM CONTROL

ENHANCED SAFETY FEATURES

JUST WHEN YOU THINK METALS PREP TECHNOLOGY CANT GET ANY BETTER, IT DOES.

The Milestone Ethos UP isnt just intelligent, its the most powerful microwave digestion system on the market today.

Featuring the highest throughput rotors, stainless steel construction and patented vent-and-reseal technology, the Ethos UP ensures market-leading safety and productivity.

Plus, new Milestone Connect offers remote system control, 24/7 technical support and direct access to a comprehensive library of content developed especially for lab professionals.

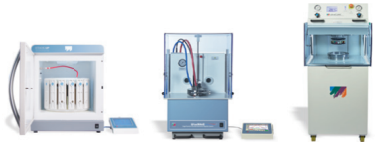

ETHOS Line | UltraWAVE | UltraCLAVE

See how Ethos UP can help you work smarter.
Go to www.milestonesrl.com/ethosup

VIDEO WEBSITE

MILESTONE

RELEASE

Perform like a PRO

Thermo Scientific™ iCAP™ PRO X ICP-OES system delivers Simplicity, Speed and Robustness

The Thermo Scientific™ iCAP™ PRO X ICP-OES system combines powerful multi-element capability with flexibility, so your lab is ready for any challenge. Produce consistent, reliable data quickly and easily. Experience enhanced sample throughput, matrix tolerance, and flexibility to produce results you can trust.

The iCAP™ PRO X ICP-OES offers fast start-up, easy-to-use software and incredible speed with pre-optimized method conditions, providing multi-element detection technology far superior to that of single-element AAS and multi element microwave plasma techniques. This system is ideal for laboratories with low sample throughput requirements. For ease of use a number of optimized settings are defined as standard, making them ideal for users new to the technique or those who require a simple solution for multi elemental analysis.

Experience more simplicity without compromising on detail

- Flexibility to fulfil demanding projects
- Long-term stability through gas MFCs and temperature control
- Full frame view immediately after measurement
- Intelligent monitoring of analytes with Qtegra ISDS Software
- Plasma optimization tool with tune sets and auto-tune for automated method development

Fast, powerful performance

- Advanced, high-speed charge injection device detection technology produces results in the fastest possible time
- A small optical tank ensures fast start up time and reduced purge gas requirements. With start up times of just 30 minutes from power off and 5 minutes from standby (model dependent)
- Detect from % range to sub ppb detection limits with a high dynamic range detector

Optimized vertical torch for ultimate robustness

- Both duo and radial view configurations of the instruments feature vertical torch orientation. When combined with the unique plasma interface, a new level of robustness is achieved
- Adjustable radial viewing height on both duo and radial view instruments, enabled by the vertical plasma interface
- Increase robustness further with dedicated accessories and analyze the most challenging samples, such as saturated brine solutions.

Accurately quantify the elemental composition of a wide range of samples in: Agricultural screening, Food production and safety, Environmental analysis, Pharmaceutical and nutraceutical compliance, Chemical QA and QC, Petrochemical, Metals and materials

Find out more at thermofisher.com/icp-oes

thermo scientific

iCAP PRO Series ICP-OES

Perform like a PRO
Simplicity, robustness and speed

Analyze even the most challenging sample matrices
The Thermo Scientific™ iCAP™ PRO Series ICP-OES combines powerful multi-element capability with flexibility so your lab is ready for any challenge.

Produce consistent, reliable data quickly and easily. Experience enhanced sample throughput, matrix tolerance and flexibility to produce results you can trust.

Achieve precise results first time, every time with the innovative Get Ready feature. This automated technology sets up the instrument for you and checks performance. Manage instrument processes using a logical dashboard interface. Trust in ICP-OES technology driven by Thermo Scientific™ Qtegra™ Intelligent Scientific Data Solution™ (ISDS) Software.

VIDEO

WEBSITE

ThermoFisher SCIENTIFIC

RELEASE

Thermo Scientific TSQ 9610 Triple Quadrupole GC-MS/MS System

Unstoppable confidence for analytical testing

To confidently stay ahead, your GC-MS/MS system must deliver ultimate performance while consistently producing trusted quantitative results. That's the reason for the Thermo Scientific™ TSQ™ 9610 Triple Quadrupole GC-MS/MS System. User-centric Thermo Scientific™ NeverVent™ technology, extended-life detector, and intelligent software eliminate unnecessary downtime to maximize your sample throughput and return on investment (ROI). New extended linear dynamic range combined with proven high sensitivity ensures you keep ahead of the toughest regulatory methods and business demands.

Combine the TSQ 9610 Triple Quadrupole GC-MS/MS System with the Thermo Scientific™ TRACE™ 1600 Series Gas Chromatograph (GC) and Thermo Scientific™ AI/AS 1610 Liquid Autosampler to optimize the performance and productivity of your solution.

Increase instrument uptime

Eliminate unnecessary and unplanned instrument downtime to deliver high-confidence quantitative results, day after day. The TSQ 9610 Triple Quadrupole GC-MS/MS System combines unstoppable robustness with the ability to change the GC column and clean the ion source without interrupting analytical workflows.

Maximize sample throughput

When high sample throughput is essential, the system delivers results on time and with ease. Automated workflows and simplified operation ensure every user produces consistent results, sample after sample. Extended linear range and rapid selected reaction monitoring (SRM) scanning enable method consolidation so you can analyze more compounds in a single run. When these capabilities are combined with best-in-class uptime and sensitivity, you stay ahead of any productivity demand.

Realize rapid return on investment

Ensuring your system delivers results as soon as it's installed is necessary to achieving rapid ROI. With built-in intelligence that simplifies instrument set up, analytical methods, and everyday operation, the TSQ 9610 Triple Quadrupole GC-MS/MS System is designed for accelerated deployment. Reduced needs for operator training and faster time to full productivity together with maximum sample throughput provide fast return on your instrument investment.

Find out more at thermofisher.com/TSQ9610

ThermoFisher SCIENTIFIC

Mass Spectrometry

Stay ahead

with unstoppable confidence

To confidently stay ahead, your GC-MS/MS system must deliver ultimate performance while consistently producing trusted quantitative results. That's the reason for the Thermo Scientific™ TSQ™ 9610 Triple Quadrupole GC-MS/MS System. User-centric Thermo Scientific™ NeverVent™ technology, extended-life detector, and intelligent software eliminate unnecessary downtime to maximize your sample throughput and return on investment (ROI). New extended linear dynamic range combined with proven high sensitivity ensures you keep ahead of the toughest regulatory methods and business demands.

GC-MS that's ready to run when you are.

VIDEO **WEBSITE**

Find out more at **thermofisher.com/TSQ9610**

thermoscientific

RELEASE

Pittcon Conference & Expo

Pittcon is a catalyst for the exchange of information, a showcase for the latest advances in laboratory science, and a venue for international connectivity.

Pittcon is a friendly, welcoming environment where analytical chemists at all professional levels meet. Pittcon is a platform for sharing ideas and cooperating to form new ones. Here, you will find that spark that drives your research, your career, and above all, your scientific perspective forward.

One of the foremost analytical chemistry conferences, Pittcon's Conference programs provide participants with direct access to the latest research and developments from top scientists and innovators throughout the world.

At Pittcon, our goal is to advance scientific endeavor through collaboration, bringing together a world of knowledge to impact, enrich, and inspire the future of science.

Proceeds from each and every Pittcon directly fund science education and outreach. Over 90% of Pittcon's net profit goes on to fund primary and secondary education, continuing education, scholarships, laboratory improvements, and outreach activities.

Pittcon also offers an employment bureau, networking opportunities, social events, and an environment that fosters knowledge and expands your network of scientific resources.

Pittcon 2023 Dates
Exposition: Monday (Mar 20) – Wednesday (Mar 22)
Short Courses: Saturday (Mar 18) – Wednesday (Mar 22)
Technical Program: Sunday (Mar 19) – Wednesday (Mar 22)
Employment Bureau: Saturday (Mar 18) – Friday (Mar 31)

Pittcon 2023 Location
Pennsylvania Convention Center
1101 Arch Street
Philadelphia, PA 19107, USA

Pittcon®
Conference and Exposition

Pittcon Conference and Exposition
Philadelphia, Pennsylvania, USA
March 18 – 22, 2023

LEADING THE LAB

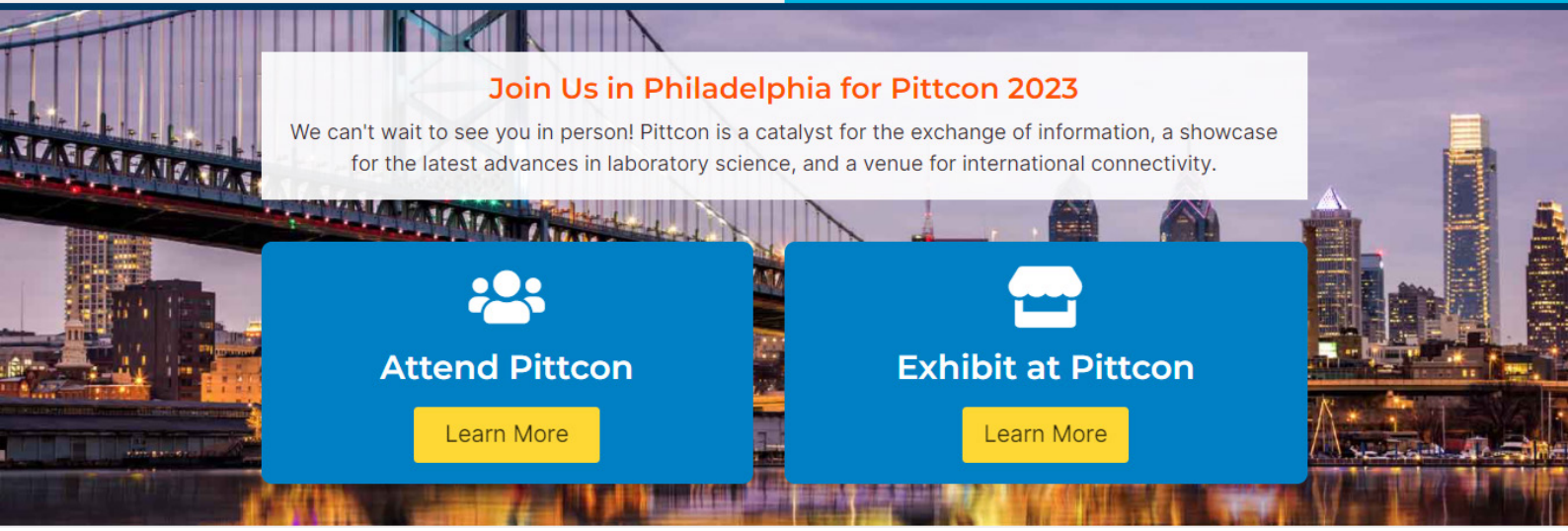

Finally, a Chance to Collaborate in Person!

Reconnect with colleagues, feel the instruments, and experience the sights. Celebrate bringing together a world of knowledge to impact, enrich, and inspire the future of science.

Why You Need to Attend

It's a matter of perspective, or maybe more a matter of gaining perspective. You'll be presented new ideas, new methods, new instrumentation, and there's so much more – the interactions, the conversations, the introductions.

March 18 - 22, 2023
Pennsylvania Convention Center
Philadelphia, Pennsylvania, USA

Be the First to Know

Connect with us and we'll let you know the latest news as we prepare for Pittcon 2023.

Connect with Us

Visit the full Pittcon website to learn more - much more!

Home Page

Pittcon®
Conference and Exposition

RELEASE

SelectScience® Pioneers online Communication and Promotes Scientific Success

SelectScience® promotes scientists and their work, accelerating the communication of successful science. Through trusted lab product reviews, virtual events, thought-leading webinars, features on hot scientific topics, eBooks and more, independent online publisher SelectScience® provides scientists across the world with vital information about the best products and techniques to use in their work.

Some recent contributions from SelecScience® to the scientific community

VIDEOS

Using mass spec to maintain the health of livestock

Researchers at the Iowa State Veterinary Diagnostic Lab help to maintain the health of livestock by analyzing drug residue samples from various species, screening for many different compound. Access **here**

Detecting allergens using mass spectrometry

Detecting and identifying allergens within foods is incredibly important. Dr Phil Johnson from the University of Nebraska-Lincoln explains how mass spectrometry can be used to detect allergens, and how they ensure they are testing the correct peptides to identify allergens in food. Access **here**

WEBINAR

Transmission Raman: A versatile tool for pharmaceutical formulation development to end-product testing

Transmission Raman is a versatile tool that presents fast, non-destructive bulk measurements of whole intact tablets, capsules, creams, vials, and well plates. This webinar explores the key pharmaceutical applications of transmission Raman spectroscopy. Access this webinar **here**

INDUSTRY NEWS

Inaugural open access issue of SLAS Discovery paves way for 2022

SLAS Discovery is an official journal of the Society for Laboratory Automation and Screening (SLAS). Volume 27, Issue 1 of *SLAS Discovery* is the first issue to be published Open Access in partnership with SLAS's new publisher, Elsevier. Access **here**

SelectScience® is the leading independent online publisher connecting scientists to the best laboratory products and applications.

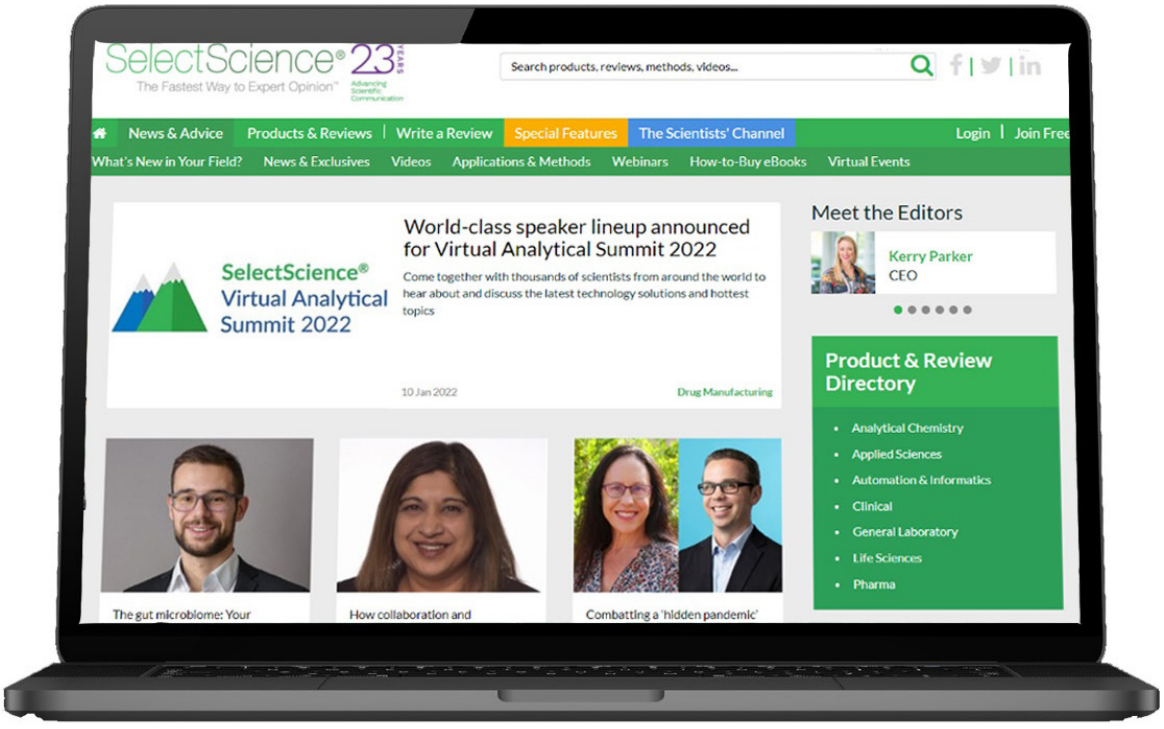

- Working with Scientists to Make the Future Healthier.
- Informing scientists about the best products and applications.
- Connecting manufacturers with their customers to develop, promote and sell technologies.

SelectScience®
The Fastest Way to Expert Opinion

RELEASE

CHROMacademy is the leading provider of eLearning for analytical science

CHROMacademy *helps scientific organizations acquire and maintain excellence in their laboratories*.

For over 10 years, CHROMacademy has increased knowledge, efficiency and productivity across all applications of chromatography. With a comprehensive library of learning resources, members can improve their skills and knowledge at a pace that suits them.

CHROMacademy covers all chromatographic applications – HPLC, GC, mass spec, sample preparation, basic lab skills, and bio chromatography. Each paradigm contains dozens of modules across theory, application, method development, troubleshooting, and more. Invest in analytical eLearning and supercharge your lab.

For more information, please visit www.chromacademy.com/

LC GC's CHROMacademy
powered by crawford scientific

CHROMacademy Lite members have access to less than 5% of our content. Premier members get so much more !

Video Training courses

Fundamental HPLC
Fundamental GC
Fundamental LCMS
Fundamental GCMS
HPLC Method Development
GC Method Development

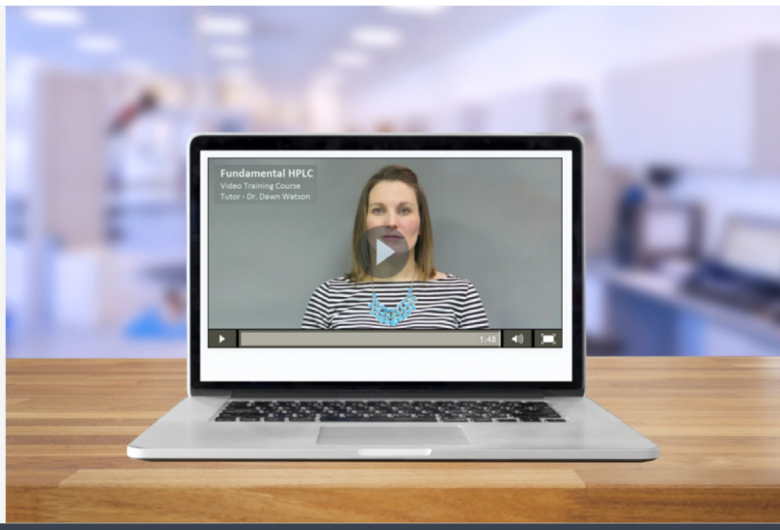

Ask the Expert

We are always on hand to help fix your instrument and chromatographic problems, offer advice on method development, help select a column for your application and more.

To find out more about Premier Membership contact:

Glen Murry: +1 732.346.3056 | Glen.Murry@ubm.com
Peter Romillo: +1 732.346.3074 | Peter.Romillo@ubm.com

www.chromacademy.com

The worlds largest e-Learning website for analytical scientists

NOTICES OF BOOKS

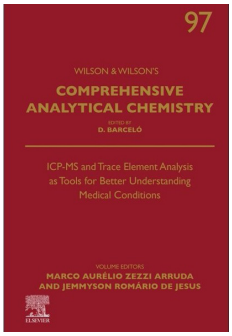

ICP-MS and Trace Element Analysis as Tools for Better Understanding Medical Conditions (Series: Comprehensive Analytical Chemistry, Volume 97)

Marco Aurélio Zezzi Arruda and Jemmyson Romário de Jesus, Editors

May, 2022. Publisher: Elsevier

This book discusses trace elements and how they play an important role in biological functions and metabolism in the human body. It covers biomedical analysis by ICP-MS: a focus on single cell, advanced statistical tools and machine learning applied to trace element analysis associated with medical conditions, ICP-MS as a tool to understand trace element homeostasis in neurological disorders, and as a versatile technique from imaging to chemical speciation, and more. Read more

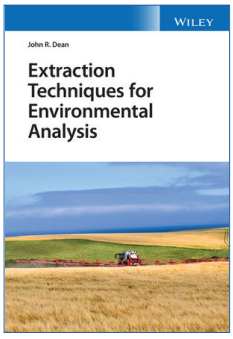

Extraction Techniques for Environmental Analysis

John R. Dean, Author

February 2022. Publisher: Wiley

Extraction techniques for aqueous, air, and solid environmental matrices are explored. Readers will find in-depth treatments of specific extraction techniques suitable for adoption in their own laboratories, as well as reviews of relevant analytical techniques used for the analysis of organic compound extracts. A chapter that extensively covers the requirements for an analytical laboratory, including health and safety standards is included. Read more

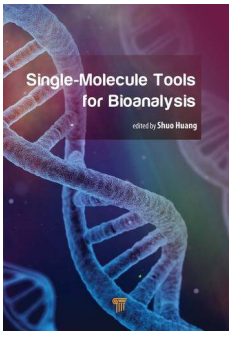

Single-Molecule Tools for Bioanalysis

Shuo Huang, Editor

May 2022. Publisher: Jenny Stanford

In the last three decades, the fast development of single-molecule techniques has revolutionized the way we observe and understand biological processes. This book summarizes and details the frontiers of the development of the single-molecule techniques as well as their applications. The systematically written content provides a thorough illustration of the mechanisms of each methodology presented. Read more

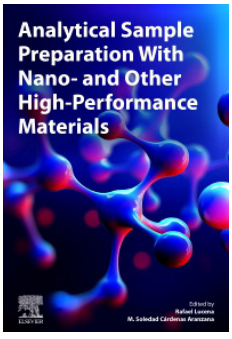

Analytical Sample Preparation with Nano- and Other High-Performance Materials

Rafael Lucena and M. Soledad Cardenas Aranzana, Editors

October, 2021. Publisher: Elsevier

This book explains the underlying principles needed to properly understand sample preparation, and also examines the latest materials - including nanomaterials - that result in greater sensitivity and specificity. The book begins with a section devoted to all the various sample preparation techniques and then continues with sections on high-performance sorbents and high-performance solvents. Read more

PERIODICALS & WEBSITES

American Laboratory

American Laboratory® is a platform that addresses basic research, clinical diagnostics, drug discovery, environmental, food and beverage, forensics and other markets, and combines in-depth articles, news, and video to deliver the latest advances in their fields. **Featured Article:** ***Achieving Energy-efficiency in Academic Labs.*** As the impacts of excess energy consumption have become more apparent, the time to act on producing greener labs has never been more urgent. Read more

LCGC

Chromatographyonline delivers practical, nuts-and-bolts information to help scientists and lab managers become more proficient in the use of chromatographic techniques and instrumentation. **Article:** ***Cracking the Code of Complex Drug Modalities via Multidimensional Liquid Chromatography Coupled to Mass Spectrometry.*** MDLC–MS is a powerful tool for the characterization of complex biopharmaceutical drug modalities, from antibody–drug conjugates to nuclear acid therapeutics like antisense oligonucleotides and small interfering RNA. Read more

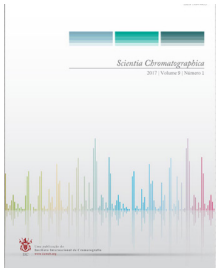

Scientia Chromatographica

Scientia Chromatographica is the first and to date the only Latin American scientific journal dedicated exclusively to Chromatographic and Related Techniques. With a highly qualified and internationally recognized Editorial Board, it covers all chromatography topics in all their formats, in addition to discussing related topics such as “The Pillars of Chromatography”, Quality Management, Troubleshooting, Hyphenation (GC-MS, LC-MS, SPE-LC-MS/MS) and others. It also provides columns containing general information, such as: calendar, meeting report, bookstore, etc. Read more

Select Science

SelectScience® has transformed global scientific communications and digital marketing over the last 23 years. Informing scientists about the best products and applications. Connecting manufacturers with their customers to develop, promote and sell technologies promotes scientists and their work, accelerating the communication of successful science. Scientists can make better decisions using independent, expert information and gain easy access to manufacturers. SelectScience® informs the global community through Editorial, Features, Video and Webinar programs. Read more

Spectroscopy

With the *Spectroscopy* journal, scientists, technicians, and lab managers gain proficiency through unbiased, peer-reviewed technical articles, trusted troubleshooting advice, and best-practice application solutions.

Feature article: ***2022 Review of Spectroscopic Instrumentation.*** Annual review of products introduced at Pittcon or during the previous year, broken down by the following categories: AAS, UV-vis, NIR, mid-IR, Raman, imaging, NMR, MS, accessories, and components. Read more

EVENTS in 2022 – It is suggested to consult the event's official website for updates.

July 18 – 21
8th International Caparica Conference on Analytical Proteomics
Caparica, Portugal
https://www.icap2022.net/

August 24 – 26
Journées de Chimie Analytique, 11th Edition (JCA2022)
Yaounde, Cameroun
https://jca-2021.sciencesconf.org

August 29 – September 2
XVIII Chemometrics in Analytical Chemistry (CAC2022)
University of Rome La Sapienza, Rome, Italy
http://cac2022.sciencesconf.org

September 5 – 8
National Meeting of Forensic Chemistry (ENQFor) & Meeting of the Brazilian Society of Forensic Sciences (SBCF)
Ribeirão Preto, SP, Brazil
https://www.enqfor.org.br/

September 5 – 8
51th Annual Meeting of the Brazilian Society of Biochemistry and Molecular Biology (SBBq) & 46th Congress of the Brazilian Society of Biophysics (SBBf)
Convention Center of the Majestic Hotel, Águas de Lindóia, SP, Brazil
https://www2.sbbq.org.br/reuniao/2022/

September 25 – 28
20th National Meeting of Analytical Chemistry (ENQA) & 8th Ibero-American Congress of Analytical Chemistry (CIAQA)
Bento Gonçalves, RS, Brazil
https://enqa.com.br/

September 25 – 29
XX Brazilian Materials Research Society Meeting (SBPMat)
Foz do Iguaçu, PR, Brazil
https://www.sbpmat.org.br/pt/

December 10 – 15
III Ibero American Conference on Mass Spectrometry (IBERO 2022)
Rio de Janeiro, RJ, Brazil
https://www.ibero2022.com/

GUIDELINES FOR AUTHORS

Scope

The *Brazilian Journal of Analytical Chemistry* (BrJAC) is dedicated to the diffusion of significant and original knowledge in all branches of Analytical Chemistry and Bioanalytics. The BrJAC is addressed to professionals involved in science, technology and innovation projects at universities, research centers and in industry.

Professional Ethics

Manuscripts submitted for publication in BrJAC cannot have been previously published or be currently submitted for publication in another journal.

The BrJAC does not consider submissions of manuscripts that have been posted to preprint servers prior to submission, and will withdraw from consideration any papers posted to those servers prior to publication.

The submitted manuscripts are the full responsibility of the authors. Manipulation/invention/omission of data, duplication of publications, the publication of papers under contract and confidentiality agreements, company data, material obtained from non-ethical experiments, publications without consent, the omission of authors, plagiarism, the publication of confidential data and undeclared conflicts of interests are considered serious ethical faults.

The BrJAC discourages and restricts the practice of excessive self-citation by the authors.

The BrJAC does not practice coercive citation, that is, it does not require authors to include references from BrJAC as a condition for achieving acceptance, purely to increase the number of citations to articles from BrJAC without any scientific justification.

Misconduct will be treated according to the COPE's recommendations (https://publicationethics.org/) and the Council of Science Editors White Paper on Promoting Integrity in Scientific Journal Publications (https://www.councilscienceeditors.org/).

For more detailed information on the BrJAC's ethics and integrity policy, please see the "About us" menu at www.brjac.com.br

Manuscripts that can be submitted to BrJAC

- **Articles:** Full descriptions of an original research finding in Analytical Chemistry. Articles undergo double-blind full peer review.
- **Reviews:** Articles on well-established subjects, including critical analyses of the bibliographic references and conclusions. Manuscripts submitted for publication as Reviews must be original and unpublished. Reviews undergo double-blind full peer review.
- **Technical Notes:** Concise descriptions of a development in analytical methods, new techniques, procedures or equipment falling within the scope of the BrJAC. Technical notes also undergo double-blind full peer review.
- **Letters:** Discussions, comments, suggestions on issues related to Analytical Chemistry, and consultations to authors. Letters are welcome and will be published at the discretion of the BrJAC editor-in-chief.

Documents Preparation

It is highly recommended that authors download and use the templates to create their four mandatory documents to avoid the suspension of a submission that does not meet the BrJAC guidelines.

Download templates here

Cover Letter

In addition to the usual content of a Cover Letter to the Editor-in-Chief of the journal, the submitting author must declare any conflicts of interest on behalf of all co-authors and their agreement with the copyright policy of the BrJAC. Please read about conflicts of interest and copyright in the About us menu at www.brjac.com.br

It is the duty of the submitting author to inform their collaborators about the manuscript content and obtain their permission for submission and eventual publication.

The Cover Letter must be signed by the submitting author.

Title Page

The Title Page must contain information for each author: full name, affiliation and full postal address in the original language, and information on the contribution of each author to the work. Acknowledgments must be entered on the Title Page. The submitting author must sign the Title Page.

Novelty Statement

The Novelty Statement must contain clear and succinct information about what is new and innovative in the study in relation to previously related works, including the works of the authors themselves.

Manuscript

It is highly recommended that authors download the Manuscript template and create their manuscript in this template, keeping the layout of this file.

- **Language**: **English** is the language adopted by BrJAC. The correct use of English is of utmost importance. In case the Editors and Reviewers consider the manuscript to require an English revision, the authors will be required to send an English proofreading certificate before the final approval of the manuscript by BrJAC.
- **Required items**: the manuscript must include a title, abstract, keywords, and the following sections: Introduction, Materials and Methods, Results and Discussion, Conclusion, and References.
- **Identification of authors**: as the BrJAC adopts a double-blind review, the manuscript file must **NOT** contain the authors' names, affiliations nor acknowledgments. Full details of the authors and their acknowledgements should be on the Title Page.
- **Layout**: the lines in the manuscript must be numbered consecutively and double-spaced.
- **Graphics and Tables**: must appear close to the discussion about them in the manuscript. For **figures** use **Arabic** numbers, and for **tables** use **Roman** numbers.
- **Permission to use content already published**: to use figures, graphs, diagrams, tables, etc. identical to others previously published in the literature, even if these materials have been published by the same submitting authors, a publication permission from the publisher or scientific society holding the copyrights must be requested by the submitting authors and included among the documents uploaded in the manuscript management system at the time of manuscript submission.
- **Chemical nomenclature, units and symbols**: should conform to the rules of the International Union of Pure and Applied Chemistry (IUPAC) and Chemical Abstracts Service. It is recommended that, whenever possible, the authors follow the International System of Units, the International Vocabulary of Metrology (VIM) and the NIST General Table of Units of Measurement. Abbreviations are not recommended except for those recognized by the International Bureau of Weights and Measures or those recorded and established in scientific publications. Use L for liters. Always use superscripts rather than /. For instance: use mg mL^{-1} and NOT mg/mL. Leave a space between numeric values and their units.
- **References throughout the manuscript:** the references must be cited as superscript numbers. It is recommended that references older than 5 (five) years be avoided, except in relevant cases. Include references that are accessible to readers.
- **References item:** This item must be thoroughly checked for errors by the authors before submission. From 2022, BrJAC is adopting the American Chemical Society's Style in the Reference item. Mendeley Reference Manager users will find the Journal of American Chemical Society citation style in the Mendeley View menu. Non-users of the Mendeley Reference Manager may refer to the ACS Reference Style Quick Guide DOI: https://doi.org/10.1021/acsguide.40303

Manuscript Submission

The BrJAC uses an online manuscript manager system for the submission of manuscripts. This system guides authors stepwise through the entire submission process.

Submit manuscripts at www.brjac.com.br

The submitting author must add all co-authors to the Authors section of the manuscript manager system. After submission, all co-authors will receive an alert and will have the opportunity to confirm whether or not they are co-authors.

Four documents are mandatorily uploaded by the submitting author: Cover letter, Title Page, Novelty Statement and the Manuscript. Templates for these documents are available at www.brjac.com.br

The four documents mentioned above must be uploaded into the manuscript manager system as Word files. The manuscript Word file will be converted by the system to a PDF file which will be used in the double-blind peer review process.

All correspondence, including notification of the Editor's decision and requests for revision, is sent by e-mail to the submitting author through the manuscript manager system.

Review process

Manuscripts submitted to the BrJAC undergo an initial check for compliance with all of the journal's guidelines. Submissions that do not meet the journal's guidelines will be suspended and an alert sent to the corresponding author. The authors will be able to resend the submission within 30 days. If the submission according to the journal's guidelines is not made within 30 days, the submission will be withdrawn on the first subsequent day and an alert will be sent to the corresponding author.

Manuscripts that are in accordance with the journal's guidelines are submitted for the analysis of similarities by the iThenticate software.

The manuscript is then forwarded to the Editor-in-Chief who will check whether the manuscript is in accordance with the journal's scope and will analyze the similarity report issued by iThenticate.

If the manuscript passes the screening described above, it will be forwarded to an Associate Editor who will also analyze the iThenticate similarity report and invite reviewers.

Manuscripts are reviewed in double-blind mode by at least 2 reviewers. A larger number of reviewers may be used at the discretion of the Editor. As evaluation criteria, the reviewers employ originality, scientific quality, contribution to knowledge in the field of Analytical Chemistry, the theoretical foundation and bibliography, the presentation of relevant and consistent results, compliance with the BrJAC's guidelines, clarity of writing and presentation, and the use of grammatically correct English.

Note: In case the Editors and Reviewers consider the manuscript to require an English revision, the authors will be required to send an English proofreading certificate, by the ProofReading Service or equivalent service, before the final approval of the manuscript by the BrJAC.

The 1st-round review process usually takes around 5-6 weeks. If the manuscript is not rejected but requires corrections, the authors will have one month to submit a corrected version of the manuscript. In another 3-4 weeks, a new decision on the manuscript may be presented to the corresponding author.

The manuscripts accepted for publication are forwarded to the article layout department. Minor changes to the manuscripts may be made, when necessary, to adapt them to BrJAC guidelines or to make them clearer in style, respecting the original content. The articles are sent to the authors for approval before publication. Once published online, a DOI number is assigned to the article.

Copyright

When submitting their manuscript for publication, the authors agree that the copyright will become the property of the Brazilian Journal of Analytical Chemistry, if and when accepted for publication. The submitting author declares in the Cover Letter, on behalf of all other co-authors, to consent to this transfer.

The copyright comprises exclusive rights of reproduction and distribution of the articles, including reprints, photographic reproductions, microfilms or any other reproductions similar in nature, including translations.

Final Considerations

Whatever the nature of the submitted manuscript, it must be original in terms of methodology, information, interpretation or criticism.

With regard to the contents of published articles and advertisements, the sole responsibility belongs to the respective authors and advertisers; the BrJAC, its editors, editorial board, editorial office and collaborators are fully exempt from any responsibility for the data, opinions or unfounded statements.